MARCOS AUGUSTO DE PAULA BARBOSA

PROGRAMMED CELL DEATH IN *in vitro* PLANTS OF *Luffa cylindrica* (L.) ROEM: A PHYSIOLOGICAL INVESTIGATION

Dissertation submitted to the Plant Physiology Graduate Program of the Universidade Federal de Viçosa in partial fulfillment of the requirements for the degree of *Magister Scientiae*.

Adviser: Wagner Campos Otoni

Co-advisers: Kleiton Lima de Godoy Machado
Tatiane Dulcineia Silva

VIÇOSA - MINAS GERAIS
2023

Ficha catalográfica elaborada pela Biblioteca Central da Universidade Federal de Viçosa - Campus Viçosa

T
B238p
2024

Barbosa, Marcos Augusto de Paula, 1994-
Programmed cell death in *in vitro* plants of *Luffa cylindrica* (L.) Roem: a physiological investigation / Marcos Augusto de Paula Barbosa. – Viçosa, MG, 2024.
1 dissertação eletrônica (151 f.): il. (algumas color.).

Texto em inglês.
Orientador: Wagner Campos Otoni.
Dissertação (mestrado) - Universidade Federal de Viçosa, Departamento de Biologia Vegetal, 2024.
Inclui bibliografia.
DOI: https://doi.org/10.47328/ufvbbt.2024.563
Modo de acesso: World Wide Web.

1. *Luffa cylindrica*. 2. Apoptose. 3. Plantas - Anatomia. 4. Proteômica. 5. Poliaminas. 6. Estresse oxidativo. 7. Plantas - Reguladores. I. Otoni, Wagner Campos, 1962-. II. Universidade Federal de Viçosa. Departamento de Biologia Vegetal. Programa de Pós-Graduação em Fisiologia Vegetal. III. Título.

CDD 22. ed. 583.63

Bibliotecário(a) responsável: Bruna Silva CRB-6/2552

MARCOS AUGUSTO DE PAULA BARBOSA

PROGRAMMED CELL DEATH IN *in vitro* PLANTS OF *Luffa cylindrica* (L.) ROEM: A PHYSIOLOGICAL INVESTIGATION

Dissertation submitted to the Plant Physiology Graduate Program of the Universidade Federal de Viçosa in partial fulfillment of the requirements for the degree of *Magister Scientiae*.

APPROVED: July 25, 2024.

Assent:

gov.br Documento assinado digitalmente
MARCOS AUGUSTO DE PAULA BARBOSA
Data: 20/09/2024 07:50:48-0300
Verifique em https://validar.iti.gov.br

Marcos Augusto de Paula Barbosa

Author

Wagner Campos Otoni

Adviser

To my wife and to my mom.

Acknowledgements

It is with immense gratitude that I express my thanks to everyone who, in their own unique way, contributed to the success of this master's thesis. I express my deep gratitude to every person who has played an essential role throughout this significant academic journey.

First and foremost, I would like to extend my sincere thanks to my devoted wife, Letícia, whose unwavering support, understanding, and encouragement were the driving force that illuminated my academic path. I am grateful for her constant presence and unconditional love, which were fundamental elements in the success we achieved.

To my mother, Neuzi, I convey my deepest thanks for always believing in me and encouraging the pursuit of my dreams. Her tireless dedication and boundless love were endless sources of strength and motivation throughout this entire journey.

I express my gratitude to my esteemed advisors, Wagner and Tatiane for their precise guidance, extensive knowledge, and patience. Their direct involvement and valuable contributions were fundamental to the development of this research, and I am thankful for the opportunity to learn from such dedicated professionals.

I extend my sincere gratitude to the Laboratório de Cultura de Tecidos II and its members. The indispensable collaboration and support from Dr. Kleiton Machado were crucial to the progress of this study. I thank each member of the laboratory, including Michelle Mayla, Michelle Araujo, Lázara, Lana, Claudinei, Jéssica, Elisandra, Pedro, Ana Cláudia, Dhilermando, Raissa, Quézia, Emerson, Luisa, Ravi, Sandy, for their collaboration, productive discussions, and camaraderie throughout this journey.

I cannot fail to express my gratitude to Bioagro, which was truly my home for three years. And to the Environmental Biophysics Laboratory, special thanks to Dr. Pedro Neves and Dr. Juraci Oliveira for their invaluable contributions and dedication, and to Dr. Tadeu Oliveira, Dra Claudete Santa-Catarina and Dr Vanildo Silveira from UENF for his support, availability and invaluable additions to our work.

To the Federal University of Viçosa, my heartfelt gratitude for providing the opportunity to undertake and complete this postgraduate course. The university's commitmentto academic excellence and research was vital for my personal and professional growth.

I thank the Coordination for the Improvement of Higher Education Personnel - Brazil (CAPES) for the crucial financial support. Their funding played a decisive role in the completion of this study, enabling me to access the necessary resources and present the

obtained results. I am also grateful to the Minas Gerais State Research Support Foundation [FAPEMIG; APQ-00772-19 and RED-00053-16 - Rede Mineira em Fisiologia de Plantas sob Condições de Estresse (Rede Mineira Estresse em Plantas)] and to the National Council for Scientific and Technological Development (CNPq; Process 313901/2018-0; Process: 406455/2022-8/Instituto Nacional de Ciência e Tecnologia em Fisiologia de Plantas em Condições de Estresse (INCT Stress Physiology)), for their financial support.

To all those mentioned and to those who may not have been explicitly cited, my sincere thanks for your constant support, encouragement, and significant contributions to the realization of this work. Without each of you, this achievement would not have been possible.

Thank you all very much!
Marcos

“If you fail to plan, you plan to fail”.

(Benjamin Franklin - 1790)

Abstract

BARBOSA, M. A. P, M.Sc, Universidade Federal de Viçosa, June, 2024. **Programmed cell death in *in vitro* plants of *Luffa cylindrica* (L.) Roem: a physiological investigation**. Adviser: Wagner Campos Otoni. Co-advisers: Kleiton Lima de Godoy Machado, Tatiane Dulcineia Silva.

Programmed cell death (PCD) is a crucial regulatory mechanism in plant life cycles, impacting various stages from reproduction to leaf aging. Polyamines, including putrescine, spermidine, and spermine, play significant roles in PCD regulation, while newer polyamines like thermospermine (TSPM) and xylem (XY) also influence plant growth and development. Synthetic auxin analogs such as 2,4-D Iso-octyl ester (2,4-D IOE) have been shown to affect root formation and xylem development. *Luffa cylindrica*, an economically important plant species, exhibits various PCD processes during its development stages, yet research into its morphological and physiological aspects, particularly concerning PCD- aspects, remains elusive. Recent studies have focused on investigating the impact of different treatments involving polyamines and growth regulators on *Luffa cylindrica* grown *in vitro*. These studies have examined growth characteristics, plant anatomy, antioxidant activity, lipid peroxidation, andgene expression. *In vitro* cultivation techniques, such as photoheterotrophic (PH) and photomixotrophic (PM) systems, have been employed to study *Luffa* growth under controlled conditions. Comparative analysis between PH and PM systems has revealed differences in growth parameters, metabolism, and stress response. Notably, PH cultivation has been associated with anatomical changes, altered metabolism, and increased antioxidant enzyme activity, indicating higher susceptibility to oxidative damage compared to the PM system. Furthermore, proteomic analysis has identified proteins potentially involved in PCD regulation, suggesting *Luffa cylindrica* as a promising model for studying PCD mechanism in plants.

Keywords: Programmed Cell Death. Plant anatomy. Proteomics. Polyamines. Oxidative stress.

Resumo

BARBOSA, M. A. P, M.Sc, Universidade Federal de Viçosa, Junho, 2024. **Morte Celular Programada em plantas de *Luffa cylindrica in vitro* (L.) Roem: uma investigação fisiológica**. Orientador: Wagner Campos Otoni. Co-orientadores: Kleiton Lima de Godoy Machado, Tatiane Dulcineia Silva.

A morte celular programada (MCP) é um mecanismo regulatório crucial nos ciclos de vidadas plantas, impactando várias etapas, desde a reprodução até o envelhecimento das folhas.As poliaminas, incluindo putrescina, espermidina e espermina, desempenham papéis significativos na regulação da MCP, enquanto poliaminas mais recentes como termospermina (TSPM) e xilemina (XY) também influenciam o crescimento e desenvolvimento das plantas. Auxinas análogas sintéticas como o éster iso-octílico de 2,4-D (2,4-D IOE) mostraram afetar aformação de raízes e o desenvolvimento do xilema. *Luffa cylindrica*, uma espécie de planta economicamente importante, exibe vários fenômenos de MCP durante suas fases de crescimento, mas a pesquisa sobre seus aspectos morfológicos e fisiológicos, especialmente em relação ao envolvimento da MCP, ainda é limitada. Estudos recentes têm se concentrado em investigar o impacto de diferentes tratamentos envolvendo poliaminas e reguladores de crescimento em *Luffa cylindrica* cultivada in vitro. Esses estudos examinaram características de crescimento, anatomia da planta, atividade antioxidante, peroxidação lipídica e aspectos moleculares. Além disso, técnicas de cultivo, como os sistemas foto-heterotrófico (PH) e fotomixotrófico (PM), foram empregadas para estudar o crescimento de *Luffa* em condições controladas. Análises comparativas entre os sistemas PH e PM revelaram diferenças em parâmetros de crescimento, metabolismo e resposta ao estresse. Notavelmente, o cultivo PH foi associado a mudanças anatômicas, metabolismo alterado e aumento da atividade enzimática antioxidante, indicando maior suscetibilidade a danos oxidativos em comparação com o sistema PM. Além disso, a análise proteômica identificou proteínas potencialmente envolvidas na regulação da MCP, sugerindo *Luffa cylindrica* como um modelo promissor paraestudar os mecanismos de MCP em plantas.

Palavras-chave: Morte Celular Programada. Anatomia. Proteômica. Poliaminas. Estresse oxidativo.

Summary

General Introduction

Plants are remarkable organisms that, during evolution, have been selected with essential mechanisms for growth and development. Those mechanisms guarantee plants to adjust to various environments challenges. As sessile organisms' plants require strategies for their survival. Among these, senescence plays an important role in remobilizing photosynthates and nutrients, such as in autophagy processes (Pérez-Llorca & Munné-Bosch, 2021). Moreover, in pathogen recognition, stress signaling, and developmental processes, a set of events of programmed cell death (PCD) occurs, which involves a series of metabolic events (Iakimova & Woltering, 2017; Burke et al., 2020; Valandro et al., 2020; Kacprzyk et al., 2021). It is known that PCD events occur in a controlled and organized manner through the activation of whole transcription pathways (Jones et al.,2013; Villanueva et al., 2021; Sychta et al., 2021).

PCD has already been studied in various plant species, acting in different developmental phases, such as the exclusion of the upper embryonic cell, trichome formation, aerenchyma formation in hypoxic roots, leaf morphogenesis, floral organ abortion,root cap cell differentiation, and formation of tracheal elements (TEs), among others (van Doorn et al., 2011;Jones et al., 2013; Escamez & Tuominen, 2014; Buchanan et al., 2015; van Durme et al., 2016; Sychta et al., 2021). There are three forms of PCD: apoptosis-like cell death, senescence-related cell death, and vacuole-mediated cell death. In the first two categories there is chromatin volume reduction, cell fragmentation, cytochrome C release, and modification of cytoplasmic organelle structures. Additionally, metacaspase activation and reactive oxygen species (ROS) production occur. During vacuolar PCD, cell contents are removed through a process similar to autophagy, involving tonoplast rupture, release of vacuolar hydrolases, and cytoplasm acidification. Another factor triggered during PCD is the increase of endogenous hormone levels such as ethylene, jasmonate, abscisic acid, and salicylate, among others(Fukuda, 1997; Demura, 2014; Escamez & Tuominen, 2014; Buchanan et al., 2015; Sukhova & Sukhov, 2021; Wang et al., 2021).

In the late 1970s, isolated cells of *Zinnia elegans* were subjected to a balance of auxin and cytokinin transdifferentiated into non-dividing tracheary elements (TEs) (Fukuda & Komamine, 1980). This process, called xylogenesis, involves the accumulation of hydrolytic enzymes in the differentiated cell, which are deposited in the secondary cell wall. It is a coordinated process involving various hormones, such as ethylene (Song et al., 2014;

Buchanan et al., 2015; Chen et al., 2020; Denbigh et al., 2020). Although, hormonal action requires a signaling cascade mediated by intermediaries (de Rybel et al., 2009; Kondo, 2015). However, there are still gaps inthe full understanding of the role of ethylene in PCD.

Several species have been the subject of PCD studies, such as *Zinnia elegans*, *Arabidopsis thaliana, Pinus pinea, Echinocystis lobata, Citrullus colocynthis, Cinnamomum zeylanicum, Phyllostachys bamboo, Musa banana, Paeonia suffruticosa,* and *Aponogeton madagascariensis* (Fukuda & Komamine, 1980; Kalev & Aloni, 1998; Wojciechowska & Olszewska, 2003; Ünlü et al., 2010; Pesquet & Tuominen, 2011; Ogita et al., 2012; Bagniewska-Zadworna et al., 2014; Negi et al., 2015; Ren et al., 2019; Denbigh et al., 2020). However, none of them possess the potential that *Luffa cylindrica* does, due to the sclerification and development of lignocellulosic fibers in its organs naturally, making it a promising model for PCD studies. These statements can be confirmed through transcriptome elucidation, which provided data regarding a range of putative genes and transcription factors related to the differentiation of tracheary elements (Demura, 2013). Functional genes encoding lignin and cellulose biosynthesis are correlated with the formation of the secondary cell wall and lignification. Such tools provide new insights into molecular mechanisms related to xylogenesis and corroborate to *L. cylindrica* as a strong candidate as a PCD model (Chen et al., 2015; Zhu et al., 2017).

Polyamine hormones are recognized as a class of organic compounds that boast a chemical structure characterized by the presence of multiple amino groups (-NH2). Their widespread distribution in living organisms, particularly in plants, highlights their crucial role in a variety of physiological processes. Studies conducted by Alcázar et al. (2010) and Pál et al. (2015) emphasize the vital importance of polyamines, such as putrescine, spermidine and spermine, in stress responses, defense mechanisms and plant development. In addition to theircontribution to cell growth and differentiation, these compounds play a central role in modulating gene expression and protein synthesis (Gill & Tuteja, 2010; Tiburcio et al., 2014).Thus, their influence goes beyond merely stimulating plant growth, encompassing moreintricate and interconnected aspects of plant biology.

The *in vitro* plant culture technique involves isolating plant cells, tissue and organs, stablishing them in a sterile culture media enriched with essential nutrients. This method facilitates large-scale micropropagation, the production of metabolites, genetic improvement and the preservation of genetic resources (Chandran et al., 2020; Khan et al., 2021). Photoheterotrophic (PH) systems, which use carbon sources, can lead to gas accumulation and low levels of CO_2 inside the flask , while photomixotrophic (PM) systems, which employ

membrane covers, increase gas exchange between inner headspace and outer atmosphere, thus improving the performance of vitroplants (Ševčíková et al., 2018; Silva et al., 2019; Santos et al., 2020; Alves et al., 2022). This technique allows the study of morphophysiological and molecular characteristics in various cultivation systems, contributing to practical applications and research in plant sciences (Shahzad et al., 2017).

This study seeks to elucidate the physiological mechanisms underlying programmed cell death (PCD) in *L. cylindrica*, positioning this species as a promising model for investigating PCD-related processes. In addition, we aim to evaluate the expression of polyamine biosynthesis genes and identify the proteins involved in the PCD signaling cascade, exploring their interaction with the antioxidant system. A comprehensive understanding of PCD phenomena is fundamental for the advancement of modern techniques aimed at strengthening plant resistance against various stressors. These insights are key to increasing crop productivity and raising product quality through targeted manipulation of PCD pathways.

References

ALCÁZAR, R.; CUEVAS, J.C.; PLANAS, J.; ZARZA, X.; BORTOLOTTI, C.; CARRASCO, P.; SALINAS, J.; TIBURCIO, A.F.; ALTABELLA, T. Integration of polyamines in the cold acclimation response. **Plant Science**, v.180, p.31–38, 2011. DOI: 10.1016/j.plantsci.2010.07.022.

ALVES, J.P.; PINHEIRO, M.V.M.; CORRÊA, T.R.; ALVES, G.L.; MARINHO, T.R.D.S.; BATISTA, D.S.; DE ASSIS FIGUEIREDO, F.A.M.M.; DE OLIVEIRA REIS, F.; FERRAZ, T.M.; CAMPOSTRINI, E. Morphophysiology of *Ananas comosus* during in vitro photomixotrophic growth and ex vitro acclimatization**. In Vitro Cellular & Developmental Biology – Plant**, v.59, p.106–120, 2022. DOI: 10.1007/s11627-022-10321-5.

BAGNIEWSKA-ZADWORNA, A.; ARASIMOWICZ-JELONEK, M.; SMOLIŃSKI, D.J.; STELMASIK, A. New insights into pioneer root xylem development: evidence obtained from*Populus trichocarpa* plants grown under field conditions. **Annals of Botany**, v.113, p.1235–1247, 2014. DOI: 10.1093/aob/mcu063.

BUCHANAN, B.B.; GRUISSEM, W.; JONES, R.L. **Biochemistry and molecular biology ofplants**. [s.l.] John Wiley & Sons, 2015.

BURKE, R.; SCHWARZE, J.; SHERWOOD, O.L.; JNAID, Y.; McCABE, P.F.; KACPRZYK, J. Stressed to death: The role of transcription factors in plant programmed cell death induced by abiotic and biotic stimuli. **Frontiers in Plant Science**, v.11, 2020. DOI: 10.3389/fpls.2020.01235.

CHEN, X.; MEI, Q.; LIANG, W.; SUN, J.; WANG, X.; ZHOU, J.; WANG, J.; ZHOU, Y.; ZHENG, B.; YANG, Y.; CHEN, J. Gene Mapping, Genome-Wide Transcriptome Analysis, and WGCNA Reveals the Molecular Mechanism for Triggering Programmed Cell Death in Rice Mutant *pir1*. **Plants**, v.9, p.1607, 2020. DOI: 10.3390/plants9111607.

CHANDRAN, H.; MEENA, M.; BARUPAL, T.; SHARMA, K. Plant tissue culture as a perpetual source for production of industrially important bioactive compounds. **BiotechnologyReports,** v.26, p.e00450, 2020. DOI: 10.1016/j.btre.2020.e00450.

CHEN, X.; TAN, T.; XU, C.; HUANG, S.; TAN, J.; ZHANG, M.; WANG, C.; XIE, C. Genome-wide transcriptome profiling reveals novel insights into *Luffa cylindrica* browning. **Biochemical and Biophysical Research Communications**, v.463, p.1243–1249, 2015. DOI:10.1016/j.bbrc.2015.06.093.

DE RYBEL, B.; AUDENAERT, D.; VERT, G.; ROZHON, W.; MAYERHOFER, J.; PEELMAN, F.; COUTUER, S.; DENAYER, T.; JANSEN, L.; NGUYEN, L.;

VANHOUTTE,I.; BEEMSTER, G.T.S.; VLEMINCKX, K.; JONAK, C.; CHORY, J.; INZÉ, D.; RUSSINOVA, E.; BEECKMAN, T. Chemical Inhibition of a Subset of *Arabidopsis thaliana* GSK3-like Kinases Activates Brassinosteroid Signaling. **Chemistry & Biology**, v.16, p.594–604, 2009. DOI: 10.1016/j.chembiol.2009.04.008.

DEMURA, T. Tracheary element differentiation. **Plant Biotechnology Reports**, v.8, p.17–21,2013. DOI: 10.1007/s11816-013-0293-0.

DENBIGH, G.L.; DAUPHINEE, A.N.; FRASER, M.S.; LACROIX, C.; GUNAWARDENA, A.H.L. A. N. The role of auxin in developmentally regulated programmed cell death in lace plant. **American Journal of Botany**, v.107, p.577–586, 2020. DOI: 10.1002/ajb2.1463.

ESCAMEZ, S.; TUOMINEN, H. Programmes of cell death and autolysis in tracheary elements: when a suicidal cell arranges its own corpse removal. **Journal of Experimental Botany**, v.65, p.1313–1321, 2014. DOI: 10.1093/jxb/eru057.

FUKUDA, H.; KOMAMINE, A. Establishment of an Experimental System for the Study of Tracheary Element Differentiation from Single Cells Isolated from the Mesophyll of *Zinnia elegans.* **Plant Physiology**, v.65, p.57–60, 1980. DOI: 10.1104/pp.65.1.57.

GILL, S.S.; TUTEJA, N. Polyamines and abiotic stress tolerance in plants. **Plant Signaling &Behavior**, v.5, p.26–33, 2010. DOI: 10.4161/psb.5.1.10291.

IAKIMOVA, E.T.; WOLTERING, E.J. Xylogenesis in zinnia (*Zinnia elegans*) cell cultures: unravelling the regulatory steps in a complex developmental programmed cell death event. **Planta**, v.245, p.681–705, 2017. DOI: 10.1007/s00425-017-2656-1.

JONES, R.L.; OUGHAM, H.J.; THOMAS, H.; WAALAND, S.D. **The molecular life of plants**. [s.l: s.n.].

KACPRZYK, J.; BURKE, R.; SCHWARZE, J.; MCCABE, P.F. Plant programmed cell deathmeets auxin signalling. **The FEBS Journal**, v.289, p.1731–1745, 2021. DOI: 10.1111/febs.16210.

KALEV, N.; ALONI, R. Role of auxin and gibberellin in regenerative differentiation of tracheids in *Pinus pinea* seedlings. **New Phytologist**, v.138, p.461–468, 1998. DOI: 10.1046/j.1469-8137.1998.00119.x.

KHAN, T.A.; KHAN, M.A.; KARAM, K.; ULLAH, N.; MASHWANI, Z.; NADHMAN, A. Plant in vitro Culture Technologies; A Promise Into Factories of Secondary Metabolites Against COVID-19. **Frontiers in Plant Science**, v.12, 2021. DOI: 10.3389/fpls.2021.610194. KONDO, Y.; FUJITA, T.; SUGIYAMA, M.; FUKUDA, H. A Novel System for Xylem Cell Differentiation in *Arabidopsis thaliana*. **Molecular Plant**, v.8, p.612–621, 2015. DOI: 10.1016/j.molp.2014.10.008.

NEGI, S.; TAK, H.; GANAPATHI, T.R. In vitro xylem vessel elements formation from banana embryogenic cells and expression analysis of vessel development-related genes. **PlantBiotechnology Reports**, v.9, p.47–54, 2015. DOI: 10.1007/s11816-015-0342-y.

OGITA, S.; NOMURA, T.; KISHIMOTO, T.; KATO, Y. A novel xylogenic suspension culture model for exploring lignification in *Phyllostachys bamboo*. **Plant Methods**, v.8, p.40, 2012. DOI: 10.1186/1746-4811-8-40.

PÁL, M.; SZALAI, G.; JANDA, T. Speculation: Polyamines are important in abiotic stress signaling. **Plant Science**, v.237, p.16–23, 2015. DOI: 10.1016/j.plantsci.2015.05.003.

PÉREZ-LLORCA, M.; MUNNÉ-BOSCH, S. Aging, stress, and senescence in plants: what can biological diversity teach us? **GeroScience**, v.43, p.167–180, 2021. DOI: 10.1007/s11357-021-00336-y.

PESQUET, E.; TUOMINEN, H. Ethylene stimulates tracheary element differentiation in *Zinnia elegans* cell cultures. **New Phytologist**, v.190, p.138–149, 2011. DOI: 10.1111/j.1469-8137.2010.03600.x.

PESQUET, E.; ZHANG, B.; GORZSÁS, A.; PUHAKAINEN, T.; SERK, H.; ESCAMEZ, S.; BARBIER, O.; GERBER, L.; COURTOIS-MOREAU, C.; ALATALO, E.; PAULÍN, L.; KANGASJÄRVI, J.; SUNDBERG, B.; GOFFNER, D.; TUOMINEN, H. Non-Cell-Autonomous Postmortem Lignification of Tracheary Elements in *Zinnia elegans*. **The Plant Cell**, v.25, p.1314–1328, 2013. DOI: 10.1105/tpc.113.110593.

RANTONG, G.; GUNAWARDENA, A.H.L. A. N. Vacuolar processing enzymes, AmVPE1 and AmVPE2, as potential executors of ethylene regulated programmed cell death in the lace plant (*Aponogeton madagascariensis*). **Botany**, v.96, p.235–247, 2018. DOI: 10.1139/cjb-2017-0184.

REN, R.; LI, Z.; ZHOU, H.; ZHANG, L.; XUE, J.; LIU, Y. Changes in apoptosis-likeprogrammed cell death and viability during the cryopreservation of pollen from *Paeonia suffruticosa*. **Plant Cell, Tissue and Organ Culture (PCTOC)**, v.140, p.357–368, 2019. DOI: 10.1007/s11240-019-01732-1.

SANTOS, G.C.; CARDOSO, F.P.; MARTINS, A.D.; PASQUAL, M.; OSSANI, P.C.; QUEIROZ, J.M.; REZENDE, R.A.L.S.; SOARES, J.D.R. Effect of light and sucrose on photoautotrophic and photomixotrophic micropropagation of *Physalis angulata*. **Bioscience Journal**, v.36, 2020. DOI: 10.14393/bj-v36n4a2020-47738.

ŠEVČÍKOVÁ, H.; LHOTÁKOVÁ, Z.; HAMET, J.; LIPAVSKÁ, H. Mixotrophic in vitro cultivations: the way to go astray in plant physiology. **Physiologia Plantarum**, v.167, p.365–377, 2019. DOI: 10.1111/ppl.12893.

SHAHZAD, A.; SHARMA, S.; PARVEEN, S.; SAEED, T.; SHAHEEN, A.; AKHTAR, R.; YADAV, V.; UPADHYAY, A.; AHMAD, Z. **Historical perspective and basic principles of plant tissue culture**. In: Springer eBooks. [s.l: s.n.]. p.1–36. DOI: 10.1007/978-981-10-2961-5_1.

SILVA, S.T.; BERTOLUCCI, S.K.V.; DA CUNHA, S.H.B.; LAZZARINI, L.E.S.; TAVARES, M.C.; PINTO, J.E.B.P. Effect of light and natural ventilation systems on the growth parameters and carvacrol content in the in vitro cultures of *Plectranthus amboinicus* (Lour.) Spreng. **Plant Cell, Tissue and Organ Culture**, v.129, p.501–510, 2017. DOI: 10.1007/s11240-017-1195-6.

SIMÕES, M.S.; FERREIRA, S.S.; GRANDIS, A.; RENCORET, J.; PERSSON, S.; FLOH, E.I.S.; FERRAZ, A.; DEL RÍO, J.C.; BUCKERIDGE, M.S.; CESARINO, I. Differentiation of tracheary elements in sugarcane suspension cells involves changes in secondary walldeposition and extensive transcriptional reprogramming. **Frontiers in Plant Science**, v.11, 2020. DOI: 10.3389/fpls.2020.617020.

SONG, S.; QI, T.; WASTERNACK, C.; XIE, D. Jasmonate signaling and crosstalk with gibberellin and ethylene. **Current Opinion in Plant Biology**, v.21, p.112–119, 2014. DOI: 10.1016/j.pbi.2014.07.005.

SUKHOVA, E.; SUKHOV, V. Electrical signals, plant tolerance to actions of stressors, and programmed cell death: is interaction possible? **Plants**, v.10, p.1704, 2021. DOI: 10.3390/plants10081704.

SYCHTA, K.; SŁOMKA, A.; KUTA, E. Insights into Plant Programmed Cell Death Induced by Heavy Metals—Discovering a *Terra Incognita*. **Cells**, v.10, p.65, 2021. DOI: 10.3390/cells10010065.

TIBURCIO, A.F.; ALTABELLA, T.; BITRIÁN, M.; ALCÁZAR, R. The roles of polyamines during the lifespan of plants: from development to stress. **Plant**a, v.240, p.1–18, 2014. DOI: 10.1007/s00425-014-2055-9.

ÜNLÜ, M.; ERGENE, E.; ÜNLÜ, G.; ZEYTİNOĞLU, H.; VURAL, N. Composition, antimicrobial activity and in vitro cytotoxicity of essential oil from *Cinnamomum zeylanicum* Blume (Lauraceae). **Food and Chemical Toxicology**, v.48, p.3274–3280, 2010. DOI: 10.1016/j.fct.2010.09.001.

VALANDRO, F.; MENGUER, P.K.; CABREIRA-CAGLIARI, C.; MARGIS-PINHEIRO, M.; CAGLIARI, A. Programmed cell death (PCD) control in plants: New insights from the *Arabidopsis thaliana* deathosome. **Plant Science**, v.299, p.110603, 2020. DOI: 10.1016/j.plantsci.2020.110603.

VAN DOORN, W.G.; BEERS, E.P.; DANGL, J.L.; FRANKLIN-TONG, V.E.; GALLOIS, P.; HARA-NISHIMURA, I.; JONES, A.M.; KAWAI-YAMADA, M.; LAM, E.; MUNDY, J.; MUR, L. A. J.; PETERSEN, M.; SMERTENKO, A.; TALIANSKY, M.; VAN BREUSEGEM,F.; WOLPERT, T.; WOLTERING, E.J.; ZHIVOTOVSKY, B.; BOZHKOV, P.V. Morphological classification of plant cell deaths. **Cell Death & Differentiation**, v.18, p.1241–1246, 2011. DOI: 10.1038/cdd.2011.36.

VILLANUEVA, S.L.; MALVESTITI, M.C.; VAN IEPEREN, W.; JOOSTEN, M.H.A.J.; VAN KAN, J.A.L. Red light imaging for programmed cell death visualization and quantification in plant–pathogen interactions. **Molecular Plant Pathology**, v.22, p.361–372, 2021. DOI: 10.1111/mpp.13027.

VORSTER, J.; CULLIS, C.A.; KUNERT, K. Plant vacuolar processing enzymes. **Frontiersin Plant Science**, v.10, 2019. DOI: 10.3389/fpls.2019.00479.

WANG, H.; ZHANG, S.; QU, Y.; GAO, R.; XIAO, Y.; WANG, Z.; ZHAI, R.; YANG, C.; XU, L. Jasmonic Acid and Ethylene Participate in the Gibberellin-Induced Ovule Programmed Cell Death Process in Seedless Pear ‘1913’ (*Pyrus* hybrid). **International Journal of Molecular Sciences**, v.22, p.9844, 2021. DOI: 10.3390/ijms22189844.

WOJCIECHOWSKA, M.; OLSZEWSKA, M. Endosperm degradation during seed development of *Echinocystis lobata* (Cucurbitaceae) as a manifestation of programmed cell death (PCD) in plants. **PubMed**, v.41, p.41–50, 2003.

ZHU, H.; JIANTING, L.; QINGFANG, W.; CHEN, M.; WANG, B.; ZHANG, Q.; XUE, Z. De novo sequencing and analysis of the transcriptome during the browning of fresh-cut *Luffa cylindrica* “Fusi-3” fruits. **PLOS ONE**, v.12, p.e0187117, 2017. DOI: 10.1371/journal.pone.0187117.

Chapter 1:

Molecular and physiological impacts of polyamines and 2,4-D isooctyl ester on programmed cell death *in vitro* in *Luffa cylindrica* (L.) Roem

Abstract

Programmed cell death (PCD) intricately regulates various stages of the plant life cycle, affecting reproductive processes, seed maturation, xylem formation and leaf aging. PCD operates through a fine-tuned genetically regulated biochemical pathways, orchestrating cell self-elimination during development, categorized into apoptotic-type, senescence-associated and vacuole-mediated cell death. Polyamines, includingputrescine, spermidine and spermine, profoundly influence PCD, modulating levels of reactive oxygen species, gene expression and enzymatic activities. Thermospermine (TSPM) and xylemin (XY), new polyamines, crucially regulate plant growth and development, affecting xylem differentiation and the formation of tracheary elements. In addition, 2,4-D Iso-octyl ester (2,4-D IOE), an auxin, influences root formation and enhances xylem development. *Luffa cylindrica*, an economically important plant, exhibits various PCD events during its growth stages, but the knowledge into its morphological and physiological aspects, especially in relation to the involvement of PCD, remains elusive. Here we investigated the impact of treatments with different combinations of polyamines and growth regulators on growth characteristics, plant anatomy, antioxidant activity, lipid peroxidation and molecular aspects in *L. cylindrica* grown *in vitro* for seven days. Visual uniformity was observed in the initial development of the seedlings, with the treatment with 2.4-D IOE standing out for promoting leaf development. Average plant height remained constant, while leaf area varied, with a significant reduction in treatments with TSPM. Analysis of the total dry weight revealed marked differences between the treatments. Anatomical descriptions revealed morphological adaptations in response to the treatments, such as trichomes in some treatments. The treatments also influenced antioxidant activity and lipid peroxidation, with increased antioxidant enzyme activity. Differential gene expression highlighted the complex regulation of polyamine biosynthesis, with significant changes in the expression of the polyamines biosynthesis genes in all treatments, suggesting a modulation of the molecular response to the experimental conditions.

Keywords: Senescence; Tracheary Elements; Plant anatomy; Gene expression

Introduction

Several stages of plant life cycles are influenced by programmed cell death (PCD), including reproductive processes, seed maturation, xylem formation and leaf aging (Buchanan et al., 2015; van Durme & Nowack, 2016; Dickman et al., 2017; Locato & De Gara, 2018). PCD occurs due to the activation of specific biochemical pathways that are genetically regulated. These pathways encompass several orchestrated process that guide cells to self-eliminate during development (Iakimova & Woltering, 2017; Locato & De Gara, 2018). In the plants domain, PCD has been categorized into three distinct types:apoptotic-type cell death, senescence-associated cell death and vacuole-mediated cell death (Fukuda & Komamine, 1980; Locato & De Gara, 2018). These PCD events can occur during plant development and represent essential processes in the life cycle (Van Hautegem et al., 2015).

Polyamines (PAs) are plant hormones that belong to a class of organic compounds that contain multiple amino groups (-NH2) in their chemical structure. They are widely distributed in living organisms, including plants, playing crucial roles in various physiological processes. As example putrescine, spermidine, and spermine, are involved in growth, development, stress responses, and plant defense mechanisms (Alcázar et al., 2010; Pál et al., 2015). One of the primary functions of PAs in plants is their role in cell division and differentiation making them essential for plant growth and development, as they regulate the cell cycle, promote cell elongation, and influence organ formation (Alcázar et al., 2010; Tiburcio et al., 2014). The PAs also regulate gene expression, including the modulation of transcription factors, which are crucial processes during plant development (Gill & Tuteja, 2010).

PAs have been revealed as crucial regulators of PCD across various plant tissues and developmental stages. Spermidine, for instance, is notably associated with inducing PCD in plant cells, particularly during senescence, leaf abscission, and responses to stress. Its regulatory role in PCD involves intricate modulation of reactive oxygen species (ROS) levels, alteration of gene expression profiles, and activation of specific PCD-related enzymes (Yoda et al., 2006; Moschou & Roubelakis-Angelakis, 2013; Cai et al.,2014). Similarly, spermine plays a significant role in PCD regulation , particularly during leaf senescence, pollen development, and stress-induced cell death. Its influence on PCD stems from its impact on redox homeostasis, modulation of PCD-related gene expression, and regulation of enzyme activities within cell death pathways (Liu et al., 2007; Mandal et al., 2012; Frett et al., 2013; Burke et al., 2023). Additionally, putrescine, the precursor of spermidine and

spermine, has been implicated in the regulation of PCD in plants. Its effects on PCD can be dualistic, either promoting or inhibiting PCD depending on the specific context, such as seed development, flower senescence, and stress-induced cell death. Putrescine's role in PCD regulation involves intricate interactions with other signaling molecules and modulation of gene expression,thereby contributing to the finely tuned regulation of PCD during different plant developmental processes (Takao et al., 2006; Alcázar et al., 2011; Sobieszczuk-Nowicka et al., 2016). The interplay between polyamine hormones and redox signaling molecules emerges as a critical determinant in orchestrating the precise regulation of PCD across variousplant developmental contexts.

Thermospermine (TSPM), a distinctive PA derivative, has garnered considerable attention in plant biology due to its unique chemical structure and emerging rolesin diverse physiological processes. Its biosynthesis entails the activity of specific enzymes, notably arginine decarboxylase (ADC) and thermospermine synthase ACAULIS5 (ACL5) (Takahashi, 2017). ADC initiates the decarboxylation of arginine, yielding agmatine, which is subsequently metabolized into TSPM by ACL5. The metabolism of TSPM involves oxidativecleavage and conjugation reactions.

Xylemin (XY), a recently identified synthetic PA acting as a plant growth regulator, has emerged as a pivotal controller of plant growth and development. It has been identified as an inducer of xylem differentiation in *Arabidopsis thaliana*. XY functions as an inhibitor of ACL5, the enzyme responsible for TSPM synthesis. TSPM, in turn, inhibits the formation of tracheary elements (TEs) through the upregulation of the transcription factor *SAC51* (Yoshimoto et al., 2016; Takamura et al., 2020).

Moreover, a proauxin significantly enhances the inductive effect of XY on xylem differentiation. 2,4-D Iso-octyl (2,4-D IOE) ester, derived from the herbicide 2,4-D, is a a plant growth regulator extensively used in agriculture and horticulture to modulate plant growth and development. It facilitates root formation, enhances fruit set, controls fruit thinning, stimulates branching, and suppresses unwanted plant growth by mimicking auxin, thereby affecting cell division, elongation, and differentiation. Interestingly, it has been observed that 2,4-D IOE promotes an increase in TE differentiation when applied to *acl5-1* mutants, which are unable to synthesize TSPM (Yoshimoto et al., 2016).

Luffa cylindrica (Cucurbitaceae) is a yearly herbaceous displaying significant economic significance linked to its fruits. It has been extensively utilized in the production of handicrafts, industrial goods, traditional medicine, and for aesthetic purposes (Partap et al., 2012; Zhu et al., 2017). Throughout the growth process, various PCD occurrences can be

observed in *L. cylindrica*, such as the formation of the fistula in the stem, high investment of vascular tissue differentiation, , and the prominent network of sclerified fibrous cells in the fruits, as maturation progresses (Chen et al., 2014).

Nonetheless, limited research exists in the literature regarding the morphological and physiological examination of *L. cylindrica*, particularly concerning its intrinsic capacity for PCD. Furthermore, there are gaps related to the understanding on how polyamines acts during PCD events. The aim of this study was to investigate the complex molecular and redox interactions that influence the progression of PCD in *L. cylindrica*. To this end, detailed analyses were carried out on the effect of Thermospermine, Xylemin and 2,4-D IOE, in order to better understand the mechanisms underlying this biological process.

Materials and Methods

Plant material and experimental design

Mature *Luffa cylindrica* seeds obtained from Feltrin® (Farroupilha, RS, Brazil) were mechanically scarified by removing the tegument using a mini-mortar. Under aseptic conditions, in a laminar flow chamber, the scarified seeds were disinfected by immersion in 70% (v/v) alcohol for 1 min, and then immersing them for 20 min in a commercial solution of sodium hypochlorite (SuperGlobo®, Contagem, MG) at 1.3% (v/v), plus two dropsof the surfactant Tween 20 per 100 mL of solution. Next, the decoated seeds were triple-rinsed in distilled and autoclaved water. Subsequently, the seeds (15 units/per plate) were inoculated into sterile 90 mm crystal polystyrene Petri dishes (Kasvi®, Curitiba, PR), arranged evenly containing 25 mL of Agar-Water medium, 6 g L^{-1} agar (PhytoTechnology Labs, USA), pH adjusted to 5.7 ± 0.1, and autoclaved at 120 °C, 108 kPa, for 20 min. The plates were sealed with microporous adhesive tape (Micropore® 3M, Sumaré, SP), which favors gas exchange between the atmosphere and the plate (Ribeiro et al., 2009; Saldanha et al., 2012; Jesus Santana et al., 2022).

After the radicle had protruded, one pre-germinated seed was inoculated above the liquid medium line per flask (600mL capacity) containing 100 mL of liquid MS medium. The seeds were arranged on an adapted support made from the base of autoclavable polypropylene plastic cups.The flasks were sealed with rigid polypropylene lids with two vents (10 mm diameter) covered with 0.45 μm PTFE membranes (MilliSeal® AVS-045 Air Vent, Tokyo, Japan) allowing for a CO_2 exchange rate of 25 μL L^{-1} s^{-1}. The following treatments were carried out: Control; TSPM; XY; 2,4-D IOE; XY plus TSPM; XY plus 2,4-D IOE; and XY plus 2,4-D IOE plus TSPM. All at a concentration of 10 μM. The cultures were maintained under light and temperature conditions as mentioned above.

The experiment was conducted in a completely randomized design, with 6 flasks (replicates) containing one explant for each treatment.

Anatomical characterization

After 7 days of culture in induction medium explants were collected and fixed in a glutaraldehyde solution 4% (Karnovsky, 1965). Fixed samples were dehydrated in an ethanolic series, included in methacrylate resin (Historesin, Leica®) and embedded in plastic histomolds. Five-micrometer thickness cross sections were obtained using an automatic rotarymicrotome (RM 2155, Leica®) and stained using toluidine blue (O'Brien & McCully,

1982). The specimens were mounted in Permount on glass slides. Photographs were taken using a microscope stereoscope Olympus SZH and microscope (Olympus AX70), U-Photo system attached.

Growth parameters

After 7 days of in vitro culture, stem length (cm), largest root length (cm), leaves number, root number and leaf area (cm^2) were evaluated. Plant tissues were collected at the end of the. The plantlet was fixed individually on white plasticized graph paper. Photographs were taken with a digital camera and processed using ImageJ software (Schneider et al., 2012).

Antioxidant activity

Activity of oxidative stress enzymes, superoxide dismutase (SOD), catalase (CAT) andperoxidase (POX) was assessed. Briefly, 50 mg of frozen fresh material (aerial part) was homogenized in 1.4 mL extraction medium containing 0.1 M potassium phosphate buffer, pH 6.8; 0.1 mM ethylenediaminetetraacetic acid; 1 mM phenylmethylsulfonyl fluoride and 1% (w/v) polyvinylpolypyrrolidone. The sample was vortexed for 10 s, centrifuged at 12,000 rpmfor 15 min at 4 °C, and the supernatant was removed and set aside on ice for enzyme assays plus protein determination (Bradford, 1976). CAT and POX activities were determined as proposed previously (Chance & Maehly, 1955; Nakano & Asada, 1981; Havir & McHale, 1987) and expressed as μmol^{-1} min^{-1} $.g^{-1}$ protein. SOD activity was measured as described earlier (Giannopolitis & Ries, 1977) and expressed as U min^{-1} g^{-1} protein, with 1 U being equivalent to the concentration of SOD required to inhibit 50% of nitro blue tetrazolium photoreduction.

Determination of lipid peroxidation

Lipid peroxidation was determined by quantifying thiobarbituric acid reactive substances (TBARS) according to the method of Hodges et al. (1999) with some modifications. The plant material, 50 mg of frozen fresh material (aerial part), was homogenized in 2 mL of ethanol-water 80:20 (v/v) and centrifuged at 10,000 *g* for 15 min at 4 °C. The supernatant (500 µL) was removed and added to 0.5 mL of 20% TCA. Another 500 µL of the supernatant was added to 500 µL of the mixture of 20% TCA and 0.5% TBA. The samples were placed in a bath at 90 °C for 1 h and then cooled in an ice bath. The samples were centrifuged again at 3000 *g* for 10 min at 4 °C and the supernatant was read at

440, 532 and 600 nm absorbances. The results were estimated using the following equations: [(Abs 532+TBA)-(Abs 600+TBA)-(Abs 532-TBA- Abs600-TBA)] = A; [(Abs 440+TBA-Abs 600+TBA) 0.05711]= B; MDA equivalents (nmol to µmol-1) = (A-B/157000)*10^{-6}; The results were expressed in nmol of fresh weight (FW).

Gene expression (RT-qPCR)

Roots and hypocotyls were harvested, macerated in liquid nitrogen and stored in an Ultrafreezer (COLDLAB; CL58-86V, Piracicaba, SP, Brazil). To extract total RNA, 100 mg of fresh plant mass was used with the addition of TRI Reagent® (Sigma Aldrich, St. Louis, MO, USA) according to the manufacturer's recommendations. 10 µg of RNA was treated with 1 µL of DNase I (Thermo Scientific NanoDrop Technologies, Wilmington, DE, USA) to avoid nuclear DNA. The quantity and quality of the RNA sample were determined using a Nanodrop 2000C (Thermo Scientific, Wilmington, DE). Moloney Murine Leukemia Virus Reverse Transcriptase (M-MLV RT) (Promega®, Woods Hollow Road-Madison, R.D, U.S.A) was used for the cDNA synthesis.As it follows: 1 µg of RNA was used.Then, was add to the mixture 1 µL of oligo (dT) 20 to 50 µM and 1 µL of dNTP (10 mM), and incubated for 5 min at 65 °C. In the next step the solution was incubated at 4 °C for 2 min, then adding 0.1 M dNTP and 1 µL of the M-MLV RT enzyme. The resultingsolution was incubated at 50 °C for 60 min, then at 70 °C for 15 min. Genes expression associated with polyamine biosynthesis were analyzed. Primers were designed based on sequences previously identified in the *Luffa cylindrica* transcriptome

RT-qPCR analyses were carried out on the CFX96 Touch™ Real Time PCR Detection System (BIO-RAD). Starting with 20 ng of cDNA, 400 nM of forward and reverse primer (Síntese Biotecnologia Ltda., Belo Horizonte, MG), and qPCR SYBR- Green Supermix (Bio- Rad) and double distilled water (ddH2O) for a final reaction volume of 10 µL. Expression levels were calculated in relation to thehousekeeping gene 40S ribosomal protein S9 (RPS9), using the $2^{-\Delta\Delta ct}$ method (Livak & Schmittgen, 2001). The real-time PCR analysis was carried out at the Laboratory of Microorganism Genetics (BIOAGRO/DMB/UFV).

Statistical analysis

Statistical analysis was carried out using Genes software version Windows/2019.89 (Cruz, 2016). The experiments were repeated twice. The data was subjected to a one-factor analysis of variance, using Duncan's test, and the means were compared Student's t-test, both at a 5% significance level.

Results and Discussion

Polyamines impact some L. cylindrica *growth parameters*

During the plant cultivation experiment in stationary liquid medium conducted over seven days, there was visual uniformity in the initial stages of seedling development (Figure 1). It was observed that first leaves developed under 2,4-D IOE, whereas the other treatments did not stimulate this development.

The total dry weight was analyzed (cotyledon, shoot and root weight) (Figure 2a). The treatments with TSPM and XY plants displayed around 20% less dry weight than control. The treatment 2,4-D IOE and the treatment XY plus TSPM plants showed similar dry weight than control. The treatment XY plus 2,4-D IOE plants had the lower dry weight, displaying 50% less than control. On the other hand, the treatment with TSPM plus XY plus 2,4-D IOE treatment showed 25% more dry weight from control, presenting the highest dry weight. The average plant height did not differ from treatment to treatment, displaying 1.3 up to 2 cm height (Figure 2b). The cotyledon area was measured based on the cotyledon and showed slight variation (Figure 2c), with a significant decrease in the treatments with TSPM while the other treatments remained homogeneous to the control group and the TSPM treatment. This behavior corroborates with total dry weight, which may show how cotyledon area is important for total dry weight.

The specific cotyledon area was analyzed (Figure 2d). There was no heterogeneous group formed. However, a tendency in smaller cotyledon in XY plus TSPM treatments and thicker cotyledons was observed. Previous research corroborates the findings, indicating that the application of PAs significantly increases the growth of plants, correlating with a reduction in electrolyte leakage, an increase in relative water content, chlorophyll fluorescence parameters, the activities of the main antioxidant enzymes, as well as an increase in the concentration of photosynthetic pigments under stress conditions (Khoshbakht et al., 2018).

Anatomical description of Luffa cylindrica *plantlets grown in vitro in stationary liquid medium with polyamines and growth regulators*

After seven days of cultivation in stationary liquid medium, a qualitative anatomical description was made of cross-sections of the hypocotyl and roots of *Luffa cylindrica* (Figures3 & 4). The explants were embedded in resin blocks and the sections were obtained and stained with toluidine blue.

When observing the control treatment, the hypocotyl (Figure 3a) shows the presence of a uniseriate epidermis around the entire perimeter of the organ. This epidermis is made up of small juxtaposed cells, where stomata and trichomes are found sparsely. Entering the structure of the hypocotyl is the angular collenchyma, made up of small cells with thick walls in the cell edges; this tissue is organized in two to three layers. Its main function is to support the plant, allowing it to grow without limiting its flexibility too much. More internally, the cortical parenchyma is characterized by less juxtaposed cells with a larger diameter than the collenchyma and the presence of spaces between the cells is also observed. This tissue plays an important role in storing nutrients and water within the plant. The vascular bundles are evenly arranged in a total of six, with a bicollateral shape, composed of xylem wrapped laterally by phloem. These structures are responsible for transporting water, nutrients and organic substances throughout the plant. Inside the hypocotyl, in addition to the medullary parenchyma with looser cells and primary wall. Also, there is a fistula, a structure formed by the death of cells with the function of allowing oxygenation of the innermost tissues. This is evidence of the plant's adaptation to flooded areas and the method of cultivation, where hypoxia is a strong abiotic signal.

After examining the images of the treatment with the application of TSPM, some differences were observed compared to the control treatment (Figure 3b). In the hypocotyl, in the unicellular epidermis, the presence of multicellular tector trichomes was noted, suggesting a possible morphological adaptation of the plant to the specific conditions dthe treatment. Angular collenchyma was also present, similar to the control, providing structural support to the hypocotyl. However, in the cortical parenchyma, the cells appeared tobe larger in diameter than in the control treatment, which may indicate an increase in the capacity to store or transport water and nutrients. The vascular bundles maintained the same pattern of lateral beak arrangement, with six bundles, as observed in the control treatment. A notable difference was observed in the medullary parenchyma, which appeared to be reduced in this treatment, and the fistula was more pronounced. Plants treated with TSPM show a fistula that is larger than those from control group. This suggests a possible alteration in the internal structure of the hypocotyl, which may have implications for the plant's function and adaptation to the environment.

When examining the image of the hypocotyl from the treatment with application of XY (Figure 3c), several distinct characteristics stand out compared to previous treatments. The epidermis exhibits a higher density of trichomes and areas where two layers of cells are present, imparting an increased thickness to the organ. This suggests a specific morphological

response to this treatment. Furthermore, both the collenchyma and cortical parenchyma are present, with the cortical parenchyma appearing more compact, with fewer spaces between cells compared to previous treatments. The vascular bundles maintain the same morphology in a bicollateral shape; however, in this treatment, they are arranged in a greater number, showing one more vascular bundle than plants from other treatments, suggesting a possible influence of the treatment on the distribution and development of these structures. Regarding the medullary parenchyma, its characteristics are similar to the control treatment, with cells of larger diameter and presence of spaces between them. The fistula is also observed in the center of the organ, indicating continuity in the adaptive responses found in previous treatments.

When analyzing the image of the hypocotyl of the 2,4-D IOE treatment (Figure 3d), it is possible to observe the presence of the uniseriate epidermis, where points of formation of pluricellular tector trichomes are visible. Stomata can also be identified by the presence of the guard cell and the stomatal cavity. The collenchyma is evident, represented bytwo layers of juxtaposed cells with thick walls. The cortical parenchyma follows the pattern of the other treatments, with large diameter cells and the presence of intracellular spaces. In the regions close to the vascular bundles, the cortical parenchyma cells become more compact.

The bicollateral vascular bundles are also arranged in six, while the medullary parenchyma shows the presence of a fistula and cells with a primary wall containing several intracellular spaces.

Analysis of the section from the treatment with XY plus TSPM (Figure 3e) reveals an epidermis with areas where there is a double layer of cells and others with uniseriate cells, where pluricellular tectorial trichomes are present. The collenchyma shows areas where it is more prominent, although it does not follow a uniform pattern throughout the cell perimeter. The cortical parenchyma shows cells arranged in such a way as to create intracellular spaces, with more compact cells near the vascular bundle. The bicollateral vascular bundle shows regions of the developed xylem and distinct regions of the phloem. It is possible to see the presence of a fistula in the medullary parenchyma, where the angular cells have thin walls.

The image of the treatment XY plus 2,4-D IOE (Figure 3f) reveals a multiseriate epidermis with globular and juxtaposed cells with signs of trichome formation. The collenchyma is visible, with layers of two to three thick-walled cells, evidenced by the intense coloration. The cortical parenchyma shows larger diameter cells, with an angular shape and intercellular spaces. The vascular bundles follow the pattern of bicollateral arrangement and morphology. The medullary parenchyma also follows the patternmentioned above, with

larger diameter cells, intracellular spaces and the presence of a fistula.

The image of the hypocotyl in the treatment with XY plus 2,4-D IOE plus TSPM (Figure 3g) shows a multiseriate epidermis with trichomes. There is also a collenchyma with two layers of cells, juxtaposed and angular in shape. The cortical parenchyma is made up of cells of different diameters, with intracellular spaces and a thin cell wall. The bicollateral vascular bundle is well developed, with distinct xylem and phloem. The medullary parenchyma is represented by cells of a similar diameter tothe cortical parenchyma, but more widely spaced, i.e. with more space between the cells, and shows the presence of a fistula.

Previous research has demonstrated the positive benefits of applying PAs during stressful situations, reflected in significant improvements in anatomical characteristics such as the length and width of the central vein, the size and width of the vascular bundle, the thickness of the phloem, xylem and collenchyma, vessel diameter and the number of xylem rows in the central vein bundle, as well as yield-related characteristics such as plant height, leaf area and lipid content (Desoky et al., 2023). Notably, in plants treated with TSPM, an increase in the size of the fistula was observed compared to those from control group. On the other hand, the plants subjected to XY showed an additional vascular bundle compared to the other treatments. Interestingly, the XY, 2,4-D IOE and XY plus 2,4-D IOE plants showed only one layer of collenchyma, suggesting a possible reduction in dry weight compared to the control group. Thus, the external application of PAs emerges as a promising strategy for improving the efficiency of water transport in crops and optimizing the yield characteristics of plants under stress conditions.

Now, looking at a cross-section of the root of control group (Figure 4a), it’s possible to see the characteristic organization of the different layers and tissues that make up its structure. On the outer surface is the uniseriate epidermis, made up of smaller diameter cells arranged in juxtaposition. This layer provides protection for the root dissection. Just below the epidermis is the cortical parenchyma, characterized by larger cells arranged in such a way as to create various intracellular spaces, giving this tissue a spongy texture. This structure helps to store nutrients, oxygen, and water. As we looked into the inner series, the cells are close together and with smaller sizes until the endodermis, with smaller cells surrounding the central cylinder, occupied mainly by conductive elements, fibers and medullar parenchyma. Inside the central cylinder are the xylem vessels, responsible for transporting water and nutrients from the root to other plant organs, while the phloematic cylinders, located on the outside, are responsible for transporting organic substances producedby the plant. In the center of the central cylinder is the protoxylem star, where the larger woody elements are in

the center and the smaller ones on the periphery. This organization contributes to efficiently transporting water and nutrients by the root.

As for the roots of TSPM treatment (Figure 4b), although there are similarities in all the tissues compared to the control, such as the presence of uniseriate epidermis, spongy cortical parenchyma and a central cylinder with well-defined xylem and phloem, it is important to note that there may be subtle variations that deserve a more detailed analysis to fully understand the impact of TSPM on root morphology.

Upon observing the image of the root in XY treatment (Figure 4c), it is noted that there is also a uniseriate epidermis with closely arranged cells. The cortical parenchyma exhibits irregularly shaped cells with large intercellular spaces, rendering this tissue spongier. The central cylinder presents the same characteristics as those observed in previous treatments, with well-defined regions of the xylem and phloem.

The image of the 2,4-D IOE treatment roots (Figure 4d) shows the presence of a uniseriate epidermis, made up of juxtaposed globular cells. This is followed by the cortical parenchyma with angular cells arranged separately from each other, giving it a spongy appearance. The central cylinder differs from the other treatments in that the vascular stele is made up of 4 segments and the protoxylem is well-developed in the center.

The cross-section of the XY plus TSPM treatment root's (Figure 4e) reveals a uniseriate epidermis made up of juxtaposed globular cells. The medullary parenchyma is represented by cells of different diameters, arranged separately, giving the tissue a spongy appearance. The image of this treatment shows the largest number of cells in the parenchyma, giving it a robust diameter. The central cylinder is evident, with xylem and phloem clearly distinct.

The image of the XY plus 2,4-D IOE treatment root's (Figure 4f) shows globular and juxtaposed cells in the epidermis, which vary in size, but are smaller compared to the medullary parenchyma. The medullary parenchyma has cells with a larger diameter at the ends and a smaller diameter nearthe central cylinder, which has distinct xylem and phloem.

The epidermis of the XY plus 2,4-D IOE plus TSPM treatment root's (Figure 4g) is made up of irregularly shaped cells arranged in a single layer, followed by the cortical parenchyma with angular cells spaced apart, resulting in a spongy tissue. The central cylinder is not evident, but the presence of poorly developed xylem and phloem inside the organ is noticeable.

Adaptations in morphology are fundamental to increasing the efficiency of water and nutrient absorption and transportation, thus guaranteeing plant survival in adverse conditions.

Polyamines act as important mediators in this mechanism, helping to alleviate the harmful impacts of various stresses by modulating the morphological and biochemical responses of plants. The changes observed in the epidermis, cortical parenchyma and central cylinder of roots submitted to treatment with polyamines highlight their regulatory function in facilitating plant adaptation to avoid stress. (Elbar et al., 2019; Desoky et al., 2023).

Treatments have an impact on the antioxidant activity and lipid peroxidation of the aerial parts and roots of Luffa cylindrica

The results of the study show the enzymatic antioxidant activity and the levels of lipid peroxidation in both aerial parts and roots of *L. cylindrica* grown *in vitro* for seven days in stationary liquid medium (Figures 5 and 6).

Examining the activity of superoxide dismutase in the aerial parts (SOD) (Figure 5a),it is clear that, compared to the control group, the treatment with the application of XY showed no statistically significant differences. Next, the treatment with the application of 2,4-D IOE showed a slightly positive change in enzyme activity. Higher positive variations in enzyme activity were observed in the treatments with XY plus TSPM and XY plus 2,4-D IOE. Notably, the treatments with TSPM and XY plus 2,4-D IOE plus TSPM showed the most significant impact by the superoxide ion, indicating nearly 2-fold higher enzymatic activity in these cases.

Concerning the enzyme Catalase (CAT) in the aerial parts (Figure 5b), XY and 2,4-D IOE treatments showed no significant differences compared to the control group, while TSPM treatment showed a lower enzyme activity than the other treatments. The data indicates a slight increase in CAT activity in XY plus TSPM treatment, although it remains statistically close to the control. Notably, there was a significant increase in enzyme activity in XY plus 2,4-D IOE and XY plus 2,4-D IOE plus TSPM treatments.

The activity of the enzyme peroxidase (POX) in the aerial part (Figure 5c) remained constant in TSPM, XY, 2,4-D IOE and XY plus TSPM treatments, with fluctuating averages statistically close to the control group. However, XY plus 2,4-D IOE and XY plus 2,4-D IOE plus TSPM treatments showed the highest enzyme activity, reaching 200% of the control.

Analysis of the lipid peroxidation data (Figure 5d) revealed a similar pattern to the CAT enzyme data, but all the averages were lower than the control group. We observed that TSPM treatment showed the lowest averages, around 50%, compared to the control group, followed by XY and 2,4-D IOE treatments. Subsequently, there was a gradual improvement in the level of lipid peroxidation in XY plus TSPM, XY plus 2,4-D IOE and XY plus 2,4-D

IOE plus TSPM treatments, the latter being statistically equivalent to the control.

The trend in SOD enzyme activity was similar in the roots (Figure 6a) for TSPM, XY, treatments, where the first showed significantly higher activity than the control group, while the other showed similar levels of activity to the control group. There was a significant increase in activity in 2,4-D IOE, XY plus TSPM and XY plus 2,4-D IOE treatments. In contrast, XY plus 2,4-D IOE plus TSPM treatment showed the lowest averages, although it maintained an activity similar to that of the control.

Enzymatic activity of CAT in the roots (Figure 6b) was higher in all treatments compared to the control group, highlighting XY plus TSPM and XY plus 2,4-D IOE treatments, with activities greater than 200% in relation to the control. In addition, TSPM, XY, 2,4-D IOE and XY plus 2,4-D IOE plus TSPM treatments showed similar activities, all slightly higher than the control.

Lipid peroxidation in *L. cylindrica* roots (Figure 6d) showed different results from the aerial part (Figure 5d), starting with the control group, in which the lowest averages were obtained for the whole experiment. There were similar averages for treatments TSPM, XY, 2,4-D IOE, XY plus TSPM and XY plus 2,4-D IOE, with approximately 20% more activity compared to the control. It is notable that XY plus 2,4-D IOE plus TSPM treatment distinguished itself from the others, showing the highest averages and achieving around 35% more activity.

The activity of the POX enzyme in the roots showed a similar trend to that of SOD (Figures 5a, 6a),where in T2 the POX activity was significantly higher than that of the control group, while in XY treatment it showed averages comparable to those of the control. However, treatments 2,4-D IOE, XY plus TSPM, XY plus 2,4-D IOE and XY plus 2,4-D IOE plus TSPM treatments showed the highest average levels of activity of these enzymes, up to four times greater than the control.

The accumulation of reactive oxygen species poses a significant risk to cells, compromising their integrity and negatively affecting plant development. Spermidine plays a crucial role in protecting against oxidative stress by neutralizing these potentially harmful molecules (Møller & Sweetlove, 2010; Li et al., 2014). Recent studies have shown that external application of spermidine can reduce superoxide production in response to heat stress, as well as increase the activity of antioxidant enzymes such as SOD, CAT and POX (Zhou et al., 2020; Benkő et al., 2022). In situations of oxidative stress, there is an increased expression of genes related to spermidine synthesis, resulting in higher levels of this polyamine and spermine in the body (Zhou et al., 2020; Benkő et al., 2022). However,

excessive accumulation of polyamines can trigger the formation of reactive oxygen species, such as hydrogen peroxide, through degradation mediated by polyamine oxidase. When in excess, these compounds can harm cells, but in adequate concentrations they can strengthen the cellular antioxidant system. Previous research with cucumbers subjected to salt stress suggests that the application of external spermidine can increase antioxidant capacity, probably due to the regulatory role of polyamine oxidase in this process (Yoda et al., 2006; An et al., 2008; Campestre et al., 2011; Wu et al., 2018).

Differential expressions of genes involved in polyamine biosynthesis were found.

The reference gene *Ribosomal Protein S9* (*LcRPS9*) and three genes associated with the polyamine biosynthetic pathway, namely *thermospermine synthase* (*LcACL5*), *polyamine oxidase* (*LcPAO1*), and *spermidine synthase* (*LcSPDE*) (Figures 7 and 8), were employed for RT-qPCR analysis of both the aerial part and roots of *L. cylindrica*.

Recently, a review was conducted on the genetic expression regulation of the polyamine metabolism-related enzymes, evidencing the endogenous PAs regulatory system. It was shown that this regulation is represented by a hierarchically organized network in which specific transcription factors, metabolism products and miRNAs are involved, demonstrating how complex is the signaling for PAs synthesis (Jiménez-Bremont et al., 2022).

In the analysis of the relative gene expression of the *LcACL5* gene in the aerial part of*L. cylindrica* (Figure 7a), it becomes clear that the averages in the treatment TSPM were remarkably and conspicuously close to those observed in the control group. However, there were no statistically significant differences between the treatments 2,4-D IOE, XY plus TSPM, XY plus 2, 4-D IOE and XY plus 2,4-D IOE plus TSPM compared to the control, there is an unequivocal inclination towards a more pronounced expression of this gene. It should be noted, however, that only in the treatment XY can it be conclusively stated that there is an overexpression of the *LcACL5* gene. As previously anticipated, the accumulation of *ACL5* transcripts was observed in seedlings treated with XY. These results are similar to those obtained by Takamura et al. (2020), where the expression of the *ACL5* gene was used as a sensitive indicator of the endogenous amount of thermospermine. The regulation of *ACL5* occurs through a feedback mechanism by TSPM, so a reduction in the amountof TSPM leads to an increase in *ACL5* expression.

A comprehensive analysis of the expression of the *LcPAO1* gene in the aerial part of

L. cylindrica (Figure 7b) reveals intriguing patterns. The control group shows the lowest relative averages, establishing a baseline for comparison. Subsequently, treatments XY plus 2,4-D IOE and TSPM follow a similar pattern, showing no statistically significant differences. On the other hand, XY, 2,4-D IOE, XY plus TSPM and XY plus 2,4-D IOE plus TSPM treatments show a noticeably high expression of the *LcPAO1* gene compared to the control group. Noteworthy, in XY plus TSPM we noticed an impressive five-fold increase in gene expression, revealing an intriguing aspect of the plant's molecular response.

After a meticulous examination of the *LcSPDE* gene data in the aerial part (Figure 7c) of *L. cylindrica*, a noteworthy trend emerges in which the averages appear to be consistently lower than those observed in the control group. Treatments TSPM, 2,4-D IOE and XY plus 2,4-D IOE plus TSPM show no statistically significant differences compared to the control, while treatments XY, XY plus TSPM and XY plus 2,4-D IOE show averages 60% lower than the control. This observation suggests a potential negative regulation of the *LcSPDE* gene in response to certain treatments, indicating a complex regulatory landscape in the aerial part of *L. cylindrica*.

During the analysis of the *LcACL5* gene in the roots (Figure 8a), no statistically significant differences were observed between the treatments. However, the averages show a noticeable degree of dispersion, although they remain close to the control group.

Expanding our analysis to the intricate network beneath the soil, examining the expression of the *LcPAO1* gene in the roots (Figure 8b) reveals important insights. Treatments TSPM, XY, 2,4-D IOE, XY plus TSPM and XY plus 2,4-D IOE plus TSPM show a substantial reduction in the relative expression of the *LcPAO1* gene, which means a notable decrease of approximately 70% when juxtaposed with the control group. This dramatic change in gene expression may suggest a differentiated modulation of polyamine metabolism in the roots. It is essential to highlight the different dynamics observed in the XY plus 2,4-D IOE treatment, which did not reach statistical significance despite showing lower averages than the control. It can be seen that the treatments with the highest *LcPAO1* gene expression also had the highest antioxidant system enzyme activity, except in XY treatment, a thermospermine synthase suppressor, was applied. Polyamine oxidases (PAOs) require flavin adenine dinucleotide (FAD) for their activity. They oxidize PAs and play a crucial role in plant growth, development and resistance to stress. The activity of the PAOs, responsible forthe oxidation of spermidine or spermine, significantly influences the homeostasis of polyamines in plant tissues, directly impacting plant defense responses under adverse conditions (Wu et al., 2022). In addition, the transformation catalyzed by PAO results in the

formation of hydrogen peroxide, triggering a cascade of signals which, in turn, negatively regulates responsive proteins (Benkő et al., 2022). Previous research with other plant species belonging to the Cucurbitaceae family has indicated that the exogenous application of spermidine leads to an enhanced antioxidant capacity in cucumbers subjected to salt stress, due to the production of hydrogen peroxide resulting from the oxidation of polyamines. Thesefindings suggest a possible protective role for polyamine oxidase in salt stress tolerance in plants (Yoda et al., 2006; An et al., 2008; Campestre et al., 2011; Wu et al., 2018).

A detailed analysis of *LcSPDE* gene expression in the roots (Figure 8c) reveals intriguing details. The XY treatment shows a notable reduction in gene expression, with a decrease of 30%. In addition, treatments XY plus TSPM, XY plus 2,4-D IOE and XY plus 2,4-D IOE plus TSPM manifest a substantial decrease of around 70% for the first two and around 60% for the last, underlining apronounced modulation of the *LcSPDE* gene under these conditions. In contrast, treatments 2,4-D IOE and TSPM showed no statistically significant differences, although the latter showed averages comparable to those of treatment XY. Spermidine plays an essential role as an intracellular regulator in plants, influencing a variety of physiological processes, including responses to oxidative and thermal stress (Song et al., 2002; Gupta & Dey, 2013; Ebeed et al., 2017; Zhou et al., 2020). The excessive increase in reactive oxygen species can cause severe damage to cells, compromising the integrity of the plasma membrane and organelles, which in turn impairs plant growth and development. Spermidine plays a critical role in defending against oxidative stress by neutralizing these harmful species (Møller & Sweetlove, 2010; Li et al., 2014). Recent studies have shown that exogenous application of spermidine reduced superoxide production induced by heat stress and increased the activity of antioxidant enzymes such as SOD, CAT and POX, evidencing its ability to influence the synthesis and activity of these enzymes. In addition, during situations of oxidative stress, an increase in the expression of genes related to spermidine synthesis has been observed, resulting in higher levels of endogenous spermidine and spermine (Zhou et al., 2020; Benkő et al., 2022).

However, our results contradict these findings, as we observed a reduction in the gene expression associated with the enzyme that synthesizes spermidine in almost all treatments, both in the aerial part and in the roots. Notably, the expression of the *LcSPDE* gene was significantly lower where XY was applied, a spermidine-like molecule that acts as a suppressor of ACL5, the enzyme responsible for TSPM synthesis.

Conclusions

In summary, our investigation into the growth parameters, anatomical characteristics, enzymatic antioxidant activity, lipid peroxidation levels, and gene expression patterns in *Luffa cylindrica* revealed intriguing insights into the plant's responses to various treatments. Despite consistent development of initial seedlings across treatments, subtle variations in leaf organ development, total dry weight, tissue organization, and antioxidant activity were observed. These variations, influenced by polyamines in the culture medium, underscore the dynamic nature of plant responses to an important growth regulator. Notably, polyamines treatments exhibited enhanced antioxidant activity and reduced lipid peroxidation, suggesting potential avenues for modulating plant stress responses in future works. Molecular analysis revealed complex patterns of gene expression, challenging existing notions of polyamine-mediated stress responses. The unexpected reduction in *LcSPDE* expression, particularly with XY treatment, highlights the intricate regulation of polyamine metabolism in *L. cylindrica*. This comprehensive study sheds light on the multifaceted mechanisms underlying plant adaptation and stress response, paving the way for further exploration in agricultural and environmental contexts.

References

ALCÁZAR, R.; CUEVAS, J.C.; PLANAS, J.; ZARZA, X.; BORTOLOTTI, C.; CARRASCO, P.; SALINAS, J.; TIBURCIO, A.F.; ALTABELLA, T. Integration of polyamines in the cold acclimation response. **Plant Science**, v.180, p.31–38, 2011. DOI: 10.1016/j.plantsci.2010.07.022.

AN, Z.; JING, W.; YOULIANG, L.; ZHANG, W. Hydrogen peroxide generated by copper amine oxidase is involved in abscisic acid-induced stomatal closure in *Vicia faba*. **Journal of Experimental Botany**, v.59, p.815–825, 2008. DOI: 10.1093/jxb/erm370.

BENKŐ, P.; GÉMES, K.; FEHÉR, A. Polyamine Oxidase-Generated Reactive Oxygen Species in Plant Development and adaptation: The Polyamine Oxidase—NADPH Oxidase Nexus. **Antioxidants**, v.11, p.2488, 2022. DOI: 10.3390/antiox11122488.

BRADFORD, M.M. A rapid and sensitive method for the quantitation of microgram quantities of protein utilizing the principle of protein-dye binding. **Analytical Biochemistry**, v.72, p.248–254, 1976. DOI: 10.1016/0003-2697(76)90527-3.

BUCHANAN, B.B.; GRUISSEM, W.; JONES, R.L. **Biochemistry and Molecular Biology of Plants**. [s.l.] John Wiley & Sons, 2015.

BURKE, R.; NICOTRA, D.; PHELAN, J.; McCABE, P.F.; KACPRZYK, J. The polyamines spermine and spermidine inhibit or induce programmed cell death in *Arabidopsis thaliana* in vitro and in vivo in a dose-dependent manner. **bioRxiv (Cold Spring Harbor Laboratory)**, 2023. DOI: 10.1101/2023.11.15.567161.

CAI, G.; SOBIESZCZUK-NOWICKA, E.; ALOISI, I.; FATTORINI, L.; SERAFINI-FRACASSINI, D.; DEL DUCA, S. Polyamines are common players in different facets of plant programmed cell death. **Amino Acids**, v.47, p.27–44, 2014. DOI: 10.1007/s00726-014-1865-1.

CAMPESTRE, M.P.; BORDENAVE, C.D.; ORIGONE, A.C.; MENÉNDEZ, A.; RUÍZ, O.A.; RODRÍGUEZ, A.A.; MAIALE, S.J. Polyamine catabolism is involved in response to salt stress in soybean hypocotyls. **Journal of Plant Physiology**, v.168, p.1234–1240, 2011. DOI: 10.1016/j.jplph.2011.01.007.

CHANCE, B.; MAEHLY, A.C. [136] Assay of catalases and peroxidases. In: **Methods in Enzymology**. [s.l: s.n.]. p.764–775. DOI: 10.1016/s0076-6879(55)02300-8.

CHEN, Q.; SHI, Q.; GORB, S.N.; LI, Z. A multiscale study on the structural and mechanical properties of the luffa sponge from *Luffa cylindrica* plant. **Journal of Biomechanics**, v.47,

p.1332–1339, 2014. DOI: 10.1016/j.jbiomech.2014.02.010.

CRUZ, C.D. Programa Genes - Ampliado e integrado aos aplicativos R, Matlab e Selegen. **Acta Scientiarum-agronomy**, v.38, p. 547–552, 2016. DOI: 10.4025/actasciagron.v38i4.32629.

DE JESUS SANTANA, M.; BARBOSA-JÚNIOR, S.M.; DIAS, L.L.L.; SILVA, L.A.S.; DA SILVA, G.Z.; FORTINI, E.A.; BATISTA, D.S.; OTONI, W.C.; DA COSTA NETTO, A.P.; ROCHA, D.I. A novel in vitro propagation system for West Indian elm [*Guazuma ulmifolia* Lam. (Malvaceae)]: a valuable medicinal woody species. **In Vitro Cellular & Developmental Biology – Plant**, v.58, p.865–875, 2022. DOI: 10.1007/s11627-022-10275-8.

DESOKY, E.-S.M.; ALHARBI, K.; RADY, M.M.; ELNAHAL, A.S.M.; SELEM, E.; ARNAOUT, S.M. A. I.; MANSOUR, E. Physiological, Biochemical, Anatomical, and Agronomic Responses of Sesame to Exogenously Applied Polyamines under Different Irrigation Regimes. **Agronomy**, v.13, p.875, 2023. DOI: 10.3390/agronomy13030875.

DICKMAN, M.B.; WILLIAMS, B.; LI, Y.; DE FIGUEIREDO, P.; WOLPERT, T. Reassessing apoptosis in plants. **Nature Plants**, v.3, p.773–779, 2017. DOI: 10.1038/s41477-017-0020-x.

EBEED, H.T.; HASSAN, N.M.; ALJARANI, A.M. Exogenous applications of Polyamines modulate drought responses in wheat through osmolytes accumulation, increasing free polyamine levels and regulation of polyamine biosynthetic genes. **Plant Physiology and Biochemistry**, v.118, p.438–448, 2017. DOI: 10.1016/j.plaphy.2017.07.014.

FRETT, T.J.; FRELICH, M.J.; MARAVOLO, N.C. The influence of spermine and hydrogen peroxide on programmed cell death in tuberculate rhizoids of *Marchantia polymorpha*. **The Bryologist**, v.116, p.134–145, 2013. DOI: 10.1639/0007-2745-116.2.134.

FUKUDA, H.; KOMAMINE, A. Establishment of an Experimental System for the Study of Tracheary Element Differentiation from Single Cells Isolated from the Mesophyll of *Zinnia elegans*. **Plant Physiology**, v.65, p.57–60, 1980. DOI: 10.1104/pp.65.1.57.

GAMBORG, O.L.; MILLER, R.; OJIMA, K. Nutrient requirements of suspension cultures of soybean root cells. **Experimental Cell Research**, v.50, p.151–158, 1968. DOI: 10.1016/0014-4827(68)90403-5.

GIANNOPOLITIS, C.N.; RIES, S.K. Superoxide dismutases. **Plant Physiology**, v.59, p.309–314, 1977. DOI: 10.1104/pp.59.2.309.

GILL, S.S.; TUTEJA, N. Polyamines and abiotic stress tolerance in plants. **Plant Signaling & Behavior**, v.5, p.26–33, 2010. DOI: 10.4161/psb.5.1.10291.

GUPTA, K.; DEY, A. Plant polyamines in abiotic stress responses. **Acta Physiologiae Plantarum**, v.35, p.2015–2036, 2013. DOI: 10.1007/s11738-013-1239-4.

HAVIR, E.A.; McHALE, N.A. Biochemical and developmental characterization of multiple forms of catalase in tobacco leaves. **Plant Physiology**, v.84, p.450–455, 1987. DOI: 10.1104/pp.84.2.450.

HODGES, D.M.; DELONG, J.M.; FORNEY, C.F.; PRANGE, R.K. Improving the thiobarbituric acid-reactive-substances assay for estimating lipid peroxidation in plant tissues containing anthocyanin and other interfering compounds. **Planta**, v.207, p.604–611, 1999. DOI: 10.1007/s004250050524.

IAKIMOVA, E.T.; WOLTERING, E.J. Xylogenesis in zinnia (*Zinnia elegans*) cell cultures: unravelling the regulatory steps in a complex developmental programmed cell death event. **Planta**, v.245, p.681–705, 2017. DOI: 10.1007/s00425-017-2656-1.

JIMÉNEZ-BREMONT, J.F.; CHÁVEZ-MARTÍNEZ, A.I.; ORTEGA-AMARO, M.A.; DE LA LUZ GUERRERO-GONZÁLEZ, M.; JASSO-ROBLES, F.I.; MARURI-LÓPEZ, I.; LIU, J.; GILL, S.S.; RODRÍGUEZ-KESSLER, M. Translational and post-translational regulation of polyamine metabolic enzymes in plants. **Journal of Biotechnology**, v.344, p.1–10, 2022. DOI: 10.1016/j.jbiotec.2021.12.004.

KARNOVSKY, M.J. A formaldehyde-glutaraldehyde fixative of high osmolality for use in electron-microscopy. **Journal of Cell Biology**, v.27, 1965.

KHOSHBAKHT, D.; ASGHARI, M.; HAGHIGHI, M. Influence of foliar application of polyamines on growth, gas-exchange characteristics, and chlorophyll fluorescence in Bakraii citrus under saline conditions. **Photosynthetica**, v.56, p.731–742, 2018.
DOI: 10.1007/s11099017-0723-2.

LI, Z.; PENG, Y.; ZHANG, X.; PAN, M.; MA, X.; HUANG, L.; YAN, Y. Exogenous spermidine improves water stress tolerance of white clover (*Trifolium repens* L.) involved in antioxidant defence, gene expression and proline metabolism. **Plant Omics**, v.7, p.517–526, 2014.

LIU, J.; KITASHIBA, H.; WANG, J.; BAN, Y.; MORIGUCHI, T. Polyamines and their ability to provide environmental stress tolerance to plants. **Plant Biotechnology**, v.24, p.117–126, 2007. DOI: 10.5511/plantbiotechnology.24.117.

LIVAK, K.J.; SCHMITTGEN, T.D. Analysis of relative gene expression data using Real-Time Quantitative PCR and the $2^{-\Delta\Delta CT}$ method. **Methods**, v.25, p.402–408, 2001. DOI: 10.1006/meth.2001.1262.

LOCATO, V.; DE GARA, L. Programmed cell Death in Plants: An Overview. In: **Methods**

inmolecular biology. [s.l: s.n.]. p.1–8. DOI: 10.1007/978-1-4939-7668-3_1.

MANDAL, C.; GHOSH, N.; MAITI, S.; DAS, K.; GUPTA, S.D.; DEY, N.; ADAK, M.K. Antioxidative responses of Salvinia (*Salvinia natans* Linn.) to aluminium stress and it's modulation by polyamine. **Physiology and Molecular Biology of Plants**, v.19, p.91–103, 2012. DOI: 10.1007/s12298-012-0144-4.

MØLLER, I.M.; SWEETLOVE, L.J. ROS signalling – specificity is required. **Trends inPlant Science**, v.15, p.370–374, 2010. DOI: 10.1016/j.tplants.2010.04.008.

MOSCHOU, P.N.; ROUBELAKIS-ANGELAKIS, K.A. Polyamines and programmed cell death. **Journal of Experimental Botany**, v.65, p.1285–1296, 2013. DOI: 10.1093/jxb/ert373.

MURASHIGE, T.; SKOOG, F. A Revised Medium for Rapid Growth and Bio Assays with Tobacco Tissue Cultures. **Physiologia Plantarum**, v.15, p.473–497, 1962. DOI: 10.1111/j.1399-3054.1962.tb08052.x.

NAKANO, Y.; ASADA, K. Hydrogen Peroxide is Scavenged by Ascorbate-specific Peroxidase in Spinach Chloroplasts. **Plant and Cell Physiology**, 1981. DOI: 10.1093/oxfordjournals.pcp.a076232.

O'BRIEN, T.P.; MCCULLY, M.E. The study of Plant Structure: Principles and Selected Methods. **Taxon**, v.31, p.789, 1982. DOI: 10.2307/1219725.

PÁL, M.; SZALAI, G.; JANDA, T. Speculation: Polyamines are important in abiotic stress signaling. **Plant Science**, v.237, p.16–23, 2015. DOI: 10.1016/j.plantsci.2015.05.003.

PARTAP, S.; KUMAR, A.; SHARMA, N.; JHA, K.K. *Luffa cylindrica*: an important medicinal plant. **Journal of Natural Product and Plant Resources**, v.2, p.127–134, 2012.

PAUL, S.; BANERJEE, A.; ROYCHOUDHURY, A. Role of polyamines in mediating antioxidant defense and epigenetic regulation in plants exposed to heavy metal toxicity. In: **Springer eBooks**. [s.l: s.n.]. p.229–247. DOI: 10.1007/978-981-13-2242-6_8.

RIBEIRO, A.; DE TOLEDO PICOLI, E.A.; LANI, E.R.G.; VENDRAME, W.A.; OTONI, W.C. The influence of flask sealing on in vitro morphogenesis of eggplant (*Solanum melongena* L.). **In Vitro Cellular & Developmental Biology – Plant**, v.45, p.421–428, 2009. DOI: 10.1007/s11627-008-9183-5.

SALDANHA, C.W.; OTONI, C.G.; DE AZEVEDO, J.L.F.; DIAS, L.L.C.; RÊGO, M.M.D.; OTONI, W.C. A low-cost alternative membrane system that promotes growth in nodal cultures of Brazilian ginseng [*Pfaffia glomerata* (Spreng.) Pedersen]. **Plant Cell, Tissue and Organ Culture**, v.110, p.413–422, 2012. DOI: 10.1007/s11240-012-0162-5.

SCHNEIDER, C.A.; RASBAND, W.; ELICEIRI, K.W. NIH Image to ImageJ: 25 years of image analysis. **Nature Methods**, v.9, p.671–675, 2012. DOI: 10.1038/nmeth.2089.

SOBIESZCZUK-NOWICKA, E.; KUBALA, S.; ŻMIEŃKO, A.; MAŁECKA, A.; LEGOCKA, J. From accumulation to degradation: reprogramming polyamine metabolism facilitates dark-Induced senescence in barley leaf cells. **Frontiers in Plant Science**, v.6, 2016. DOI: 10.3389/fpls.2015.01198.

SONG, J.; NADA, K.; TACHIBANA, S. Suppression of S-adenosylmethionine Decarboxylase Activity is a Major Cause for High-Temperature Inhibition of Pollen Germination and Tube Growth in Tomato (*Lycopersicon esculentum* Mill.). **Plant and Cell Physiology**, v.43, p.619–627, 2002. DOI: 10.1093/pcp/pcf078.

TAKAHASHI, T. Thermospermine: an evolutionarily ancient but functionally new compound in plants. In: **Methods in Molecular Biology**. [s.l: s.n.]. p.51–59. DOI: 10.1007/978-1-4939-7398-9_4.

TAKAMURA, H.; MOTOSE, H.; OTSU, T.; SHINOHARA, S.; KOUNO, R.; KADOTA, I.; TAKAHASHI, T. Chemical synthesis and biological effect on xylem formation of xylemin and its analogues. **European Journal of Organic Chemistry**, v.2020, p.2745–2753, 2020. DOI: 10.1002/ejoc.202000322.

TAKAO, K.; RICKHAG, M.; HEGARDT, C.; OREDSSON, S.; PERSSON, L. Induction of apoptotic cell death by putrescine. **The International Journal of Biochemistry & Cell Biology**, v.38, p.621–628, 2006. DOI: 10.1016/j.biocel.2005.10.020.

TIBURCIO, A.F.; ALTABELLA, T.; BITRIÁN, M.; ALCÁZAR, R. The roles of polyamines during the lifespan of plants: from development to stress. **Planta**, v.240, p.1–18, 2014. DOI: 10.1007/s00425-014-2055-9.

VAN DURME, M.; NOWACK, M.K. Mechanisms of developmentally controlled cell death in plants. **Current Opinion in Plant Biology**, v.29, p.29–37, 2016. DOI: 10.1016/j.pbi.2015.10.013.

VAN HAUTEGEM, T.; WATERS, A.J.; GOODRICH, J.; NOWACK, M.K. Only in dying, life: programmed cell death during plant development. **Trends in Plant Science**, v.20, p.102–113, 2015. DOI: 10.1016/j.tplants.2014.10.003.

WU, J.; LIU, W.; JAHAN, M.S.; SHU, S.; SUN, J.; GUO, S. Characterization of polyamine oxidase genes in cucumber and roles of CsPAO3 in response to salt stress. **Environmental and Experimental Botany**, v.194, p.104696, 2022. DOI: 10.1016/j.envexpbot.2021.104696.

WU, J.; SHU, S.; LI, C.; SUN, J.; GUO, S. Spermidine-mediated hydrogen peroxide signaling enhances the antioxidant capacity of salt-stressed cucumber roots. **Plant Physiology and Biochemistry**, v.128, p.152–162, 2018. DOI: 10.1016/j.plaphy.2018.05.002.

YODA, H.; HIROI, Y.; SUZUKI, H. Polyamine oxidase is one of the key elements for

oxidative burst to induce programmed cell death in tobacco cultured cells. **Plant Physiology**, v.142, p.193–206, 2006. DOI: 10.1104/pp.106.080515.

YOSHIMOTO, K.; TAKAMURA, H.; KADOTA, I.; MOTOSE, H.; TAKAHASHI, T. Chemical control of xylem differentiation by thermospermine, xylemin and auxin. **Scientific Reports**, v.6, 2016. DOI: 10.1038/srep21487.

ZHOU, R.; HU, Q.; PU, Q.; CHEN, M.; ZHU, X.; GAO, C.; ZHOU, G.; LIU, L.; WANG, Z.; YANG, J.; ZHANG, J.; CAO, Y. Spermidine Enhanced Free Polyamine Levels and Expression of Polyamine Biosynthesis Enzyme Gene in Rice Spikelets under Heat Tolerance before Heading. **Scientific Reports**, v.10, 2020. DOI: 10.1038/s41598-020-64978-2.ZHU, H.; JIANTING, L.; QINGFANG, W.; CHEN, M.; WANG, B.; ZHANG, Q.; XUE, Z.

De novo sequencing and analysis of the transcriptome during the browning of fresh-cut *Luffa cylindrica* "Fusi-3" fruits. **PLOS ONE**, v.12, p.e0187117, 2017. DOI: 10.1371/journal.pone.0187117.

Figures

Figure 1 - Experimental design. *Luffa cylindrica* after 7 days of *in vitro* cultivation under stationary liquid medium. a) Control; b) Thermospermine (TSPM); c) Xylemin (XY); d) 2,4-D Iso-octyl ester (2,4-D IOE); e) XY plus TSPM; f) XY plus 2,4-D IOE; f) XY plus 2,4-D IOE plus TSPM. *Bar* = 100 mm.

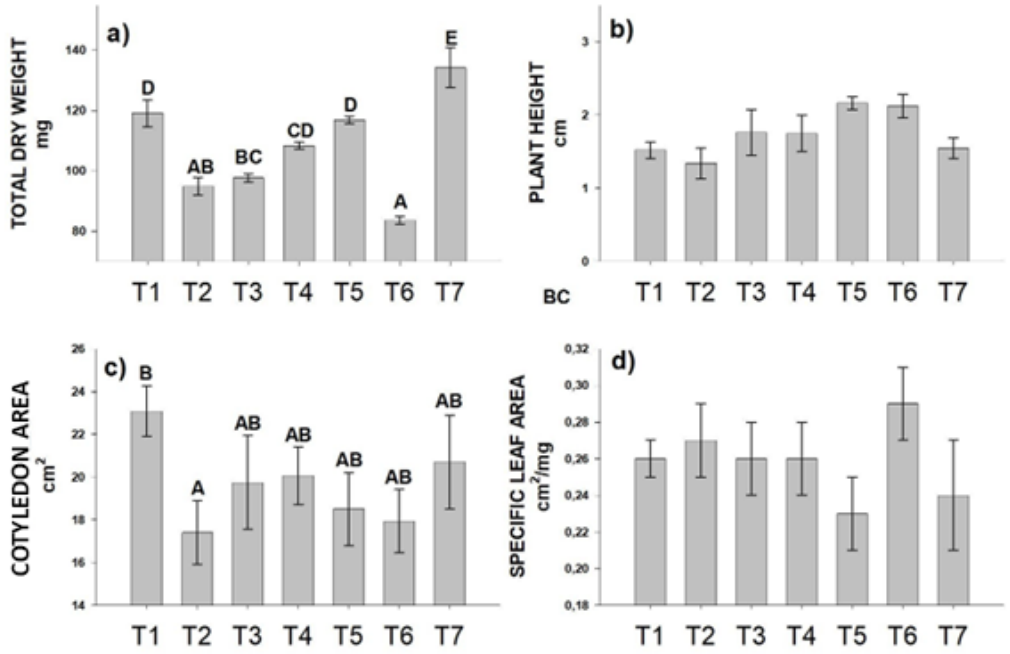

Figure 2 - Analysis of growth parameters of *Luffa cylindrica* grown *in vitro* under stationary liquid medium for 7 days. T1 = Control; T2 = Thermospermine (TSPM); T3 = Xylemin (XY); T4 = 2,4-D Iso-octyl ester (2,4-D IOE); T5 = XY plus TSPM; T6 = XY plus 2,4-D IOE, and T7 = XY plus 2,4-D IOE plus TSPM. All concentrations in 10 µM. Equal letters denote no difference at the 5% level by Duncan's test; values represent the mean ± standard error ($n = 5$)

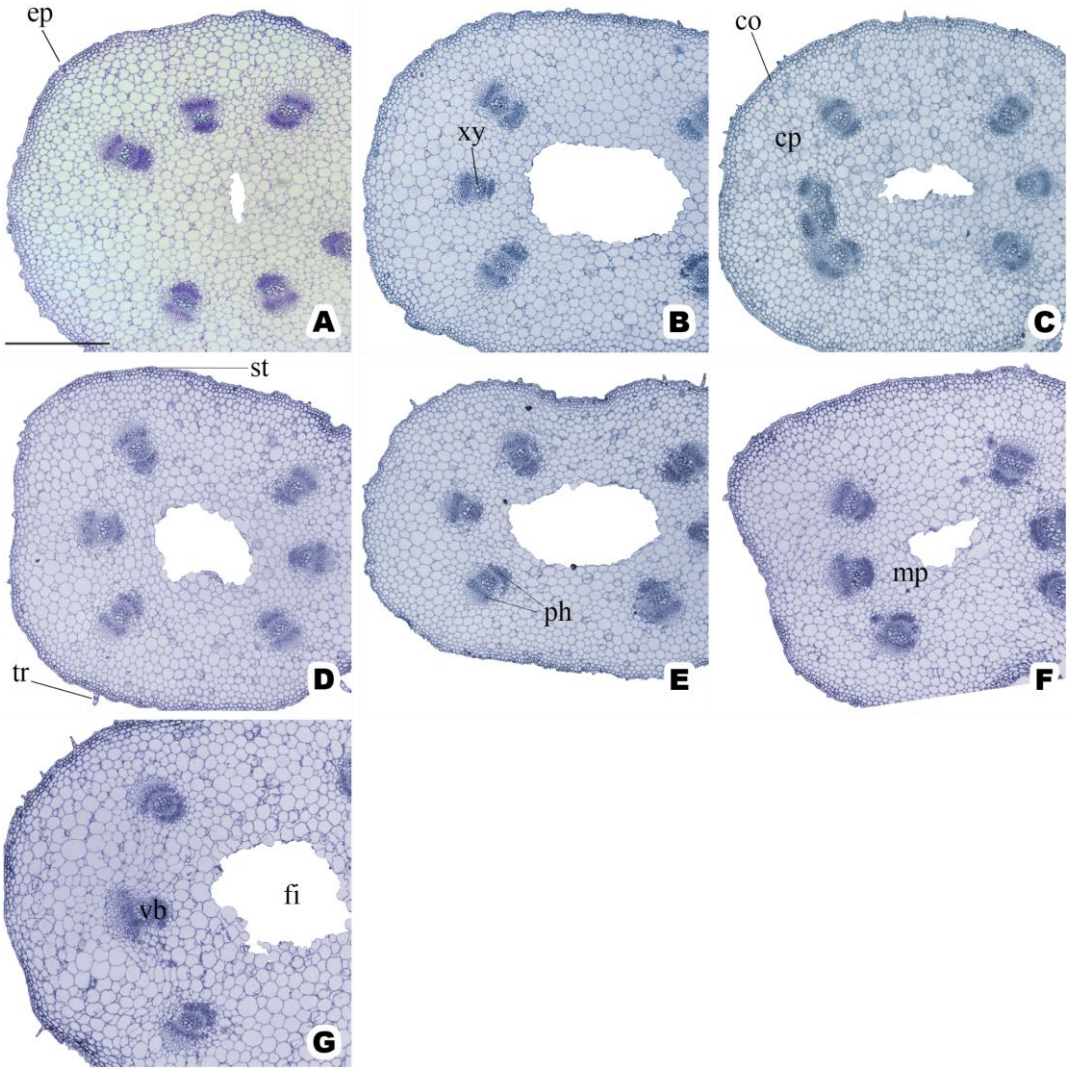

Figure 3 - Hypocotyl transversal sections (a-g) of *Luffa cylindrica* plants grown in vitro under stationary liquid medium for 7 days. A = Control; B = Thermospermine (TSPM); C = Xylemin (XY); D = 2,4-D Iso-octyl ester (2,4-D IOE); E = XY plus TSPM; F = XY plus 2,4-D IOE, and G = XY plus 2,4-D IOE plus TSPM. All concentrations in 10 µM. *Abbreviations*: *co*, collenchyma; *cp*, cortical parenchyma; *ep*, epidermis; *fi*, fistula; *mp*, medullary parenchyma; *ph*, phloem; *st*; stomata; *tr*, trichome; *vb*, vascular bundle; *xy*, xylem. *Bar* = 1000 µm.

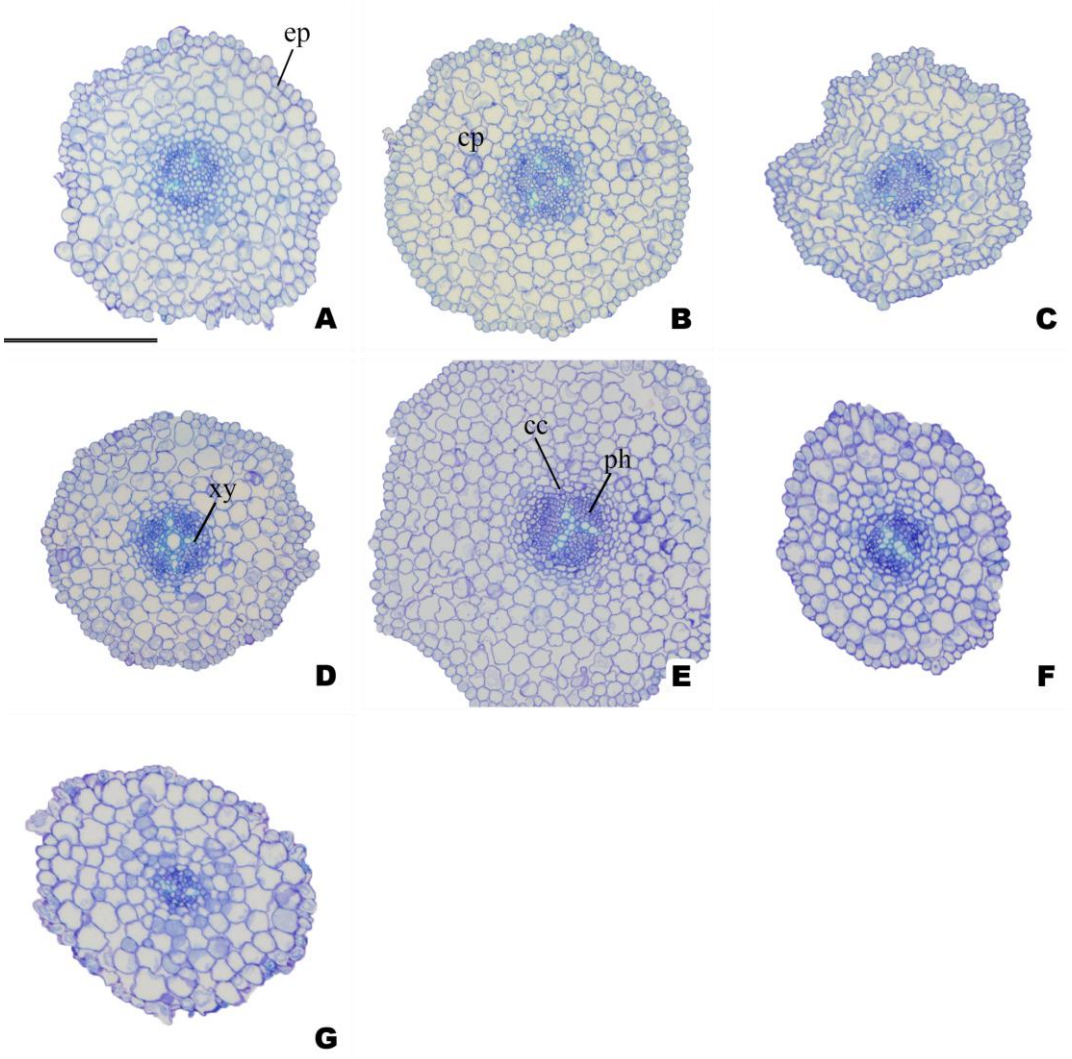

Figure 4 - Root transversal sections (a-g) of *Luffa cylindrica* plants grown *in vitro* under stationary liquid medium for7 days. A = Control; B = Thermospermine (TSPM); C = Xylemin (XY); D = 2,4-D Iso-octyl ester (2,4-D IOE); E = XY plus TSPM; F = XY plus 2,4-D IOE, and G = XY plus 2,4-D IOE plus TSPM. All concentrations in 10 µM. *Abbreviations*: *cc*, central cylinder; *cp*, cortical parenchyma; *ep*, epidermis; *ph*, phloem; *xy*, xylem. *Bar* = 600 µm.

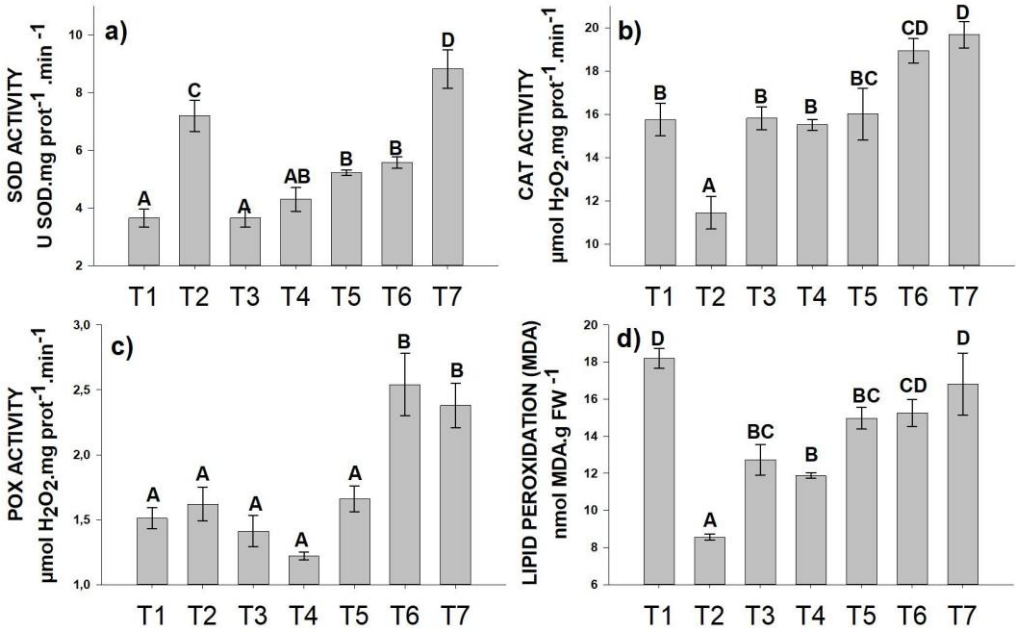

Figure 5 - Antioxidant enzyme activity and lipid peroxidation in aerial parts of *Luffa cylindrica* grown *in vitro* at 7 days of cultivation under stationary liquid medium. T1 = Control; T2 = Thermospermine (TSPM); T3 = Xylemin (XY); T4 = 2,4-D Iso-octyl ester (2,4-D IOE); T5 = XY plus TSPM; T6 = XY plus 2,4-D IOE, and T7 = XY plus 2,4-D IOE plus TSPM. All concentrations in 10 µM. Equal letters denote no difference at the 5% level by Duncan's test; values represent the mean ± standard error ($n = 5$).

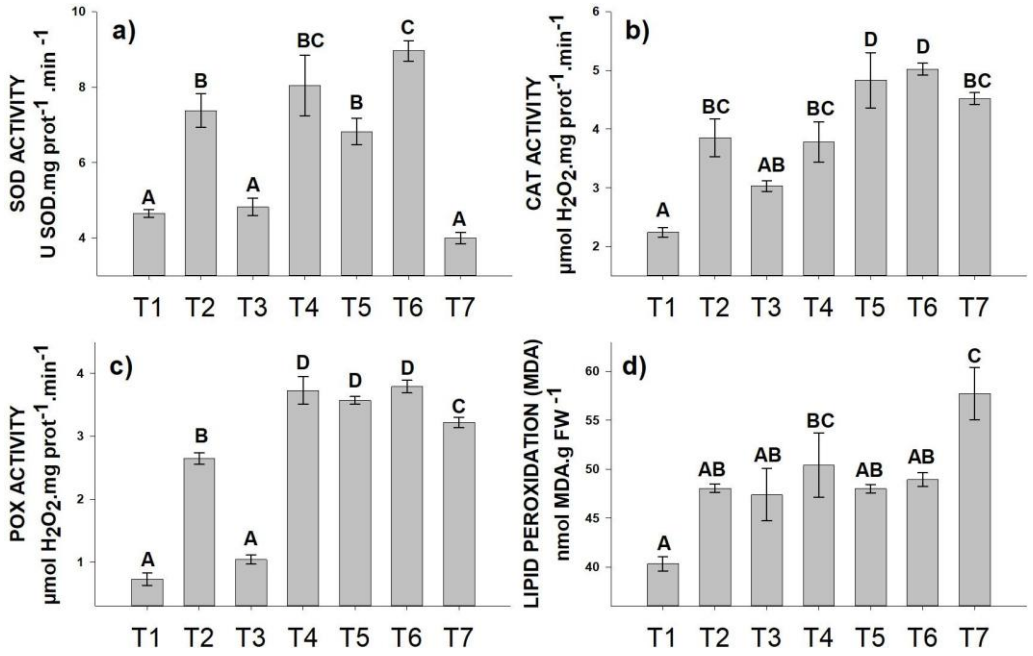

Figure 6 - Antioxidant enzyme activity and lipid peroxidation in roots of *Luffa cylindrica* plants grown *in vitro* at 7 days of cultivation, under stationary liquid medium. T1 = Control; T2 = Thermospermine (TSPM); T3 = Xylemin (XY); T4 = 2,4-D Iso-octyl ester (2,4-D IOE); T5 = XY plus TSPM; T6 = XY plus 2,4-D IOE, and T7 = XY plus 2,4-D IOE plus TSPM. All concentrations in 10 µM. Equal letters denote no difference at the 5% level by Duncan's test; values represent the mean ± standard error ($n = 5$).

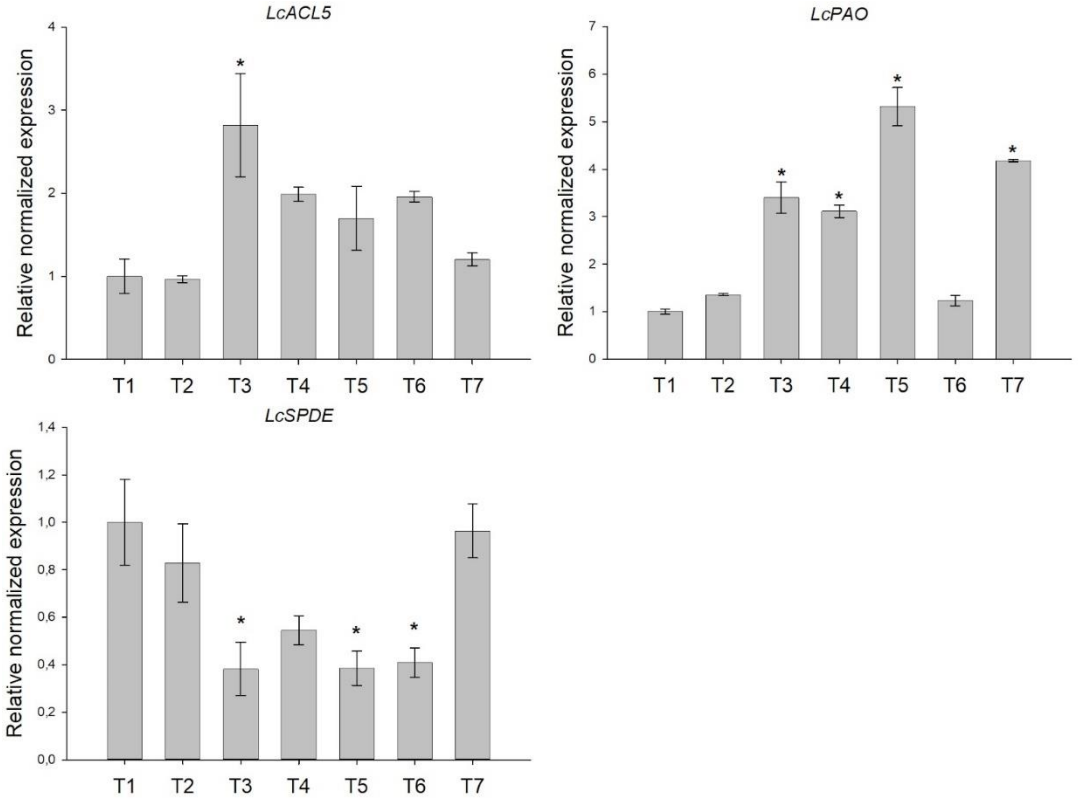

Figure 7 - Real-time reverse transcription-polymerase chain reaction (RT-qPCR) for *Luffa cylindrica* genes —*Thermospermine Sintase* (*LcACL5*); *Polyamine Oxidase* (*LcPAO1*) and *Spermidine synthase* (*LcSPDE*) — after 7 days of cultivation *in vitro*. Relative gene expression of *Luffa cylindrica* aerial parts at seven different conditions: T1 = Control; T2 = Thermospermine (TSPM); T3 = Xylemin (XY); T4 = 2,4-D Iso-octyl ester (2,4-D IOE); T5 = XY plus TSPM; T6 = XY plus 2,4-D IOE, and T7 = XY plus 2,4-D IOE plus TSPM. All concentrations in 10 µM. Gene expression relative to *Ribosomal Protein S9* (RPS9). Data presented as mean ± standard deviation (n = 4), *$p < 0.05$

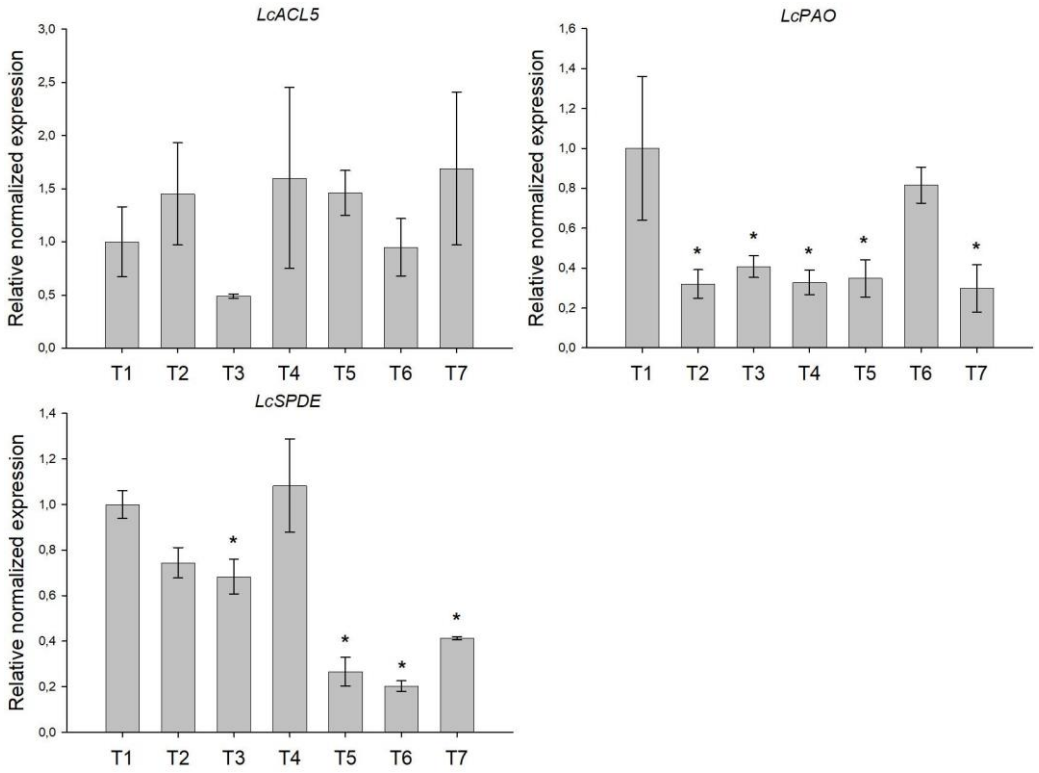

Figure 8 - Real-time reverse transcription-polymerase chain reaction (RT-qPCR) for *Luffa cylindrica* genes — *Thermospermine Sintase* (*LcACL5*); *Polyamine Oxidase* (*LcPAO1*) and *Spermidine synthase* (*LcSPDE*) — after 7 days of cultivation *in vitro*. Relative gene expression of Luffa roots at seven different conditions: T1 = Control; T2 = Thermospermine (TSPM); T3 = Xylemin (XY); T4 = 2,4-D Iso-octyl ester (2,4-D IOE); T5 = XY plus TSPM; T6 = XY plus 2,4-D IOE, and T7 = XY plus 2,4-D IOE plus TSPM. All concentrations in 10 µM. Gene expression relative to *Ribosomal Protein S9* (RPS9). Data presented as mean ± standard deviation ($n = 4$), *$p < 0.05$

Chapter 2:

Influence of microporous membranes on the physiology of programmed cell death of Luffa cylindrica (L.) Roem in vitro through modulation of the protein profile

Abstract

Plants, during evolution, have developed crucial mechanisms for growth and adaptation to different environments. Senescence plays a vital role in the remobilization of nutrients, in the response to pathogens and stress, and in the development involving programmed cell death (PCD) events. Plant tissue culture is widely used in various cultivation methods to study morphophysiological and molecular characteristics. The photoheterotrophic (PH) system, which uses a carbon source in the culture medium, can accumulate undesirable gasses, such as ethylene, in sealed flasks. On the other hand, the photomixotrophic system (PM), which uses membrane lids, improves gas exchange, renewing the internal atmosphere of the growing containers and thus improving the performance of the vitroplants. Here, we investigated the anatomy, metabolism, stress response and protein profile of *Luffa cylindrica* vitroplants using the PH and PM sealing techniques. The plants were grown *in vitro* for 20 days in Murashige and Skoog medium under PH and PM conditions. Compared to the PM, PH treatment reduced growth and showed anatomical changes in the leaves and stem.Photosynthetic rates and photosynthetic pigment content were the same in both treatments. However, the PH treatment reduced the levels of starch, total amino acids, and protein, and increased sucrose, fructose and glucose. The analysis of the antioxidant system enzymes showed that the vitroplants under the PH cultivation system were more subject to oxidative damage and had higher enzyme activity. Comparative proteomic analysis revealed 128 differentially accumulated proteins involved in 34 biological processes, including proteins involved in PCD and their different biological roles. Taken together, our results help to understand *Luffa cylindrica* how PCD works and their possible regulatory protein system, opening the avenue for future investigations into the mechanisms involved in this regulation.

Keywords: Gas exchange. Plant Tissue Culture. Photoheterotrophic growth. Photomixotrophic growth.Proteomic.

Introduction

Over the course of evolution, crucial adaptation and development mechanisms evolved in plants due to environment pressures, since as sessile organisms are susceptible to a diverse range ofbiotic and abiotic challenges. Senescence plays an essential role in the remobilization of nutrients and photoassimilates, as well as in response to pathogens, stresses and development, involving programmed cell death (PCD) events (Iakimova & Woltering, 2017; Burke et al., 2020; Valandro et al., 2020; Jones etal., 2013; Villanueva et al., 2021; Sychta et al., 2021).

The in vitro plant culture technique is a biotechnological procedure that involves isolating plant organs, tissues, and cells from living organisms, followed by disinfestation to eliminate bacteria and fungi from the explants. Subsequently, these explants are transferred to sterile tissue culture media, defined and enriched with essential nutrients for plant tissue growth and multiplication. Within meticulously controlled environments, this approach enables effective observation and manipulation of plant growth (Shahzad et al., 2017; Panis et al., 2020). The *in vitro* technique is widely used for large-scale micropropagation, production of metabolites of industrial interest, breeding purposes, embryo rescue, ploidy manipulations, protoplast fusions and somatic embryogenesis, and is an appropriate tool for the temporary storage of plant genetic resources (Chandran et al., 2020; Khan et al., 2021). Cloning, primarily through *in vitro* cultivation, has emerged as an efficient strategy for maintaining the genetic purity of species with recalcitrant seeds, allowing the preservation of different accessions in limited spaces. Plant tissue culture is widely used for practical applications and research, allowing the study of morphophysiological and molecular characteristics in different cultivation systems (Shahzad et al., 2017).

The photoheterotrophic (PH) system, which uses a sugar as a principal carbon source in the culture medium, can lead to the accumulation of undesired gases inside sealed flasks (Park et al., 2018). In contrast, the photomixotrophic (PM) system defends the use of lids combined with membranes, improving gas shifts with the external environment. This approach effectively renews the internal atmosphere of the growing containers, thus improving the performance of the vitroplants (Ševčíková et al., 2018; Silva et al., 2019; Santos et al., 2020; Alves et al., 2022).

Cultivating explants under a PH regime can result in plants adapted to a high-water content environment, increasing the risk of dehydration and mortality during acclimatization (Kubota & Kozai, 1992; Arigita et al., 2002). However, these effects can be mitigated by

simultaneously increasing the CO_2 concentration and reducing the relative humidity and ethylene levels around the plant, achieved through the use of PM system lids (Kozai & Nguyen, 2003).

Raising the concentration of CO2 through the PM system proves to be an effective strategy in promoting an increase in photosynthesis, exerting a direct influence on the Rubisco enzyme carboxylation rate (Bowes, 1993; Arigita et al., 2002). This solves the challenges linked to the PH regime and establishes an environment conducive to the optimized functioning of the photosynthetic system throughout the subsequent stages of cultivation.

At the same time, the reduction in relative humidity reduces the likelihood of plant hyperhydricity, encouraging the development of cuticle on the leaves and normalizing the functioning of the stomata to the external environment. This adaptive measure increases tolerance to water deficit (Zobayed et al., 2001) and speeds up the acclimatization process, creating more favourable conditions for the overall development of the plant later on.

Ethylene plays an important role in PCD, increasing the efficiency of tracheary elements (TEs) differentiation, participating in the lignification process and affecting the transcription rates and patterns of genes encoding vacuolar processing enzymes (VPEs), responsible for the collapse of the tonoplast resulting in the release of proteases into the cytoplasm and the initiation of the proteolytic cascade of PCD (Pesquet & Tuominen, 2011; Pesquet et al., 2013; Rantong & Gunawardena, 2018; Vorster et al., 2019; Simões et al., 2020).

Even though several species have been studied in relation to PCD, *Luffa cylindrica* stands out for its innate ability to undergo sclerification and develop lignocellulosic fibers in its fruits (Demura, 2014). This distinctive feature emphasizes the need for a comprehensive understanding of PCD-related processes and potential methods to activate and regulate these processes. As a direct effect, the comprehensive characterization of the physiological mechanisms triggered in response to specific *in vitro* sealing methods remains incomplete for this species. With this in mind, the present study explores and compares the differences between PCD-related aspects in the anatomy, metabolism, stress response and protein profile of *Luffa cylindrica* vitroplants using the PH and PM sealing techniques.

L. cylindrica has the potential to fill knowledge gaps, shed light on stress mechanisms, treat pathologies, and increase productivity. This research aims to contribute to a deeper understanding of the signaling pathways and events that occur during the PCD process in *L. cylindrica*, thus integrating new knowledge for the development of plants.

Materials and Methods

Plant material and experimental design

Mature *Luffa cylindrica* seeds obtained from Feltrin® (Farroupilha, RS, Brazil) were mechanically scarified by removing the tegument using a mini-mortar. Under aseptic conditions, in a laminar flow chamber, the scarified seeds were disinfected by immersing them in 70% (v/v) alcohol for 1 min, and then immersing them for 20 min in a commercial solution of sodium hypochlorite (SuperGlobo®, Contagem, MG) at 1.3% (v/v), plus two dropsof the surfactant Tween 20 per 100 mL of solution. Next, the decoated seeds were triple rinsedin distilled and autoclaved water. Subsequently, the seeds (15 units/per plate) were inoculated into sterile 90 mm crystal polystyrene Petri dishes (Kasvi®, Curitiba, PR), arranged evenly containing 25 mL of Agar-Water medium, 6 g L^{-1} agar (PhytoTechnology Labs, USA), pH adjusted to 5.7 ± 0.1, and autoclaved at 120 °C, 108 kPa, for 20 min. The plates were sealed with hypoallergenic microporous adhesive tape (Micropore® 3M, Sumaré, SP), which favors higher gas exchange between the atmosphere and the headspace of the plate (Ribeiro et al., 2009; Saldanha et al., 2012; Jesus Santana et al., 2022). The cultures were kept in a growth room at 25 ± 2 °C, witha 16/8 h light photoperiod, under an irradiance of 60 µmol m^{-2} s^{-1}, using two LED lamps (SMD 100, 18 W, Vilux®, Vitória, ES, Brazil).

After radicle protrusion (~ 2-3 mm), 2 pre-germinated seeds were inoculated into glassflasks (600 mL capacity) containing 100 mL of semi-solid MS medium (Murashige and Skoog, 1962) plus vitamins B5, 30 g L^{-1} sucrose, 0.1 g L^{-1} myo-inositol, 6 g L^{-1} agar (PhytoTechnology Labs, USA), pH adjusted to 5.7 ± 0.1, and autoclaved at 120 °C, 108 kPa, for 20 min. The flasks were closed with rigid polypropylene lids with two 10 mm holes, covered with 0.45 µm-pore size hydrophobic polytetrafluoroethylene (PTFE) membranes (Photomixotrophic(PM)) or with rigid polypropylene lids without membranes (Photoheterotrophic(PH)), and kept under the light and temperature conditions mentioned above. The experiment was conducted in a completely randomized design (DIC), with 15 flasks (repetitions), containing two explants for each repetition, with the experimental unit consisting of flasks.

Anatomical characterization

After 20 days of culture, the explants were collected and fixed in Karnovsky's solution(Karnovsky, 1965). The fixed samples were dehydrated in an ethanolic series,

embedded in methacrylate resin (Historesin, Leica®), and embedded in plastic molds. Five-micrometer-thick cross-sections were obtained using an automatic rotary microtome(RM 2155, Leica) and stained with toluidine blue (O'Brien and McCully, 1981). The specimens were mounted in Permount on glass slides. Photographs were taken with anOlympus SZH stereoscopic microscope and a microscope (Olympus AX70) with an attached U-Photo system.

Growth parameters

After 20 days of *in vitro* culture, the length of the stem (cm), the length of the largest root (cm), the number of leaves, the number of roots, the fresh weight (FW) (g), the dryweight (DW) (g) and the leaf area (cm^2) were evaluated. The plant tissues were collected at the end of the experiment and sectioned into shoot and root parts. The leaves were detached and fixed individually on plasticized white paper. Photographs were taken with a digital camera and the images were processed using ImageJ software (Schneider et al., 2012). DW (g) was obtained by drying the plant material in an oven at 50 °C for 72 h.

Antioxidant activity

Activity of oxidative stress enzymes, superoxide dismutase (SOD), catalase (CAT) andascorbate peroxidase (APX) was assessed. Briefly, 50 mg of frozen fresh material (aerial part)were homogenized in 1.4 mL extraction medium containing 0.1 M potassium phosphate buffer, pH 6.8; 0.1 mM ethylenediaminetetraacetic acid; 1 mM phenylmethylsulfonyl fluoride and 1% (w/v) polyvinylpolypyrrolidone. The sample was vortexed for 10 s, centrifuged at 12,000 rpm for 15 min at 4 °C, and the supernatant was removed and set aside on ice for enzyme assays plus protein determination (Bradford, 1976). CAT and POX activities were determined as proposed previously (Chance & Maehly, 1955; Nakano & Asada, 1981; Havir & McHale, 1987) and expressed as μmol^{-1} min^{-1} g^{-1} protein. SOD activity was measured as described earlier (Giannopolitis & Ries, 1977) and expressed as U min^{-1} g^{-1} protein, with 1 U being equivalent to the concentration of SOD required to inhibit 50% of nitro blue tetrazoliumphotoreduction.

Determination of lipid peroxidation

Lipid peroxidation was determined by quantifying thiobarbituric acid reactive

substances (TBARS) according to Hodges et al. (1999), with modifications. The plant material, 50 mg of frozen fresh material (aerial part), was homogenized in 2 mL of ethanol-water 80:20 (v/v) and centrifuged at 10,000 *g* for 15 min at 4 °C. The supernatant(500 µL) was removed and added to 0.5 mL of 20% TCA. Another 500 µL of the supernatant was added to 500 µL of the mixture of 20% TCA and 0.5% TBA. The samples were placed ina bath at 90 °C for 1 h and then cooled in an ice bath. The samples were centrifuged again at 3000 *g* for 10 min at 4 °C and the supernatant was read at absorbances of 440, 532 and 600 nm. The results were estimated using the following equations: [(Abs 532+TBA)-(Abs 600+TBA)-(Abs 532-TBA- Abs600-TBA)] = A; [(Abs 440+TBA-Abs 600+TBA) 0.05711] = B; MDA equivalents (nmol to µmol-1) = (A-B/157000)*10^{-6}; The results were expressed in nmol of fresh weight (FW).

Proteome analyses

Proteomic analyses were performed using freeze-dried and macerated aerial part samples (three biological replicates, 30 mg DW per sample). Extraction was performed as described by Damerval et al. (1986). The samples were suspended in a buffer solution of 10% (w/v) trichloroacetic acid/acetone (Sigma-Aldrich, St. Louis, MO, USA) together with 20 mM dithiothreitol (GE Healthcare, Piscataway, NJ, USA), and subsequently vortexed for5 min at 8 °C. The solution was kept for 60 min at −20 °C and then centrifuged at 16,000×*g* for30 min at 4 °C. The pellets from the previous step were washed thrice in cold acetone solution with 20 mM dithiothreitol and centrifuged for 5 min between each wash. Following, the pellets were air dried and solubilized in a buffer containing 7 M urea, 2 M thiourea (all GE Healthcare), 2% Triton X-100 (Sigma-Aldrich), 1% dithiothreitol, 1 mM phenylmethylsulfonyl fluoride (Sigma-Aldrich), and vortexed for 30 min at 8 °C. The samples were centrifuged at 16,000 × *g* for 30 min at 4 °C, the supernatants were collected, and the protein concentration was measured using a 2-D Quant Kit (GE Healthcare). Before trypsin digestion, protein samples (100 µg from each biological replicate) were precipitated using methanol/ chloroform and resuspended in buffer containing 7 M urea and 2 M thiourea. Proteins were digested using the Microcon-30 kDa filter units (Merck Millipore, Burlington, MA, USA) with the filter-aided sample preparation methodology (Reis et al., 2021). Peptides and proteins were quantified on a NanoDrop™ 2000c spectrophotometer at 205 nm.

The differential accumulated proteins (DAPs) data were used for enrichment analyses of gene ontology (GO), biological processes and Kyoto Encyclopedia of Genes and Genomes

(KEGG).

A protein-protein interaction (PPI) network was created using orthologs identified by STRING (https://string-db.org/). v11.5 (Szklarczyk et al. 2023). based on the *Luffa cylindrica* amino acid sequence. Predicted interaction networks of DAPs were constructed using proteome *Luffa cylindrica* identified through a STRING search (Sharable organism identifier; STRG0A29BBS; https://version-12-0.string-db.org/organism/STRG0A29BBS), followed by downstream analysis in Cytoscape v 3.9 (Shannon et al. 2003).

Statistical analysis

Statistical analysis was carried out using Genes software version Windows/2019.89 (Cruz, 2016). The experiments were repeated twice. The data was subjected to a one-factor analysis of variance using Duncan's test and the means were compared using Student's t-test, both at a 5% significance level.

Results and Discussion

Evaluation of growth parameters on the 20th day of cultivation under PH and PM systems

The growth and development of plants under the photoheterotrophic (PH) system showed adverse changes when compared to plants grown under photomixotrophic (PM) conditions (Figure 1), such as lower shoot growth and organ death. These changes may have occurred due to the accumulation of gases such as ethylene inside the flask under PH conditions. It is possible to observe phenotypic characteristics resulting from the symptoms ofthe triple response to ethylene in the PH system, characterized by the shortening of stems and the death of meristems. These factors culminate in the death of the plant, characteristics that have been recognized and validated for decades (Pratt & Goeschl, 1969; Wang et al., 2023).

After these first observations, we quantified the dry mass of leaf, stem and roots (Figure2a). Despite the trend of higher values for stem and root dry mass, only the leaves were significantly higher in the PM treatment. We also calculate the biomass partition (Figure 2b). The leaves biomass was amplified in the PM cultivation method, under stem and root biomass penalty. The plant height was also assessed (Figure 2c). Here PM was 14.06% higher than PH counterparts. The specific leaf area is an important feature to plant physiology since it relates both leaf weight and area (Figure 2d). Plants cultivated in these two methods do not differ each other. On the other hand, when we analyzed the leaf area, we observed 30.61% more leaves area in the PM treatment (Figure 2e)

Anatomical characterization of Luffa cylindrica *vitroplants under photoheterotrophy and photomixotrophy*

The results showed that the PH system favors the accumulation of gases such ethylene, through exchange deficit of gases inside the flasks. This condition led to anatomical changes in all the plant organs evaluated.

These changes may be associated with the accumulation of gases such as ethylene, as several studies have shown the relationship between this gas and various physiological responses in plants, including PCD events. Microscopy showed some anatomical differences in the stems and leaves of *L. cylindrica* plants grown *in vitro* under different conditions of gasexchange in *in vitro* cultivation (Figures 3 and 4).

The stems of *L. cylindrica* plants grown in the PH system showed more compact and

similar collenchyma at 15 and 20 days (Figure 3a, g), with well-defined regions than when compared to the PM system. The latter, however, showed a more pronounced development with gradual evolution until the 20th day of harvest (Figure 3d, j). The medullary parenchyma cells of the plants grown on the PH system on the 15th day of cultivation (Figure 3a) were larger and had well-defined extra-cellular spaces when compared to the PM culture of the same age (Figure 3d). This result was similar when observed on the 20th day of cultivation (Figure 3g, j).

The lower development of collenchyma in the stems of plants grown under PH may explain the lower growth of these plants. This is corroborated by the findings of Leroux (2012), who indicated that the collenchyma is reduced in size under stress conditions, thus inhibiting stem elongation. Indeed, most elongation occurs after the collenchyma cells thicken their walls in order to sustain the increased growth demand.

Some studies have shown that during events such as aerenchyma formation, xylem development, and senescence, there are significant increases in ethylene production by plants that coincide with the occurrence PCD events (Pesquet & Tuominen, 2011; Schneider et al., 2018; Tavares et al., 2018; Liu et al., 2019).

The plants grown in the PH system showed a more pronounced development of sclerenchyma and vascular tissue in the stem, evidenced by the greater development of vascular bundles and the high formation of metaxylem and protoxylem. It was also observed by Martins et al. (2015), reporting, which indicates an accelerated effort by *Billbergia zebrina* plant's machinery to overcome the stress caused by the high concentration of gases in the headspace of the flasks, similar to the symptoms caused by water stress (Li et al., 2023)

In addition, there was a difference in the development of the vascular bundles betweenthe treatments. In the PM system, the number of vascular bundles was greater (Figure 3j) thanin the PH system (Figure 3g) and the hydraulic system was designed in a more individualised way, which, although it is more susceptible to failure, demonstrates the tendency for efficiencyover protection (Anderegg & Venturas, 2020). The number of leaf structures was also higher in the PM (Figure 3b), showing that the plant invests in vascular structures for the survivaland development of the leaves. These findings are similar to those found by Li et al. (2023), where plants exposed to abiotic stresses show less stem development and damage to the xylem vessels.

We observed that *L. cylindrica* leaves have a uniseriate epidermis with trichomes, the palisade parenchyma is well defined and spongy parenchyma is evident. These characteristics were not affected by the treatment; however, our results showed, in contrast

to the stem results, that there was a greater development of collenchyma in the leaves of the plants grown under the PM system (Fig. 4h).

The use of lids with membranes, which allow greater gas exchange, maintains an adequate concentration of CO_2 and reduces ethylene concentration inside the flask (Saldanha et al., 2012). Like *Pfaffia glomerata*, *L. cylindrica* plants grown under PM showed greater vigor and leaf development (Silva et al., 2019). Lids with no membranes restrict gas exchange and consequently maintain higher levels of ethylene in the headspace inside the flasks, which affects plant growth, including other factors (Batista et al., 2017; Silva et al., 2017; De Paula Alves et al., 2022).

The leaves of the plants grown under PM conditions showed a more evident and well-developed region of collenchyma (Figure 4j), corroborating the results found by Iarema et al. (2012), where the cultivation of the species *P. glomerata* in membrane treatments showed similar results. The lower development of collenchyma in the leaves of plants grown under pH justifies the reduction in leaf area due to the limitation in gas exchange which prevents complete leaf development. According to Leroux (2012), plastic deformation of the walls of young collenchyma is crucial during leaf development. This tissue is often persistent as the primary mechanical support in plant organs without sclerification or secondary growth, such as leaves. Its more elastic walls provide essential support during leaf growth and expansion.

In addition, we observed that plants grown under PH conditions displayed a more differentiated vascular tissue with a more pronounced vascular system (Fig. 4i) compared to the PM system (Figure 4l). Under photoheterotrophic system, leaf anatomy tends towards cell compaction, leading to smaller cells and fewer spaces between them. This results in more cells, thicker cellwalls and increased production of cellulose compounds.

Cultivation with microporous membranes affects the activity of antioxidant enzymes

Oxidative stress results from an imbalance in the homeostasis of reactive oxygen species (ROS) and occurs when plants are exposed to various types of stress. High levels of ethylene can result in the overproduction of these enzymes, which in turn can induce programmed cell death (PCD) pathways. Oxidative stress is a biochemical phenomenon that occurs when the delicate balance in the cellular environment of (ROS) is disturbed (Li et al., 2011b; Kapoor et al., 2018). The results obtained showed that the PH and PM cultures differed significantly in antioxidant enzyme activity (Figure 5)

When analyzing the activity of the enzyme superoxide dismutase (SOD) (Figure 5a), on the 10th day, similar activity was observed in both treatments. Only on the 15th day of cultivation was there a significant difference between the treatments due to a decrease in SODactivity in the PH treatment. However, as the days progressed, the difference in activity between the treatments decreased and reached similar levels, suggesting a possible adaptation of the plants to similar oxidative stress conditions. The observation of a trend of reduction in SOD activity over time may indicate a natural response to the reduction in the presence of the superoxide radical (Gechev et al., 2006).

When analyzing the activity of the enzyme catalase (CAT) (Figure 5b), it is clear thatit remained similar on the 10th day of cultivation in both treatments. However, this stability was not maintained in the PM treatment, which showed significant drop-in activity on the 15th and 20th days. In the case of the PH treatment, CAT seemed to maintain stability over time, with an upward trend. These observations point to a difference in the oxidative state between the two treatments, with PH showing greater consumption and higher production of H2O2 compared to PM. Catalase (CAT) stands out as a crucial antioxidant enzyme present in several organisms, playing a central role in the decomposition of hydrogen peroxide (H2O2) and the fine regulation of the levels of this vital cell signaling molecule (Chelikani et al., 2004). CAT is the most abundant protein in the plant peroxisome domain, boasting one of the highest catalytic rates in biology (Zhi-Sheng et al., 2016). Its impact has repercussions on essential functions in plant development, influencing seed aging, viability and organ senescence. As proposed by Baker et al. (2023), CAT appears to be a determining factor in the longevity of plants, animals and yeasts.

Notably, all CAT isoforms contribute to PCD responses. Although mainly located in the peroxisomes, CAT's adaptability is demonstrated as it involves interactions in the cytosol or nucleus, especially in the face of biotic and abiotic stress conditions (Zhang et al., 2014; Li et al., 2015; Kneeshaw et al., 2017). This flexibility suggests that CAT plays diverse roles in cellular compartments beyond the peroxisome, demonstrating its potential to respond to various environmental challenges.

Gadjev et al. (2008a) highlighted CAT's unique ability to degrade H_2O_2 without providing reducing power, offering plants an energy-efficient mechanism to remove H_2O_2. This adds another layer to the multifaceted contributions of catalase in cellular processes, highlighting its importance in maintaining the cellular redox balance.

Regarding the ascorbate peroxidase (APX) enzyme activity (Figure 5c), it is clear that there was a reduction between the 10th and 15th days of cultivation in the PH treatment.

However, there was a significantly drop in APX activity in the PM treatment from the 20th day onwards. Such pattern can be translated on an oxidative stress sensitivity by both plant groups, since the response over time was different, with the PM treatment showing a later response. The suggestion is that ROS are crucial in directing nitric oxide (NO) into the cell death pathway. According to the study by Murgia et al. (2004), increased resistance to NO-induced cell death is observed in Arabidopsis plants that overexpress the APX enzyme.

Due to the ephemeral nature of ROS, direct measurement of their concentration is a challenge. Therefore, TiBARS assays, which measure malondialdehyde (MDA) (Figure 5d) present in the samples, are valid alternatives for assessing oxidative damage to membranes (Blokhina & Fagerstedt, 2010).

On the 10th day of cultivation, there was a significant difference in MDA activity between the treatments, suggesting an immediate response by the plants to oxidative stress. The observation of an increase in MDA in *L. cylindrica* at this point indicates that plants grown under the PH system tend to raise ROS levels as a cell protection strategy during stressful conditions. This suggests that, even with the higher antioxidant enzyme activity inthe PH treatment, the damage caused to the membranes by reactive oxygen species was similar between the treatments tested.

These findings highlight the complexity of the antioxidant response and the importance of considering not only antioxidant enzymes but also the end products of oxidative stress when assessing the impact of stress on plants. This situation resembles the phenomenon observed in maize embryos, where elevated ethylene levels also resulted in ROSactivation and subsequent cell death (Huang et al., 2014; Kapoor et al., 2018).

Gas shift regimes affects the levels of primary metabolites

In general, *L. cylindrica*, when cultivated under photomixotrophic (PM) and photoheterotrophic (PH) conditions, showed similar chlorophyll *a*/*b* rate and total chlorophyll contents (Figure 6), with no variations in the chlorophyll fluorescence parameters examined such as the maximum quantum yield of photosystem II (Figure 7a); The non-photochemical quenching (Figure 7b); photochemical quenching (Figure 7c); electron transport rate (Figure 7d). However, gasexchange impacted compounds linked to primary metabolism, including protein, starch, glucose, fructose, sucrose and amino acids (Figure 8). It was noted that growth under photoheterotrophic (PH) conditions resulted in a reduction in the levels of protein (12%), starch (58.32%), and amino acids (37.52%) (Figure 8a, b, f).

Conversely, the levels of sugars (glucose, fructose and sucrose) increased considerably in the plants grown in the system (120, 62.6 and 106%, respectively) (Figure 8c, d, e).

Although gas exchange causes changes in leaf structure, it did not impact the chlorophyll contents, and chlorophyll fluorescence parameters were evaluated. However, there were changes in the accumulation of metabolites and the activity of antioxidant enzymes. These changes may be linked to the accumulation of ethylene, as several studies have revealed the influence of this compound on various morphophysiological responses in plants, including its role in regulating programmed cell death (PCD).

Gas exchange influences primary metabolism and, as observed in *L. cylindrica*, photoheterotrophic (PH) conditions result in a reduction in protein, starch and amino acid levels, while there is an increase in soluble sugar levels. Sucrose, glucose and fructose, crucialmolecules for cell biosynthesis, can be used as a source of carbon and energy. The treatments did not affect the chlorophyll content, and some of the chlorophyll fluorescence parameters were analyzed. *Fv/Fm* values close to 0.8 indicate the integrity of the photosynthetic machinery, suggesting that photosynthesis was not impaired (Roháček, 2002; Zhang et al., 2023). The presence of sucrose in the culture medium may have contributed to the maintenance of the photosynthetic machinery since the plant preferentially absorbs sucrose as the end product of the photosynthetic process (Kozai & Sekimoto, 1988; Paiva Neto & Otoni, 2003).

The high content of these sugars favors processes such as cell division, expansion, differentiation and maturation, and it is recognized that sugar metabolism plays a significant role in responses to biotic and abiotic stresses (Ruan et al., 2010; Ruan, 2014).

Stress caused by high levels of ethylene triggered PCD pathways in *L. cylindrica*, and in this context, sugars also have signaling functions, interacting with hormone and reactive oxygen species (ROS) signaling pathways, inducing cell division and PCD (Liu et al., 2013). The greater availability of carbon keeps amino acid levels low, as there is no need to provide an additional source of energy for substrate respiration (Hildebrandt et al., 2015). In addition, the degradation of starch and proteins is expected in some PCD events, such as autophagy (Izumi et al., 2013; Barros et al., 2017)

Gas shift system affects proteome screening of programmed cell death-related proteins

Principal component analysis (PCA) (Figure 9) showed a clear segregation of proteins, highlighting the discrepancies between the two treatments under analysis:

photoheterotrophic (PH) and photomixotrophic (PM). This evaluation was meticulously conducted in order to compare the protein profiles in the different in vitro cultivation conditions of *Luffa cylindrica*.

The results indicate that the two principal components, PC1 and PC2, together can explain 81.5% of all the variations present in the proteomic data. This methodology improves the validity and interpretation of the results obtained, providing aricher context for the proteomic analysis carried out in this specific study.

A total of 894 proteins were identified (Supplementary Table 1) in the aerial part of *L. cylindrica*, of which 887 were found in both treatments. Comparing the proteins identified in both treatments, based on the PH system as a reference, we observed that almost 10% of proteins showed down-accumulation and almost 5% of proteins showedup-accumulation in the PM system (Figure 10a). These results indicated which metabolic routes are modulated by gas shift system.

The discrepancy in the differential accumulation of proteins (DAP's) becomes evident when we analyze the volcano plot (Figure 10b). There is a remarkable trend of accumulation in both directions of the graph, reinforcing even more the crucial importance of the type of flask gas exchange rate in the development of plants during *in vitro* growth.

When analyzing the biological processes involved in these PADs (Figure 11a), we observed a lower accumulation of proteins related to catabolic cellular processes, such as the catabolism of carbohydrates, proteins and macromolecules. as well as processes associated with the catabolism of reactive oxygen species (ROS), cellular detoxification and stress responses in the PM system. Among the down-regulated PM's DAPs (Table 1), it was possible to identify several proteins closely related to PCD, as described in the literature. The following proteins can be grouped according to their function in the plant.

The proteins calreticulin (TRINITY_DN8513_c0_g1_i1_p1Calreticulin), ATP synthase β-mitochondrial subunit (TRINITY_DN13431_c0_g1_i1_p2spA7N0Y1ATPB1_VIBC1) and the heat shock 70 proteins (TRINITY_DN16818_c0_g1_i2_p1spQ9S7C0HSP7O_ARATH, (TRINITY_DN43107_c0_g2_i1_p1spP0DMV8HS71A_HUMAN, (TRINITY_DN121394_c0_g1_i1_p1spP09189HSP7C_PETHY) are resistant to proteolysis and are associated with PCD in the mitochondria and endoplasmic reticulum. In addition, the association of calreticulins with the Ca^{2+} ion, known to play an essential role in cell signaling and to be one of the main agents in the PCD process, further strengthens the link between these proteins and the regulation of the cell death mechanism (Krebs, 1998;

Nakamura et al., 2000; Rao et al., 2004; Giorgi et al., 2008).

The 26s Proteasome (TRINITY_DN638_c0_g1_i17_p1spO64982PRS7_PRUPE, TRINITY_DN397_c0_g1_i1_p1spQ9C5U3PRS8A_ARATH) and PCD have a complex relationship. The 26s proteasome, a highly conserved subunit protein complex, plays a crucial role in the degradation of cytosolic and nuclear proteins. Studies using proteasome inhibitors, such as Ac-APnLD-CHO and β-lactone, have revealed that these inhibitors can block PCD induced by avirulent bacteria (Hatsugai et al., 2009; Pajerowska-Mukhtar & Dong, 2009). This highlights the crucial interaction between the 26s proteasome and PCD in plants.

The DEAD-box ATP-dependent RNA helicase (TRINITY_DN8254_c1_g1_i1_p1spQ93ZG7RH38 _ARATH) is crucial in pre-mRNA splicing and mRNA export out of the nucleus, playing an essential role in PCD, especially in structural cells during anther development. Forming a dimer with AIP1, it binds to the promoter region of the cysteine protease CP1. The silencing of AIP1 and AIP2 in plants results in a male-sterile phenotype, highlighting the importance of these components in plant reproduction (Li et al., 2011a).

Endochitinases (TRINITY_DN1165_c0_g3_i1_p1spP36907CHIX_PEA) are accumulated in response to abiotic stress, the accumulation of transcripts and proteins was observed in Arabidopsis in a study proposed by Passarinho et al., 2001, and it was later proposed that these chitinases were involved in PCD (De a Gerhardt et al., 2004). It has also been shown that the expression of plant endochitinases is regulated spatially and temporally during plant development processes in which PCD occurs, such as somatic embryogenesis (deJong et al., 1992 & 1993).

The Endoplasmic reticulum (ER) chaperoneBiP (TRINITY_DN7395_c0_g1_i5_p1spP11021BIP_HUMAN), present in plants, plays an essential role in the formation and maturation of proteins. Studies have shown its relevance in controlling cell death induced by endoplasmic reticulum stress (Schröder & Kaufman, 2005; Valente et al., 2009; Reis et al., 2011). BiP regulates drought-induced cell death by modulating N-Rich-Protein-mediated signaling (Reis & Fontes, 2012). Involved in the regulation of programmed cell death in immune response in plants (Wang et al., 2007; Reis et al., 2011; Xu et al., 2012).

The group of proteins called Metacaspases (MCs) (TRINITY_DN11900_c0_g1_i1_p1spO64517MCA4_ARATH) are proteins with structures homologous to plant caspases, which differ from animal caspases in their way. They are the main proteins for PCD, from initiation to execution. Ethylene is a strong signal for the

synthesis of MC in plant cells (Sun et al., 2024). MCs play a fundamental role in programmed cell death during the development process of plants and in their defense responses (Huh, 2022).

The 14-3-3-like protein (TRINITY_DN10969_c1_g3_i2_p1spP462661433_PEA), actin (TRINITY_DN2280_c2_g1_i1_p1101241at33090_Actin) and lipoxygenase (LOX) (TRINITY_DN3440_c0_g1_i7_p1UniRef100_A0A6J1J654) play interconnected roles in cellular processes. The 14-3-3-like protein regulates several biological processes, including programmed cell death (PCD), transcription, apoptosis and pathogen tolerance. Actin, as a fundamental cellular component, acts as a cellular sensor and plays a key role in regulating apoptosis/PCD. In addition, LOX influences the organization of the cytoskeleton and the phosphorylation of proteins, playing a crucial role in promoting PCD. The early activation of LOX in apoptotic pathways, distinct from necrosis, suggests a biochemical difference between vacuolar PCD and necrosis processes. Together, these proteins form a network of interconnected regulators that influence cellular responses, with 14-3-3, actin and LOX contributing to the orchestration of PCD, apoptosis and related processes in different cellular kingdoms (Aducci et al., 2002; Obsilova et al., 2008; Chevalier, 2009; de Boer et al., 2013; Franklin-Tong & Gourlay, 2008; Provost et al., 1999; Maccarrone et al., 1997, 1999, 2001).

Aconitate hydratase (TRINITY_DN8633_c0_g1_i1_p1spQ42560ACO1_ARATH) and peroxidase enzymes (TRINITY_DN564_c0_g2_i9_p1UniRef100_A0A6J1H0T4, TRINITY_DN209_c1_g2_i3_p1spP19135PER2_CUCSA, TRINITY_DN39_c3_g1_i1_p1spQ42580PER21_ARATH,TRINITY_DN20234_c0_g1_i2_p1spO23044PER3_ARATH, TRINITY_DN10870_c0_g1_i3_p1spA7NY33PER4_VITVI, TRINITY_DN16124_c1_g1_i5_p1spQ9SZB9PER47_ARATH, TRINITY_DN12127_c0_g1_i2_p1spQ96509PER55_ARATH, TRINITY_DN11172_c0_g1_i4_p1spQ43873PER73_ARATH) are interconnected components of cellular defense mechanisms against oxidative stress and programmed cell death (PCD) in plants. Aconitate hydratase, a key enzyme in the citric acid cycle, is sensitive to oxidative inactivation by hydrogen peroxide (H_2O_2). Its activity serves as an indicator of intracellular H_2O_2 levels and oxidative damage. Studies have shown a significant decrease in aconitase activity before the onset of PCD, underlining its role as a marker for assessing the effects of oxidative stress and impending PCD in plant cells (Ishikawa et al., 2009).

Peroxidase enzymes neutralize hydrogen peroxide generated in cellular compartments (Gadjev et al., 2008a, 2008b) due to energy transfer reactions, electron leakage and oxidase activities (Apel & Hirt, 2004). This function aligns with the role of aconitate hydratase in the

oxidative stress response. The interaction between the aconitate hydratase and peroxidase enzymes shows a cellular defense strategy.

This comparative analysis suggests less potential for accumulating PCD-linked proteins in the PM system, where the container is sealed with membranes. While the lower concentration of these proteins reduces the catabolic processes mentioned, proteins linked to processes related to full development, such as photosynthesis and metabolic intermediates, aremore prominent in PM (Figure 11b).

Conclusions

In conclusion, our investigation into the growth parameters, anatomical characteristics, enzymatic antioxidant activity, primary metabolism, and proteomic profiles of Luffa cylindrica under different cultivation systems revealed significant insights into the plant's physiological responses. The comparison between photoheterotrophic (PH) and photomixotrophic (PM) conditions demonstrated distinct effects on plant growth and development.

Proteomic profiling highlighted distinct protein accumulation patterns between PH and PM treatments, particularly proteins related to programmed cell death (PCD). PH-grown plants showed higher accumulation of PCD-related proteins, suggesting a potential link between ethylene accumulation, oxidative stress, and PCD induction.

Overall, our findings underscore the importance of gas exchange regimes in influencing plant physiology, metabolism, and stress responses. The dynamic interplay between ethylene, antioxidant systems, primary metabolism, and PCD-related proteins reveals the intricate mechanisms underlying plant adaptation to different environmental conditions. These insights contribute to our understanding of plant responses to stress and may inform strategies for optimizing cultivation practices in agricultural and environmental contexts.

References

ADUCCI, P.; CAMONI, L.; MARRA, M.; VISCONTI, S. From cytosol to organelles: 14-3-3proteins as multifunctional regulators of plant cell. **IUBMB Life**, v.53, p.49–55, 2002. DOI: 10.1080/15216540210813.

ALVES, J.P.; PINHEIRO, M.V.M.; CORRÊA, T.R.; ALVES, G.L.; MARINHO, T.R.D.S.; BATISTA, D.S.; FIGUEIREDO, F.A.M.M.A.; REIS, F.O; FERRAZ, T.M.; CAMPOSTRINI, E. Morphophysiology of *Ananas comosus* during in vitro photomixotrophic growth and ex vitro acclimatization. **In Vitro Cellular & Developmental Biology – Plant**, v.59, p.106–120, 2022. DOI: 10.1007/s11627-022-10321-5.

ANDEREGG, W.R.L.; VENTURAS, M.D. Plant hydraulics play a critical role in Earth system fluxes. **New Phytologist**, v.226, p.1535–1538, 2020. DOI: 10.1111/nph.16548.

APEL, K.; HIRT, H. Reactive oxygen species: metabolism, oxidative stress, and signal transduction. **Annual Review of Plant Biology**, v.55, p.373–399, 2004. DOI: 10.1146/annurev.arplant.55.031903.141701.

ARIGITA, L.; GONZÁLEZ, A.; TAMÉS, R.S. Influence of CO_2 and sucrose on photosynthesis and transpiration of *Actinidia deliciosa* explants cultured in vitro. **Physiologia Plantarum**, v.115, p.166–173, 2002. DOI: 10.1034/j.1399-3054.2002.1150119.x.

BAKER, A.; LIN, C.-C.; LETT, C.; KARPIŃSKA, B.; WRIGHT, M.H.; FOYER, C.H. Catalase: A critical node in the regulation of cell fate. **Free Radical Biology and Medicine**, v.199, p.56–66, 2023. DOI: 10.1016/j.freeradbiomed.2023.02.009.

BARROS, J. A S.; CAVALCANTI, J.M.B.; MEDEIROS, D.B.; NUNES-NESI, A.; AVIN-WITTENBERG, T.; FERNIE, A.R.; ARAÚJO, W.L. Autophagy Deficiency Compromises Alternative Pathways of Respiration following Energy Deprivation in *Arabidopsis thaliana*. **Plant Physiology**, v.175, p.62–76, 2017. DOI: 10.1104/pp.16.01576.

BATISTA, D.S.; DE CASTRO, K.M.; RIBEIRO, D.M.; CAIXETA, E.T.; DE OLIVEIRA SANTOS, M.; VICCINI, L.F.; OTONI, W.C. Ethylene Responses and ACC oxidase Gene Expression in *Lippia alba* (Verbenaceae) Chemotypes with Varying Ploidy Levels. **In Vitro Cellular & Developmental Biology – Plant**, v.53, p.278–284, 2017. DOI: 10.1007/s11627-017-9827-4.

BLOKHINA, O.; FAGERSTEDT, K. Oxidative metabolism, ROS and NO under oxygen deprivation. **Plant Physiology and Biochemistry**, v.48, p.359–373, 2010. DOI: 10.1016/j.plaphy.2010.01.007.

BOWES, G. Facing the inevitable: plants and increasing atmospheric CO_2. **Annual Review of Plant Physiology and Plant Molecular Biology**, v.44, p.309–332, 1993. DOI: 10.1146/annurev.pp.44.060193.001521.

BRADFORD, M.M. A rapid and sensitive method for the quantitation of microgram quantities of protein utilizing the principle of protein-dye binding. **Analytical Biochemistry**, v.72, p.248–254, 1976. DOI: 10.1016/0003-2697(76)90527-3.

BURKE, R.; SCHWARZE, J.; SHERWOOD, O.L.; JNAID, Y.; MCCABE, P.F.; KACPRZYK, J. Stressed to death: The role of transcription factors in plant programmed cell death induced by abiotic and biotic stimuli. **Frontiers in Plant Science**, v.11, 2020. DOI: 10.3389/fpls.2020.01235.

CHANCE, B.; MAEHLY, A.C. [136] Assay of catalases and peroxidases. In: **Methods in Enzymology**. [s.l: s.n.]. p.764–775. DOI: 10.1016/s0076-6879(55)02300-8.

CHANDRAN, H.; MEENA, M.; BARUPAL, T.; SHARMA, K. Plant tissue culture as a perpetual source for production of industrially important bioactive compounds. **Biotechnology Reports**, v.26, p.e00450, 2020. DOI: 10.1016/j.btre.2020.e00450.

CHELIKANI, P.; FITA, I.; LOEWEN, P.C. Diversity of structures and properties among catalases. **Cellular and Molecular Life Sciences**, v.61, p.192–208, 2004. DOI: 10.1007/s00018-003-3206-5.

CHEN, Q.; SHI, Q.; GORB, S.N.; LI, Z. A multiscale study on the structural and mechanical properties of the luffa sponge from *Luffa cylindrica* plant. **Journal of Biomechanics**, v.47, p.1332–1339, 2014. DOI: 10.1016/j.jbiomech.2014.02.010.

CHEVALIER, D.; MORRIS, E.R.; WALKER, J.C. 14-3-3 and FHA domains mediate phosphoprotein interactions. **Annual Review of Plant Biology**, v.60, p.67–91, 2009. DOI: 10.1146/annurev.arplant.59.032607.092844.

CRUZ, C.D. Programa Genes - Ampliado e integrado aos aplicativos R, Matlab e Selegen. **Acta Scientiarum-agronomy**, v.38, p.547–552, 2016. DOI: 10.4025/actasciagron. v38i4.32629.

DAMERVAL, C.; DE VIENNE, D.; ZIVY, M.; THIELLEMENT, H. Technical improvements in two-dimensional electrophoresis increase the level of genetic variation detected in wheat-seedling proteins. **Electrophoresis**, v.7, p.52–54, 1986. DOI: 10.1002/elps.1150070108.

DE BOER, A.H.; VAN KLEEFF, P.J.M.; GAO, J. Plant 14-3-3 proteins as spiders in a web ofphosphorylation. **Protoplasma**, v.250, p.425–440, 2012. DOI: 10.1007/s00709-012-0437-z.

DE JESUS SANTANA, M.; BARBOSA-JÚNIOR, S.M.; DIAS, L.L.L.; SILVA, L.A.S.; DA

SILVA, G.Z.; FORTINI, E.A.; BATISTA, D.S.; OTONI, W.C.; DA COSTA NETTO, A.P.; ROCHA, D.I. A novel in vitro propagation system for West Indian elm [*Guazuma ulmifolia* Lam. (Malvaceae)]: a valuable medicinal woody species. **In Vitro Cellular & Developmental Biology – Plant**, v.58, p.865–875, 2022. DOI: 10.1007/s11627-022-10275-8.

DE JONG, A.J.; CORDEWENER, J.; LO SCHIAVO, F.; TERZI, M.; VANDEKERCKHOVE, J.; VAN KAMMEN, A.; DE VRIES, S.C. A carrot somatic embryo mutant is rescued by chitinase. **The Plant Cell**, v.4, p.425–433, 1992. DOI: 10.1105/tpc.4.4.425.

DE JONG, A.J.; HEIDSTRA, R.; SPAINK, H.P.; HARTOG, M.; MEIJER, E.; HENDRIKS, T.; LO SCHIAVO, F.; TERZI, M.; BISSELING, T.; VAN KAMMEN, A.; DE VRIES, S.C. *Rhizobium* lipooligosaccharides rescue a carrot somatic embryo mutant. **The Plant Cell**, p.615–620, 1993. DOI: 10.1105/tpc.5.6.615.

DEMURA, T. Tracheary element differentiation. **Plant Biotechnology Reports**, v.8, p.17–21,2013. DOI: 10.1007/s11816-013-0293-0.

DICKMAN, M.B.; WILLIAMS, B.; LI, Y.; DE FIGUEIREDO, P.; WOLPERT, T. Reassessing apoptosis in plants. **Nature Plants**, v.3, p.773–779, 2017. DOI: 10.1038/s41477-017-0020-x.

FRANKLIN-TONG, V.E.; GOURLAY, C.W. A role for actin in regulating apoptosis/programmed cell death: evidence spanning yeast, plants and animals. **Biochemical Journal**, v.413, p.389–404, 2008. DOI: 10.1042/bj20080320.

FUKUDA, H.; KOMAMINE, A. Establishment of an Experimental System for the Study of Tracheary Element Differentiation from Single Cells Isolated from the Mesophyll of *Zinnia elegans.* **Plant Physiology**, v.65, p.57–60, 1980. DOI: 10.1104/pp.65.1.57.

GADJEV, I.; STONE, J.M.; GECHEV, T. Chapter 3: Programmed Cell Death in Plants. In: **International Review of Cell and Molecular Biology**. [s.l: s.n.]. p.87–144. DOI: 10.1016/s1937-6448(08)01403-2.

GAMBORG, O.L.; MILLER, R.; OJIMA, K. Nutrient requirements of suspension cultures of soybean root cells. **Experimental Cell Research**, v.50, p.151–158, 1968. DOI: 10.1016/0014-4827(68)90403-5.

GECHEV, T.; VAN BREUSEGEM, F.; STONE, J.M.; DENEV, I.; LALOI, C. Reactive oxygen species as signals that modulate plant stress responses and programmed cell death. **BioEssays**, v.28, p.1091–1101, 2006. DOI: 10.1002/bies.20493.

GERHARDT, L.B.A; MAGIOLI, C.; MARGIS, R.; SACHETTO-MARTINS, G.;

MARGIS-PINHEIRO, M. AtchitIV gene expression is stimulated under abiotic stresses and is spatially and temporally regulated during embryo development. **Genetics and Molecular Biology**, v.27, p.118–123, 2004. DOI: 10.1590/s1415-47572004000100020.

GIANNOPOLITIS, C.N.; RIES, S.K. Superoxide dismutases. **Plant Physiology**, v.59, p.309–314, 1977. DOI: 10.1104/pp.59.2.309.

GIORGI, C.; ROMAGNOLI, A.; PINTON, P.; MENEGHESSO, G. CA_{2+} signaling, mitochondria and cell death. **Current Molecular Medicine**, v.8, p.119–130, 2008. DOI: 10.2174/156652408783769571.

HATSUGAI, N.; IWASAKI, S.; TAMURA, K.; KONDO, M.; FUJI, K.; OGASAWARA, K.; NISHIMURA, M.; HARA-NISHIMURA, I. A novel membrane fusion-mediated plant immunity against bacterial pathogens. **Genes & Development**, v.23, p.2496–2506, 2009. DOI: 10.1101/gad.1825209.

HAVIR, E.A.; McHALE, N.A. Biochemical and developmental characterization of multiple forms of catalase in tobacco leaves. **Plant Physiology**, v.84, p.450–455, 1987. DOI: 10.1104/pp.84.2.450.

HILDEBRANDT, T.M.; NUNES-NESI, A.; ARAÚJO, W.L.; BRAUN, H. Amino acid catabolism in plants. **Molecular Plant**, v.8, p.1563–1579, 2015. DOI: 10.1016/j.molp.2015.09.005.

HODGES, D.M.; DELONG, J.M.; FORNEY, C.F.; PRANGE, R.K. Improving the thiobarbituric acid-reactive-substances assay for estimating lipid peroxidation in plant tissues containing anthocyanin and other interfering compounds. **Planta**, v.207, p.604–611, 1999. DOI: 10.1007/s004250050524.

HUANG, S.; HILL, R.D.; WALLY, O.; DIONISIO, G.; AYELE, B.T.; JAMI, S.K.; STASOLLA, C. Hemoglobin Control of Cell Survival/Death decision regulates in vitro plant embryogenesis. **Plant Physiology**, v.165, p.810–825, 2014. DOI: 10.1104/pp.114.239335.

HUH, S.U. Evolutionary diversity and function of metacaspases in plants: similar to but not caspases. **International Journal of Molecular Sciences**, v.23, p.4588, 2022. DOI: 10.3390/ijms23094588.

IAKIMOVA, E.T.; WOLTERING, E.J. Xylogenesis in zinnia (*Zinnia elegans*) cell cultures: unravelling the regulatory steps in a complex developmental programmed cell death event. **Planta**, v.245, p.681–705, 2017. DOI: 10.1007/s00425-017-2656-1.

IAREMA, L.; DA CRUZ, A.C.F.; SALDANHA, C.W.; DIAS, L.L.C.; VIEIRA, R.F.; DE OLIVEIRA, E.J.; OTONI, W.C. Photoautotrophic propagation of Brazilian ginseng [*Pfaffia glomerata* (Spreng.) Pedersen]. **Plant Cell, Tissue and Organ Culture**, v.110, p.227–238,

2012. DOI: 10.1007/s11240-012-0145-6.

ISHIKAWA, T.; TAKAHARA, K.; HIRABAYASHI, T.; MATSUMURA, H.; FUJISAWA, S.; TERAUCHI, R.; UCHIMIYA, H.; KAWAI-YAMADA, M. Metabolome analysis of responseto oxidative stress in rice suspension cells overexpressing cell death suppressor BAX inhibitor-1. **Plant & Cell Physiology**, v.51, p.9–20, 2009. DOI: 10.1093/pcp/pcp162.

IZUMI, M.; HIDEMA, J.; MAKINO, A.; ISHIDA, H. Autophagy contributes to nighttime energy availability for growth in arabidopsis. **Plant Physiology**, v.161, p.1682–1693, 2013. DOI: 10.1104/pp.113.215632.

JONES, R.L.; OUGHAM, H.J.; THOMAS, H.; WAALAND, S.D. **The molecular life of plants**. [s.l: s.n.].

KAPOOR, K.; MIRA, M.M.; AYELE, B.T.; NGUYEN, T.-N.; HILL, R.D.; STASOLLA, C. Phytoglobins regulate nitric oxide-dependent abscisic acid synthesis and ethylene-induced program cell death in developing maize somatic embryos. **Planta**, v.247, p.1277–1291, 2018. DOI: 10.1007/s00425-018-2862-5.

KARNOVSKY, M.J. A formaldehyde-glutaraldehyde fixative of high osmolality for use in electron-microscopy. **Journal of Cell Biology**, v.27, 1965.

KHAN, T.A.; KHAN, M.A.; KARAM, K.; ULLAH, N.; MASHWANI, Z.; NADHMAN, A. Plant in vitro Culture Technologies; A Promise Into Factories of Secondary Metabolites Against COVID-19. **Frontiers in Plant Science**, v.12, 2021. DOI: 10.3389/fpls.2021.610194.KNEESHAW, S.; KEYANI, R.; DELORME-HINOUX, V.; IMRIE, L.; LOAKE, G.J.;

BIHAN, T.L.; REICHHELD, J.; SPOEL, S.H. Nucleoredoxin guards against oxidative stress by protecting antioxidant enzymes. **Proceedings of the National Academy of Sciences of the United States of America**, v.114, p.8414–8419, 2017. DOI: 10.1073/pnas.1703344114.

KOZAI, T.; NGUYEN, Q.T. Photoautotrophic micropropagation of woody and tropical plants. In: **Forestry sciences**. [s.l: s.n.]. p.757–781. DOI: 10.1007/978-94-010-0125-0_26.

KOZAI, T.; SEKIMOTO, K. Effects of the number of air changes per hour of the closed vessel and the photosynthetic photon flux on the carbon dioxide concentration inside the vessel and the growth of strawberry plantlets in vitro. **Seibutsu Kankyō ChōSetsu**, v.26, p.21–29, 1988. DOI: 10.2525/ecb1963.26.21.

KREBS, J. The role of calcium in apoptosis. **BioMetals**, v.11, p.375–382, 1998. DOI: 10.1023/a:1009226316146.

KUBOTA, C.; KOZAI, T. Growth and Net Photosynthetic Rate of *Solanun tuberosum* in Vitrounder Forced and Natural Ventilation. **Hortscience**, v.27, p.1312–1314, 1992. DOI:

10.21273/hortsci.27.12.1312.

LEROUX, O. Collenchyma: a versatile mechanical tissue with dynamic cell walls. **Annals of Botany**, v.110, p.1083–1098, 2012. DOI: 10.1093/aob/mcs186.

LI, J.; LIU, J.; WANG, G.; YUNG, J.; LI, G.; CHEN, S.; LI, Z.; GUO, J.; ZHANG, C.; YANG, Y.; KIM, W.Y.; YUN, D.J.; SCHUMAKER, K.S.; CHEN, Z.; GUO, Y. A chaperone function of NO CATALASE ACTIVITY1 is required to maintain catalase activity and for multiple stress responses in arabidopsis. **The Plant Cell**, v.27, p.908–925, 2015. DOI: 10.1105/tpc.114.135095.

LI, S.; SHEN, L.; WANG, J.; CHEN, Z.; ZHANG, Y.; DUAN, J.; LIU, P.; WANG, X.; GUO, J. Responses of physiological, morphological and anatomical traits to abiotic stress in woody plants. **Forests**, v.14, p.1784, 2023. DOI: 10.3390/f14091784.

LI, X.; GAO, X.; WEI, Y.; DENG, L.; OUYANG, Y.; CHEN, G.; LI, X.; ZHANG, Q.; WU, C. Rice APOPTOSIS INHIBITOR5 Coupled with Two DEAD-Box Adenosine 5′-Triphosphate-Dependent RNA Helicases Regulates Tapetum Degeneration. **The Plant Cell**, v.23, p.1416–1434, 2011a. DOI: 10.1105/tpc.110.082636.

LI, X.; ROY, K.L.; MOGHADDAM, M.R.B.; VANHAECKE, M.; LAMMENS, W.; ROLLAND, F.; VAN DEN ENDE, W. Exploring the neutral invertase–oxidative stress defence connection in Arabidopsis thaliana. **Journal of Experimental Botany**, v.62, p.3849–3862, 2011b. DOI: 10.1093/jxb/err069.

LIU, H.; HAO, N.; JIA, Y.; LIU, X.; NI, X.; WANG, M.; LIU, W. The ethylene receptor regulates *Typha angustifolia* leaf aerenchyma morphogenesis and cell fate. **Planta**, v.250, p.381–390, 2019. DOI: 10.1007/s00425-019-03177-4.

LIU, Y.; OFFLER, C.E.; RUAN, Y. Regulation of fruit and seed response to heat and drought by sugars as nutrients and signals. **Frontiers in Plant Science**, v.4, 2013. DOI: 10.3389/fpls.2013.00282.

LOCATO, V.; DE GARA, L. Programmed cell Death in Plants: An Overview. In: **Methods inmolecular biology**. [s.l: s.n.]. p.1–8. DOI: 10.1007/978-1-4939-7668-3_1.

MACCARRONE, M.; CATANI, M.V.; AGRÒ, A.F.; MELINO, G. Involvement of 5-lipoxygenase in programmed cell death of cancer cells. **Cell Death & Differentiation**, v.4, p.396–402, 1997. DOI: 10.1038/sj.cdd.4400255.

MACCARRONE, M.; MELINO, G.; FINAZZI-AGRÒ, A. Lipoxygenases and their involvement in programmed cell death. **Cell Death & Differentiation**, v.8, p.776–784, 2001. DOI: 10.1038/sj.cdd.4400908.

MACCARRONE, M.; SALUCCI, M.L.; MELINO, G.; ROSATO, N.; FINAZZI-AGRÒ, A.

The early phase of apoptosis in human neuroblastoma CHP100 cells is characterized by Lipoxygenase-dependent ultraweak light emission. **Biochemical and Biophysical Research Communications**, v.265, p.758–762, 1999. DOI: 10.1006/bbrc.1999.1744.

MARTINS, J.P.R.; VERDOODT, V.; PASQUAL, M.; DE PROFT, M. Impacts of photoautotrophic and photomixotrophic conditions on in vitro propagated *Billbergia zebrina* (Bromeliaceae). **Plant Cell, Tissue and Organ Culture**, v.123, p.121–132, 2015. DOI: 10.1007/s11240-015-0820-5.

MURASHIGE, T.; SKOOG, F. A Revised Medium for Rapid Growth and Bio Assays with Tobacco Tissue Cultures. **Physiologia Plantarum**, v.15, p.473–497, 1962. DOI: 10.1111/j.1399-3054.1962.tb08052.x.

MURGIA, I.; TARANTINO, D.; VANNINI, C.; BRACALE, M.; CARRAVIERI, S.; SOAVE, C. Arabidopsis thaliana plants overexpressing thylakoidal ascorbate peroxidase show increased resistance to Paraquat-induced photooxidative stress and to nitric oxide-induced cell death. **The Plant Journal**, v.38, p.940–953, 2004. DOI: 10.1111/j.1365-313x.2004.02092. x.

NAKAMURA, K.; BOSSY-WETZEL, E.; BURNS, K.; FADEL, M.P.; LOZYK, M.D.; GOPING, I.S.; OPAS, M.; BLEACKLEY, R.C.; GREEN, D.R.; MICHALAK, M. Changes in endoplasmic reticulum luminal environment affect cell sensitivity to apoptosis. **Journal of Cell Biology**, v.150, p.731–740, 2000. DOI: 10.1083/jcb.150.4.731.

NAKANO, Y.; ASADA, K. Hydrogen Peroxide is Scavenged by Ascorbate-specific Peroxidase in Spinach Chloroplasts. **Plant and Cell Physiology**, 1981. DOI: 10.1093/oxfordjournals.pcp.a076232.

O'BRIEN, T.P.; McCULLY, M.E. The study of Plant Structure: Principles and Selected Methods. **Taxon**, v.31, p.789, 1982. DOI: 10.2307/1219725.

OBŠILOVÁ, V.; ŠILHÁN, J.; BOUŘA, E.; TEISINGER, J.; OBŠIL, T. 14-3-3 proteins: a family of versatile molecular regulators. **Physiological Research**, p.S11–S21, 2008. DOI: 10.33549/physiolres.931598.

PAIVA NETO, V.B.; OTONI, W.C. Carbon sources and their osmotic potential in plant tissue culture: does it matter? **Scientia Horticulturae**, v.97, p.193–202, 2003. DOI: 10.1016/s0304-4238(02)00231-5.

PAJEROWSKA-MUKHTAR, K.M.; DONG, X. A kiss of death—proteasome-mediated membrane fusion and programmed cell death in plant defense against bacterial infection. **Genes & Development**, v.23, p.2449–2454, 2009. DOI: 10.1101/gad.1861609.

PANIS, B.; NAGEL, M.; VAN DEN HOUWE, I. Challenges and prospects for the

conservation of crop genetic resources in field genebanks, in in vitro collections and/or in liquid nitrogen. **Plants**, v.9, p.1634, 2020. DOI: 10.3390/plants9121634.

PARK, J.E.; THI, L.; LIU, Y.; JEONG, B.R. Sucrose Concentration, Light Intensity, and CO_2Concentration Affect Growth and Development of Micropropagated Carnation. **Han-gukwahweyeon-guhoeji**, v.26, p.61–67, 2018. DOI: 10.11623/frj.2018.26.2.04.

PARTAP, S.; KUMAR, A.; SHARMA, N.; JHA, K.K. *Luffa cylindrica*: an important medicinal plant. **Journal of Natural Product and Plant Resources**, v.2, p.127–134, 2012.

PESQUET, E.; TUOMINEN, H. Ethylene stimulates tracheary element differentiation in *Zinnia elegans* cell cultures. **New Phytologist**, v.190, p.138–149, 2011. DOI: 10.1111/j.1469-8137.2010.03600.x.

PESQUET, E.; ZHANG, B.; GORZSÁS, A.; PUHAKAINEN, T.; SERK, H.; ESCAMEZ, S.; BARBIER, O.; GERBER, L.; COURTOIS-MOREAU, C.; ALATALO, E.; PAULÍN, L.; KANGASJÄRVI, J.; SUNDBERG, B.; GOFFNER, D.; TUOMINEN, H. Non-Cell-Autonomous Postmortem Lignification of Tracheary Elements in *Zinnia elegans.* **The Plant Cell**, v.25, p.1314–1328, 2013. DOI: 10.1105/tpc.113.110593.

PRATT, A.H.K.; GOESCHL, J.D. Physiological roles of ethylene in plants. **Annual Review of Plant Physiology**, v.20, p.541–584, 1969. DOI: 10.1146/annurev.pp.20.060169.002545.

PROVOST, P.; SAMUELSSON, B.; RÅDMARK, O. Interaction of 5-lipoxygenase with cellular proteins. **Proceedings of the National Academy of Sciences of the United States ofAmerica**, v.96, p.1881–1885, 1999. DOI: 10.1073/pnas.96.5.1881.

RANTONG, G.; GUNAWARDENA, A.H.L. A. N. Vacuolar processing enzymes, AmVPE1 and AmVPE2, as potential executors of ethylene regulated programmed cell death in the lace plant (*Aponogeton madagascariensis*). **Botany**, v.96, p.235–247, 2018. DOI: 10.1139/cjb-2017-0184.

RAO, R.V.; ELLERBY, H.M.; BREDESEN, D.E. Coupling endoplasmic reticulum stress to the cell death program. **Cell Death & Differentiation**, v.11, p.372–380, 2004. DOI: 10.1038/sj.cdd.4401378.

REIS, P. A. B.; FONTES, E.P.B. N-rich protein (NRP)-mediated cell death signaling. **Plant Signaling & Behavior**, v.7, p.628–632, 2012. DOI: 10.4161/psb.20111.

REIS, P.A.; ROSADO, G.L.; SILVA, L.A.C.; DE OLIVEIRA, L.C.; OLIVEIRA, L.B.; COSTA, M.D.L.; ALVIM, F.C.; FONTES, E.P.B. The binding protein BIP attenuates Stress-Induced cell death in soybean via modulation of the N-Rich Protein-Mediated signaling pathway. **Plant Physiology**, v.157, p.1853–1865, 2011. DOI: 10.1104/pp.111.179697.

REIS, R.L.; VALE, E.M.; DE SOUSA, K.R.; SANTA–CATARINA, C.; SILVEIRA, V.

Pretreatment free of 2,4-dichlorophenoxyacetic acid improves the differentiation of sugarcane somatic embryos by affecting the hormonal balance and the accumulation of reserves. **Plant Cell, Tissue and Organ Culture**, v.145, p.101–115, 2021. DOI: 10.1007/s11240-020-01995-z.

RIBEIRO, A.; DE TOLEDO PICOLI, E.A.; LANI, E.R.G.; VENDRAME, W.A.; OTONI, W.C. The influence of flask sealing on in vitro morphogenesis of eggplant (*Solanum melongena* L.). **In Vitro Cellular & Developmental Biology – Plant**, v.45, p.421–428, 2009.DOI: 10.1007/s11627-008-9183-5.

ROHÁČEK, K. Chlorophyll Fluorescence Parameters: the definitions, photosynthetic meaning, and mutual relationships. **Photosynthetica**, v.40, p.13–29, 2002. DOI: 10.1023/a:1020125719386.

RUAN, Y. Sucrose metabolism: gateway to diverse carbon use and sugar signaling. **Annual Review of Plant Biology**, v.65, p.33–67, 2014. DOI:10.1146/annurev-arplant-050213-040251.

RUAN, Y.; JIN, Y.; YANG, Y.; LI, G.; BOYER, J.S. Sugar input, metabolism, and signaling mediated by invertase: roles in development, yield potential, and response to drought andheat. **Molecular Plant**, v.3, p.942–955, 2010. DOI: 10.1093/mp/ssq044.

SALDANHA, C.W.; OTONI, C.G.; DE AZEVEDO, J.L.F.; DIAS, L.L.C.; RÊGO, M.M.D.; OTONI, W.C. A low-cost alternative membrane system that promotes growth in nodal cultures of Brazilian ginseng [*Pfaffia glomerata* (Spreng.) Pedersen]. **Plant Cell, Tissue and Organ Culture**, v.110, p.413–422, 2012. DOI: 10.1007/s11240-012-0162-5.

SANTOS, G.C.; CARDOSO, F.P.; MARTINS, A.D.; PASQUAL, M.; OSSANI, P.C.; QUEIROZ, J.M.; REZENDE, R.A.L.S.; SOARES, J.D.R. Effect of light and sucrose on photoautotrophic and photomixotrophic micropropagation of *Physalis angulata*. **Bioscience Journal**, v.36, 2020. DOI: 10.14393/bj-v36n4a2020-47738.

SCHNEIDER, C.A.; RASBAND, W.; ELICEIRI, K.W. NIH Image to ImageJ: 25 years of image analysis. **Nature Methods**, v.9, p.671–675, 2012. DOI: 10.1038/nmeth.2089.

SCHNEIDER, H.; WOJCIECHOWSKI, T.; POSTMA, J.; BROWN, K.M.; LYNCH, J.P. Ethylene modulates root cortical senescence in barley. **Annals of Botany**, v.122, p.95–105, 2018. DOI: 10.1093/aob/mcy059.

SCHRÖDER, M.; KAUFMAN, R.J. ER stress and the unfolded protein response. **Mutation Research/Fundamental and Molecular Mechanisms of Mutagenesis**, v.569, p.29–63, 2005. DOI: 10.1016/j.mrfmmm.2004.06.056.

ŠEVČÍKOVÁ, H.; LHOTÁKOVÁ, Z.; HAMET, J.; LIPAVSKÁ, H. Mixotrophic in vitro

cultivations: the way to go astray in plant physiology. **Physiologia Plantarum**, v.167, p.365–377, 2019. DOI: 10.1111/ppl.12893.

SHAHZAD, A.; SHARMA, S.; PARVEEN, S.; SAEED, T.; SHAHEEN, A.; AKHTAR, R.; YADAV, V.; UPADHYAY, A.; AHMAD, Z. Historical perspective and basic principles of plant tissue culture. In: **Springer eBooks**. [s.l: s.n.]. p.1–36. DOI:10.1007/978-981-10-2961-5_1.

SHANNON, P.; MARKIEL, A.; OZIER, O.; BALIGA, N.S.; WANG, J.T.; RAMAGE, D.; AMIN, N.; SCHWIKOWSKI, B.; IDEKER, T. Cytoscape: a software environment for integrated models of biomolecular interaction networks. **Genome Research**, v.13, p.2498–2504, 2003. DOI: 10.1101/gr.1239303.

SILVA, S.T.; BERTOLUCCI, S.K.V.; DA CUNHA, S.H.B.; LAZZARINI, L.E.S.; TAVARES, M.C.; PINTO, J.E.B.P. Effect of light and natural ventilation systems on the growth parameters and carvacrol content in the in vitro cultures of *Plectranthus amboinicus* (Lour.) Spreng. **Plant Cell, Tissue and Organ Culture**, v.129, p.501–510, 2017. DOI: 10.1007/s11240-017-1195-6.

SILVA, T.D.; CHAGAS, K.; BATISTA, D.S.; FELIPE, S.H.S.; LOUBACK, E.; MACHADO,L.T.; FERNANDES, A.M.; BUTTRÓS, V.H.T.; KOEHLER, A.D.; FARIAS, L.M.; SANTOS, A.F.; SILVA, P.O.; OTONI, W.C. Morphophysiological in vitro performance of Brazilian ginseng (*Pfaffia glomerata* (Spreng.) Pedersen) based on culture medium formulations. **In Vitro Cellular & Developmental Biology – Plant**, v.55, p.454–467, 2019. DOI: 10.1007/s11627-019-10003-9.

SIMÕES, M.S.; FERREIRA, S.S.; GRANDIS, A.; RENCORET, J.; PERSSON, S.; FLOH, E.I.S.; FERRAZ, A.; DEL RÍO, J.C.; BUCKERIDGE, M.S.; CESARINO, I. Differentiation of tracheary elements in sugarcane suspension cells involves changes in secondary walldeposition and extensive transcriptional reprogramming. **Frontiers in Plant Science**, v.11, 2020. DOI: 10.3389/fpls.2020.617020.

SUN, M.; LV, J.; ZHANG, Y.; ZHANG, L.; CHEN, J.; GE, Y.; LǏ, J. Expression analysis of metacaspase (MC) gene family in response to ethylene signal during apple fruit ripening. **Plant Molecular Biology Reporter**, 2024. DOI: 10.1007/s11105-024-01435-8.

SYCHTA, K.; SŁOMKA, A.; KUTA, E. Insights into Plant Programmed Cell Death Induced by Heavy Metals—Discovering a Terra Incognita. **Cells**, v.10, p.65, 2021. DOI: 10.3390/cells10010065.

SZKLARCZYK, D.; KIRSCH, R.; KOUTROULI, M.; NASTOU, K.C.; MEHRYARY, F.;HACHILIF, R.; GABLE, A.L.; FANG, T.; DONCHEVA, N.T.; PYYSALO, S.; BORK,

P.; JENSEN, L.J.; VON MERING, C. The STRING database in 2023: protein–protein association networks and functional enrichment analyses for any sequenced genome of interest. **Nucleic Acids Research**, v.51, p.D638–D646, 2022. DOI: 10.1093/nar/gkac1000.

TAIZ, L.; ZEIGER, E.; MØLLER, I.M.; MURPHY, A.S. Plant physiology and development. In: **Oxford University Press eBooks**. [s.l: s.n.]. DOI: 10.1093/hesc/9780197614204.001.0001.

TAVARES, E.Q.P.; GRANDIS, A.; LEMBKE, C.G.; SOUZA, G.M.; PURGATTO, E.; DE SOUZA, A.P.; BUCKERIDGE, M.S. Roles of auxin and ethylene in aerenchyma formation in sugarcane roots. **Plant Signaling & Behavior**, v.13, p.e1422464, 2018. DOI: 10.1080/15592324.2017.1422464.

VALANDRO, F.; MENGUER, P.K.; CABREIRA-CAGLIARI, C.; MARGIS-PINHEIRO, M.; CAGLIARI, A. Programmed cell death (PCD) control in plants: New insights from the Arabidopsis thaliana deathosome. **Plant Science**, v.299, p.110603, 2020. DOI: 10.1016/j.plantsci.2020.110603.

VALENTE, M.; FARIA, J.A.Q.A.; SOARES-RAMOS, J.R.L.; REIS, P. A. B.; PINHEIRO, G.L.; PIOVESAN, N.D.; MORAIS, A.T.; DE MENEZES, C.C.E.; CANO, M.A.O.; FIETTO, L.G.; LOUREIRO, M.E.; ARAGÃO, F.J.L.; FONTES, E.P.B. The ER luminal binding protein(BiP) mediates an increase in drought tolerance in soybean and delays drought-induced leaf senescence in soybean and tobacco. **Journal of Experimental Botany**, v.60, p.533–546, 2008. DOI: 10.1093/jxb/ern296.

VAN DURME, M.; NOWACK, M.K. Mechanisms of developmentally controlled cell death in plants. **Current Opinion in Plant Biology**, v.29, p.29–37, 2016. DOI: 10.1016/j.pbi.2015.10.013.

VAN HAUTEGEM, T.; WATERS, A.J.; GOODRICH, J.; NOWACK, M.K. Only in dying, life: programmed cell death during plant development. **Trends in Plant Science**, v.20, p.102–113, 2015. DOI: 10.1016/j.tplants.2014.10.003.

VILLANUEVA, S.L.; MALVESTITI, M.C.; VAN IEPEREN, W.; JOOSTEN, M.H.A.J.; VAN KAN, J.A.L. Red light imaging for programmed cell death visualization and quantification in plant–pathogen interactions. **Molecular Plant Pathology**, v.22, p.361–372, 2021. DOI: 10.1111/mpp.13027.

VORSTER, J.; CULLIS, C.A.; KUNERT, K. Plant vacuolar processing enzymes. **Frontiersin Plant Science**, v.10, 2019. DOI: 10.3389/fpls.2019.00479.

WANG, H.; ZHANG, S.; QU, Y.; GAO, R.; XIAO, Y.; WANG, Z.; ZHAI, R.; YANG, C.; XU,

L. Jasmonic Acid and Ethylene Participate in the Gibberellin-Induced Ovule Programmed Cell Death Process in Seedless Pear ‘1913’ (*Pyrus* hybrid). **International Journal of Molecular Sciences**, v.22, p.9844, 2021. DOI: 10.3390/ijms22189844.

WANG, S.; NARENDRA, S.; FEDOROFF, N.V. Heterotrimeric G protein signaling in the Arabidopsis unfolded protein response. **Proceedings of the National Academy of Sciences of the United States of America**, v.104, p.3817–3822, 2007. DOI: 10.1073/pnas.0611735104.

XU, G.; LI, S.; XIE, K.; ZHANG, Q.; WANG, Y.; TANG, Y.; LIU, D.; HONG, Y.; HE, C.; LIU, Y. Plant ERD2-like proteins function as endoplasmic reticulum luminal protein receptors and participate in programmed cell death during innate immunity. **The Plant Journal**, v.72, p.57–69, 2012. DOI: 10.1111/j.1365-313x.2012.05053.x.

ZHANG, C.; AKHLAQ, M.; YAN, H.; NI, Y.; LIANG, S.; ZHOU, J.; XUE, R.; LI, M.; ADNAN, R.M.; LI, J. Chlorophyll fluorescence parameter as a predictor of tomato growth and yield under CO2 enrichment in protective cultivation. **Agricultural Water Management**,v.284, p.108333, 2023. DOI: 10.1016/j.agwat.2023.108333.

ZHANG, M.; LI, Q.; LIU, T.; LIU, L.; SHEN, D.; ZHU, Y.; LIU, P.; ZHOU, J.; DOU, D. Two Cytoplasmic Effectors of Phytophthora sojae Regulate Plant Cell Death via Interactions with Plant Catalases. **Plant Physiology**, v.167, p.164–175, 2014. DOI: 10.1104/pp.114.252437.

ZHI-SHENG; ZHANG, B.; YUANYUAN; XU, J.; ZONGWANG; XIE, W.; XIANGYANG, X.; LI, Q.; ZHENG-HUI; HE, J.; XINXIANG; PENG, P. Association-Dissociation of Glycolate Oxidase with Catalase in Rice：A Potential Switch to Modulate Intracellular H_2O_2 Levels. **Molecular Plants**, p.737–748, 2016.

ZHU, H.; JIANTING, L.; QINGFANG, W.; CHEN, M.; WANG, B.; ZHANG, Q.; XUE, Z. De novo sequencing and analysis of the transcriptome during the browning of fresh-cut *Luffa cylindrica* “Fusi-3” fruits. **PLOS ONE**, v.12, p.e0187117, 2017. DOI: 10.1371/journal.pone.0187117.

ZOBAYED, S.M.A.; AFREEN, F.; KOZAI, T. Physiology of Eucalyptus plantlets grown photoautotrophically in a scaled-up vessel. **In Vitro Cellular & Developmental Biology – Plant**, v.37, p.807–813, 2001. DOI: 10.1007/s11627-001-0134-7.

Figures and tables

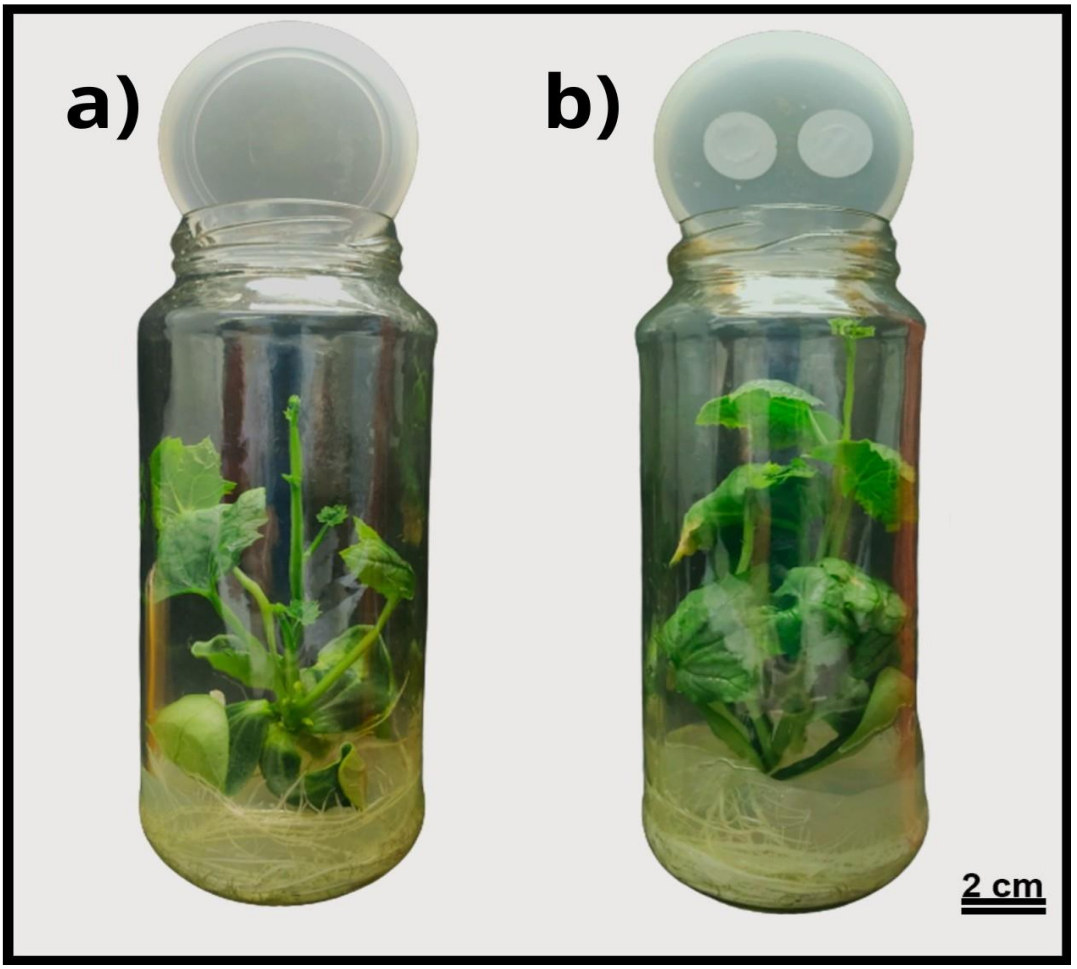

Figure 1. Experimental design. *Luffa cylindrica* after 20 days of in vitro cultivation. **a)** -Photoheterotrophic system (PH); **b)** - Photomixotrophic system (PM).

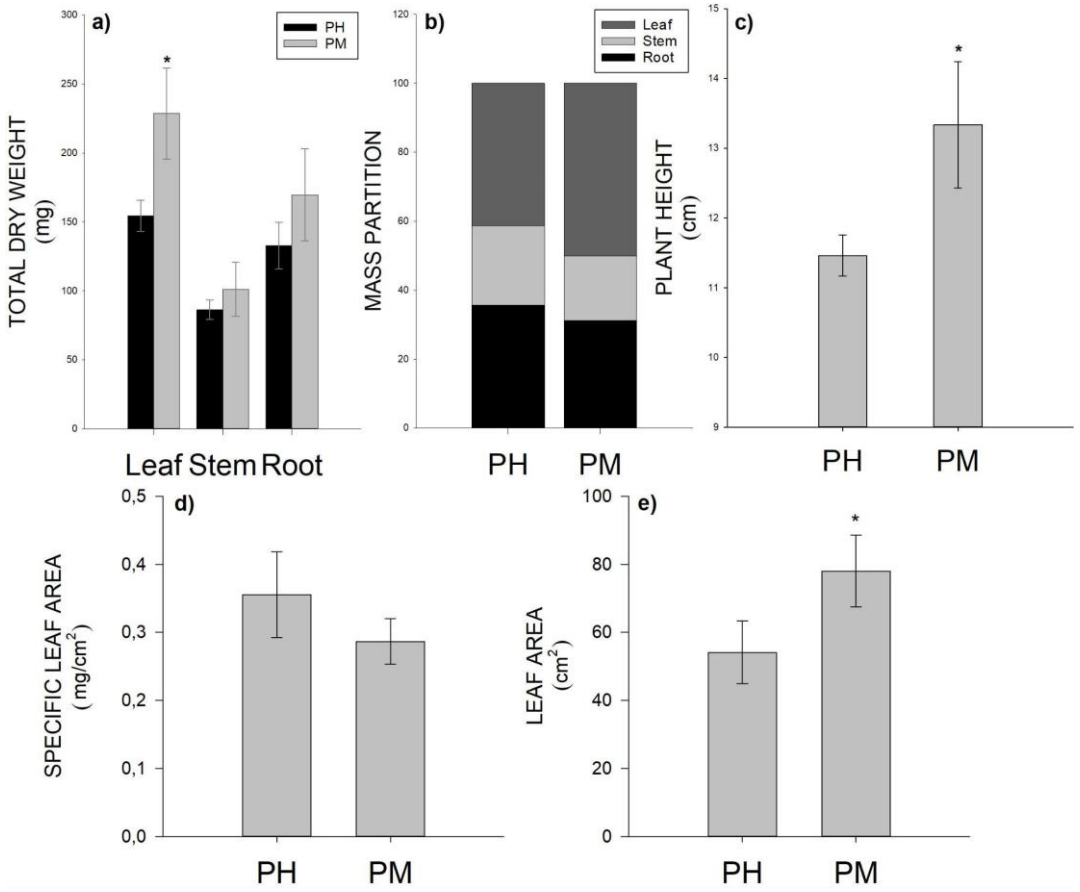

Figure 2. Growth parameters of *Luffa cylindrica* after 20 days of in vitro cultivation under photoheterotrophy (PH) and photomixotrophy (PM). **a)** Dry weight; **b)** Mass partition; **c)** Plant height; **d)** Specific leaf area; **e)** Leaf area. Comparison of means at different CO_2 exchange rates; Asterisks indicate means that differ from each other by Student's t-test at 5% probability; values represent means (n =5) ± standard error.

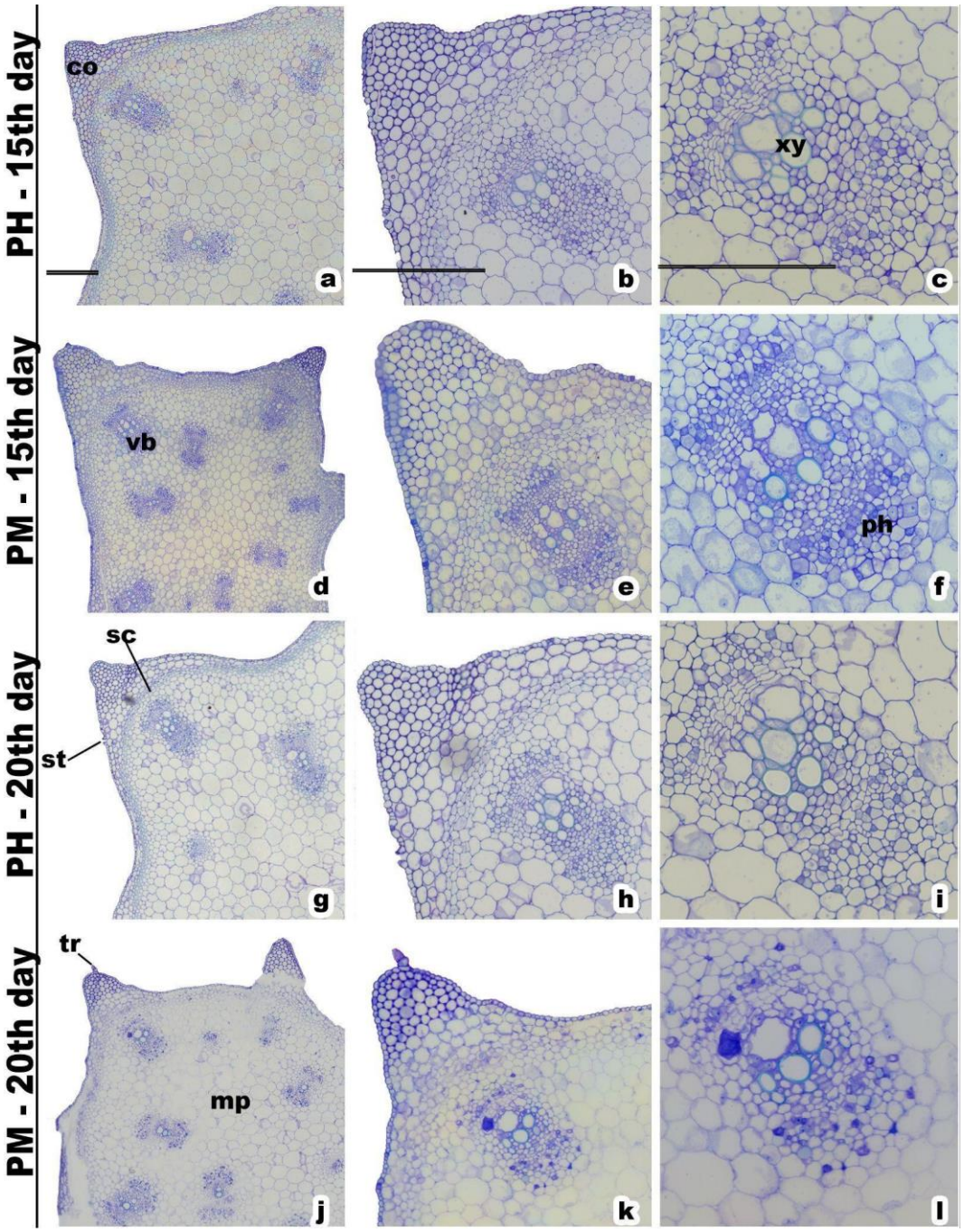

Figure 3: Stem transversal sections (a-l) of *Luffa cylindrica* plants grown in vitro under photoheterotrophy (PH) and photomixotrophy (PM) for 15 and 20 days under different gas exchange conditions. *Abbreviations*: *co*, collenchyma; *sc*, sclerenchyma; *vb*, vascular bundle; *xy*, xylem; *ph*, phloem; *mp*, medullary parenchyma; *st*, stomata; *tr*, trichome. Bars 300 µm (a;b; d; e, g; h; j and k); 200 µm(c; f; i and l).

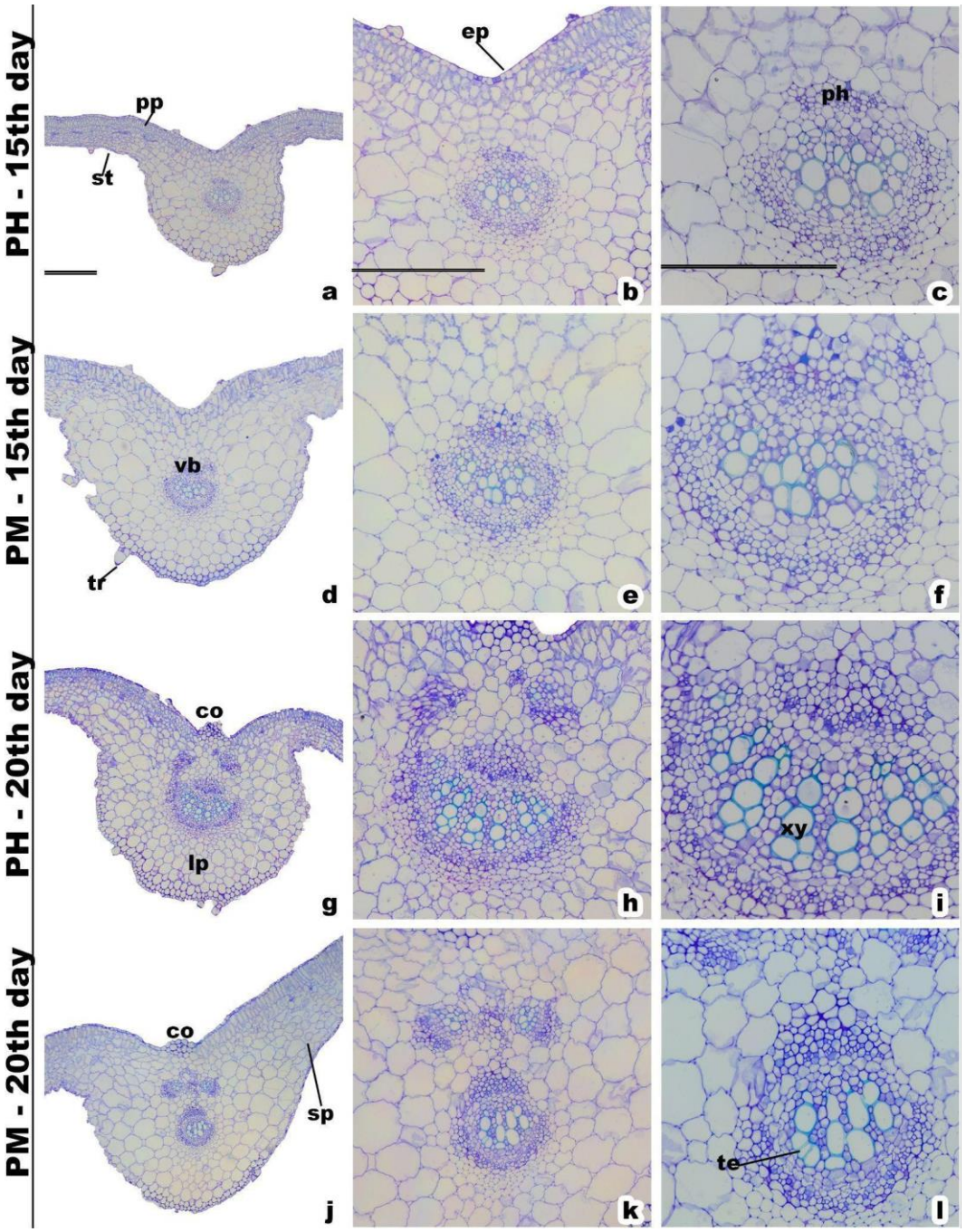

Figure 4: Leaf transversal sections (a-l) in *Luffa cylindrica* plants grown in vitro under photoheterotrophy (PH) and photomixotrophy (PM), 15 and 20 days under different gas exchange conditions. *Abbreviations*: *co*, collenchyma; *ep*, epidermis; *vb*, vascular bundle; *xy*, xylem; *ph*, phloem; *lp*, lacunose parenchyma; *pp*, palisade parenchyma; *sp*, spongy parenchyma; *st*, stomata; *tr*, trichome; *te*, tracheary element. Bars 300 µm (a; b; d; e, g; h; j and k); 200 µm (c; f; i and l).

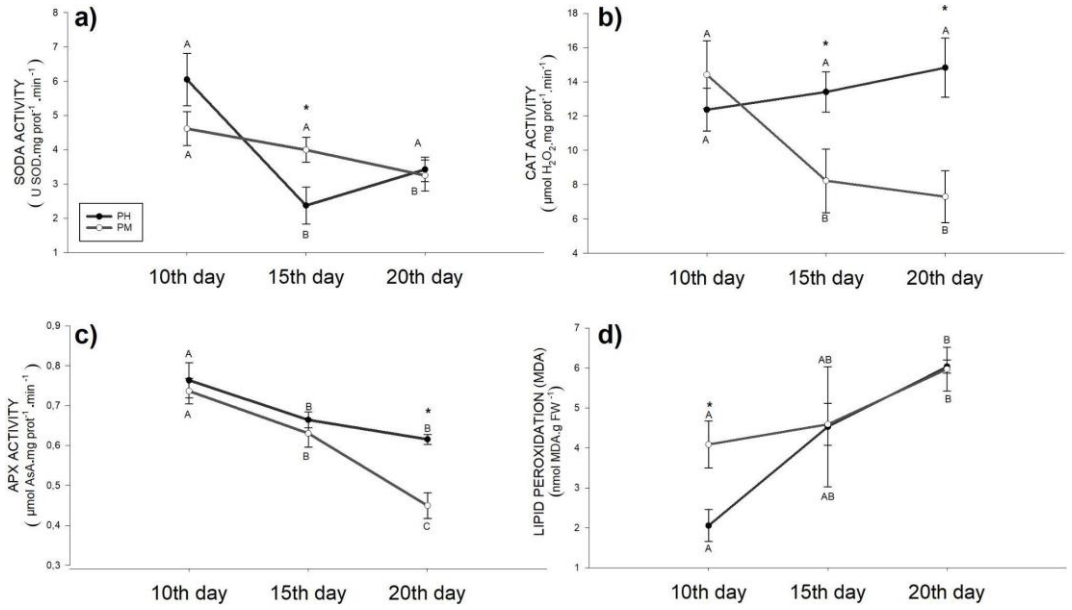

Figure 5. Antioxidant enzyme activity and lipid peroxidation in *Luffa cylindrica* plants grownin vitro under photoheterotrophy (PH) and photomixotrophy (PM) at 10, 15 and 20 days of cultivation. **a)** SOD; **b)** CAT; **c)** APX; **d)** MDA. Capital letters compare means within treatments on different days. Means followed by the same letter do not differ by Duncan's test at 5% probability; values represent means ($n = 5$) ± standard error. Comparison of means at different CO_2 exchange rates; Asterisks indicate means that differ by Student's t-test at 5% probability.

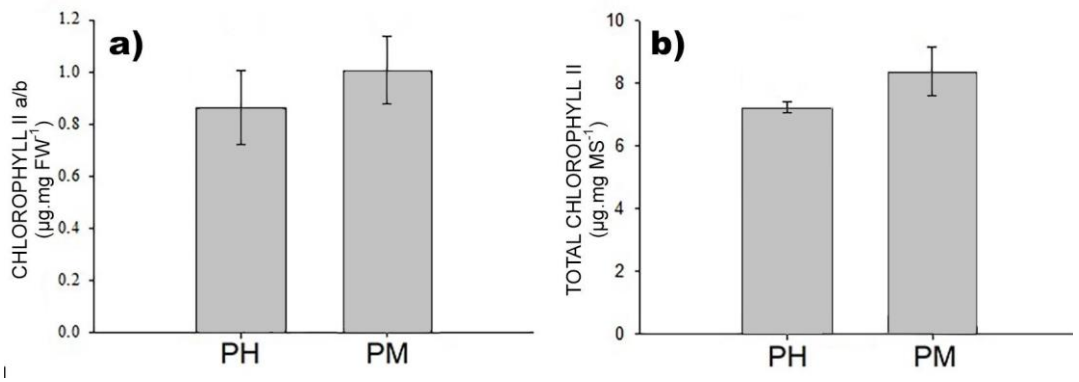

Figure 6: Chlorophyll content in 20-day-old *Luffa cylindrica* plants grown under different gas exchange conditions (photoheterotrophic_PH and photomixotrophic_PM). **a)** Chlorophyll *a*/*b* ratio; **b)** total chlorophyll. Means did not that differ by Student's t-test at 5% probability; values represent means ($n = 5$) ± standard error.

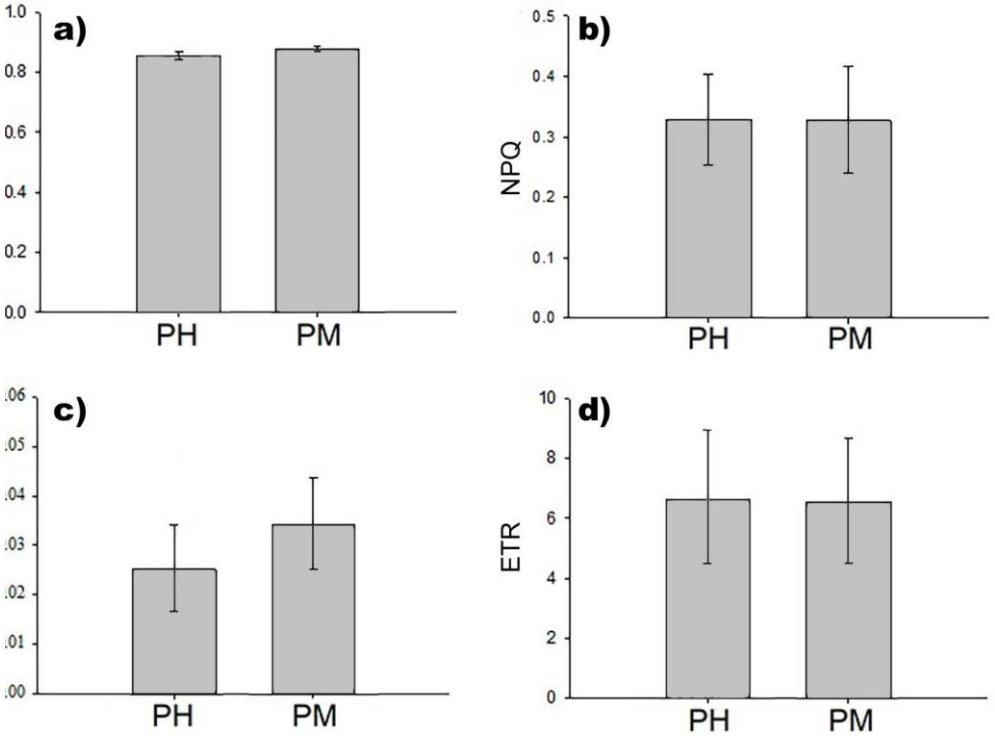

Figure 7: Chlorophyll fluorescence parameters in 20-day-old *Luffa cylindrica* plants grown under different gas exchange conditions (photoheterotrophic_PH and photomixotrophic_PM).

a) maximum quantum yield of photosystem II (*Fv/Fm*); **b)** non-photochemical quenching (NQP); **c)** photochemical quenching (qP); **d)** electron transport rate (ETR). Student's t-test at 5% probability; values represent means ($n = 5$) ± standard error.

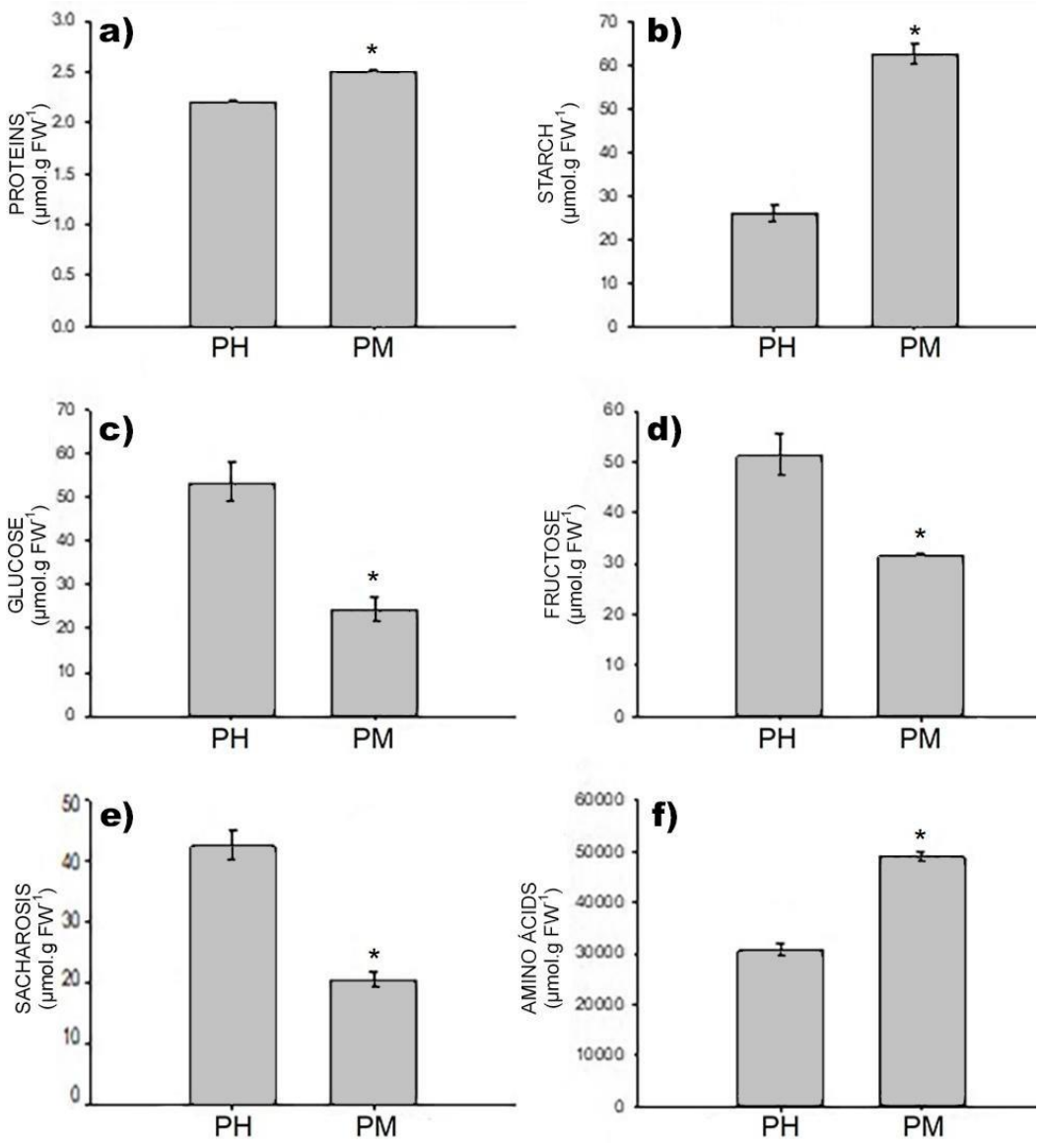

Figure 8: Metabolite levels and protein and starch content in 20-day-old *Luffa cylindrica* plants grown under different gas exchange conditions (photoheterotrophic_PH and photomixotrophic_PM). **a)** Protein; **b)** Starch; **c)** Glucose; **d)** Fructose; **e)** Sucrose; **f)** Amino acids. Asterisks indicate means that differ from each other by Student's t-test at 5% probability; values represent means (n =5) ± standard error.

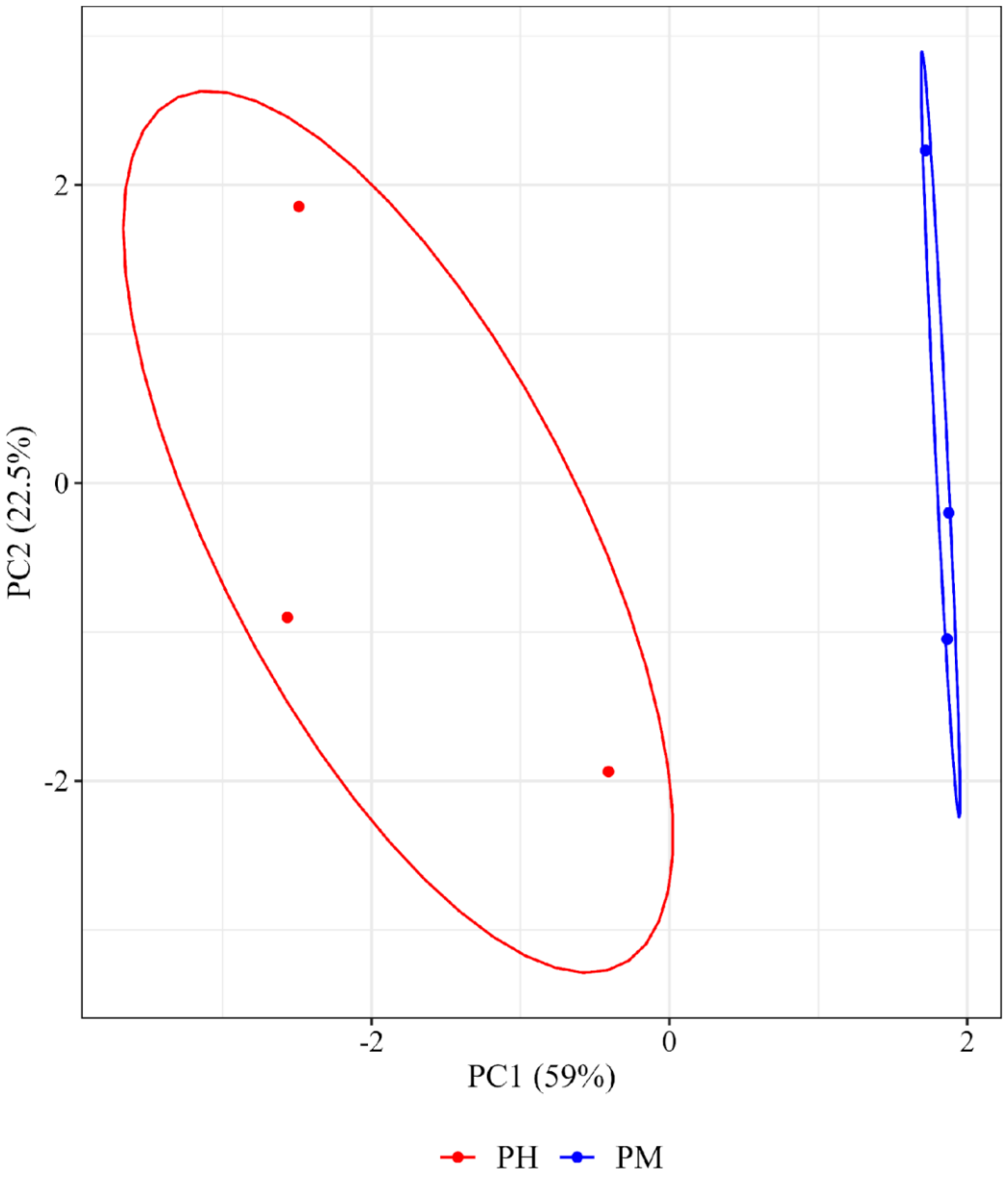

Figure 9. Proteome screening in *Luffa cylindrica* plants grown in vitro under photoheterotrophy (PH) and photomixotrophy (PM), for 20 days of cultivation. Principal component analyses (PCA) results show the separation of protein abundances based on PH and PM treatments.

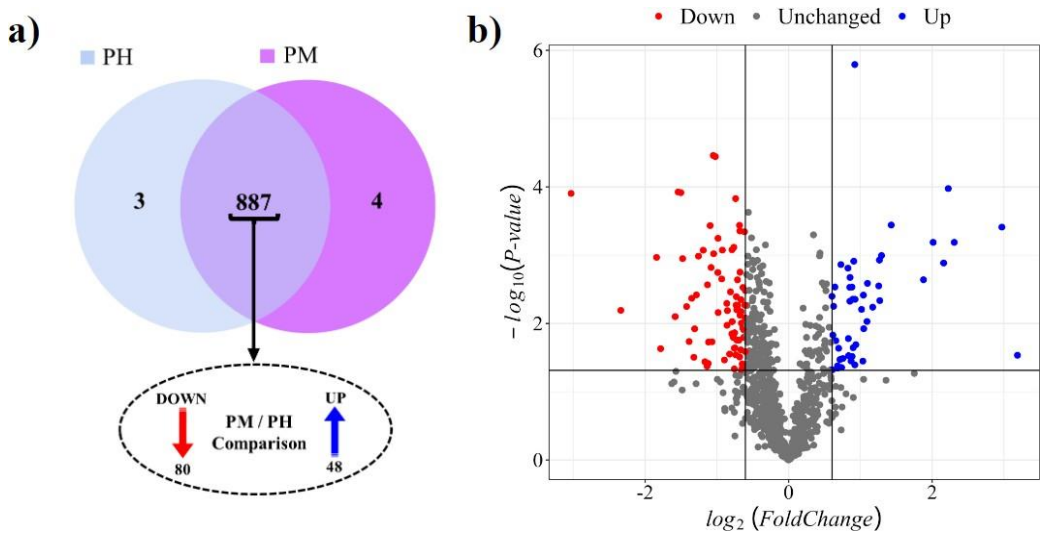

Figure 10. Proteome screening in *Luffa cylindrica* plants grown in vitro under photoheterotrophy_PH and photomixotrophy_PM, for 20 days of cultivation. **a)** Venn diagramof proteins identified in *Luffa cylindrica* comparing PH with PM treatments; **b)**. Volcano plot of differentially accumulated proteins (DAPs) identified from the PM/PH comparison. Proteins with significant Student's t-test (two-tailed; $P < 0.05$) results were considered DAPs,considering up-accumulated if the $\log_2$ fold change (FC) was greater than 0.6 and down-accumulated if the $\log_2$ FC was less than -0.6.

Figure 11. Proteome screening in *Luffa cylindrica* plants grown in vitro under

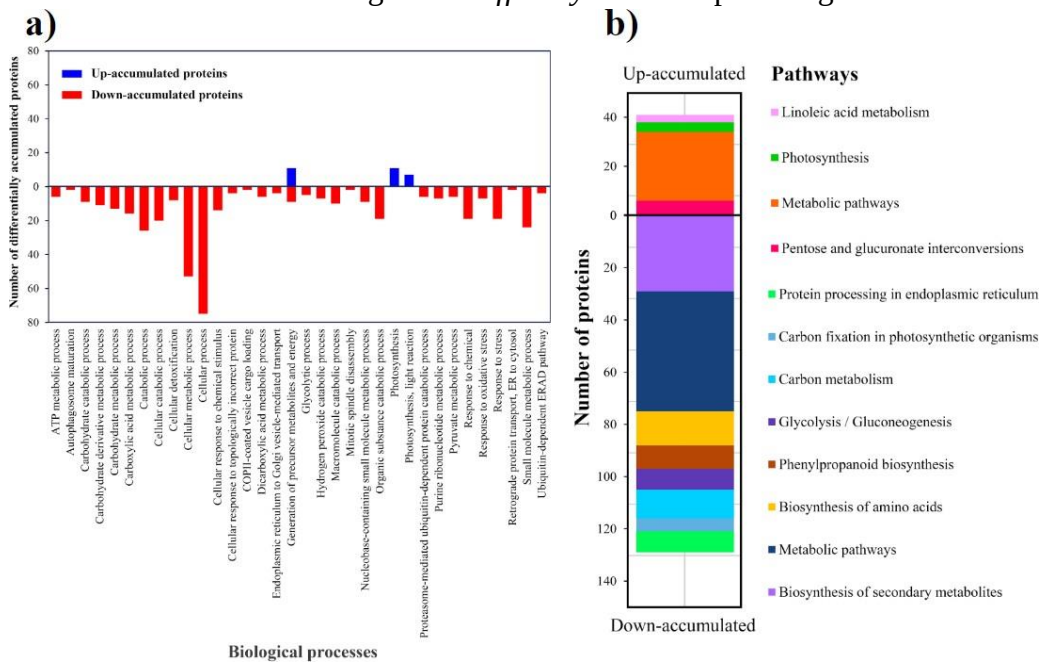

photoheterotrophy and photomixotrophy 20 days of cultivation. **a)** KEGG pathway 128 enrichment analysis ($P \leq 0.01$) of differentially accumulated proteins (DAPs) identified from the PM/PH comparison. **b)** Functional annotation of differentially altered proteins. Biological processes 128 were enriched via Fisher's exact test with $P = 0.01$ to compare proteins in PM/PH comparison.

Suplementary Table 1 - Complete list of identified proteins, functional protein annotations, and configuration parameters in *Luffa cilyndrica* aerial parts grown *in vitro* for 20 days under photoheterotrophy (PH) and photomixotrophy (PM) treatments. Differentially accumulated proteins (DAPs) identified from the PM/PH comparison are characterised by DOWN and UP.

			Normalized total ion account (TIC)						Average				
Accession	**Protein Description (Blast2GO)**	**Reported peptides**	**PH 1**	**PH 2**	**PH 3**	**PM 1**	**PM 2**	**PM 3**	**PH**	**PM**	**T-Test**	**Log2 of Fold Change**	**Differential accumulation**
TRINITY_DN836_c0_g1_i15_p1UniRef100_UPI0002B41AE8	(R)-mandelonitrile lyase 1-like	3	16211	11617	7576	14469	8148	7107	11801	9908	0,60664	-0,25	UNCHANGED
TRINITY_DN129_c1_g1_i6_p1spQ8GYB8OPR2_ARATH	12-oxophytodienoate reductase 2	3	8284	8465	10062	5987	5210	6828	8937	6009	0,01620	-0,57	UNCHANGED
TRINITY_DN51984_c0_g1_i8_p114-3-3	14-3-3	8	128368	134988	122277	81050	92257	86955	128544	86754	0,00103	-0,57	UNCHANGED
TRINITY_DN13777_c0_g3_i2_p1spP9320714310_SOLLC	14-3-3 protein 10	11	38712	47332	49991	31412	44144	43318	45345	39625	0,34435	-0,19	UNCHANGED
TRINITY_DN10183_c0_g1_i1_p1spP9321214337_SOLLC	14-3-3 protein 7	5	27176	31589	28741	20240	23764	21802	29169	21935	0,01173	-0,41	UNCHANGED
TRINITY_DN10969_c1_g3_i2_p1spP462661433_PEA	14-3-3-like protein	11	34631	39278	34399	17768	19826	14916	36103	17503	0,00095	-1,04	DOWN
TRINITY_DN10969_c1_g1_i2_p1spP462661433_PEA	14-3-3-like protein	12	58395	61624	54373	40130	40510	36938	58131	39193	0,00136	-0,57	UNCHANGED
TRINITY_DN7389_c1_g1_i12_p1spQ964531433D_SOYBN	14-3-3-like protein D	6	57331	56392	57396	54180	31521	24571	57040	36757	0,08597	-0,63	UNCHANGED
TRINITY_DN15468_c0_g1_i3_p1spQ9630014337_ARATH	14-3-3-like protein GF14 nu	5				29306	34512	72997	-	45605	-	-	Unique_PM
TRINITY_DN9263_c0_g1_i1_p1spQ96291BAS1A_ARATH	2-Cys peroxiredoxin BAS1, chloroplastic	13	248873	237645	269029	276206	286881	280488	251849	281192	0,03886	0,16	UNCHANGED

TRINITY_DN354_c0_g1_i4_p1UniRef100_UPI000C9D9499	2-iminobutanoate/2-iminopropanoate deaminase-like	3	33756	32191	30160	52487	57617	49206	32036	53103	0,00137	0,73	UP
TRINITY_DN709_c0_g1_i15_p1spQ9C550LEU12_ARATH	2-isopropylmalate synthase 2, chloroplastic	7	11011	15443	15232	16363	19031	22749	13896	19381	0,07969	0,48	UNCHANGED
TRINITY_DN3583_c0_g1_i11_p1spQ9LY74BQMT_ARATH	2-methyl-6-phytyl-1,4-hydroquinone methyltransferase, chloroplastic	5	19051	18802	20222	24094	24948	24808	19358	24617	0,00050	0,35	UNCHANGED
TRINITY_DN28021_c0_g2_i4_p1spQ84V25ENOXE_FRAAN	2-methylene-furan-3-one reductase	4	7462	8777	13263	9006	8516	11483	9834	9669	0,93739	-0,02	UNCHANGED
TRINITY_DN28021_c0_g3_i4_p1spQ84V25ENOXE_FRAAN	2-methylene-furan-3-one reductase	14	176791	202689	185669	151107	160546	179277	188383	163644	0,09248	-0,20	UNCHANGED
TRINITY_DN18587_c0_g1_i1_p1spQ42908PMGI_MESCR	2,3-bisphosphoglycerate-independent phosphoglycerate mutase	20	54208	83543	85267	45245	86395	99015	74339	76885	0,90045	0,05	UNCHANGED
TRINITY_DN42493_c1_g1_i2_p1spO65282CH20_ARATH	20 kDa chaperonin, chloroplastic	7	50034	48570	40563	38050	53160	44694	46389	45301	0,84660	-0,03	UNCHANGED
TRINITY_DN4911_c1_g1_i1_p1UniRef100_UPI0019003BF4	23 kDa jasmonate-induced protein-like	4	4947	7671	7222	5374	8831	10882	6613	8362	0,38977	0,34	UNCHANGED
TRINITY_DN767_c1_g2_i1_p1UniRef100_UPI0019003BF4	23 kDa jasmonate-induced protein-like	6	99735	117960	88437	79004	75245	80069	102044	78106	0,05169	-0,39	UNCHANGED
TRINITY_DN767_c0_g1_i12_p1UniRef100_UPI0019003BF4	23 kDa jasmonate-induced protein-like	11	171772	199215	172768	142331	166093	156718	181252	155047	0,08189	-0,23	UNCHANGED
TRINITY_DN8933_c0_g1_i1_p1spQ39227SMT2_ARATH	24-methylenesterol C-methyltransferase 2	2	8414	8107	7247	6517	5473	6930	7922	6306	0,04401	-0,33	UNCHANGED
TRINITY_DN24347_c2_g1_i10_p1spO48844PSD1A_ARATH	26S proteasome non-ATPase regulatory subunit 1 homolog A	7	27514	27328	27314	20267	18783	21772	27386	20274	0,00119	-0,43	UNCHANGED
TRINITY_DN29_c1_g1_i1_p1spQ9LP45PSD11_ARATH	26S proteasome non-ATPase regulatory subunit 11 homolog	5	16944	20684	20704	20749	16488	18445	19444	18561	0,64123	-0,07	UNCHANGED
TRINITY_DN2544_c0_g4_i2_p1spQ9FIB6PS12A_ARATH	26S proteasome non-ATPase regulatory subunit 12 homolog A	5	17005	19176	18281	10725	13072	14915	18154	12904	0,01842	-0,49	UNCHANGED

TRINITY_DN10445_c0_g1_i1_p1spQ9SIV2PSD2A_ARATH	26S proteasome non-ATPase regulatory subunit 2 homolog A	14	30767	29132	31184	24556	21448	22361	30361	22789	0,00245	-0,41	UNCHANGED
TRINITY_DN3140_c0_g1_i2_p1spO82143PSMDA_ORYSJ	26S proteasome non-ATPase regulatory subunit 4 homolog	2	24606	27623	30588	21107	21385	27115	27605	23202	0,16698	-0,25	UNCHANGED
TRINITY_DN16811_c0_g1_i2_p1spQ93Y35PSMD6_ARATH	26S proteasome non-ATPase regulatory subunit 6 homolog	5	12677	14647	17738	11049	11739	15540	15021	12776	0,33072	-0,23	UNCHANGED
TRINITY_DN169555_c0_g1_i1_p1spO24412PSD7A_ARATH	26S proteasome non-ATPase regulatory subunit 7 homolog A	3	20983	19135	20770	16298	14324	17306	20296	15976	0,01480	-0,35	UNCHANGED
TRINITY_DN11119_c0_g4_i2_p1spQ9SGW3PSD8A_ARATH	26S proteasome non-ATPase regulatory subunit 8 homolog A	5	14662	16156	11418	8271	9505	10989	14079	9588	0,04887	-0,55	UNCHANGED
TRINITY_DN1433_c2_g1_i2_p1spQ9SZD4PRS4A_ARATH	26S proteasome regulatory subunit 4 homolog A	7	21503	22291	19258	11990	15346	15203	21017	14179	0,00862	-0,57	UNCHANGED
TRINITY_DN551_c0_g2_i1_p1spO23894PRS6A_BRACM	26S proteasome regulatory subunit 6A homolog	12	54593	35859	26930	33646	22805	29394	39127	28615	0,29538	-0,45	UNCHANGED
TRINITY_DN7248_c0_g1_i1_p1spP85200PRS6B_HELAN	26S proteasome regulatory subunit 6B homolog	12	27734	22910	26557	29787	27093	32610	25734	29830	0,13016	0,21	UNCHANGED
TRINITY_DN638_c0_g1_i17_p1spO64982PRS7_PRUPE	26S proteasome regulatory subunit 7	5	20114	22250	18667	11775	12107	13362	20344	12415	0,00230	-0,71	DOWN
TRINITY_DN397_c0_g1_i1_p1spQ9C5U3PRS8A_ARATH	26S proteasome regulatory subunit 8 homolog A	6	28152	32508	26120	16846	17562	21374	28927	18594	0,01173	-0,64	DOWN
TRINITY_DN2984_c0_g1_i10_p1spQ9MAK9PS10B_ARATH	26S proteasome regulatory subunit S10B homolog B	17	30056	29442	25482	19429	17414	26419	28327	21087	0,07860	-0,43	UNCHANGED
TRINITY_DN4657_c0_g2_i1_p1UniRef100_UPI000C9D9EC8	28 kDa ribonucleoprotein, chloroplastic	2	6285	7292	10472	10220	11209	14363	8016	11931	0,09220	0,57	UNCHANGED
TRINITY_DN7983_c0_g1_i4_p1spP28644ROC1_SPIOL	28 kDa ribonucleoprotein, chloroplastic	17	93437	100915	102523	119582	126663	140125	98958	128790	0,01090	0,38	UNCHANGED
TRINITY_DN6732_c0_g1_i10_p1UniRef100_UPI0018FFC29A	29 kDa ribonucleoprotein A, chloroplastic	2	13954	15845	13532	11354	16714	17223	14444	15097	0,76122	0,06	UNCHANGED
TRINITY_DN8291_c0_g2_i3_p12OG-FeII_Oxy	2OG-Fe(II)	7	61697	58429	61187	51326	37300	46365	60438	44997	0,02177	-0,43	UNCHANGED

TRINITY_DN26050_c0_g1_i4_p1sp U3KRF2DHQS_ACTCC	3-dehydroquinate synthase, chloroplastic	4	10100	14268	11803	8879	10931	10388	12057	10066	0,21605	-0,26	UNCHANGED
TRINITY_DN14287_c0_g1_i1_p1 UniRef100_A0A6J1EUE3	3-hydroxyacyl-[acyl-carrier-protein] dehydratase	3	27238	26981	9181	45228	36640	24422	21133	35430	0,16765	0,75	UNCHANGED
TRINITY_DN13190_c1_g1_i13_p1 146469at33090 3HCDH_N	3-hydroxyacyl-CoA_ECH_1 Enoyl-CoA	6	18959	16101	20093	12959	12264	15183	18384	13468	0,02925	-0,45	UNCHANGED
TRINITY_DN6316_c0_g1_i1_p1sp Q94AR8LEUC_ARATH	3-isopropylmalate dehydratase large subunit, chloroplastic	6	21191	17059	17899	19962	17214	16638	18716	17938	0,65698	-0,06	UNCHANGED
TRINITY_DN169665_c0_g1_i1_p1 spQ9ZW85LEUD3_ARATH	3-isopropylmalate dehydratase small subunit 1	4	7322	8685	7156	7230	6325	8951	7721	7502	0,82144	-0,04	UNCHANGED
TRINITY_DN7670_c0_g1_i24_p1s pQ56WD9THIK2_ARATH	3-ketoacyl-CoA thiolase 2, — peroxisomal	15	44909	53012	63681	50133	44473	57498	53867	50701	0,65724	-0,09	UNCHANGED
TRINITY_DN6813_c0_g1_i1_p1sp P28643FABG_CUPLA	3-oxoacyl-[acyl-carrier-protein] reductase, chloroplastic	8	45903	47682	61115	56467	41040	39379	51567	45628	0,45908	-0,18	UNCHANGED
TRINITY_DN9414_c0_g1_i5_p1sp P52410KASC1_ARATH	3-oxoacyl-[acyl-carrier-protein] synthase I, chloroplastic	6	27848	37762	41887	27932	32466	38759	35832	33053	0,62232	-0,12	UNCHANGED
TRINITY_DN7924_c0_g1_i2_p1sp P23981AROA1_TOBAC	3-phosphoshikimate 1-carboxyvinyltransferase 1, chloroplastic	7	26753	32768	26792	18007	18995	16900	28771	17967	0,00663	-0,68	DOWN
TRINITY_DN812_c0_g3_i1_p1spP 29344RR1_SPIOL	30S ribosomal protein S1, chloroplastic	7	21047	22121	22817	29660	31183	34297	21995	31713	0,00264	0,53	UNCHANGED
TRINITY_DN4127_c0_g1_i1_p1sp Q9M4Y3RR10_MESCR	30S ribosomal protein S10, chloroplastic	2	20845	25024	28765	19461	28454	31268	24878	26394	0,73825	0,09	UNCHANGED
TRINITY_DN12182_c0_g1_i1_p5s pQ4VZK2RR11_CUCSA	30S ribosomal protein S11, chloroplastic	5	17767	21074	18655	17911	21110	20144	19165	19722	0,70524	0,04	UNCHANGED
TRINITY_DN4171_c1_g1_i10_p5s pQ4VZP4RR2_CUCSA	30S ribosomal protein S2, chloroplastic	6	18909	21347	22283	28831	32450	28121	20846	29801	0,00591	0,52	UNCHANGED
TRINITY_DN7684_c0_g1_i3_p2sp Q4VZN0RR3_CUCSA	30S ribosomal protein S3, chloroplastic	5	69808	17399	16154	24625	26565	25786	34454	25659	0,64515	-0,43	UNCHANGED
TRINITY_DN11369_c1_g1_i1_p1s pQ9ST69RR5_SPIOL	30S ribosomal protein S5, chloroplastic	4	33587	34858	39351	42545	42673	41368	35932	42195	0,02524	0,23	UNCHANGED

TRINITY_DN9032_c0_g1_i2_p1sp F4K0E8ISPG_ARATH	4-hydroxy-3-methylbut-2-en-1-yl diphosphate synthase (ferredoxin), chloroplastic	8	10248	12142	13247	11704	12323	14794	11879	12940	0,45628	0,12	UNCHANGED
TRINITY_DN6448_c3_g1_i1_p1sp Q94B35ISPH_ARATH	4-hydroxy-3-methylbut-2-enyl diphosphate reductase, chloroplastic	2	5345	7627	6969	7783	8433	8538	6647	8251	0,08925	0,31	UNCHANGED
TRINITY_DN10626_c0_g1_i10_p1 40S_S4_C	40S	6	58811	61990	40414	23757	45961	40363	53738	36694	0,14626	-0,55	UNCHANGED
TRINITY_DN2076_c1_g1_i6_p1sp Q9M5M1RS11_EUPES	40S ribosomal protein S11	8	93263	88559	66087	41214	69899	73981	82636	61698	0,19024	-0,42	UNCHANGED
TRINITY_DN2261_c0_g1_i4_p1sp P62302RS13_SOYBN	40S ribosomal protein S13	4	27831	20901	25302	16765	22959	25379	24678	21701	0,41387	-0,19	UNCHANGED
TRINITY_DN11304_c4_g1_i1_p1s pQ9CAX6RS142_ARATH	40S ribosomal protein S14-2	3	10171	15758	8071	7035	8383	8792	11333	8070	0,23796	-0,49	UNCHANGED
TRINITY_DN7927_c0_g1_i1_p1sp Q08112RS151_ARATH	40S ribosomal protein S15-1	2	14932	37069	7267	6426	17054	11800	19756	11760	0,44499	-0,75	UNCHANGED
TRINITY_DN23501_c0_g1_i1_p1s pQ00332RS15A_BRANA	40S ribosomal protein S15a	9	30585	33929	29125	25064	24003	24932	31213	24666	0,01097	-0,34	UNCHANGED
TRINITY_DN86483_c0_g1_i1_p2s pP42798R15A1_ARATH	40S ribosomal protein S15a-1	9	101658	116111	99670	78079	87165	90537	105813	85260	0,03221	-0,31	UNCHANGED
TRINITY_DN1922_c2_g1_i1_p1sp P46293RS16_GOSHI	40S ribosomal protein S16	2	13867	24250	11254	4970	8528	13141	16457	8880	0,17635	-0,89	UNCHANGED
TRINITY_DN5893_c0_g1_i1_p1sp P49215RS17_SOLLC	40S ribosomal protein S17	3	99741	110081	107059	59464	73445	83275	105627	72061	0,01133	-0,55	UNCHANGED
TRINITY_DN37991_c0_g1_i2_p1 UniRef100_UPI00162F028D	40S ribosomal protein S2-4-like	7	122664	131991	96040	69663	91699	79921	116899	80428	0,04346	-0,54	UNCHANGED
TRINITY_DN103726_c0_g1_i2_p2 spQ9STY6RS202_ARATH	40S ribosomal protein S20-2	4	79066	71090	64769	44503	58021	53800	71642	52108	0,02734	-0,46	UNCHANGED
TRINITY_DN2935_c0_g1_i6_p1sp P46297RS23_FRAAN	40S ribosomal protein S23	3	14777	13084	20101	26356	21460	19613	15987	22477	0,09026	0,49	UNCHANGED
TRINITY_DN2964_c3_g1_i1_p1sp Q9LYK9RS263_ARATH	40S ribosomal protein S26-3	3	22351	22100	31889	22010	23644	24652	25447	23435	0,57652	-0,12	UNCHANGED

TRINITY_DN13335_c0_g1_i2_p1sp|Q9FJA6|RS33_ARATH	40S ribosomal protein S3-3	14	40222	49784	31027	18095	21219	18456	40344	19257	0,01860	-1,07	DOWN
TRINITY_DN11891_c0_g1_i3_p1sp|Q9FJA6|RS33_ARATH	40S ribosomal protein S3-3	15	50366	69027	38853	34784	45147	35478	52749	38470	0,20362	-0,46	UNCHANGED
TRINITY_DN85584_c1_g2_i2_p1sp|Q8GTE3|RS3A_CICAR	40S ribosomal protein S3a	10	126895	109254	134619	95285	101639	110667	123589	102530	0,07344	-0,27	UNCHANGED
TRINITY_DN85584_c1_g1_i1_p1sp|P49397|RS3A_ORYSJ	40S ribosomal protein S3a	10	58610	57760	60800	50086	63889	61541	59057	58506	0,90548	-0,01	UNCHANGED
TRINITY_DN10626_c0_g1_i1_p1sp|Q8VYK6|RS43_ARATH	40S ribosomal protein S4-3	10	37029	31240	21745	15884	32656	26016	30005	24852	0,47893	-0,27	UNCHANGED
TRINITY_DN2972_c0_g1_i1_p1sp|Q9ZUT9|RS51_ARATH	40S ribosomal protein S5-1	11	90132	86941	82367	83741	81615	95333	86480	86896	0,93532	0,01	UNCHANGED
TRINITY_DN448_c1_g1_i10_p1sp|O48549|RS61_ARATH	40S ribosomal protein S6-1	6	45687	41921	67769	74797	49511	60472	51792	61594	0,41899	0,25	UNCHANGED
TRINITY_DN48905_c0_g1_i4_p1sp|Q9ZNS1|RS7_AVIMR	40S ribosomal protein S7	9	42963	51034	31007	12921	28123	16453	41668	19165	0,03856	-1,12	DOWN
TRINITY_DN3359_c0_g1_i5_p1sp|Q9C514|RS71_ARATH	40S ribosomal protein S7-1	6	36719	48232	18262	2510	19837	14590	34404	12312	0,09453	-1,48	UNCHANGED
TRINITY_DN1877_c0_g1_i10_p1sp|Q08069|RS8_MAIZE	40S ribosomal protein S8	3	15147	20560	29068	17394	21486	28022	21592	22301	0,89613	0,05	UNCHANGED
TRINITY_DN20719_c0_g1_i1_p1sp|Q9FLF0|RS92_ARATH	40S ribosomal protein S9-2	5	30560	32189	24585	15979	27841	27825	29111	23882	0,31707	-0,29	UNCHANGED
TRINITY_DN6671_c0_g2_i3_p1sp|Q2QLY5|METE1_ORYSJ	5-methyltetrahydropteroyltriglutamate--homocysteine methyltransferase 1	21	70044	76059	68620	45418	54308	56429	71574	52052	0,00868	-0,46	UNCHANGED
TRINITY_DN150333_c0_g1_i1_p1sp|Q9LY66|RK1_ARATH	50S ribosomal protein L1, chloroplastic	3	10438	9974	12142	10942	12686	12053	10851	11894	0,27911	0,13	UNCHANGED
TRINITY_DN1674_c0_g3_i1_p1sp|Q4VZK5|RK2_CUCSA	50S ribosomal protein L2, chloroplastic	6	14042	11973	19260	12279	21034	21659	15092	18324	0,43446	0,28	UNCHANGED
TRINITY_DN4556_c1_g1_i1_p1sp|O80360|RK3_TOBAC	50S ribosomal protein L3, chloroplastic (Fragment)	8	20757	19980	23748	17949	20783	26466	21495	21733	0,93537	0,02	UNCHANGED

TRINITY_DN169205_c0_g1_i1_p1 spO50061RK4_ARATH	50S ribosomal protein L4, chloroplastic	3	11366	10186	15900	12277	8353	16626	12484	12418	0,98332	-0,01	UNCHANGED
TRINITY_DN4335_c0_g1_i2_p1sp P82192RK5_SPIOL	50S ribosomal protein L5, chloroplastic	6	50507	45119	67052	61538	59843	64075	54226	61819	0,32123	0,19	UNCHANGED
TRINITY_DN12481_c0_g1_i1_p1s pQ9FWA36PGD2_ARATH	6-phosphogluconate dehydrogenase, decarboxylating 2	8	9714	10047	7971	5796	6496	7794	9244	6695	0,04285	-0,47	UNCHANGED
TRINITY_DN2818_c0_g1_i1_p1sp Q9FWA36PGD2_ARATH	6-phosphogluconate dehydrogenase, decarboxylating 2	13	45834	46372	36986	31062	35003	39649	43064	35238	0,11704	-0,29	UNCHANGED
TRINITY_DN16556_c6_g1_i1_p1s pQ9FFR36PGD3_ARATH	6-phosphogluconate dehydrogenase, decarboxylating 3, chloroplastic	13	18080	20724	18979	15764	16784	22447	19261	18332	0,69679	-0,07	UNCHANGED
TRINITY_DN4339_c0_g1_i1_p1U niRef100_UPI0019002CBD	6,7-dimethyl-8-ribityllumazine synthase, chloroplastic	6	53282	65639	56908	60205	72018	64148	58610	65457	0,24662	0,16	UNCHANGED
TRINITY_DN3902_c0_g1_i1_p1sp Q9M5M7RL10_EUPES	60S ribosomal protein L10	9	109682	77595	81748	60478	79700	88398	89675	76192	0,35894	-0,24	UNCHANGED
TRINITY_DN2248_c0_g1_i17_p1s pB8B9K6R10A_ORYSI	60S ribosomal protein L10a	5	35622	34650	19598	10967	15795	13504	29957	13422	0,03699	-1,16	DOWN
TRINITY_DN132488_c0_g1_i1_p1 spP42795RL111_ARATH	60S ribosomal protein L11-1	6	149094	154578	122972	116972	114727	133734	142215	121811	0,14926	-0,22	UNCHANGED
TRINITY_DN17935_c0_g1_i1_p1s pQ9FF52RL123_ARATH	60S ribosomal protein L12-3	11	135190	146016	125264	84541	114002	104928	135490	101157	0,03146	-0,42	UNCHANGED
TRINITY_DN13376_c0_g3_i1_p1s pQ9FKC0R13A4_ARATH	60S ribosomal protein L13a-4	3	49136	13325	45059	99966	40697	38042	35840	59568	0,36361	0,73	UNCHANGED
TRINITY_DN21579_c1_g1_i2_p1s pP42791RL182_ARATH	60S ribosomal protein L18-2	2	27927	25547	21659	17206	20293	22366	25044	19955	0,09759	-0,33	UNCHANGED
TRINITY_DN539_c3_g1_i2_p1spQ 940B0RL183_ARATH	60S ribosomal protein L18-3	3	39686	42352	41993	15883	21753	20506	41344	19380	0,00037	-1,09	DOWN
TRINITY_DN3807_c0_g1_i3_p1sp Q9ATF5RL18A_CASSA	60S ribosomal protein L18a	3	33947	32776	26014	16955	41637	37582	30912	32058	0,89347	0,05	UNCHANGED

TRINITY_DN27649_c0_g1_i9_p1sp|P49693|RL193_ARATH	60S ribosomal protein L19-3	2	29626	25603	35333	25627	24657	31984	30187	27423	0,48982	-0,14	UNCHANGED
TRINITY_DN13675_c0_g1_i2_p1sp|Q9M9W1|RL222_ARATH	60S ribosomal protein L22-2	2	15749	22765	8109	5876	7878	11452	15541	8402	0,19060	-0,89	UNCHANGED
TRINITY_DN263_c1_g1_i6_p2sp|P49690|RL23_ARATH	60S ribosomal protein L23	3	54738	76832	41693	19528	35390	34683	57754	29867	0,07215	-0,95	UNCHANGED
TRINITY_DN10472_c0_g1_i4_p1sp|Q9AT35|RL23A_DAUCA	60S ribosomal protein L23a	2	23564	13980	29204	12900	11880	20622	22249	15134	0,24536	-0,56	UNCHANGED
TRINITY_DN71667_c0_g1_i1_p1sp|P51414|RL261_ARATH	60S ribosomal protein L26-1	3	27082	16902	47946	24985	25889	30214	30643	27030	0,71676	-0,18	UNCHANGED
TRINITY_DN32349_c0_g1_i10_p1sp|P49637|R27A3_ARATH	60S ribosomal protein L27a-3	2	10260	14637	11226	11578	15774	16535	12041	14629	0,27222	0,28	UNCHANGED
TRINITY_DN86167_c0_g1_i1_p1sp|Q9M0E2|RL282_ARATH	60S ribosomal protein L28-2	5	56684	75063	33580	23962	30948	32886	55109	29265	0,10359	-0,91	UNCHANGED
TRINITY_DN5050_c0_g1_i12_p1sp|P35684|RL3_ORYSJ	60S ribosomal protein L3	7	24493	28294	31149	20757	35747	28074	27979	28193	0,96612	0,01	UNCHANGED
TRINITY_DN1979_c4_g1_i1_p1sp|Q9XHE4|RL37A_GOSHI	60S ribosomal protein L37a	2	41750	48693	43134	21756	30068	37168	44526	29664	0,03945	-0,59	UNCHANGED
TRINITY_DN4401_c0_g1_i1_p1sp|Q9XF97|RL4_PRUAR	60S ribosomal protein L4	13	64437	68644	65193	55751	79711	57934	66091	64465	0,84424	-0,04	UNCHANGED
TRINITY_DN68582_c0_g1_i1_p1sp|Q9XF97|RL4_PRUAR	60S ribosomal protein L4	14	72646	76110	72996	56391	71117	60936	73917	62815	0,06878	-0,23	UNCHANGED
TRINITY_DN41858_c2_g1_i6_p1sp|Q6UNT2|RL5_CUCSA	60S ribosomal protein L5	9	36918	39108	69318	60121	52179	56209	48448	56170	0,51052	0,21	UNCHANGED
TRINITY_DN2904_c0_g1_i4_p1sp|Q9C9C6|RL62_ARATH	60S ribosomal protein L6-2	7	73955	61081	55270	38589	62957	69480	63435	57009	0,58722	-0,15	UNCHANGED
TRINITY_DN10685_c0_g1_i1_p1sp|Q9LHP1|RL74_ARATH	60S ribosomal protein L7-4	8	71291	94517	41799	32264	54635	56626	69202	47842	0,28061	-0,53	UNCHANGED
TRINITY_DN4424_c15_g1_i1_p1sp|P29766|RL8_SOLLC	60S ribosomal protein L8	5	39661	22500	85760	59376	43936	59674	49307	54329	0,81033	0,14	UNCHANGED
TRINITY_DN10443_c0_g1_i4_p1sp|P30707|RL9_PEA	60S ribosomal protein L9	8	66926	67258	48837	38794	46436	42993	61007	42741	0,04777	-0,51	UNCHANGED

TRINITY_DN10206_c0_g1_i2_p2s pP30707RL9_PEA	60S ribosomal protein L9	9	83882	89410	65422	57646	68843	69152	79571	65213	0,15409	-0,29	UNCHANGED
TRINITY_DN132000_c0_g1_i1_p1 spP27819ILVB3_BRANA	Acetolactate synthase 3, chloroplastic	2	11616	8330	7564	8586	8247	8631	9170	8488	0,61406	-0,11	UNCHANGED
TRINITY_DN365_c0_g1_i12_p1sp Q9C5C4ARGE_ARATH	Acetylornithine deacetylase	12	82372	65323	87548	76354	80486	66416	78414	74419	0,63988	-0,08	UNCHANGED
TRINITY_DN12277_c0_g1_i3_p1s pP29000INVA_SOLLC	Acid beta-fructofuranosidase	4	14517	15069	23372	10843	11747	15898	17653	12830	0,21306	-0,46	UNCHANGED
TRINITY_DN4602_c1_g1_i1_p1U niRef100_A0A6J1DKC3	Acid phosphatase 1-like	5	2798	2396	1879	21056	31694	11777	2358	21509	0,02925	3,19	UP
TRINITY_DN9011_c0_g1_i4_p1U niRef100_A0A6J1G2F8	Acid phosphatase 1-like isoform X2	13	119240	117077	104647	166357	143664	145306	113655	151776	0,01142	0,42	UNCHANGED
TRINITY_DN958_c1_g2_i2_p1Uni Ref100_A0A6J1DVP2	Acidic endochitinase-like	5	8117	9593	11814	10461	12279	11203	9841	11314	0,28581	0,20	UNCHANGED
TRINITY_DN958_c1_g2_i3_p1Uni Ref100_A0A6J1DVP2	Acidic endochitinase-like	8	73109	91796	94647	63988	84890	63599	86517	70826	0,18287	-0,29	UNCHANGED
TRINITY_DN7290_c1_g2_i15_p1 Aconitase_C	Aconitase	3				2034	2140	2213	-	2129	-	-	Unique_PM
TRINITY_DN8633_c0_g1_i1_p1sp Q42560ACO1_ARATH	Aconitate hydratase 1	18	36963	43876	35491	23445	22996	23759	38777	23400	0,00406	-0,73	DOWN
TRINITY_DN8633_c0_g2_i1_p1sp P49608ACOHC_CUCMA	Aconitate hydratase, cytoplasmic	31	163083	200398	177852	159618	174013	147241	180444	160291	0,20496	-0,17	UNCHANGED
TRINITY_DN33998_c0_g1_i5_p1 UniRef100_A0A6J1K838	ACT domain-containing protein ACR	5	30548	23083	22542	47207	51940	42444	25391	47197	0,00443	0,89	UP
TRINITY_DN2280_c2_g1_i1_p110 1241at33090 Actin	Actin	3	2548	3412	3667	2052	1717	2230	3209	2000	0,03095	-0,68	DOWN
TRINITY_DN2578_c1_g2_i1_p110 1241at33090 Actin	Actin	7	47543	55007	38199	40087	36658	34815	46916	37187	0,12917	-0,34	UNCHANGED
TRINITY_DN2578_c0_g3_i1_p2A ctin	Actin	7				1794	2158	2150	-	2034	-	-	Unique_PM

TRINITY_DN2578_c0_g2_i1_p1UniRef100_A0A7S9VMD1	Actin 6 (Fragment)	6	5656	5046	4959	4268	3187	3953	5220	3802	0,02181	-0,46	UNCHANGED
TRINITY_DN2578_c0_g2_i5_p1spP53492ACT7_ARATH	Actin-7	27	344771	375399	280586	247549	295737	303606	333585	282297	0,19485	-0,24	UNCHANGED
TRINITY_DN2578_c0_g1_i1_p1spP60712ACTB_BOVIN	Actin, cytoplasmic 1	9	5241	3920	4192	9012	8166	4964	4451	7381	0,08679	0,73	UNCHANGED
TRINITY_DN6906_c2_g1_i1_p1spP32061STAD_CUCSA	Acyl-[acyl-carrier-protein] desaturase, chloroplastic	2	4181	5569	4993	2687	5665	6318	4914	4890	0,98464	-0,01	UNCHANGED
TRINITY_DN3548_c0_g2_i2_p1Adaptin_N	Adaptin	4	5459	6762	5478	3507	4437	3955	5899	3966	0,01902	-0,57	UNCHANGED
TRINITY_DN6605_c0_g1_i3_p1Adap_comp_sub	Adaptor	2	14216	11276	12158	7991	6890	7943	12550	7608	0,00632	-0,72	DOWN
TRINITY_DN1277_c0_g1_i5_p1spQ43199APT1_WHEAT	Adenine phosphoribosyltransferase 1	2	32857	26480	26926	23461	18255	18641	28754	20119	0,03117	-0,52	UNCHANGED
TRINITY_DN8762_c0_g1_i4_p1spQ9LZG0ADK2_ARATH	Adenosine kinase 2	12	44649	41665	44675	23040	23999	28780	43663	25273	0,00083	-0,79	DOWN
TRINITY_DN2743_c0_g1_i12_p1spQ9LZG0ADK2_ARATH	Adenosine kinase 2	8	51454	61894	56938	74545	74957	106493	56762	85332	0,06026	0,59	UNCHANGED
TRINITY_DN8762_c0_g1_i13_p1spQ9LZG0ADK2_ARATH	Adenosine kinase 2	10	9687	8425	9500	14187	11830	14845	9204	13621	0,01138	0,57	UNCHANGED
TRINITY_DN30257_c0_g1_i3_p1spP93253SAHH_MESCR	Adenosylhomocysteinase	23	180068	181297	178327	108816	114888	128598	179897	117434	0,00045	-0,62	DOWN
TRINITY_DN30257_c0_g1_i6_p1spP50246SAHH_MEDSA	Adenosylhomocysteinase	11	45373	48349	48845	33596	35514	38598	47522	35903	0,00306	-0,40	UNCHANGED
TRINITY_DN11681_c0_g2_i10_p1Adenylsucc_synt	Adenylosuccinate	2	16192	16861	14529	12476	16979	19475	15861	16310	0,84546	0,04	UNCHANGED
TRINITY_DN132476_c0_g1_i1_p1spP34727ARF_AJECA	ADP-ribosylation factor	5	15268	21499	22347	15191	18351	25219	19705	19587	0,97615	-0,01	UNCHANGED
TRINITY_DN14508_c0_g1_i10_p1spP51823ARF2_ORYSJ	ADP-ribosylation factor 2	7	66858	66592	56186	52902	51058	59976	63212	54645	0,12606	-0,21	UNCHANGED

TRINITY_DN2703_c0_g1_i1_p1sp O22342ADT1_GOSHI	ADP,ATP carrier protein 1, mitochondrial	16	124461	135146	128555	98198	99969	104498	129387	100888	0,00143	-0,36	UNCHANGED
TRINITY_DN1768_c0_g1_i3_p1sp O49447ADT3_ARATH	ADP,ATP carrier protein 3, mitochondrial	6	9683	12963	10499	8430	9844	11522	11048	9932	0,44892	-0,15	UNCHANGED
TRINITY_DN2484_c0_g1_i4_p1U niRef100_A0A5A7TEN6	Agglutinin domain-containing protein	16	182364	173454	196564	149544	150342	184440	184127	161442	0,16388	-0,19	UNCHANGED
TRINITY_DN491_c0_g1_i5_p1Uni Ref100_A0A0A0KD65	Agglutinin domain-containing protein	18	12053	14972	17908	10608	12197	17956	14978	13587	0,64536	-0,14	UNCHANGED
TRINITY_DN491_c0_g1_i6_p1Uni Ref100_A0A0A0KD65	Agglutinin domain-containing protein	22	82304	113828	125993	62390	75952	115326	107375	84556	0,32866	-0,34	UNCHANGED
TRINITY_DN2231_c0_g2_i1_p1U niRef100_A0A0A0LGX2	Aha1_N domain-containing protein	2	11672	10974	12194	10831	7585	9705	11613	9373	0,09196	-0,31	UNCHANGED
TRINITY_DN7474_c0_g1_i6_p1sp P34106ALA2_PANMI	Alanine aminotransferase 2	2	8153	8921	8890	5390	5268	9306	8655	6654	0,21243	-0,38	UNCHANGED
TRINITY_DN8346_c0_g1_i2_p1sp P36428SYA_ARATH	Alanine--tRNA ligase	12	20874	23517	22340	17250	17876	20006	22244	18377	0,02684	-0,28	UNCHANGED
TRINITY_DN567_c0_g2_i1_p1spP 12886ADH1_PEA	Alcohol dehydrogenase 1	8	37384	43436	34202	8627	9127	14377	38341	10710	0,00108	-1,84	DOWN
TRINITY_DN2810_c0_g1_i3_p1sp Q96533ADHX_ARATH	Alcohol dehydrogenase class-3	11	71157	85813	82466	49210	55541	65902	79812	56884	0,02528	-0,49	UNCHANGED
TRINITY_DN29073_c0_g1_i25_p1 Aldedh	Aldehyde	3	6843	6556	5427	4569	3981	6612	6275	5054	0,24928	-0,31	UNCHANGED
TRINITY_DN5869_c1_g1_i1_p1U niRef100_A0A6J1JLJ4	Allene-oxide cyclase	4	34406	35697	44725	27157	27528	26565	38276	27084	0,02641	-0,50	UNCHANGED
TRINITY_DN9154_c0_g1_i26_p1 Melibiase_2	Alpha	4	17637	20017	28229	12558	14009	17079	21961	14549	0,09981	-0,59	UNCHANGED
TRINITY_DN1773_c0_g3_i1_p1sp P04045PHSL1_SOLTU	Alpha-1,4 glucan phosphorylase L-1 isozyme, chloroplastic/amyloplastic	12	31905	36110	34228	19623	16240	29651	34081	21838	0,04364	-0,64	DOWN
TRINITY_DN19946_c0_g2_i2_p1s pP06733ENOA_HUMAN	Alpha-enolase	10	13255	16788	16490	14280	16609	18865	15511	16585	0,57074	0,10	UNCHANGED

TRINITY_DN16734_c0_g1_i17_p1 spQ9FT97AGAL1_ARATH	Alpha-galactosidase 1	21	71987	77158	107609	82554	78393	91591	85585	84179	0,91076	-0,02	UNCHANGED
TRINITY_DN7167_c1_g1_i2_p1sp Q8VXZ7AGAL3_ARATH	Alpha-galactosidase 3	9	26021	26499	27417	24797	21960	29108	26646	25288	0,55648	-0,08	UNCHANGED
TRINITY_DN6590_c0_g1_i11_p1 UniRef100_UPI0019014658	Alpha-galactosidase mel1	6	11180	14844	20612	12591	15282	16751	15545	14875	0,83426	-0,06	UNCHANGED
TRINITY_DN1307_c0_g1_i1_p1sp Q9S7Y7XYL1_ARATH	Alpha-xylosidase 1	5	7405	10467	20562	17828	18965	23581	12811	20125	0,16777	0,65	UNCHANGED
TRINITY_DN1307_c0_g2_i1_p1sp Q9S7Y7XYL1_ARATH	Alpha-xylosidase 1	5	24440	20566	19725	25827	25401	26040	21577	25756	0,04617	0,26	UNCHANGED
TRINITY_DN4538_c1_g1_i1_p1sp A0A0E3T3B5AADH2_MALDO	Aminoaldehyde dehydrogenase 2, peroxisomal	16	34229	34660	35281	27700	27286	35318	34723	30101	0,15352	-0,21	UNCHANGED
TRINITY_DN13017_c0_g2_i2_p1s pP54260GCST_SOLTU	Aminomethyltransferase, mitochondrial	25	141943	141961	142048	169025	172557	149105	141984	163562	0,04173	0,20	UNCHANGED
TRINITY_DN352_c0_g1_i42_p1Pe ptidase_M18	Aminopeptidase	3	2174	3618	4920	7813	10360	17890	3571	12021	0,05399	1,75	UNCHANGED
TRINITY_DN352_c0_g1_i1_p1Pep tidase_M18	Aminopeptidase	4	8141	11506	11053	8558	9930	12231	10233	10239	0,99695	0,00	UNCHANGED
TRINITY_DN44176_c0_g1_i10_p1 Aminotran_1_2	Aminotransferase	8	20596	18726	18197	12511	15363	16854	19173	14910	0,04387	-0,36	UNCHANGED
TRINITY_DN4181_c0_g1_i2_p1U niRef100_A0A6J1JEL9	Ankyrin repeat domain-containing protein 2B-like n=2 Tax=Cucurbita TaxID=3660 RepID=A0A6J1JEL9_CUCMA	5	21961	27694	17487	14737	25720	22942	22381	21133	0,79203	-0,08	UNCHANGED
TRINITY_DN9203_c0_g1_i1_p1sp Q9XEE2ANXD2_ARATH	Annexin D2	7	26705	22192	23459	24176	13439	14209	24119	17275	0,13883	-0,48	UNCHANGED
TRINITY_DN12237_c0_g1_i4_p1s pP51074ANX4_FRAAN	Annexin-like protein RJ4	14	43869	45105	32860	36045	31811	36191	40611	34682	0,22616	-0,23	UNCHANGED
TRINITY_DN12237_c0_g2_i1_p1s pP51074ANX4_FRAAN	Annexin-like protein RJ4	19	123138	101075	92172	87060	69819	93393	105462	83424	0,13004	-0,34	UNCHANGED

TRINITY_DN2396_c1_g2_i1_p1sp S5ZH89PIP11_MUSAC	Aquaporin PIP1-1	4	44532	48663	61701	44544	47998	54788	51632	49110	0,69513	-0,07	UNCHANGED
TRINITY_DN2396_c1_g2_i2_p1sp Q9ATM4PIP27_MAIZE	Aquaporin PIP2-7	4	109433	123544	143583	116853	148138	158799	125520	141263	0,38134	0,17	UNCHANGED
TRINITY_DN7298_c0_g1_i3_p1sp P46637ARGI1_ARATH	Arginase 1, mitochondrial	10	79458	72479	80302	68013	61343	66688	77413	65348	0,01979	-0,24	UNCHANGED
TRINITY_DN7920_c0_g1_i7_p1sp Q3C251ARGJ_CITLA	Arginine biosynthesis bifunctional protein ArgJ, chloroplastic	7	19952	18301	23145	18387	17151	21996	20466	19178	0,56085	-0,09	UNCHANGED
TRINITY_DN2480_c0_g2_i1_p1sp Q9LEU8ARLY_ARATH	Argininosuccinate lyase, chloroplastic	7	15657	20504	16873	14020	13989	14252	17678	14087	0,06951	-0,33	UNCHANGED
TRINITY_DN21865_c0_g1_i6_p1s pQ9C969ISS1_ARATH	Aromatic aminotransferase ISS1	7	12856	20714	13560	10369	16308	12539	15710	13072	0,43609	-0,27	UNCHANGED
TRINITY_DN65197_c0_g1_i1_p1s pP46644AAT3_ARATH	Aspartate aminotransferase 3, chloroplastic	13	39983	41762	43342	31132	24465	32561	41696	29386	0,01004	-0,50	UNCHANGED
TRINITY_DN12340_c0_g1_i5_p1s pP26563AATM_LUPAN	Aspartate aminotransferase P2, mitochondrial (Fragment)	13	25805	25586	28720	28117	31262	33947	26704	31109	0,08838	0,22	UNCHANGED
TRINITY_DN13320_c0_g1_i2_p1s pP46643AAT1_ARATH	Aspartate aminotransferase, mitochondrial	4	19036	21036	17902	19344	16724	17448	19325	17839	0,28460	-0,12	UNCHANGED
TRINITY_DN6347_c0_g2_i1_p1sp Q8H104SYDC1_ARATH	Aspartate--tRNA ligase 1, cytoplasmic	15	24623	27016	25401	15370	16091	19299	25680	16920	0,00331	-0,60	DOWN
TRINITY_DN1931_c0_g4_i1_p1U niRef100_A0A6J1FS25	Aspartate-semialdehyde dehydrogenase	5	18434	21297	21283	16184	16472	20051	20338	17569	0,15179	-0,21	UNCHANGED
TRINITY_DN13552_c1_g2_i1_p1s pO04057ASPR_CUCPE	Aspartic proteinase	4	9940	11535	9726	7367	7546	9197	10400	8037	0,04420	-0,37	UNCHANGED
TRINITY_DN11538_c0_g1_i5_p11 15240at33090 Asp_protease	Aspartyl	3	6203	7301	8059	5124	5138	6386	7188	5549	0,07416	-0,37	UNCHANGED
TRINITY_DN206565_c2_g1_i1_p1 spO04496AED3_ARATH	Aspartyl protease AED3	5	32977	37595	23775	33468	27459	28042	31449	29656	0,71006	-0,08	UNCHANGED
TRINITY_DN33745_c0_g1_i2_p1 UniRef100_A0A5A7SU62	Aspartyl protease AED3 n=3 Tax=Cucumis melo TaxID=3656 RepID=A0A5A7SU62_CUCME	9	33014	54548	71902	93336	89137	86800	53155	89758	0,03264	0,76	UP

TRINITY_DN2683_c0_g2_i5_p1UniRef100_A0A6J1KW81	Aspartyl protease family protein 2	2	5465	7666	8832	7133	7055	6916	7321	7035	0,78697	-0,06	UNCHANGED
TRINITY_DN2683_c0_g2_i1_p1spQ9LNJ3APF2_ARATH	Aspartyl protease family protein 2	6	17833	16878	18539	16908	11787	18617	17750	15771	0,40094	-0,17	UNCHANGED
TRINITY_DN3157_c1_g2_i1_p1UniRef100_A0A6J1FDU3	Aspartyl protease family protein At5g10770-like isoform X2	10	33137	39425	34178	40463	38669	34513	35580	37882	0,43013	0,09	UNCHANGED
TRINITY_DN12658_c0_g1_i1_p1spO80934Y2766_ARATH	At2g37660, chloroplastic	10	41100	52540	40857	32618	50240	36072	44832	39643	0,47740	-0,18	UNCHANGED
TRINITY_DN17966_c0_g1_i11_p1spQ8GSJ1HIS1B_ARATH	ATP phosphoribosyltransferase 2, chloroplastic	7	18166	23188	15988	18197	18381	20602	19114	19060	0,98203	0,00	UNCHANGED
TRINITY_DN16393_c0_g1_i1_p2spQ4VZG9ATPE_CUCSA	ATP synthase epsilon chain, chloroplastic	6	27544	37085	52970	55823	66754	73595	39200	65391	0,04428	0,74	UP
TRINITY_DN1727_c0_g3_i1_p1spP29790ATPG_TOBAC	ATP synthase gamma chain, chloroplastic	6	21783	23029	21826	27926	27064	33779	22213	29590	0,02645	0,41	UNCHANGED
TRINITY_DN1727_c0_g2_i1_p1spP29790ATPG_TOBAC	ATP synthase gamma chain, chloroplastic	14	95210	99333	117106	128803	137622	162108	103883	142844	0,03160	0,46	UNCHANGED
TRINITY_DN19570_c0_g2_i1_p1spA8FJR0ATPA_CAMJ8	ATP synthase subunit alpha	4	2906	3368	3202	3192	3865	3499	3158	3519	0,20272	0,16	UNCHANGED
TRINITY_DN13431_c0_g2_i1_p2spQ88BX2ATPA_PSEPK	ATP synthase subunit alpha	4	1904	2554	2339	3734	4725	4458	2266	4305	0,00443	0,93	UP
TRINITY_DN4171_c1_g1_i10_p2spB1NWD5ATPA_MANES	ATP synthase subunit alpha, chloroplastic	23	316840	301452	355848	346952	358206	335908	324713	347022	0,26957	0,10	UNCHANGED
TRINITY_DN18301_c0_g2_i1_p1spP37211ATPA_NEUCR	ATP synthase subunit alpha, mitochondrial	9	5991	7425	6728	7866	9180	9852	6714	8966	0,03457	0,42	UNCHANGED
TRINITY_DN10553_c0_g1_i2_p1spP05492ATPAM_OENBI	ATP synthase subunit alpha, mitochondrial	23	156616	189705	175521	104591	115522	143970	173947	121361	0,02557	-0,52	UNCHANGED

TRINITY_DN4171_c1_g1_i10_p6s pQ4VZP7ATPF_CUCSA	ATP synthase subunit b, chloroplastic	5	53660	37481	49403	71634	62134	55345	46848	63038	0,07490	0,43	UNCHANGED
TRINITY_DN13431_c0_g1_i1_p2s pA7N0Y1ATPB1_VIBC1	ATP synthase subunit beta 1	2	84603	83130	66655	31389	25868	26946	78129	28068	0,00112	-1,48	DOWN
TRINITY_DN16393_c0_g1_i1_p1s pQ4VZI5ATPB_CUCSA	ATP synthase subunit beta, chloroplastic	36	341046	389404	414699	347168	413308	451838	381716	404105	0,58196	0,08	UNCHANGED
TRINITY_DN16526_c0_g1_i3_p1s pP06576ATPB_HUMAN	ATP synthase subunit beta, mitochondrial	10	9750	7284	8176	12658	9777	8089	8403	10175	0,30758	0,28	UNCHANGED
TRINITY_DN1753_c0_g1_i7_p1sp P29685ATPBM_HEVBR	ATP synthase subunit beta, mitochondrial	23	189282	218345	185373	146377	150777	155679	197667	150944	0,01216	-0,39	UNCHANGED
TRINITY_DN28963_c0_g2_i1_p1s pQ9SSS9ATPD_ARATH	ATP synthase subunit delta, chloroplastic	4	13095	13470	14278	36421	34885	28941	13614	33415	0,00101	1,30	UP
TRINITY_DN15095_c0_g1_i4_p1s pP26360ATPG3_IPOBA	ATP synthase subunit gamma, mitochondrial	6	17327	30158	23565	14919	21312	21715	23683	19315	0,36810	-0,29	UNCHANGED
TRINITY_DN1372_c0_g3_i10_p1s pQ9FGX1ACLB2_ARATH	ATP-citrate synthase beta chain protein 2	11	17282	16984	18589	10275	11638	13524	17619	11812	0,00546	-0,58	UNCHANGED
TRINITY_DN15874_c0_g1_i2_p1s pQ94AA4PFKA3_ARATH	ATP-dependent 6-phosphofructokinase 3	2	4307	4133	7107	5402	3070	2691	5182	3721	0,31847	-0,48	UNCHANGED
TRINITY_DN3971_c0_g2_i2_p1U niRef100_A0A6J1CI79	ATP-dependent Clp protease ATP-binding subunit CLPT1, chloroplastic-like	3	8707	10794	12824	12380	8608	7106	10775	9365	0,51323	-0,20	UNCHANGED
TRINITY_DN9595_c0_g1_i10_p1s pQ3C1K4CLPP_NICSY	ATP-dependent Clp protease proteolytic subunit	2	11291	7715	11530	12766	12638	13924	10179	13109	0,08717	0,37	UNCHANGED
TRINITY_DN208516_c0_g1_i1_p1 UniRef100_A0A6J1CWB9	ATP-dependent Clp protease proteolytic subunit	2	21652	23624	29018	30050	30577	29768	24765	30131	0,07247	0,28	UNCHANGED
TRINITY_DN9256_c0_g1_i4_p1sp Q9SXJ6CLPP3_ARATH	ATP-dependent Clp protease proteolytic subunit 3, chloroplastic	3	9021	9595	11184	9397	10859	13369	9933	11208	0,39134	0,17	UNCHANGED

TRINITY_DN14121_c1_g1_i2_p1sp|Q9S834|CLPP5_ARATH	ATP-dependent Clp protease proteolytic subunit 5, chloroplastic	7	50748	60636	60083	58991	72285	66862	57156	66046	0,15116	0,21	UNCHANGED
TRINITY_DN2958_c0_g1_i14_p1sp|Q8L770|CLPR3_ARATH	ATP-dependent Clp protease proteolytic subunit-related protein 3, chloroplastic	2	15852	20236	9416	25196	19700	26822	15168	23906	0,08354	0,66	UNCHANGED
TRINITY_DN22056_c0_g1_i1_p1sp|Q7RV88|IF4A_NEUCR	ATP-dependent RNA helicase eIF4A	2	5548	5790	3793				5043		-	-	Unique_PH
TRINITY_DN28119_c0_g2_i16_p1sp|Q655S1|FTSH2_ORYSJ	ATP-dependent zinc metalloprotease FTSH 2, chloroplastic	16	49671	53572	75493	67906	70505	68208	59579	68873	0,31403	0,21	UNCHANGED
TRINITY_DN28119_c0_g2_i14_p1sp|Q655S1|FTSH2_ORYSJ	ATP-dependent zinc metalloprotease FTSH 2, chloroplastic	16	23581	21305	36406	48629	43690	52467	27097	48262	0,01666	0,83	UP
TRINITY_DN10542_c0_g2_i1_p1sp|O82150|FTSH_TOBAC	ATP-dependent zinc metalloprotease FTSH, chloroplastic	13	29042	30241	38830	34375	34000	46431	32704	38269	0,33787	0,23	UNCHANGED
TRINITY_DN4843_c0_g1_i3_p1sp|Q9LV11|PMA11_ARATH	ATPase 11, plasma membrane-type	12	23076	13105	20479	11636	13827	14691	18887	13385	0,15278	-0,50	UNCHANGED
TRINITY_DN1089_c0_g1_i10_p2sp|Q9ZRA4|AB19A_PRUPE	Auxin-binding protein ABP19a	6	155108	202740	314555	355572	395539	478830	224134	409980	0,03557	0,87	UP
TRINITY_DN6294_c0_g1_i2_p1sp|Q9ZRA4|AB19A_PRUPE	Auxin-binding protein ABP19a	8	169006	203100	316478	376348	354467	399355	229528	376723	0,03383	0,71	UP
TRINITY_DN5531_c0_g1_i3_p1sp|C7A2A0|BALDH_ANTMA	Benzaldehyde dehydrogenase, mitochondrial	19	62308	65510	52460	36397	49431	41569	60093	42466	0,03196	-0,50	UNCHANGED
TRINITY_DN3520_c2_g1_i4_p1sp|Q94CE4|BCA4_ARATH	Beta carbonic anhydrase 4	9	23247	35661	42921	27303	30871	31026	33943	29734	0,51304	-0,19	UNCHANGED
TRINITY_DN4213_c0_g1_i5_p1sp|Q9FGY1|BXL1_ARATH	Beta-D-xylosidase 1	8	13307	11256	21752	11846	9315	13546	15438	11569	0,32350	-0,42	UNCHANGED
TRINITY_DN10142_c0_g1_i1_p1sp|Q5N8X6|BGAL3_ORYSJ	Beta-galactosidase 3	9	30096	33146	42924	29126	23558	35098	35389	29261	0,29630	-0,27	UNCHANGED

TRINITY_DN11163_c0_g1_i1_p1UniRef100_A0A6J1HKE9	Beta-glucosidase	2	5394	6441	7568	5652	5020	6509	6467	5727	0,38603	-0,18	UNCHANGED
TRINITY_DN7224_c0_g1_i4_p1spQ9LV33BGL44_ARATH	Beta-glucosidase 44	20	90047	98705	82202	63794	60402	71131	90318	65109	0,01164	-0,47	UNCHANGED
TRINITY_DN802_c0_g1_i4_p1UniRef100_UPI00190062B1	Beta-glucosidase BoGH3B-like	10	26635	20659	30789	21838	16627	24225	26028	20896	0,23756	-0,32	UNCHANGED
TRINITY_DN6326_c0_g1_i4_p1UniRef100_UPI0019015060	Beta-glucosidase BoGH3B-like	14	185549	134761	130968	202640	146940	138719	150426	162766	0,66794	0,11	UNCHANGED
TRINITY_DN11021_c0_g1_i5_p1spQ8H183BUP1_ARATH	Beta-ureidopropionase	4	7962	8885	12928	7992	5582	8379	9925	7318	0,21221	-0,44	UNCHANGED
TRINITY_DN15477_c0_g2_i2_p1spA5JTQ2XYL1_MEDSV	Beta-xylosidase/alpha-L-arabinofuranosidase 1 (Fragment)	8	17270	16622	18526	14304	16127	17314	17473	15915	0,20803	-0,13	UNCHANGED
TRINITY_DN34142_c0_g1_i6_p1spP25696ENO2_ARATH	Bifunctional enolase 2/transcriptional activator	10	78244	69246	60466	106280	75829	76949	69319	86352	0,20334	0,32	UNCHANGED
TRINITY_DN22046_c0_g1_i3_p1spQ9LHH7FOLD2_ARATH	Bifunctional protein FolD 2	4	12600	15098	16105	8978	12524	15114	14601	12206	0,30976	-0,26	UNCHANGED
TRINITY_DN513_c1_g1_i11_p1spB9HBA8ACCC1_POPTR	Biotin carboxylase 1, chloroplastic	11	21725	60242	43162	48026	42243	48688	41710	46319	0,70492	0,15	UNCHANGED
TRINITY_DN615_c0_g1_i1_p1UniRef100_UPI0019003352	Blue copper protein-like	2	16532	21515	25882	28016	28354	28824	21310	28398	0,05915	0,41	UNCHANGED
TRINITY_DN13334_c2_g1_i3_p1spQ43609COMT1_PRUDU	Caffeic acid 3-O-methyltransferase	5	11555	14102	11958	7765	10312	14604	12538	10894	0,48628	-0,20	UNCHANGED
TRINITY_DN136075_c0_g1_i1_p1spQ43095CAMT_POPTM	Caffeoyl-CoA O-methyltransferase	2	3145	5706	2952	3416	3331	3623	3934	3457	0,62061	-0,19	UNCHANGED
TRINITY_DN2779_c2_g1_i1_p1spQ9FN48CAS_ARATH	Calcium sensing receptor, chloroplastic	11	27173	27903	32935	40879	41303	42086	29337	41423	0,00281	0,50	UNCHANGED
TRINITY_DN4242_c0_g1_i3_p1spP49101CDPK2_MAIZE	Calcium-dependent protein kinase 2	5	13832	15558	22666	14470	17497	18770	17352	16912	0,89011	-0,04	UNCHANGED
TRINITY_DN8513_c0_g1_i1_p1Calreticulin	Calreticulin	11	33813	32681	36001	17205	21912	28354	34165	22490	0,02584	-0,60	DOWN

TRINITY_DN8017_c1_g1_i3_p1Calreticulin	Calreticulin_Calreticulin Calreticulin	12	88440	105970	82067	50985	76772	85964	92159	71240	0,17424	-0,37	UNCHANGED
TRINITY_DN6952_c0_g1_i1_p1spQ42601CARB_ARATH	Carbamoyl-phosphate synthase large chain, chloroplastic	10	13918	24246	26521	11578	21336	23816	21562	18910	0,64815	-0,19	UNCHANGED
TRINITY_DN5377_c1_g1_i13_p1spP17067CAHC_PEA	Carbonic anhydrase, chloroplastic	16	185924	208131	294894	307087	338827	387954	229650	344623	0,04768	0,59	UNCHANGED
TRINITY_DN7825_c0_g1_i5_p1spP48350CATA1_CUCPE	Catalase isozyme 1	18	280353	265741	273270	249606	248872	227600	273121	242026	0,02047	-0,17	UNCHANGED
TRINITY_DN12894_c0_g1_i12_p1UniRef100_UPI001900E02F	Cathepsin B-like protease 2 isoform X1	8	87434	81302	80754	90787	75108	76541	83163	80812	0,68802	-0,04	UNCHANGED
TRINITY_DN12341_c0_g1_i1_p1spQ5AWS6CDC48_EMENI	Cell division control protein 48	2	16459	23987	20295	9903	12358	18023	20247	13428	0,10318	-0,59	UNCHANGED
TRINITY_DN180_c0_g1_i3_p1spQ9SCN8CD48D_ARATH	Cell division control protein 48 homolog D	28	20716	24273	23049	12136	13218	16244	22680	13866	0,00545	-0,71	DOWN
TRINITY_DN8148_c1_g1_i2_p1spP54774CDC48_SOYBN	Cell division cycle protein 48 homolog	21	16532	19667	17380	8862	10026	11662	17860	10183	0,00345	-0,81	DOWN
TRINITY_DN180_c0_g3_i1_p1spP54774CDC48_SOYBN	Cell division cycle protein 48 homolog	29	49259	57728	54808	35759	38946	47871	53932	40859	0,04093	-0,40	UNCHANGED
TRINITY_DN816_c0_g1_i6_p1spP35100CLPC_PEA	Chaperone protein ClpC, chloroplastic	22	30817	34164	38460	38051	40505	41257	34480	39938	0,08666	0,21	UNCHANGED
TRINITY_DN816_c0_g1_i3_p1spP35100CLPC_PEA	Chaperone protein ClpC, chloroplastic	23	22090	27393	30344	31596	33314	36537	26609	33816	0,06268	0,35	UNCHANGED
TRINITY_DN20090_c0_g1_i1_p1spP21240CPNB1_ARATH	Chaperonin 60 subunit beta 1, chloroplastic	27	104528	109031	88143	87583	105053	108832	100567	100490	0,99359	0,00	UNCHANGED
TRINITY_DN31_c0_g1_i1_p1spQ05046CH62_CUCMA	Chaperonin CPN60-2, mitochondrial	6	11469	13312	8207	8577	9607	8654	10996	8946	0,25106	-0,30	UNCHANGED
TRINITY_DN15658_c0_g1_i2_p1spQ05046CH62_CUCMA	Chaperonin CPN60-2, mitochondrial	10	30998	38656	24224	24319	28466	28687	31293	27157	0,40089	-0,20	UNCHANGED
TRINITY_DN169771_c12_g1_i1_p1spP27489CB23_SOLLC	Chlorophyll a-b binding protein 13, chloroplastic	7	127657	187025	229120	179891	254365	256935	181267	230397	0,27402	0,35	UNCHANGED

TRINITY_DN4065_c0_g1_i1_p1sp P27518CB21_GOSHI	Chlorophyll a-b binding protein 151, chloroplastic	9	361228	445817	445860	367523	426429	441445	417635	411799	0,87946	-0,02	UNCHANGED
TRINITY_DN2361_c0_g2_i10_p1s pP09756CB23_SOYBN	Chlorophyll a-b binding protein 3, chloroplastic	8	380981	546874	596268	451006	552870	590035	508041	531303	0,77830	0,06	UNCHANGED
TRINITY_DN16242_c0_g1_i6_p1s pP12360CB11_SOLLC	Chlorophyll a-b binding protein 6A, chloroplastic	8	184211	187512	214720	258013	133988	135660	195481	175887	0,66648	-0,15	UNCHANGED
TRINITY_DN48363_c0_g1_i1_p1s pP10708CB12_SOLLC	Chlorophyll a-b binding protein 7, chloroplastic	6	125866	141405	160558	173382	206619	195440	142610	191814	0,02457	0,43	UNCHANGED
TRINITY_DN35_c10_g1_i1_p1spP 27524CB4A_SOLLC	Chlorophyll a-b binding protein CP24 10A, chloroplastic	9	295313	239075	379712	361543	416631	441191	304700	406455	0,09718	0,42	UNCHANGED
TRINITY_DN5438_c1_g1_i1_p1sp Q9XF89CB5_ARATH	Chlorophyll a-b binding protein CP26, chloroplastic	14	295074	288690	335657	309838	356428	368726	306474	344997	0,17206	0,17	UNCHANGED
TRINITY_DN6813_c0_g2_i2_p1sp Q07473CB4A_ARATH	Chlorophyll a-b binding protein CP29_1, chloroplastic	12	152075	150483	187528	190144	201929	218943	163362	203672	0,05179	0,32	UNCHANGED
TRINITY_DN6813_c0_g2_i5_p1sp Q07473CB4A_ARATH	Chlorophyll a-b binding protein CP29_1, chloroplastic	14	386383	377737	411404	404935	399441	448599	391841	417658	0,23619	0,09	UNCHANGED
TRINITY_DN2361_c1_g1_i1_p1sp P08221CB21_CUCSA	Chlorophyll a-b binding protein of LHCII type I, chloroplastic (Fragment)	8	186225	164186	156114	264394	308087	226730	168842	266404	0,01790	0,66	UP
TRINITY_DN3901_c1_g1_i1_p1sp Q9SQL2CB24_PEA	Chlorophyll a-b binding protein P4, chloroplastic	5	59191	35068	88738	70209	129761	88009	60999	95993	0,21071	0,65	UNCHANGED
TRINITY_DN6894_c0_g1_i5_p1Un iRef100_UPI0019019E52	Chloroplast stem-loop binding protein of 41 kDa a, chloroplastic-like	14	65868	58336	89299	81479	78583	88204	71168	82755	0,30032	0,22	UNCHANGED
TRINITY_DN4794_c0_g1_i6_p1sp Q9SA52CP41B_ARATH	Chloroplast stem-loop binding protein of 41 kDa b, chloroplastic	16	61304	71153	102368	93991	97020	105663	78275	98891	0,18422	0,34	UNCHANGED
TRINITY_DN89345_c0_g1_i3_p1U niRef100_UPI000C9D9134	Cinnamoyl-CoA reductase 1-like	9	48150	53625	48792	31809	34243	41508	50189	35853	0,01334	-0,49	UNCHANGED
TRINITY_DN1934_c2_g1_i8_p1Cit rate_synt	Citrate	2	8844	9510	6553	8908	7278	8745	8302	8310	0,99420	0,00	UNCHANGED

TRINITY_DN25062_c0_g1_i7_p1sp|P49298|CISY_CITMA	Citrate synthase, mitochondrial	9	19533	22884	20858	8384	12689	18306	21092	13126	0,05844	-0,68	UNCHANGED
TRINITY_DN1971_c1_g2_i14_p1sp|Q0WNJ6|CLAH1_ARATH	Clathrin heavy chain 1	23	42180	47402	42022	26962	34422	34277	43868	31887	0,01679	-0,46	UNCHANGED
TRINITY_DN114078_c0_g1_i5_p1 UniRef100_A0A1S3BRT4	Co-chaperone protein p23	3	43793	45833	41301	39031	45324	51194	43642	45183	0,70205	0,05	UNCHANGED
TRINITY_DN792_c0_g1_i2_p1Uni Ref100_A0A6J1JB53	Coatomer subunit alpha	5	7628	13861	8458	4542	4968	5543	9982	5018	0,06585	-0,99	UNCHANGED
TRINITY_DN10344_c0_g1_i2_p1sp|Q9SV21|COPB1_ARATH	Coatomer subunit beta-1	5	22560	23800	17477	11995	16197	15919	21279	14704	0,04966	-0,53	UNCHANGED
TRINITY_DN3548_c0_g1_i1_p1sp|Q6Z382|COPG2_ORYSJ	Coatomer subunit gamma-2	10	14587	19399	16263	9561	12157	13056	16750	11591	0,04255	-0,53	UNCHANGED
TRINITY_DN10303_c0_g1_i6_p1sp|Q6Z844|COPZ2_ORYSJ	Coatomer subunit zeta-2	2	14075	13770	14936	10207	7581	10789	14260	9525	0,01063	-0,58	UNCHANGED
TRINITY_DN976_c0_g1_i1_p1Meth_synt_2	Cobalamin-independent	13	164789	155248	139296	118275	114708	130206	153111	121063	0,02185	-0,34	UNCHANGED
TRINITY_DN11045_c0_g1_i14_p1 231151at33090 CIA30	Complex	3	4000	5790	8460	6134	7861	8532	6083	7509	0,38987	0,30	UNCHANGED
TRINITY_DN11922_c1_g1_i1_p1sp|B2LSD2|MUCIN_MUCPR	Cysteine proteinase mucunain (Fragment)	8	147872	170370	162140	129232	143885	147638	160127	140252	0,08301	-0,19	UNCHANGED
TRINITY_DN1024_c4_g1_i1_p1sp|Q43317|CYSK_CITLA	Cysteine synthase	17	104423	108121	114964	77839	73601	96644	109169	82695	0,02661	-0,40	UNCHANGED
TRINITY_DN11410_c0_g2_i1_p1sp|P32260|CYSKP_SPIOL	Cysteine synthase, chloroplastic/chromoplastic	10	40704	44704	36936	46383	50080	48332	40781	48265	0,03944	0,24	UNCHANGED
TRINITY_DN518_c0_g3_i1_p2COX2	Cytochrome	2	50063	41431	42564	40273	33343	30882	44686	34832	0,06507	-0,36	UNCHANGED
TRINITY_DN12182_c0_g1_i30_p3sp|Q49KW8|CYB6_EUCGG	Cytochrome b6	3	84133	100707	109429	73508	114181	110998	98090	99562	0,92661	0,02	UNCHANGED
TRINITY_DN4538_c2_g2_i9_p1sp|P26291|UCRIA_PEA	Cytochrome b6-f complex iron-sulfur subunit, chloroplastic	9	101506	131258	136069	91578	150338	160050	122944	133989	0,66886	0,12	UNCHANGED

TRINITY_DN12182_c0_g1_i19_p4 spQ7FNS2PETD_ATRBE	Cytochrome b6-f complex subunit 4	2	62280	51400	81088	91729	69163	102277	64922	87723	0,15579	0,43	UNCHANGED
TRINITY_DN2614_c0_g1_i1_p1sp Q9FKS5CYC1B_ARATH	Cytochrome c1 2, heme protein, mitochondrial	2	13646	12363	19345	3764	12784	13377	15118	9975	0,24509	-0,60	UNCHANGED
TRINITY_DN12244_c0_g1_i2_p3s pQ2QD76CYF_CUCSA	Cytochrome f	16	154210	133924	160960	154545	146490	166123	149698	155719	0,57676	0,06	UNCHANGED
TRINITY_DN4550_c1_g1_i1_p1sp O49485SERA1_ARATH	D-3-phosphoglycerate dehydrogenase 1, chloroplastic	13	27891	34285	33532	22133	28546	26455	31903	25711	0,08855	-0,31	UNCHANGED
TRINITY_DN16180_c0_g1_i4_p1s pO04130SERA2_ARATH	D-3-phosphoglycerate dehydrogenase 2, chloroplastic	5	5901	8555	7371	4043	4718	5701	7276	4821	0,05357	-0,59	UNCHANGED
TRINITY_DN5120_c0_g1_i8_p1sp Q56XG6RH15_ARATH	DEAD-box ATP-dependent RNA helicase 15	8	64206	50058	55020	75459	50041	62086	56428	62529	0,50932	0,15	UNCHANGED
TRINITY_DN9529_c0_g1_i3_p1sp Q84W89RH37_ARATH	DEAD-box ATP-dependent RNA helicase 37	9	21498	23057	24343	19476	16373	19963	22966	18604	0,03514	-0,30	UNCHANGED
TRINITY_DN8254_c1_g1_i1_p1sp Q93ZG7RH38_ARATH	DEAD-box ATP-dependent RNA helicase 38	5	12418	16886	17279	8508	9379	11872	15527	9920	0,03913	-0,65	DOWN
TRINITY_DN1991_c0_g1_i4_p1sp Q8RXK6RH8_ARATH	DEAD-box ATP-dependent RNA helicase 8	2	9078	10749	12900	7243	7272	9023	10909	7846	0,07086	-0,48	UNCHANGED
TRINITY_DN11568_c0_g1_i13_p1 ILVD_EDD	Dehydratase	2	17498	18977	16913	11524	10596	14514	17796	12211	0,01378	-0,54	UNCHANGED
TRINITY_DN2463_c0_g1_i24_p1A LAD	Delta-aminolevulinic	7	16354	18558	23015	21233	21543	24174	19309	22316	0,23807	0,21	UNCHANGED
TRINITY_DN2463_c0_g1_i25_p1s pP43210HEM2_SOYBN	Delta-aminolevulinic acid dehydratase, chloroplastic	6	30015	31836	31383	20440	22615	23680	31078	22245	0,00130	-0,48	UNCHANGED
TRINITY_DN5602_c0_g1_i2_p1sp F4JLP5PLPD2_ARATH	Dihydrolipoyl dehydrogenase 2, chloroplastic	2	12535	14159	14416	13445	11661	14302	13703	13136	0,59218	-0,06	UNCHANGED
TRINITY_DN6262_c0_g1_i1_p1sp Q8RWN9ODP22_ARATH	Dihydrolipoyllysine-residue acetyltransferase component 2 of pyruvate dehydrogenase complex, mitochondrial	7	14624	18387	14829	10977	13100	12497	15947	12192	0,05240	-0,39	UNCHANGED

TRINITY_DN264_c0_g3_i1_p1spQ9SQI8ODP24_ARATH	Dihydrolipoyllysine-residue acetyltransferase component 4 of pyruvate dehydrogenase complex,chloroplastic	5	11587	13242	11604	12266	14785	16195	12144	14415	0,14909	0,25	UNCHANGED
TRINITY_DN264_c0_g2_i1_p1spQ9C8P0ODP25_ARATH	Dihydrolipoyllysine-residue acetyltransferase component 5 of pyruvate dehydrogenase complex, chloroplastic	5	10313	10073	10270	9901	10692	11943	10219	10845	0,35441	0,09	UNCHANGED
TRINITY_DN26857_c1_g2_i1_p1UniRef100_A0A5A7T9F1	Dirigent protein n=2 Tax=Cucumis melo TaxID=3656 RepID=A0A5A7T9F1_CUCME	2	37011	61838	51175	46018	53826	47216	50008	49020	0,90271	-0,03	UNCHANGED
TRINITY_DN23041_c0_g2_i1_p1UniRef100_UPI001C3442C0	DNA damage-repair/toleration protein DRT-like protein	6	12910	16926	22058	11724	10813	16895	17298	13144	0,27093	-0,40	UNCHANGED
TRINITY_DN5677_c0_g1_i1_p1spQ944K2OST48_ARATH	Dolichyl-diphosphooligosaccharide--protein glycosyltransferase 48 kDa subunit	6	10272	11964	13249	7329	7525	12071	11828	8975	0,18278	-0,40	UNCHANGED
TRINITY_DN3268_c0_g1_i12_p1DUF3458_C	Domain_DUF3458 Domain	5	14902	18303	19069	11584	12526	17188	17425	13766	0,16471	-0,34	UNCHANGED
TRINITY_DN6335_c0_g1_i1_p1UniRef100_A0A7J8T5L1	Domain-containing protein	4	23560	34072	16360	21399	13120	15295	24664	16605	0,23085	-0,57	UNCHANGED
TRINITY_DN23979_c0_g1_i1_p1UniRef100_UPI001C343A77	Early nodulin-like protein 3 n=2 Tax=Cucurbita TaxID=3660 RepID=UPI001C343A77	4	15969	17478	28544	16779	10984	17425	20664	15063	0,27774	-0,46	UNCHANGED
TRINITY_DN83807_c0_g5_i1_p1GTP_EFTU_D3	Elongation	4	6066	5768	5118	3097	2784	3058	5651	2980	0,00084	-0,92	DOWN
TRINITY_DN2790_c1_g1_i4_p1spO64937EF1A_ORYSJ	Elongation factor 1-alpha	22	303430	298971	269356	212384	220219	252691	290585	228431	0,01899	-0,35	UNCHANGED
TRINITY_DN2790_c1_g1_i9_p1spO64937EF1A_ORYSJ	Elongation factor 1-alpha	22	121632	133039	113897	81333	80831	83818	122856	81994	0,00192	-0,58	UNCHANGED
TRINITY_DN12303_c0_g1_i1_p1spP17507EF1A2_XENLA	Elongation factor 1-alpha, oocyte form	5	12728	11790	10625	12154	11248	11612	11715	11672	0,95135	-0,01	UNCHANGED

TRINITY_DN16830_c0_g2_i1_p1spP93447EF1D_SPUBR	Elongation factor 1-delta	11	148299	164891	131241	94780	92612	123450	148144	103614	0,03277	-0,52	UNCHANGED
TRINITY_DN49145_c0_g2_i3_p1spP93447EF1D_SPUBR	Elongation factor 1-delta	11	84515	93577	62913	46146	56838	61241	80335	54742	0,06508	-0,55	UNCHANGED
TRINITY_DN206718_c0_g1_i1_p1spQ9FUM1EF1G_PRUAV	Elongation factor 1-gamma	11	50375	59734	64514	35187	35779	47448	58208	39471	0,03130	-0,56	UNCHANGED
TRINITY_DN149568_c9_g1_i1_p1spQ9FUM1EF1G_PRUAV	Elongation factor 1-gamma	20	135015	152225	163946	111829	131294	164836	150395	135986	0,45925	-0,15	UNCHANGED
TRINITY_DN4018_c0_g1_i2_p1spQ9ASR1EF2_ARATH	Elongation factor 2	36	148711	151353	125448	103639	98629	108554	141837	103607	0,01181	-0,45	UNCHANGED
TRINITY_DN4018_c0_g1_i1_p1spQ9ASR1EF2_ARATH	Elongation factor 2	38	61558	62652	58346	48053	44125	48566	60852	46915	0,00186	-0,38	UNCHANGED
TRINITY_DN7997_c0_g1_i1_p1spP34811EFGC1_SOYBN	Elongation factor G-1, chloroplastic	18	27766	30379	35568	30371	33261	37037	31237	33556	0,48228	0,10	UNCHANGED
TRINITY_DN17629_c0_g1_i1_p1spQ9ZT91EFTM_ARATH	Elongation factor Tu, mitochondrial	10	21849	25809	24833	16947	22338	25301	24164	21529	0,38749	-0,17	UNCHANGED
TRINITY_DN7855_c0_g1_i1_p1GTP_EFTU	Elongation_GTP_EFTU_D3 Elongation	22	133844	148971	167121	144728	165720	191361	149979	167270	0,35546	0,16	UNCHANGED
TRINITY_DN1165_c0_g3_i1_p1spP36907CHIX_PEA	Endochitinase	2	10708	12344	12976	1339	1935	1133	12009	1469	0,00012	-3,03	DOWN
TRINITY_DN1165_c0_g2_i6_p1spP93680CHIT_PERAE	Endochitinase	4	15045	22774	39515	6081	10665	8267	25778	8338	0,07637	-1,63	UNCHANGED
TRINITY_DN7395_c0_g1_i5_p1spP11021BIP_HUMAN	Endoplasmic reticulum chaperone BiP	5	5116	5250	3436	189	970	1570	4601	910	0,00644	-2,34	DOWN
TRINITY_DN6098_c0_g2_i4_p1spP35016ENPL_CATRO	Endoplasmin homolog	15	46684	39761	34093	29593	32229	31087	40179	30970	0,06853	-0,38	UNCHANGED
TRINITY_DN5103_c0_g1_i6_p1spQ42971ENO_ORYSJ	Enolase	12	8084	6467	5896	6080	3444	3799	6816	4441	0,08743	-0,62	UNCHANGED
TRINITY_DN68087_c0_g1_i25_p1spP42896ENO_RICCO	Enolase	27	212940	239971	219057	140605	160427	195400	223989	165477	0,03129	-0,44	UNCHANGED

TRINITY_DN34142_c0_g1_i9_p1Enolase_C	Enolase,	6	16322	8032	7717	2211	3232	5156	10690	3533	0,07207	-1,60	UNCHANGED
TRINITY_DN9116_c0_g2_i1_p1spQ9SLA8FABI_ARATH	Enoyl-[acyl-carrier-protein] reductase [NADH], chloroplastic	8	36272	45826	43110	41327	33358	38962	41736	37883	0,35601	-0,14	UNCHANGED
TRINITY_DN7723_c0_g1_i1_p1spQ9ZVA2EP1L2_ARATH	EP1-like glycoprotein 2	8	22481	29058	31173	19973	23830	34039	27570	25947	0,75920	-0,09	UNCHANGED
TRINITY_DN1556_c0_g1_i7_p1UniRef100_UPI000C9D6029	Epidermis-specific secreted glycoprotein EP1-like	10	117844	125599	125413	59336	58384	64062	122952	60594	0,00004	-1,02	DOWN
TRINITY_DN1910_c0_g1_i28_p1spM1CZC0EBP1_SOLTU	ERBB-3 BINDING PROTEIN 1	10	59199	59106	40047	41166	48096	46436	52784	45233	0,32290	-0,22	UNCHANGED
TRINITY_DN8180_c0_g1_i5_p1PMM	Eukaryotic	5	94186	91032	102812	128921	69122	78167	96010	92070	0,84536	-0,06	UNCHANGED
TRINITY_DN13552_c0_g1_i2_p1Asp	Eukaryotic	9	42759	40965	38107	44545	42165	42625	40611	43111	0,17931	0,09	UNCHANGED
RINITY_DN19243_c0_g1_i1_p1spP41380IF4A3_NICPL	Eukaryotic initiation factor 4A-3	3	10954	14577	14795	10309	11050	11378	13442	10913	0,12039	-0,30	UNCHANGED
TRINITY_DN3867_c0_g1_i1_p1spP41381IF4A8_TOBAC	Eukaryotic initiation factor 4A-8	18	143284	144313	128331	96391	88523	114329	138643	99748	0,01349	-0,48	UNCHANGED
TRINITY_DN4393_c0_g1_i3_p1spQ3SZ54IF4A1_BOVIN	Eukaryotic initiation factor 4A-I	6	12908	14621	14291				13940		-	-	Unique_PH
TRINITY_DN18409_c0_g1_i18_p1spQ3SZ65IF4A2_BOVIN	Eukaryotic initiation factor 4A-II	9	17386	18250	18253	24325	22307	27588	17963	24740	0,01235	0,46	UNCHANGED
TRINITY_DN14504_c1_g1_i4_p1UniRef100_A0A6J1DVK8	Eukaryotic peptide chain release factor GTP-binding subunit ERF3A	4	9678	12135	11821	6948	8576	10454	11212	8659	0,11561	-0,37	UNCHANGED
TRINITY_DN7454_c0_g1_i1_p1spP41091IF2G_HUMAN	Eukaryotic translation initiation factor 2 subunit 3	4	13563	20286	15197	11091	14887	15658	16349	13879	0,37352	-0,24	UNCHANGED
TRINITY_DN4502_c0_g1_i1_p1spQ9SIZ2IF2AH_ARATH	Eukaryotic translation initiation factor 2 subunit alpha homolog	2	22506	25362	25232	20597	33336	19864	24366	24599	0,96103	0,01	UNCHANGED
TRINITY_DN20541_c0_g1_i1_p1spO49160EIF3C_ARATH	Eukaryotic translation initiation factor 3 subunit C	3	10493	14324	13646	12492	11377	11464	12821	11778	0,44530	-0,12	UNCHANGED

TRINITY_DN12862_c0_g1_i1_p1spP56820EIF3D_ARATH	Eukaryotic translation initiation factor 3 subunit D	4	10014	16785	13507	7747	10320	13467	13435	10511	0,31727	-0,35	UNCHANGED
TRINITY_DN137_c0_g1_i1_p1spO04202EIF3F_ARATH	Eukaryotic translation initiation factor 3 subunit F	5	46424	53107	44160	43335	44485	41138	47897	42986	0,16106	-0,16	UNCHANGED
TRINITY_DN4149_c0_g1_i1_p2spP24922IF5A2_NICPL	Eukaryotic translation initiation factor 5A-2	5	61473	49561	46550	45287	48539	47966	52528	47264	0,32226	-0,15	UNCHANGED
TRINITY_DN848_c2_g1_i2_p1UniRef100_A0A5D3BDQ9	Expansin	3	42010	55062	64154	31715	30587	39714	53742	34005	0,04862	-0,66	DOWN
TRINITY_DN5487_c0_g1_i8_p1spQ38865EXPA6_ARATH	Expansin-A6	3	43248	73141	75489	40881	41903	56919	63959	46567	0,20818	-0,46	UNCHANGED
TRINITY_DN15915_c0_g1_i1_p1UniRef100_A0A1S3CJS6	Fasciclin-like arabinogalactan protein 1	2	22967	29556	28278	37205	28774	31824	26934	32601	0,14982	0,28	UNCHANGED
TRINITY_DN6680_c0_g1_i1_p1UniRef100_UPI0019017EDA	Fasciclin-like arabinogalactan protein 10	4	23822	24020	22901	35913	34877	30683	23581	33824	0,00332	0,52	UNCHANGED
TRINITY_DN7011_c0_g1_i23_p1spK4CF70HPL_SOLLC	Fatty acid hydroperoxide lyase, chloroplastic	5	16909	27442	32160	23339	35721	53965	25503	37675	0,28928	0,56	UNCHANGED
TRINITY_DN4290_c1_g1_i3_p1spP10933FENR1_PEA	Ferredoxin--NADP reductase, leaf isozyme, chloroplastic	20	163809	180750	238640	204513	209144	262518	194400	225392	0,35010	0,21	UNCHANGED
TRINITY_DN7230_c0_g1_i6_p1spQ41014FENR2_PEA	Ferredoxin--NADP reductase, root isozyme, chloroplastic	5	30118	29000	30949	22542	20613	22794	30022	21983	0,00083	-0,45	UNCHANGED
TRINITY_DN30250_c0_g1_i2_p1spP38500NIR_BETPN	Ferredoxin--nitrite reductase, chloroplastic	6	12130	11646	14012	9239	8737	12989	12596	10321	0,20963	-0,29	UNCHANGED
TRINITY_DN149598_c3_g1_i1_p1spO04090FER1_ARATH	Ferredoxin-1, chloroplastic	3	178129	228580	283451	259479	309079	304316	230053	290958	0,15019	0,34	UNCHANGED
TRINITY_DN26829_c0_g3_i2_p1spQ43155GLTB_SPIOL	Ferredoxin-dependent glutamate synthase, chloroplastic	47	113629	167763	191631	159304	192115	223152	157674	191524	0,31566	0,28	UNCHANGED
TRINITY_DN35375_c0_g1_i8_p1spQ948P6FRI3_SOYBN	Ferritin-3, chloroplastic	2	29213	36154	33165	28242	27785	42298	32844	32775	0,98999	0,00	UNCHANGED
TRINITY_DN1152_c0_g1_i14_p1Fibrillarin	Fibrillarin	10	36034	32865	29173	31485	28264	34274	32691	31341	0,63552	-0,06	UNCHANGED

TRINITY_DN5306_c0_g1_i4_p1sp Q07511FDH_SOLTU	Formate dehydrogenase, mitochondrial	14	118746	148898	144934	89526	93490	101661	137526	94893	0,01352	-0,54	UNCHANGED
TRINITY_DN14447_c3_g1_i2_p1s pP28723FTHS_SPIOL	Formate--tetrahydrofolate ligase	14	26220	32392	29675	23253	19645	27752	29429	23550	0,11687	-0,32	UNCHANGED
TRINITY_DN3519_c0_g1_i2_p1sp Q42896SCRK2_SOLLC	Fructokinase-2	13	39824	45728	48468	19284	51870	42177	44673	37777	0,52800	-0,24	UNCHANGED
TRINITY_DN12337_c0_g1_i1_p1F BPase	Fructose-1-6-bisphosphatase,_FB Pase_C Fructose-1-6-bisphosphatase,	4	5666	6387	10242	9934	11577	10111	7432	10541	0,10909	0,50	UNCHANGED
TRINITY_DN131564_c0_g1_i2_p1 spP46275F16P1_PEA	Fructose-1,6-bisphosphatase, chloroplastic	10	202521	161510	164211	225060	203763	207212	176081	212012	0,07211	0,27	UNCHANGED
TRINITY_DN7144_c0_g1_i17_p1s pQ944G9ALFP2_ARATH	Fructose-bisphosphate aldolase 2, chloroplastic	19	269446	320630	392789	284072	325586	378202	327622	329287	0,97224	0,01	UNCHANGED
TRINITY_DN131705_c0_g1_i1_p1 spQ9ZU52ALFP3_ARATH	Fructose-bisphosphate aldolase 3, chloroplastic	11	36058	42743	45214	19483	22123	30085	41338	23897	0,01422	-0,79	DOWN
TRINITY_DN7086_c0_g1_i1_p1sp Q9SJQ9ALFC6_ARATH	Fructose-bisphosphate aldolase 6, cytosolic	12	61691	84687	72512	35663	39566	45529	72963	40253	0,01065	-0,86	DOWN
TRINITY_DN4841_c0_g1_i20_p2s pP46256ALF1_PEA	Fructose-bisphosphate aldolase, cytoplasmic isozyme 1	13	60734	78909	114517	99991	112976	121579	84720	111515	0,19003	0,40	UNCHANGED
TRINITY_DN12154_c0_g1_i1_p1F AA_hydrolase_N	Fumarylacetoacetase_FAA_hydrol ase Fumarylacetoacetate	4	12305	12333	14742	11584	10147	12341	13126	11357	0,16180	-0,21	UNCHANGED
TRINITY_DN8554_c0_g1_i2_p1sp Q9SEE5GALK1_ARATH	Galactokinase	15	64255	70221	71914	50934	50959	61453	68797	54449	0,02693	-0,34	UNCHANGED
TRINITY_DN2106_c3_g1_i4_p1Un iRef100_UPI0019016D46	Galactose mutarotase	2	11647	13906	17156	14909	11173	13596	14236	13226	0,62967	-0,11	UNCHANGED
TRINITY_DN3702_c0_g1_i2_p1Un iRef100_UPI00190202EA	Galactose mutarotase-like	3	13250	14699	35656	20377	20649	35373	21202	25466	0,65230	0,26	UNCHANGED
TRINITY_DN727_c0_g1_i5_p1spQ 84P54GATP1_SOLLC	Gamma aminobutyrate transaminase 1, mitochondrial	9	16164	16457	17925	13380	12540	15724	16849	13881	0,05386	-0,28	UNCHANGED

TRINITY_DN2375_c0_g3_i1_p1sp Q9FWR5GCA1_ARATH	Gamma carbonic anhydrase 1, mitochondrial	7	23545	26692	25464	19259	21346	23178	25234	21261	0,05252	-0,25	UNCHANGED
TRINITY_DN208609_c0_g1_i1_p1 spQ9SMN1GCAL2_ARATH	Gamma carbonic anhydrase-like 2, mitochondrial	2	12178	11116	11444	10745	9722	9249	11579	9905	0,03657	-0,23	UNCHANGED
TRINITY_DN553_c0_g1_i5_p1Uni Ref100_UPI001900D0D3	Gamma-glutamyl hydrolase 2-like	15	108043	109561	80736	98150	88122	103814	99446	96695	0,80496	-0,04	UNCHANGED
TRINITY_DN4879_c0_g1_i3_p1sp A2Z7B3GME1_ORYSI	GDP-mannose 3,5-epimerase 1	6	17432	49206	46407	20461	38549	47110	37682	35373	0,86607	-0,09	UNCHANGED
TRINITY_DN14412_c0_g1_i1_p1s pP93031GMD2_ARATH	GDP-mannose 4,6 dehydratase 2	2	12079	16606	12191	8922	7626	7645	13625	8064	0,02307	-0,76	DOWN
TRINITY_DN3133_c1_g1_i1_p1Li pase_GDSL	GDSL-like	2	4526	6678	5187	5455	8489	6972	5464	6972	0,23605	0,35	UNCHANGED
TRINITY_DN6210_c0_g1_i1_p1sp Q9ZS34CHLP_TOBAC	Geranylgeranyl diphosphate reductase, chloroplastic	14	83235	81735	88180	104242	97318	110908	84383	104156	0,01071	0,30	UNCHANGED
TRINITY_DN1646_c0_g1_i1_p1sp P36401E13H_TOBAC	Glucan endo-1,3-beta-glucosidase, acidic isoform PR-Q'	12	103825	101309	66602	70737	71647	52701	90578	65028	0,13140	-0,48	UNCHANGED
TRINITY_DN9104_c0_g1_i5_p1sp P55229GLGL1_ARATH	Glucose-1-phosphate adenylyltransferase large subunit 1, chloroplastic	10	8684	10218	13935	20581	24510	22530	10946	22540	0,00385	1,04	UP
TRINITY_DN12777_c0_g3_i3_p1s pP52417GLGS2_VICFA	Glucose-1-phosphate adenylyltransferase small subunit 2, chloroplastic	12	18950	19299	19417	36927	36646	35714	19222	36429	0,00000	0,92	UP
TRINITY_DN6187_c0_g1_i1_p1sp P37830G6PD_SOLTU	Glucose-6-phosphate 1-dehydrogenase, cytoplasmic isoform	10	29422	30757	40225	23564	22198	33680	33468	26481	0,23229	-0,34	UNCHANGED
TRINITY_DN5990_c0_g1_i10_p1s pB2J5F1G6PI_NOSP7	Glucose-6-phosphate isomerase	7	13034	18834	17546	15338	18451	21697	16471	18495	0,47053	0,17	UNCHANGED
TRINITY_DN1435_c3_g1_i1_p1sp P54243G6PI_OENSH	Glucose-6-phosphate isomerase, cytosolic	3	15212	16964	15188	11457	9220	11910	15788	10862	0,00842	-0,54	UNCHANGED
TRINITY_DN20522_c1_g1_i5_p1s pQ07346DCE_PETHY	Glutamate decarboxylase	25	115158	149757	149808	73630	78024	88856	138241	80170	0,00942	-0,79	DOWN

TRINITY_DN7666_c0_g1_i3_p1sp P54767DCE_SOLLC	Glutamate decarboxylase	16	48118	35962	37457	36474	24384	29467	40512	30108	0,11549	-0,43	UNCHANGED
TRINITY_DN31480_c0_g2_i1_p1U niRef100_A0A6J1HIB5	Glutamate decarboxylase	6	3733	4658	5268	13656	17063	19544	4553	16754	0,00229	1,88	UP
TRINITY_DN5380_c0_g2_i1_p1sp Q38946DHE2_ARATH	Glutamate dehydrogenase 2	5	17238	21259	20743	18422	17557	20982	19747	18987	0,66509	-0,06	UNCHANGED
TRINITY_DN2474_c0_g1_i3_p1sp Q9S7E9GGT2_ARATH	Glutamate--glyoxylate aminotransferase 2	19	49056	67034	80696	66565	84131	92503	65595	81066	0,26450	0,31	UNCHANGED
TRINITY_DN2474_c0_g1_i18_p1s pQ9S7E9GGT2_ARATH	Glutamate--glyoxylate aminotransferase 2	22	48062	55658	67634	76153	92453	88873	57118	85826	0,01902	0,59	UNCHANGED
TRINITY_DN4083_c0_g1_i1_p1sp Q42522GSA2_ARATH	Glutamate-1-semialdehyde 2,1-aminomutase 2, chloroplastic	13	92201	85316	79337	93201	89773	96134	85618	93036	0,14812	0,12	UNCHANGED
TRINITY_DN3490_c0_g1_i5_p1G CS2	Glutamate-cysteine	5	11883	10767	14525	10261	11769	10507	12392	10846	0,26980	-0,19	UNCHANGED
TRINITY_DN5380_c0_g1_i1_p1EL FV_dehydrog	Glutamate/Leucine/Phenylalanine/ Valine_ELFV_dehydrog_N Glu/Leu/Phe/Val	4	8773	9637	8022	6388	5530	5815	8811	5911	0,00544	-0,58	UNCHANGED
TRINITY_DN83339_c0_g1_i18_p1 spQ42899GLNA1_LOTJA	Glutamine synthetase cytosolic isozyme	7	24205	33229	32431	21876	29736	40210	29955	30607	0,91927	0,03	UNCHANGED
TRINITY_DN72240_c3_g1_i5_p1s pQ42899GLNA1_LOTJA	Glutamine synthetase cytosolic isozyme	16	92660	94962	92543	68956	72640	79483	93388	73693	0,00347	-0,34	UNCHANGED
TRINITY_DN6302_c0_g1_i8_p1sp P32289GLNA_VIGAC	Glutamine synthetase nodule isozyme	6	11135	13512	13217	5131	6235	6542	12621	5969	0,00152	-1,08	DOWN
TRINITY_DN4382_c0_g1_i14_p1s pQ43621GSHRC_PEA	Glutathione reductase, cytosolic	7	25410	30574	31516	21908	23143	25039	29167	23364	0,05102	-0,32	UNCHANGED
TRINITY_DN1516_c0_g1_i18_p1s pQ9FRL8DHAR2_ARATH	Glutathione S-transferase DHAR2	3	14690	19836	16944	14114	19614	16431	17157	16720	0,85108	-0,04	UNCHANGED
TRINITY_DN1516_c0_g1_i15_p1s pQ9FRL8DHAR2_ARATH	Glutathione S-transferase DHAR2	3	12601	15417	7059	6883	8375	5985	11692	7081	0,14508	-0,72	UNCHANGED
TRINITY_DN2308_c0_g1_i4_p1Un iRef100_A0A5A7VCW2	Glutathione transferase	4	45380	49041	40145	34710	35654	36324	44855	35562	0,02397	-0,33	UNCHANGED

TRINITY_DN13748_c0_g2_i5_p1Gp_dh_C	Glyceraldehyde	15	78361	82450	99792	108664	109825	107593	86868	108694	0,02975	0,32	UNCHANGED
TRINITY_DN2402_c0_g1_i10_p1spQ7FAH2G3PC2_ORYSJ	Glyceraldehyde-3-phosphate dehydrogenase 2, cytosolic	23	126440	130885	106124	107693	106333	98338	121150	104121	0,10524	-0,22	UNCHANGED
TRINITY_DN18589_c0_g1_i1_p1spP0A9B4G3P1_ECO57	Glyceraldehyde-3-phosphate dehydrogenase A	3	10123	11656	9676	6055	7493	7146	10485	6898	0,00834	-0,60	DOWN
TRINITY_DN5404_c0_g1_i5_p1spP12859G3PB_PEA	Glyceraldehyde-3-phosphate dehydrogenase B, chloroplastic	21	137327	145691	156168	156571	169710	161825	146395	162702	0,07041	0,15	UNCHANGED
TRINITY_DN13748_c0_g2_i1_p1spQ9LPW0G3PA2_ARATH	Glyceraldehyde-3-phosphate dehydrogenase GAPA2, chloroplastic	21	125757	148572	194693	155404	167504	193364	156341	172090	0,53382	0,14	UNCHANGED
TRINITY_DN2245_c0_g1_i15_p1spQ5E924G3PP2_ARATH	Glyceraldehyde-3-phosphate dehydrogenase GAPCP2, chloroplastic	4	5831	6693	8095	4031	4263	4472	6873	4255	0,01760	-0,69	DOWN
TRINITY_DN2402_c0_g1_i11_p2spP25861G3PC_ANTMA	Glyceraldehyde-3-phosphate dehydrogenase, cytosolic	23	137344	148448	136562	84082	82522	86543	140785	84382	0,00015	-0,74	DOWN
TRINITY_DN2402_c0_g1_i12_p1spP26520G3PC_PETHY	Glyceraldehyde-3-phosphate dehydrogenase, cytosolic	21	129739	148279	119561	138711	136067	143171	132526	139316	0,47673	0,07	UNCHANGED
TRINITY_DN1264_c0_g1_i23_p1spP13443DHGY_CUCSA	Glycerate dehydrogenase	14	84180	80098	95168	108337	104326	97145	86482	103269	0,03929	0,26	UNCHANGED
TRINITY_DN101_c2_g1_i1_p1UniRef100_UPI001C360F2C	Glycerophosphodiester phosphodiesterase GDPDL4	10	40073	39154	34808	45278	42264	40902	38012	42815	0,08166	0,17	UNCHANGED
TRINITY_DN7087_c0_g1_i1_p1spQ39732GCSH_FLAAN	Glycine cleavage system H protein, mitochondrial	8	50324	63423	53685	78403	126325	104534	55810	103087	0,03041	0,89	UP
TRINITY_DN13459_c0_g1_i1_p1spP49361GCSPA_FLAPR	Glycine dehydrogenase (decarboxylating) A, mitochondrial	31	5346	5869	7448	8539	8462	9945	6221	8982	0,02551	0,53	UNCHANGED
TRINITY_DN13459_c0_g1_i2_p1spO49954GCSP_SOLTU	Glycine dehydrogenase (decarboxylating), mitochondrial	35	120493	132286	167876	145877	144558	169905	140218	153446	0,46646	0,13	UNCHANGED
TRINITY_DN37620_c0_g1_i4_p1spO23627SYGM1_ARATH	Glycine--tRNA ligase, mitochondrial 1	13	17409	16551	17817	17131	16651	15919	17259	16567	0,24890	-0,06	UNCHANGED

TRINITY_DN1734_c0_g1_i1_p1UniRef100_A0A6J1K0M4	Glycine-rich RNA-binding protein 4, mitochondrial-like	4	40199	36520	23906	31095	27896	28431	33542	29141	0,43114	-0,20	UNCHANGED
TRINITY_DN73407_c0_g1_i13_p1spQ9LRR9GLO1_ARATH	Glycolate oxidase 1	23	185972	232999	191362	221587	240293	255351	203444	239077	0,11559	0,23	UNCHANGED
TRINITY_DN4321_c0_g1_i1_p1Glyco_hydro_17	Glycosyl	2	4437	6354	11757	9504	12795	11183	7516	11160	0,20173	0,57	UNCHANGED
TRINITY_DN1529_c1_g1_i11_p1Glyco_hydro_1	Glycosyl	8				4554	4724	5867	-	5048	-	-	Unique_PM
TRINITY_DN533_c0_g1_i8_p1spF4I907GLYR2_ARATH	Glyoxylate/succinic semialdehyde reductase 2, chloroplastic	5	8765	11308	17290	14138	17880	17599	12454	16539	0,21820	0,41	UNCHANGED
TRINITY_DN3007_c0_g1_i4_p1spP38548RAN_VICFA	GTP-binding nuclear protein Ran/TC4	10	127836	147729	118774	106027	114841	107164	131446	109344	0,06976	-0,27	UNCHANGED
TRINITY_DN8283_c0_g1_i1_p1spO04834SAR1A_ARATH	GTP-binding protein SAR1A	5	27424	26578	27311	22041	17948	22802	27104	20930	0,01568	-0,37	UNCHANGED
TRINITY_DN1142_c0_g1_i10_p1spO04834SAR1A_ARATH	GTP-binding protein SAR1A	6	25587	20327	23214	28023	21901	26691	23043	25538	0,35741	0,15	UNCHANGED
TRINITY_DN64798_c0_g1_i5_p1spQ39836GBLP_SOYBN	Guanine nucleotide-binding protein subunit beta-like protein	14	115607	152393	118536	71660	95836	116993	128845	94830	0,12591	-0,44	UNCHANGED
TRINITY_DN7020_c0_g1_i9_p1spO24653GDI2_ARATH	Guanosine nucleotide diphosphate dissociation inhibitor 2	13	38979	53826	43285	28753	34443	37228	45363	33475	0,07882	-0,44	UNCHANGED
TRINITY_DN13201_c0_g1_i3_p1spQ01233HSP70_NEUCR	Heat shock 70 kDa protein	3	13869	12484	14947	12787	12413	11193	13767	12131	0,13004	-0,18	UNCHANGED
TRINITY_DN2982_c1_g2_i1_p1spP26413HSP70_SOYBN	Heat shock 70 kDa protein	8	1523	1762	1413	2913	3042	2551	1566	2835	0,00212	0,86	UP
TRINITY_DN16818_c0_g1_i2_p1spQ9S7C0HSP7O_ARATH	Heat shock 70 kDa protein 14	19	45830	84416	61240	28957	24300	32048	63829	28435	0,03641	-1,17	DOWN
TRINITY_DN43107_c0_g2_i1_p1spP0DMV8HS71A_HUMAN	Heat shock 70 kDa protein 1A	10	11428	14835	10040	5581	7636	7317	12101	6845	0,02812	-0,82	DOWN
TRINITY_DN7785_c0_g1_i1_p1spQ01899HSP7M_PHAVU	Heat shock 70 kDa protein, mitochondrial	14	59917	56858	66146	39399	42755	47112	60974	43088	0,00714	-0,50	UNCHANGED

TRINITY_DN121394_c0_g1_i1_p1 spP09189HSP7C_PETHY	Heat shock cognate 70 kDa protein	24	95660	102714	100512	59095	59618	67286	99629	62000	0,00037	-0,68	DOWN
TRINITY_DN2982_c1_g3_i2_p1sp P09189HSP7C_PETHY	Heat shock cognate 70 kDa protein	19	114387	114970	119760	83069	93898	101514	116372	92827	0,01377	-0,33	UNCHANGED
TRINITY_DN26598_c0_g1_i1_p1s pP27322HSP72_SOLLC	Heat shock cognate 70 kDa protein 2	29	87150	106786	121345	126647	106913	107700	105094	113753	0,50451	0,11	UNCHANGED
TRINITY_DN3960_c0_g1_i1_p1sp P36181HSP80_SOLLC	Heat shock cognate protein 80	31	231032	221526	210005	179978	175320	153155	220854	169484	0,00747	-0,38	UNCHANGED
TRINITY_DN11832_c0_g1_i1_p1s pQ9SIF2HS905_ARATH	Heat shock protein 90-5, chloroplastic	13	23250	25927	25532	23748	29266	30323	24903	27779	0,26162	0,16	UNCHANGED
TRINITY_DN18829_c0_g1_i1_p1U niRef100_UPI001C36A2DA	Heme-binding protein 2	5	32919	39607	40845	38957	49642	49841	37790	46147	0,12760	0,29	UNCHANGED
TRINITY_DN30340_c0_g1_i2_p1s pO22582H2B_GOSHI	Histone H2B	6	182807	162584	180192	155496	161202	165509	175194	160736	0,10709	-0,12	UNCHANGED
TRINITY_DN17916_c0_g1_i11_p1 spP62785H41_WHEAT	Histone H4 variant TH011	8	126002	104084	78603	88260	76849	76254	102896	80454	0,19020	-0,35	UNCHANGED
TRINITY_DN5689_c0_g1_i4_p1Un iRef100_H6TB35	HSP27_8	3	10555	11776	15169	8420	8119	10842	12500	9127	0,10690	-0,45	UNCHANGED
TRINITY_DN43107_c0_g3_i1_p1H SP70	Hsp70	9	80410	79828	79804	51519	53972	64495	80014	56662	0,00423	-0,50	UNCHANGED
TRINITY_DN8967_c0_g1_i2_p1H SP90	Hsp90	2	6333	20275	20915	9997	18000	20363	15841	16120	0,96328	0,03	UNCHANGED
TRINITY_DN7320_c0_g1_i3_p1sp O22478IMA_SOLLC	Importin subunit alpha	13	21185	22166	22352	17740	16720	18478	21901	17646	0,00243	-0,31	UNCHANGED
TRINITY_DN42199_c0_g1_i2_p1s pQ96321IMPA1_ARATH	Importin subunit alpha-1	10	30406	30723	32481	21484	20203	21767	31203	21151	0,00024	-0,56	UNCHANGED
TRINITY_DN71_c0_g1_i11_p1spQ 9FJD4IMB1_ARATH	Importin subunit beta-1	6	26940	31195	32594	17436	13561	16562	30243	15853	0,00223	-0,93	DOWN
TRINITY_DN3116_c0_g1_i1_p1Py rophosphatase	Inorganic	2	8421	12185	13472	9072	15795	10425	11359	11764	0,88168	0,05	UNCHANGED

TRINITY_DN8778_c0_g1_i2_p1sp Q9SA34IMDH2_ARATH	Inosine-5'-monophosphate dehydrogenase 2	2	14406	16611	10039	12146	13778	16783	13685	14235	0,82718	0,06	UNCHANGED
TRINITY_DN8577_c0_g1_i8_p1sp P54928IMP3_SOLLC	Inositol monophosphatase 3	3	11310	13416	15691	12915	14717	16663	13472	14765	0,48080	0,13	UNCHANGED
TRINITY_DN24056_c0_g3_i3_p1s pQ945K7IDH5_ARATH	Isocitrate dehydrogenase [NAD] catalytic subunit 5, mitochondrial	11	31352	34287	35351	25213	24771	31929	33663	27304	0,07121	-0,30	UNCHANGED
TRINITY_DN881_c1_g1_i4_p1spQ 8LFC0IDH1_ARATH	Isocitrate dehydrogenase [NAD] regulatory subunit 1, mitochondrial	4	19929	25765	25324	13138	18166	22005	23673	17770	0,13696	-0,41	UNCHANGED
TRINITY_DN66426_c0_g1_i11_p1 spQ06197IDHC_SOYBN	Isocitrate dehydrogenase [NADP]	13	64569	66670	53578	40360	43638	45287	61606	43095	0,01270	-0,52	UNCHANGED
TRINITY_DN353_c0_g1_i13_p1Un iRef100_A0A6J1IPQ6	Isocitrate lyase	4	35381	44762	44503	27610	32923	36627	41549	32387	0,08621	-0,36	UNCHANGED
TRINITY_DN5541_c0_g1_i17_p1Is o_dh	Isocitrate/isopropylmalate	3	11080	13341	13296	11081	11645	16936	12572	13221	0,76309	0,07	UNCHANGED
TRINITY_DN12707_c0_g1_i3_p1s pQ05758ILV5_ARATH	Ketol-acid reductoisomerase, chloroplastic	11	47969	74090	49171	35263	40892	42458	57076	39538	0,11673	-0,53	UNCHANGED
TRINITY_DN8748_c0_g1_i5_p1Un iRef100_A0A6J1H3Q6	KH domain-containing protein HEN4-like	5	21736	16851	16167	19874	14471	14778	18252	16374	0,49101	-0,16	UNCHANGED
TRINITY_DN5455_c0_g1_i14_p1s pQ1KLZ2CAS1_MALDO	L-3-cyanoalanine synthase 1, mitochondrial	12	38855	38661	37697	39601	35965	36067	38404	37211	0,39310	-0,05	UNCHANGED
TRINITY_DN11221_c0_g2_i1_p1s pP14133ASO_CUCSA	L-ascorbate oxidase	2	9986	13458	8570	4158	4554	4208	10671	4307	0,01199	-1,31	DOWN
TRINITY_DN5999_c0_g1_i1_p1U niRef100_UPI0018FF2EEE	L-ascorbate oxidase homolog	5	22283	22002	24425	13927	14170	14806	22903	14301	0,00044	-0,68	DOWN
TRINITY_DN606_c1_g1_i1_p1Uni Ref100_UPI0019000686	L-ascorbate oxidase homolog	3	1982	2315	1941	1907	1743	2083	2080	1911	0,33410	-0,12	UNCHANGED
TRINITY_DN18180_c0_g1_i3_p1s pQ05431APX1_ARATH	L-ascorbate peroxidase 1, cytosolic	6	100919	123343	112672	75535	101287	122102	112312	99642	0,44428	-0,17	UNCHANGED
TRINITY_DN40954_c0_g1_i18_p1 spP48534APX1_PEA	L-ascorbate peroxidase, cytosolic	11	124937	157273	73768	87320	128299	111399	118659	109006	0,73933	-0,12	UNCHANGED

TRINITY_DN19516_c0_g1_i3_p1spO65398GLX1_ARATH	Lactoylglutathione lyase GLX1	9	47872	52440	59032	41224	45953	52922	53115	46700	0,24352	-0,19	UNCHANGED
TRINITY_DN4957_c0_g1_i1_p1UniRef100_A0A0A0LID3	Late embryogenesis abundant protein, LEA-14	7	36443	40537	30029	24380	22663	26231	35670	24425	0,02524	-0,55	UNCHANGED
TRINITY_DN2159_c0_g1_i4_p1spQ9SPB1LEGRE_VIGUN	Leghemoglobin reductase	12	71580	73599	86414	68068	77391	83007	77198	76155	0,87794	-0,02	UNCHANGED
TRINITY_DN3346_c0_g1_i13_p1spQ944P7AMPL2_ARATH	Leucine aminopeptidase 2, chloroplastic	15	31894	39837	37719	27842	34421	36456	36483	32906	0,36709	-0,15	UNCHANGED
TRINITY_DN3346_c0_g1_i1_p1spP31427AMPL_SOLTU	Leucine aminopeptidase, chloroplastic	16	74264	69768	64326	89609	112589	117339	69453	106512	0,01481	0,62	UP
TRINITY_DN3556_c1_g2_i1_p1spF4I116SYLC_ARATH	Leucine--tRNA ligase, cytoplasmic	4	8875	8840	7641	5221	5312	8003	8452	6179	0,08517	-0,45	UNCHANGED
TRINITY_DN706_c0_g1_i8_p1spO24370LOX21_SOLTU	Linoleate 13S-lipoxygenase 2-1, chloroplastic	36	119046	120730	146023	147434	163843	154237	128600	155171	0,05560	0,27	UNCHANGED
TRINITY_DN706_c0_g1_i6_p1spO24370LOX21_SOLTU	Linoleate 13S-lipoxygenase 2-1, chloroplastic	36	27593	24755	28762	31613	29130	27861	27037	29535	0,19828	0,13	UNCHANGED
TRINITY_DN349_c0_g1_i19_p1spQ41238LOX16_SOLTU	Linoleate 9S-lipoxygenase 6 (Fragment)	13	11129	12603	18787	15505	18009	13526	14173	15680	0,60405	0,15	UNCHANGED
TRINITY_DN349_c0_g1_i18_p1spQ41238LOX16_SOLTU	Linoleate 9S-lipoxygenase 6 (Fragment)	19	10536	12525	12887	52792	56435	68860	11983	59362	0,00065	2,31	UP
TRINITY_DN3440_c0_g1_i7_p1UniRef100_A0A6J1J654	Lipoxygenase	23	91910	101311	80859	48263	44180	32779	91360	41740	0,00272	-1,13	DOWN
TRINITY_DN349_c0_g1_i15_p1Lipoxygenase	Lipoxygenase	2	12869	11037	15796	34794	33713	38493	13234	35666	0,00036	1,43	UP
TRINITY_DN6636_c0_g1_i5_p1Lipoxygenase	Lipoxygenase	5	3819	5430	6605	19447	26472	24979	5285	23632	0,00130	2,16	UP
TRINITY_DN10801_c0_g1_i4_p1spQ93ZN9DAPAT_ARATH	LL-diaminopimelate aminotransferase, chloroplastic	12	66956	69587	90660	36170	37904	60448	75735	44841	0,04635	-0,76	DOWN
TRINITY_DN5607_c0_g1_i3_p1spQ9CAP8LACS9_ARATH	Long chain acyl-CoA synthetase 9, chloroplastic	6	23174	21136	22034	19177	19813	18854	22115	19281	0,01230	-0,20	UNCHANGED

TRINITY_DN620_c0_g1_i3_p1Lyase_1	Lyase	6	21522	23939	17468	17483	15835	18023	20976	17114	0,12551	-0,29	UNCHANGED
TRINITY_DN559_c0_g1_i15_p1UniRef100_A0A6J1HRS5	Macrophage migration inhibitory factor homolog isoform X2	2	6357	6788	1351	10911	17233	8995	4832	12379	0,06799	1,36	UNCHANGED
TRINITY_DN11945_c0_g2_i1_p1spP93162CHLI_SOYBN	Magnesium-chelatase subunit ChlI, chloroplastic	14	44141	50351	50894	52461	58827	70115	48462	60468	0,09857	0,32	UNCHANGED
TRINITY_DN57320_c0_g1_i4_p1spQ6SJV8CRD1_GOSHI	Magnesium-protoporphyrin IX monomethyl ester [oxidative] cyclase, chloroplastic	10	27885	25813	27347	27302	26544	34262	27015	29369	0,40524	0,12	UNCHANGED
TRINITY_DN2396_c1_g4_i1_p1MIP	Major	3	92844	100694	104377	87568	129226	124192	99305	113662	0,34944	0,19	UNCHANGED
TRINITY_DN700_c8_g1_i1_p1MIP	Major	5	43664	46670	78265	52671	59081	73759	56200	61837	0,68020	0,14	UNCHANGED
TRINITY_DN6104_c0_g1_i2_p1spQ9FSF0MDH_TOBAC	Malate dehydrogenase	8	6914	8936	8641	10738	11228	12780	8164	11582	0,01785	0,50	UNCHANGED
TRINITY_DN18796_c1_g1_i3_p1spO48902MDHP_MEDSA	Malate dehydrogenase [NADP], chloroplastic	10	30837	34798	31999	28707	30518	34427	32545	31217	0,55384	-0,06	UNCHANGED
TRINITY_DN5415_c0_g1_i1_p1spQ9SN86MDHP_ARATH	Malate dehydrogenase, chloroplastic	11	17362	21266	13350	17900	16766	15198	17326	16622	0,78512	-0,06	UNCHANGED
TRINITY_DN15956_c4_g1_i2_p1spO48905MDHC_MEDSA	Malate dehydrogenase, cytoplasmic	18	231068	292228	262767	179850	198910	210884	262021	196548	0,02992	-0,41	UNCHANGED
TRINITY_DN5959_c0_g1_i36_p1spP19446MDHG_CITLA	Malate dehydrogenase, glyoxysomal	13	74449	81740	72559	122384	121608	103833	76250	115942	0,00401	0,60	UP
TRINITY_DN13592_c0_g1_i8_p1spP17783MDHM_CITLA	Malate dehydrogenase, mitochondrial	19	116220	127355	118123	124124	129062	114515	120566	122567	0,73363	0,02	UNCHANGED
TRINITY_DN141_c5_g1_i1_p1MSP	Manganese-stabilising	10	298911	247868	329669	314345	332669	339986	292150	329000	0,21514	0,17	UNCHANGED
TRINITY_DN64020_c3_g2_i2_p1spQ9XFM6MSBP1_ARATH	Membrane steroid-binding protein 1	2	18670	19179	12170	16097	14726	14562	16673	15128	0,53995	-0,14	UNCHANGED
TRINITY_DN11900_c0_g1_i1_p1spO64517MCA4_ARATH	Metacaspase-4	7	38953	41708	33689	21252	21778	25853	38117	22961	0,00540	-0,73	DOWN

TRINITY_DN10580_c0_g2_i1_p1sp|O80585|MTHR2_ARATH	Methylenetetrahydrofolate reductase 2	13	20930	28575	30418	16469	25186	22755	26641	21470	0,25514	-0,31	UNCHANGED
TRINITY_DN14438_c0_g1_i4_p2 Mt_ATP-synt_B	Mitochondrial	5	35265	32271	37704	22273	23648	27884	35080	24602	0,01047	-0,51	UNCHANGED
TRINITY_DN9545_c0_g1_i1_p1sp|Q93XM7|MCAT_ARATH	Mitochondrial carnitine/acylcarnitine carrier-like protein	6	15997	19367	17920	16592	18380	21446	17761	18806	0,57657	0,08	UNCHANGED
TRINITY_DN8735_c0_g2_i1_p1sp|Q9C5M0|DTC_ARATH	Mitochondrial dicarboxylate/tricarboxylate transporter DTC	8	20870	20170	30733	34303	29685	30843	23924	31611	0,10509	0,40	UNCHANGED
TRINITY_DN2634_c0_g1_i1_p1sp|Q9C5M0|DTC_ARATH	Mitochondrial dicarboxylate/tricarboxylate transporter DTC	9	35334	40632	34748	30230	34827	34008	36904	33022	0,17331	-0,16	UNCHANGED
TRINITY_DN11554_c0_g1_i3_p1sp|Q9LHE5|TO401_ARATH	Mitochondrial import receptor subunit TOM40-1	3	11349	14805	11626	8761	11900	15305	12593	11989	0,79618	-0,07	UNCHANGED
TRINITY_DN6880_c1_g1_i2_p1sp|Q9FJX3|VDAC2_ARATH	Mitochondrial outer membrane protein porin 2	3	33692	20657	31359	31933	31421	31717	28569	31690	0,48049	0,15	UNCHANGED
TRINITY_DN14757_c0_g1_i2_p1sp|Q9FKM2|VDAC4_ARATH	Mitochondrial outer membrane protein porin 4	6	26406	28950	29116	23161	20084	24279	28157	22508	0,02099	-0,32	UNCHANGED
TRINITY_DN9566_c0_g1_i6_p1sp|P42055|VDAC1_SOLTU	Mitochondrial outer membrane protein porin of 34 kDa	5	67434	82565	83358	69178	71592	76269	77786	72347	0,38512	-0,10	UNCHANGED
TRINITY_DN1874_c0_g1_i1_p1sp|P42056|VDAC2_SOLTU	Mitochondrial outer membrane protein porin of 36 kDa	3	20692	19002	26507	17578	39350	19850	22067	25593	0,65325	0,21	UNCHANGED
TRINITY_DN19056_c0_g1_i1_p1sp|Q9FMU6|MPCP3_ARATH	Mitochondrial phosphate carrier protein 3, mitochondrial	3	15601	18335	12476	11415	17064	15199	15471	14559	0,72048	-0,09	UNCHANGED
TRINITY_DN2928_c2_g1_i3_p1sp|P29677|MPPA_SOLTU	Mitochondrial-processing peptidase subunit alpha	12	26113	31226	30711	13680	20539	24207	29350	19475	0,04725	-0,59	UNCHANGED

TRINITY_DN3822_c0_g2_i1_p1UniRef100_A0A6J1I826	MLP-like protein 43	3	25787	30394	12110	14770	21818	12580	22764	16389	0,35902	-0,47	UNCHANGED
TRINITY_DN3822_c0_g1_i14_p1spQ9SSK5MLP43_ARATH	MLP-like protein 43	4	48151	50111	55740	33837	40127	36931	51334	36965	0,00783	-0,47	UNCHANGED
TRINITY_DN7534_c0_g1_i1_p1spP92947MDAR_ARATH	Monodehydroascorbate reductase, chloroplastic/mitochondrial	2	8811	11846	13899	11471	14888	18391	11518	14917	0,24325	0,37	UNCHANGED
TRINITY_DN556_c0_g2_i1_p1spQ42711MDARS_CUCSA	Monodehydroascorbate reductase, seedling isozyme	9	48020	49247	38570	28629	32175	27154	45279	29319	0,01237	-0,63	DOWN
TRINITY_DN556_c0_g1_i13_p1spQ42711MDARS_CUCSA	Monodehydroascorbate reductase, seedling isozyme	10	38897	41083	42815	24872	45049	44227	40932	38049	0,68873	-0,11	UNCHANGED
TRINITY_DN8644_c0_g1_i3_p1UniRef100_A0A0D2QK58	MPN domain-containing protein	4	21056	21141	21570	17985	16011	18077	21255	17358	0,00490	-0,29	UNCHANGED
TRINITY_DN606_c0_g1_i1_p1Cu-oxidase	Multicopper	8	44348	42870	52659	22714	22943	24950	46625	23536	0,00180	-0,99	DOWN
TRINITY_DN5224_c0_g1_i3_p2Cu-oxidase_2	Multicopper	2	10147	10515	10623	9306	10876	6993	10428	9058	0,29472	-0,20	UNCHANGED
TRINITY_DN5322_c0_g1_i4_p1Cu-oxidase	Multicopper	8	10732	13965	13162	8513	10656	11726	12620	10298	0,16187	-0,29	UNCHANGED
TRINITY_DN2829_c0_g2_i1_p1Cu-oxidase	Multicopper_Cu-oxidase_3 Multicopper	4	20859	22183	21955	17587	24823	24167	21665	22192	0,83329	0,03	UNCHANGED
TRINITY_DN184_c0_g1_i1_p1spQ3HVN1AGUB_SOLTU	N-carbamoylputrescine amidase	3	12995	16667	17595	8696	10416	15581	15753	11564	0,16924	-0,45	UNCHANGED
TRINITY_DN3969_c1_g3_i1_p1spP37225MAON_SOLTU	NAD-dependent malic enzyme 59 kDa isoform, mitochondrial	8	20511	23224	21330	13973	14218	16302	21689	14831	0,00328	-0,55	UNCHANGED
TRINITY_DN3177_c0_g1_i20_p1spQ9LSQ5FQR1_ARATH	NAD(P)H dehydrogenase (quinone) FQR1	7	47982	33075	39361	36861	29511	32514	40139	32962	0,21063	-0,28	UNCHANGED
TRINITY_DN12727_c0_g1_i1_p2spQ4VZH2NDHJ_CUCSA	NAD(P)H-quinone oxidoreductase subunit J, chloroplastic	3	3985	4729	5924	8522	11446	8063	4879	9343	0,02050	0,94	UP

TRINITY_DN11148_c0_g1_i1_p1sp|Q9SK66|NDUA9_ARATH	NADH dehydrogenase [ubiquinone] 1 alpha subcomplex subunit 9, mitochondrial	3	9459	9751	9533	9455	8509	10780	9581	9581	0,99950	0,00	UNCHANGED
TRINITY_DN2238_c0_g1_i1_p1sp|Q9FNN5|NDUV1_ARATH	NADH dehydrogenase [ubiquinone] flavoprotein 1, mitochondrial	2	7105	12773	8483	7011	9341	9029	9453	8460	0,62107	-0,16	UNCHANGED
TRINITY_DN14443_c1_g1_i1_p1sp|Q43644|NDUS1_SOLTU	NADH dehydrogenase [ubiquinone] iron-sulfur protein 1, mitochondrial	3	16155	15657	16080	12368	11617	13627	15964	12538	0,00484	-0,35	UNCHANGED
TRINITY_DN6762_c0_g1_i5_p1sp|P93306|NDUS2_ARATH	NADH dehydrogenase [ubiquinone] iron-sulfur protein 2	9	22203	21784	22698	15486	16946	19852	22228	17428	0,02151	-0,35	UNCHANGED
TRINITY_DN8198_c0_g1_i10_p1sp|Q95748|NDUS3_ARATH	NADH dehydrogenase [ubiquinone] iron-sulfur protein 3	5	9251	10312	9014	5724	5788	5329	9526	5614	0,00077	-0,76	DOWN
TRINITY_DN9565_c0_g1_i9_p1sp|P28475|S6PD_MALDO	NADP-dependent D-sorbitol-6-phosphate dehydrogenase	3	19927	26617	34219	22352	28589	27887	26921	26276	0,89471	-0,03	UNCHANGED
TRINITY_DN9384_c0_g1_i1_p1sp|P93338|GAPN_NICPL	NADP-dependent glyceraldehyde-3-phosphate dehydrogenase	6	16726	21132	23450	21372	22151	23758	20436	22427	0,39532	0,13	UNCHANGED
TRINITY_DN11243_c0_g1_i17_p1sp|P51615|MAOX_VITVI	NADP-dependent malic enzyme	27	180805	230591	195921	94212	117573	124537	202439	112107	0,00650	-0,85	DOWN
TRINITY_DN9158_c0_g1_i22_p1sp|Q9CA83|MAOP4_ARATH	NADP-dependent malic enzyme 4, chloroplastic	6	28593	42990	28277	16250	24234	20403	33287	20296	0,07291	-0,71	UNCHANGED
TRINITY_DN6292_c0_g1_i1_p1sp|Q0PGJ6|AKRC9_ARATH	NADPH-dependent aldo-keto reductase, chloroplastic	10	25415	33207	28931	27267	29136	31508	29184	29304	0,96510	0,01	UNCHANGED
TRINITY_DN3520_c2_g2_i1_p1sp|Q9ZUC1|AOR_ARATH	NADPH-dependent alkenal/one oxidoreductase, chloroplastic	12	19751	21094	32079	31773	33313	39749	24308	34945	0,08207	0,52	UNCHANGED
TRINITY_DN4855_c1_g1_i3_p1UniRef100_UPI0018FF2DC4	NADPH-dependent thioredoxin reductase 3	4	5885	6419	8185	11819	12301	13683	6830	12601	0,00294	0,88	UP

TRINITY_DN13106_c0_g1_i10_p1 spQ9M612NACA_PINTA	Nascent polypeptide-associated complex subunit alpha-like protein	8	105366	107126	66332	46243	87486	79658	92941	71129	0,30061	-0,39	UNCHANGED
TRINITY_DN14470_c0_g1_i2_p1s pQ9CAT7BTF3L_ARATH	Nascent polypeptide-associated complex subunit beta	2	6629	10811	3754	5893	11434	5956	7065	7761	0,81273	0,14	UNCHANGED
TRINITY_DN14382_c0_g1_i3_p1s pQ9SCP7NAMT1_ARATH	Nicotinate N-methyltransferase 1	3	8027	7699	8036	14854	12399	15667	7921	14307	0,00296	0,85	UP
TRINITY_DN10580_c1_g1_i19_p1 spA0A077EW86NOMT2_NARAP	Norbelladine 4'-O-methyltransferase 2	8	50159	49427	69216	60576	51077	69704	56267	60453	0,64516	0,10	UNCHANGED
TRINITY_DN2080_c0_g3_i1_p1sp Q9C7F5NTF2B_ARATH	Nuclear transport factor 2B	4	45869	62654	44134	32452	49481	54612	50886	45515	0,57996	-0,16	UNCHANGED
TRINITY_DN999_c2_g1_i3_p1Uni Ref100_UPI0018FF7295	Nucleoside diphosphate kinase	6	35439	39150	38735	40396	50243	52938	37775	47859	0,06476	0,34	UNCHANGED
TRINITY_DN41365_c0_g1_i16_p2 spQ02254NDK1_SPIOL	Nucleoside diphosphate kinase 1	4	45895	64122	67033	43878	61162	80419	59017	61820	0,83295	0,07	UNCHANGED
TRINITY_DN4383_c4_g1_i1_p1sp O49203NDK3_ARATH	Nucleoside diphosphate kinase III, chloroplastic/mitochondrial	2	43147	47219	52722	38785	48503	63206	47696	50165	0,76222	0,07	UNCHANGED
TRINITY_DN11017_c0_g1_i2_p1U niRef100_A0A2P5G1S3	Nucleoside phosphorylase	12	149398	186059	129289	137971	153459	178409	154915	156613	0,93757	0,02	UNCHANGED
TRINITY_DN11953_c1_g1_i4_p1N AP	Nucleosome	9	66188	70255	60403	27909	47214	59830	65616	44984	0,10086	-0,54	UNCHANGED
TRINITY_DN234_c0_g1_i1_p1spQ 8L831NUDT3_ARATH	Nudix hydrolase 3	2	6723	8408	7848	8664	9069	9746	7660	9159	0,06310	0,26	UNCHANGED
TRINITY_DN3312_c0_g1_i1_p1M ethyltransf_3	O-methyltransferase	3	22872	25966	18076	13216	14190	14781	22305	14062	0,02440	-0,67	DOWN
TRINITY_DN14051_c0_g1_i3_p1s pQ9SA73OLA1_ARATH	Obg-like ATPase 1	10	43247	52849	101833	54947	74497	98658	65976	76034	0,67280	0,20	UNCHANGED
TRINITY_DN8239_c0_g1_i1_p1sp Q8RUF8NILP3_ARATH	Omega-amidase, chloroplastic	5	13717	15599	22921	19995	8660	27119	17412	18591	0,85530	0,09	UNCHANGED
TRINITY_DN9595_c1_g1_i1_p1sp Q94AM1OOPDA_ARATH	Organellar oligopeptidase A, chloroplastic/mitochondrial	11	5952	7017	6046	5129	5550	4962	6339	5214	0,04241	-0,28	UNCHANGED

TRINITY_DN9595_c1_g1_i13_p1sp|Q94AM1|OOPDA_ARATH	Organellar oligopeptidase A, chloroplastic/mitochondrial	11	23871	29409	32006	23685	21431	24437	28429	23184	0,11020	-0,29	UNCHANGED
TRINITY_DN3340_c0_g1_i11_p1sp|Q9FNK4|OAT_ARATH	Ornithine aminotransferase, mitochondrial	7	23293	23819	17569	15087	15498	17437	21560	16007	0,05948	-0,43	UNCHANGED
TRINITY_DN45821_c0_g1_i1_p1sp|Q41350|OLP1_SOLLC	Osmotin-like protein	8	60866	72707	49488	39108	73576	74024	61020	62236	0,93190	0,03	UNCHANGED
TRINITY_DN6940_c0_g1_i3_p1sp|Q1H5C9|OP24A_ARATH	Outer envelope pore protein 24A, chloroplastic	4	15057	19154	22722	20219	18770	21748	18978	20246	0,62175	0,09	UNCHANGED
TRINITY_DN12358_c0_g2_i1_p1sp|Q4LDF9|OEP37_PEA	Outer envelope pore protein 37, chloroplastic	4	17358	14568	15370	16404	12191	13736	15766	14110	0,32703	-0,16	UNCHANGED
TRINITY_DN7049_c0_g2_i12_p1NAD_binding_1	Oxidoreductase	4	21351	28262	30490	19754	19774	23762	26701	21097	0,14069	-0,34	UNCHANGED
TRINITY_DN12414_c0_g1_i3_p1UniRef100_A0A1S3CGI3	Oxoglutarate dehydrogenase (succinyl-transferring) n=2 Tax=Cucumis melo TaxID=3656 RepID=A0A1S3CGI3_CUCME	9	19784	21598	17834	14714	16684	13715	19739	15038	0,02794	-0,39	UNCHANGED
TRINITY_DN3015_c1_g1_i1_p1sp|P35055|HEM6_SOYBN	Oxygen-dependent coproporphyrinogen-III oxidase, chloroplastic	9	46211	44241	48396	51457	44684	59434	46283	51858	0,27646	0,16	UNCHANGED
TRINITY_DN6525_c0_g1_i1_p2sp|Q41932|PSBQ2_ARATH	Oxygen-evolving enhancer protein 3-2, chloroplastic	8	54645	53258	100509	152697	135598	156165	69471	148153	0,00938	1,09	UP
TRINITY_DN13664_c0_g1_i1_p1UniRef100_A0A6J1DYX2	Palmitoyl-protein thioesterase 1-like	6	28480	26765	25112	35172	36838	36420	26786	36143	0,00102	0,43	UNCHANGED
TRINITY_DN49382_c1_g1_i3_p1Peptidase_C1	Papain	2	14157	15889	20468	15886	20026	30740	16838	22217	0,32600	0,40	UNCHANGED
TRINITY_DN2618_c0_g1_i4_p1UniRef100_UPI0018FFEC99	Patellin-3-like	6	16297	18446	36089	23282	25271	26717	23610	25090	0,82717	0,09	UNCHANGED
TRINITY_DN1818_c0_g1_i23_p1sp|Q6DBP4|PAE8_ARATH	Pectin acetylesterase 8	14	123429	78750	101212	57585	36646	45750	101131	46660	0,01874	-1,12	DOWN
TRINITY_DN6999_c1_g2_i1_p1sp|P85076|PME_ACTDE	Pectinesterase	7	23350	24372	29305	16325	19339	25829	25676	20498	0,19742	-0,32	UNCHANGED

TRINITY_DN13036_c0_g4_i1_p1Pectinesterase	Pectinesterase	6	24597	30171	31916	75128	72468	60800	28895	69465	0,00118	1,27	UP
TRINITY_DN9406_c2_g4_i2_p1spO04887PME2_CITSI	Pectinesterase 2	2	4949	7705	4666	2287	4683	3468	5773	3479	0,12633	-0,73	UNCHANGED
TRINITY_DN3268_c0_g1_i1_p1Peptidase_M1	Peptidase_DUF3458 Domain	4	14020	16880	17428	12830	14938	15765	16109	14511	0,30842	-0,15	UNCHANGED
TRINITY_DN15538_c1_g2_i5_p1UniRef100_A0A6J1JQJ8	Peptidyl-prolyl cis-trans isomerase	10	99037	115296	144529	104018	124359	133921	119621	120766	0,94625	0,01	UNCHANGED
TRINITY_DN19849_c0_g2_i1_p1UniRef100_UPI001900E2CB	Peptidyl-prolyl cis-trans isomerase A1	4	34003	41562	44598	34593	32768	39136	40054	35499	0,28295	-0,17	UNCHANGED
TRINITY_DN1098_c0_g3_i1_p1spQ38867CP19C_ARATH	Peptidyl-prolyl cis-trans isomerase CYP19-3	2	15209	14745	14206	11620	13075	13088	14720	12594	0,01994	-0,22	UNCHANGED
TRINITY_DN15769_c0_g1_i1_p1spQ9SP02CP20A_ARATH	Peptidyl-prolyl cis-trans isomerase CYP20-1	4	18236	22428	27372	10780	17290	23127	22679	17065	0,27453	-0,41	UNCHANGED
TRINITY_DN845_c0_g1_i3_p1spQ9SSA5CYP38_ARATH	Peptidyl-prolyl cis-trans isomerase CYP38, chloroplastic	9	40934	37145	49094	27139	59832	61528	42391	49500	0,57729	0,22	UNCHANGED
TRINITY_DN19164_c0_g1_i1_p1spQ9FJL3FKB65_ARATH	Peptidyl-prolyl cis-trans isomerase FKBP65	2	20482	22559	17217	16625	17624	21152	20086	18467	0,47864	-0,12	UNCHANGED
TRINITY_DN564_c0_g2_i9_p1UniRef100_A0A6J1H0T4	Peroxidase	5	41206	33988	29077	13790	12137	14973	34757	13633	0,00429	-1,35	DOWN
TRINITY_DN209_c1_g2_i1_p1UniRef100_A0A345BTH3	Peroxidase	9	2304	2726	2270				2434		-	-	Unique_PH
TRINITY_DN20774_c0_g1_i2_p1spQ9LEH3PER15_IPOBA	Peroxidase 15	3	22701	17594	4383	21313	17160	14488	14893	17654	0,65928	0,25	UNCHANGED
TRINITY_DN209_c1_g2_i3_p1spP19135PER2_CUCSA	Peroxidase 2 (Fragment)	13	165187	207213	184430	101063	127627	124140	185610	117610	0,00991	-0,66	DOWN
TRINITY_DN23219_c0_g2_i3_p1spP19135PER2_CUCSA	Peroxidase 2 (Fragment)	10	188912	250740	153197	133532	182545	175309	197616	163795	0,35454	-0,27	UNCHANGED
TRINITY_DN39_c3_g1_i1_p1spQ42580PER21_ARATH	Peroxidase 21	7	16879	22025	10960	3160	5463	5857	16621	4827	0,02342	-1,78	DOWN

TRINITY_DN20234_c0_g1_i2_p1spO23044PER3_ARATH	Peroxidase 3	10	46759	72574	43628	16802	26539	30820	54320	24720	0,04236	-1,14	DOWN
TRINITY_DN10870_c0_g1_i3_p1spA7NY33PER4_VITVI	Peroxidase 4	13	85905	80988	72543	39316	41531	40209	79812	40352	0,00057	-0,98	DOWN
TRINITY_DN10153_c0_g1_i3_p1spA7NY33PER4_VITVI	Peroxidase 4	4	14051	19498	5893	4276	11587	15536	13147	10466	0,63005	-0,33	UNCHANGED
TRINITY_DN16124_c1_g1_i5_p1spQ9SZB9PER47_ARATH	Peroxidase 47	4	8983	11584	11248	3976	3486	5601	10605	4354	0,00382	-1,28	DOWN
TRINITY_DN12127_c0_g1_i2_p1spQ96509PER55_ARATH	Peroxidase 55	9	25644	34366	17890	9385	10754	11057	25967	10399	0,03131	-1,32	DOWN
TRINITY_DN11172_c0_g1_i4_p1spQ43873PER73_ARATH	Peroxidase 73	14	129746	143971	105314	65822	70940	55153	126344	63972	0,00694	-0,98	DOWN
TRINITY_DN4757_c0_g1_i8_p1spQ9XIV8PERN1_TOBAC	Peroxidase N1	9	25541	24645	15970	23084	24177	19803	22052	22355	0,93173	0,02	UNCHANGED
TRINITY_DN602_c0_g1_i2_p1spQ6QPJ6PRXQ_POPJC	Peroxiredoxin Q, chloroplastic	4	6009	11378	14267	9590	18192	17938	10551	15240	0,27605	0,53	UNCHANGED
TRINITY_DN5407_c1_g1_i7_p1spQ9XEX2PRX2B_ARATH	Peroxiredoxin-2B	4	19537	34784	17180	11845	23261	20361	23834	18489	0,45676	-0,37	UNCHANGED
TRINITY_DN874_c0_g1_i3_p1spQ9M7T0PRX2F_ARATH	Peroxiredoxin-2F, mitochondrial	2	17745	14104	20879	24452	21881	21130	17576	22488	0,08945	0,36	UNCHANGED
TRINITY_DN78078_c0_g1_i10_p1UniRef100_A0A6J1G3D6	PGR5-like protein 1B, chloroplastic	2	9043	9645	13176	14595	18393	18687	10621	17225	0,02311	0,70	UP
TRINITY_DN12750_c0_g1_i7_p1spA0A0B6VQ48PAR1_ROSHC	Phenylacetaldehyde reductase	4	10526	25930	23872	10343	22981	24460	20109	19261	0,90377	-0,06	UNCHANGED
TRINITY_DN98088_c5_g1_i1_p1spB6VRE8TP7_TOBAC	Phenylcoumaran benzylic ether reductase TP7	6	17649	20056	15019	17915	18224	24390	17575	20176	0,36728	0,20	UNCHANGED
TRINITY_DN4422_c0_g1_i2_p1spP27608AROF_TOBAC	Phospho-2-dehydro-3-deoxyheptonate aldolase 1, chloroplastic	4	15608	21762	8353	8513	8682	9231	15241	8809	0,17279	-0,79	UNCHANGED
TRINITY_DN269_c0_g2_i2_p1spQ9FV65CAPPC_FLATR	Phosphoenolpyruvate carboxylase 2	13	22952	19641	20033	19682	17037	22062	20875	19594	0,51319	-0,09	UNCHANGED

TRINITY_DN269_c0_g1_i2_p1spQ02909CAPP1_SOYBN	Phosphoenolpyruvate carboxylase, housekeeping isozyme	16	20375	16662	17385	17131	15563	20282	18141	17659	0,80127	-0,04	UNCHANGED
TRINITY_DN614_c0_g1_i1_p1spQ9SCY0PGMP_ARATH	Phosphoglucomutase, chloroplastic	3	11186	15252	20378	16340	16225	17908	15605	16824	0,67667	0,11	UNCHANGED
TRINITY_DN1214_c0_g1_i16_p1spQ9ZSQ4PGMC_POPTN	Phosphoglucomutase, cytoplasmic	15	32544	48427	31152	31580	33090	34081	37374	32917	0,46978	-0,18	UNCHANGED
TRINITY_DN4336_c4_g1_i3_p1spQ9LD57PGKH1_ARATH	Phosphoglycerate kinase 1, chloroplastic	22	227233	297799	327972	246120	292289	344171	284335	294193	0,82242	0,05	UNCHANGED
TRINITY_DN6499_c0_g1_i2_p1spQ42962PGKY_TOBAC	Phosphoglycerate kinase, cytosolic	21	107433	151103	134084	93751	107512	132096	130873	111120	0,30860	-0,24	UNCHANGED
TRINITY_DN12687_c0_g1_i5_p1spP0DKC3PGP1A_ARATH	Phosphoglycolate phosphatase 1A, chloroplastic	8	37244	37251	43962	35651	40545	37677	39486	37958	0,59516	-0,06	UNCHANGED
TRINITY_DN605_c0_g2_i1_p1spQ41142PLDA1_RICCO	Phospholipase D alpha 1	17	43430	39234	47408	48866	48280	50691	43357	49279	0,07450	0,18	UNCHANGED
TRINITY_DN605_c0_g1_i1_p1spQ41142PLDA1_RICCO	Phospholipase D alpha 1	20	60181	71220	87115	48916	53538	54129	72838	52194	0,06107	-0,48	UNCHANGED
TRINITY_DN6032_c0_g1_i1_p1PRK	Phosphoribulokinase	7	11426	10313	15102	13864	13192	14127	12280	13728	0,38158	0,16	UNCHANGED
TRINITY_DN6032_c0_g3_i1_p1spP27774KPPR_MESCR	Phosphoribulokinase, chloroplastic	14	144387	137506	186533	175192	168808	175110	156142	173037	0,33616	0,15	UNCHANGED
TRINITY_DN4017_c0_g1_i4_p1UniRef100_UPI0019018B43	Phosphoserine aminotransferase 2, chloroplastic	10	30133	31045	28738	21647	22939	27089	29972	23892	0,02657	-0,33	UNCHANGED
TRINITY_DN63507_c6_g1_i6_p1spQ9SY97LHCA3_ARATH	Photosystem I chlorophyll a/b-binding protein 3-1, chloroplastic	10	316547	374590	424944	394828	402153	478420	372027	425133	0,26662	0,19	UNCHANGED
TRINITY_DN2157_c0_g2_i1_p1spQ2QD89PSAA_CUCSA	Photosystem I P700 chlorophyll a apoprotein A1	13	134529	135340	151181	175160	215606	175852	140350	188873	0,02821	0,43	UNCHANGED
TRINITY_DN2157_c0_g2_i1_p2spQ4VZN4PSAB_CUCSA	Photosystem I P700 chlorophyll a apoprotein A2	14	237909	244732	264137	299874	308647	279255	248926	295925	0,01604	0,25	UNCHANGED

TRINITY_DN131502_c7_g1_i1_p1 spP32869PSAD_CUCSA	Photosystem I reaction center subunit II, chloroplastic	8	40216	54392	50935	43815	55018	57521	48514	52118	0,58029	0,10	UNCHANGED
TRINITY_DN47999_c0_g1_i11_p1 spQ9SHE8PSAF_ARATH	Photosystem I reaction center subunit III, chloroplastic	8	187540	189885	222959	246435	209960	238840	200128	231745	0,11840	0,21	UNCHANGED
TRINITY_DN50594_c0_g1_i6_p1s pP49107PSAN_ARATH	Photosystem I reaction center subunit N, chloroplastic	3	27756	18902	44185	68487	46546	43167	30281	52733	0,10746	0,80	UNCHANGED
TRINITY_DN6336_c2_g1_i5_p1sp Q9SUI5PSAK_ARATH	Photosystem I reaction center subunit psaK, chloroplastic	2	64190	63665	42691	56437	65424	63151	56849	61670	0,55912	0,12	UNCHANGED
TRINITY_DN18054_c0_g1_i1_p1s pQ9S7N7PSAG_ARATH	Photosystem I reaction center subunit V, chloroplastic	5	147532	138587	158456	175717	172961	175479	148192	174719	0,01031	0,24	UNCHANGED
TRINITY_DN54367_c1_g1_i14_p1 spP22179PSAH_SPIOL	Photosystem I reaction center subunit VI, chloroplastic	2	71335	94832	33720	108090	134785	136179	66629	126351	0,04054	0,92	UP
TRINITY_DN31851_c0_g1_i10_p1 spQ39654PSAL_CUCSA	Photosystem I reaction center subunit XI, chloroplastic	2	122936	117844	145957	153679	151332	177600	128912	160870	0,05687	0,32	UNCHANGED
TRINITY_DN5361_c0_g1_i8_p1sp Q40519PSBR_TOBAC	Photosystem II 10 kDa polypeptide, chloroplastic	6	84652	92672	144012	109326	115329	160422	107112	128359	0,43668	0,26	UNCHANGED
TRINITY_DN87919_c0_g3_i1_p1s pQ9FPP4PSBS_SOLSG	Photosystem II 22 kDa protein, chloroplastic	7	104009	91774	104655	104710	104628	113616	100146	107651	0,21824	0,10	UNCHANGED
TRINITY_DN5438_c0_g1_i17_p1s pQ2QD93PSBC_CUCSA	Photosystem II CP43 reaction center protein	19	458356	423164	426774	440756	421962	429172	436098	430630	0,68311	-0,02	UNCHANGED
TRINITY_DN12182_c0_g1_i14_p1 spQ2QD63PSBB_CUCSA	Photosystem II CP47 reaction center protein	19	323936	326766	350826	392230	381848	378677	333843	384251	0,00598	0,20	UNCHANGED
TRINITY_DN5438_c0_g1_i17_p2s pQ4VZN8PSBD_CUCSA	Photosystem II D2 protein	11	359898	356618	402576	351167	394464	378506	373031	374712	0,93531	0,01	UNCHANGED
TRINITY_DN6787_c0_g1_i1_p1sp Q7FNT3PSBA_ATRBE	Photosystem II protein D1	10	350631	319249	328196	291938	342740	312647	332692	315775	0,38731	-0,08	UNCHANGED
TRINITY_DN14469_c0_g1_i1_p1s pQ5Z5A8P2SAF_ORYSJ	Photosystem II stability/assembly factor HCF136, chloroplastic	15	238553	178186	166328	248608	195762	186463	194356	210278	0,61886	0,11	UNCHANGED

TRINITY_DN4923_c0_g1_i11_p1sp|Q03194|PMA4_NICPL	Plasma membrane ATPase 4	15	29237	28975	29808	25547	30293	25375	29340	27072	0,23650	-0,12	UNCHANGED
TRINITY_DN4849_c0_g1_i3_p1UniRef100_UPI0018FFFB27	Plastid-lipid-associated protein 6, chloroplastic	4	10411	12260	10447	29467	27672	21962	11039	26367	0,00282	1,26	UP
TRINITY_DN22166_c0_g1_i2_p1sp|Q9FVQ4|PLGG1_ARATH	Plastidal glycolate/glycerate translocator 1, chloroplastic	2	9736	9672	17329	18802	20011	20148	12245	19654	0,04527	0,68	UP
TRINITY_DN3030_c0_g1_i10_p1sp|P00289|PLAS_SPIOL	Plastocyanin, chloroplastic	6	107560	115722	106873	127437	155242	117745	110052	133475	0,11341	0,28	UNCHANGED
TRINITY_DN39165_c1_g1_i10_p1sp|P42731|PABP2_ARATH	Polyadenylate-binding protein 2	5	14204	16285	17284	11893	12750	14784	15924	13142	0,08968	-0,28	UNCHANGED
TRINITY_DN4678_c0_g1_i8_p1UniRef100_A0A6J1GRK0	Polyadenylate-binding protein RBP45-like isoform X2	6	16188	15017	18116	11775	12585	14731	16440	13030	0,05403	-0,34	UNCHANGED
TRINITY_DN6665_c0_g4_i1_p1UniRef100_A0A6J1HMU3	Polygalacturonase inhibitor-like	9	18109	23162	33259	55690	68382	55729	24843	59934	0,00463	1,27	UP
TRINITY_DN563_c0_g1_i13_p1sp|P43309|PPO_MALDO	Polyphenol oxidase, chloroplastic	4	15969	20966	15343	5971	8362	5186	17426	6506	0,00566	-1,42	DOWN
TRINITY_DN5996_c0_g1_i1_p1sp|Q43082|HEM3_PEA	Porphobilinogen deaminase, chloroplastic	17	37544	38274	45145	45590	46050	58937	40321	50193	0,11956	0,32	UNCHANGED
TRINITY_DN18858_c0_g1_i1_p1sp|Q9LJL3|PREP1_ARATH	Presequence protease 1, chloroplastic/mitochondrial	3	3820	6195	3476	5006	7750	7726	4497	6827	0,13545	0,60	UNCHANGED
TRINITY_DN11403_c0_g1_i1_p1sp|A0A072UTP9|CATB_MEDTR	Pro-cathepsin H	3	5539	8952	9707	5850	9929	10633	8066	8804	0,72634	0,13	UNCHANGED
TRINITY_DN11382_c0_g1_i1_p1sp|Q9SZE1|3HID1_ARATH	Probable 3-hydroxyisobutyrate dehydrogenase-like 1, mitochondrial	3	11006	14061	9410	8973	10579	10797	11493	10116	0,40526	-0,18	UNCHANGED
TRINITY_DN12857_c2_g1_i1_p1sp|Q7XT99|AKR2_ORYSJ	Probable aldo-keto reductase 2	4	14512	12472	12929	11352	10404	10387	13304	10714	0,02041	-0,31	UNCHANGED
TRINITY_DN22668_c0_g1_i3_p1sp|Q8LPJ3|MANA2_ARATH	Probable alpha-mannosidase At5g13980	8	19082	17771	26461	25184	20422	24649	21104	23418	0,49637	0,15	UNCHANGED
TRINITY_DN1716_c0_g1_i1_p1sp|Q9FKW9|MANA3_ARATH	Probable alpha-mannosidase At5g66150	10	17994	19550	28089	22402	20927	25571	21877	22967	0,76634	0,07	UNCHANGED

TRINITY_DN13207_c0_g3_i1_p1spP0DO21GIP2_NICBE	Probable aspartic proteinase GIP2	8	44173	48741	58717	80669	79190	77311	50544	79057	0,00293	0,65	UP
TRINITY_DN239_c0_g1_i1_p1spP48255ABCX_CYAPA	Probable ATP-dependent transporter ycf16	2	3427	4770	6667	5985	8161	5130	4955	6425	0,32211	0,37	UNCHANGED
TRINITY_DN5636_c0_g1_i3_p1spQ9SGZ5BXL7_ARATH	Probable beta-D-xylosidase 7	13	35995	37157	48072	23423	19664	29719	40408	24268	0,02893	-0,74	DOWN
TRINITY_DN4027_c1_g1_i6_p1spM4IQQ7CCL9_HUMLU	Probable CoA ligase CCL9	5	35103	35705	36666	20085	20146	27667	35825	22633	0,00671	-0,66	DOWN
TRINITY_DN12272_c0_g1_i1_p1spQ9C524SCRK6_ARATH	Probable fructokinase-6, chloroplastic	2	14058	11013	14809	12037	10013	10982	13293	11010	0,15373	-0,27	UNCHANGED
TRINITY_DN2296_c0_g1_i1_p1spQ8RX87RFS6_ARATH	Probable galactinol--sucrose galactosyltransferase 6	16	26620	40299	25383	24410	31220	37390	30767	31007	0,97046	0,01	UNCHANGED
TRINITY_DN12752_c0_g1_i1_p1spQ8VZF3CGEP_ARATH	Probable glutamyl endopeptidase, chloroplastic	8	16453	19535	19559	14861	13533	16378	18516	14924	0,05279	-0,31	UNCHANGED
TRINITY_DN1772_c0_g1_i1_p1spQ03666GSTX4_TOBAC	Probable glutathione S-transferase	4	46283	61629	40112	46373	70723	45535	49341	54211	0,66541	0,14	UNCHANGED
TRINITY_DN992_c0_g1_i17_p1spQ5MAU8PPA27_ARATH	Probable inactive purple acid phosphatase 27	9	9492	9358	10601	20941	18250	23885	9817	21025	0,00259	1,10	UP
TRINITY_DN885_c2_g1_i1_p1spQ8W593LGUC_ARATH	Probable lactoylglutathione lyase, chloroplastic	5	13418	16328	14249	14745	14570	28580	14665	19298	0,38199	0,40	UNCHANGED
TRINITY_DN1320_c0_g1_i1_p1spQ9ZRF1MTDH_FRAAN	Probable mannitol dehydrogenase	3	7746	7209	4318	9898	9202	9246	6424	9449	0,04984	0,56	UNCHANGED
TRINITY_DN22720_c0_g3_i3_p1spO82515MTDH_MEDSA	Probable mannitol dehydrogenase	14	58656	59214	61886	50883	44887	50013	59919	48594	0,00591	-0,30	UNCHANGED
TRINITY_DN1063_c0_g3_i1_p1spQ42290MPPB_ARATH	Probable mitochondrial-processing peptidase subunit beta, mitochondrial	13	37522	38426	38773	32601	29955	32665	38240	31740	0,00256	-0,27	UNCHANGED
TRINITY_DN453_c2_g1_i14_p1UniRef100_UPI000C9D4E30	Probable N-acetyl-gamma-glutamyl-phosphate reductase, chloroplastic	4	18620	17289	20843	20091	17962	20864	18917	19639	0,62187	0,05	UNCHANGED

TRINITY_DN9767_c0_g1_i2_p1sp Q6NQE2FQRL1_ARATH	Probable NAD(P)H dehydrogenase (quinone) FQR1-like 1	10	195920	221480	190969	136274	151642	140832	202790	142916	0,00467	-0,50	UNCHANGED
TRINITY_DN1705_c0_g1_i5_p1Un iRef100_A0A6J1EWP9	Probable nucleoredoxin 1	11	33130	38764	15626	16686	22311	28064	29173	22354	0,42592	-0,38	UNCHANGED
TRINITY_DN4418_c1_g5_i2_p1sp Q93WF1PLY20_ARATH	Probable pectate lyase 20	2	6358	5773	7499	3764	3306	3737	6543	3602	0,00509	-0,86	DOWN
TRINITY_DN4418_c1_g3_i8_p1sp Q9M8Z8PLY8_ARATH	Probable pectate lyase 8	4	10879	10586	13856	9403	8607	8592	11774	8867	0,05437	-0,41	UNCHANGED
TRINITY_DN6057_c2_g1_i3_p1sp Q8S9M1PAP13_ARATH	Probable plastid-lipid-associated protein 13, chloroplastic	6	8751	13671	11372	15226	30533	17375	11265	21045	0,12163	0,90	UNCHANGED
TRINITY_DN12724_c0_g2_i1_p1s pA7PZL3PGLR_VITVI	Probable polygalacturonase	4	15832	19833	13057	7240	10441	11978	16241	9886	0,05788	-0,72	UNCHANGED
TRINITY_DN81379_c0_g1_i1_p1s pP38661PDIA6_MEDSA	Probable protein disulfide-isomerase A6	8	39056	44325	36816	34302	35440	33692	40066	34478	0,07071	-0,22	UNCHANGED
TRINITY_DN1728_c0_g2_i1_p1sp Q39963PDX1_HEVBR	Probable pyridoxal 5'-phosphate synthase subunit PDX1	7	48141	45287	43539	41427	37694	47675	45656	42265	0,34986	-0,11	UNCHANGED
TRINITY_DN28676_c2_g1_i1_p1s pQ9S726RPI3_ARATH	Probable ribose-5-phosphate isomerase 3, chloroplastic	4	14978	13435	17847	23732	22415	19510	15420	21885	0,02278	0,51	UNCHANGED
TRINITY_DN374_c0_g1_i2_p1spQ 8RU27RGP2_SOLTU	Probable UDP-arabinopyranose mutase 2	15	75953	78172	83889	56434	52619	59347	79338	56133	0,00163	-0,50	UNCHANGED
TRINITY_DN374_c0_g4_i1_p1spQ 8RU27RGP2_SOLTU	Probable UDP-arabinopyranose mutase 2	19	66017	66246	70379	59371	50702	56218	67547	55430	0,01398	-0,29	UNCHANGED
TRINITY_DN5080_c0_g1_i4_p1sp Q8LER3XTH7_ARATH	Probable xyloglucan endotransglucosylase/hydrolase protein 7	3	15515	16219	29362	17039	17637	20726	20365	18467	0,70378	-0,14	UNCHANGED
TRINITY_DN81768_c0_g2_i1_p1s pO49460PHB1_ARATH	Prohibitin-1, mitochondrial	4	20151	34645	16804	17044	20909	14743	23867	17565	0,33564	-0,44	UNCHANGED
TRINITY_DN4150_c0_g1_i1_p1sp Q9M1R2SYPC_ARATH	Proline--tRNA ligase, cytoplasmic	13	127851	137130	132858	115587	125703	115807	132613	119032	0,03376	-0,16	UNCHANGED

TRINITY_DN9331_c1_g1_i5_p1sp O22609DEGP1_ARATH	Protease Do-like 1, chloroplastic	3	7104	8653	7666	12875	15067	13609	7808	13851	0,00155	0,83	UP
TRINITY_DN9634_c0_g1_i6_p1sp P52428PSA1_ORYSJ	Proteasome subunit alpha type-1	7	17210	29191	27693	18993	23039	27325	24698	23119	0,74177	-0,10	UNCHANGED
TRINITY_DN15932_c0_g1_i3_p1s pQ8L4A7PSA2B_ARATH	Proteasome subunit alpha type-2-B	8	43922	53326	51679	38289	43153	51954	49643	44465	0,35373	-0,16	UNCHANGED
TRINITY_DN5488_c0_g2_i2_p1sp O24362PSA3_SPIOL	Proteasome subunit alpha type-3	6	35809	42537	37643	33743	30190	39173	38663	34369	0,26241	-0,17	UNCHANGED
TRINITY_DN643_c0_g1_i2_p1spP 52427PSA4_SPIOL	Proteasome subunit alpha type-4	5	26866	29925	26698	18187	19062	23792	27830	20347	0,02117	-0,45	UNCHANGED
TRINITY_DN11129_c0_g1_i3_p1s pQ9XG77PSA6_TOBAC	Proteasome subunit alpha type-6	6	13915	13951	14139	14581	13890	14134	14002	14202	0,40221	0,02	UNCHANGED
TRINITY_DN3133_c0_g6_i1_p1sp O48551PSA6_SOYBN	Proteasome subunit alpha type-6	7	30039	32754	30443	27605	27803	30322	31079	28577	0,10887	-0,12	UNCHANGED
TRINITY_DN1618_c0_g1_i3_p1sp Q9SXU1PSA7_CICAR	Proteasome subunit alpha type-7	3	30457	25604	18195	21487	20026	17448	24752	19654	0,24618	-0,33	UNCHANGED
TRINITY_DN13184_c0_g1_i2_p1s pO82531PSB1_PETHY	Proteasome subunit beta type-1	6	81538	89846	69763	61969	62206	65153	80382	63109	0,04325	-0,35	UNCHANGED
TRINITY_DN1422_c1_g1_i2_p1sp O23714PSB2A_ARATH	Proteasome subunit beta type-2-A	5	37243	42741	29059	27227	29760	29902	36348	28963	0,14371	-0,33	UNCHANGED
TRINITY_DN69941_c0_g1_i2_p1s pQ9XI05PSB3A_ARATH	Proteasome subunit beta type-3-A	3	20388	25650	18010	20090	22997	15631	21349	19573	0,59862	-0,13	UNCHANGED
TRINITY_DN9788_c0_g1_i2_p1sp Q7DLR9PSB4_ARATH	Proteasome subunit beta type-4	7	25414	26747	23937	25635	25129	31423	25366	27396	0,40375	0,11	UNCHANGED
TRINITY_DN3227_c0_g1_i1_p1sp O24361PSB5_SPIOL	Proteasome subunit beta type-5	7	32659	32836	32013	34625	35203	32012	32503	33947	0,22715	0,06	UNCHANGED
TRINITY_DN4608_c0_g2_i2_p1sp Q8LD27PSB6_ARATH	Proteasome subunit beta type-6	6	27159	28748	24366	25695	27023	27999	26758	26906	0,92338	0,01	UNCHANGED
TRINITY_DN4239_c0_g1_i2_p1sp O23710PSB7A_ARATH	Proteasome subunit beta type-7-A	2	42791	36668	36001	31090	34426	33972	38487	33162	0,09078	-0,21	UNCHANGED
TRINITY_DN3364_c0_g1_i3_p1sp Q9ZVD5AGO4_ARATH	Protein argonaute 4	7	16122	27260	20146	11826	14348	16417	21176	14197	0,11818	-0,58	UNCHANGED

TRINITY_DN1907_c1_g1_i4_p1sp O04616CUT1A_ARATH	Protein CURVATURE THYLAKOID 1A, chloroplastic	4	50869	56544	78041	78278	70822	76422	61818	75174	0,19427	0,28	UNCHANGED
TRINITY_DN15642_c3_g1_i1_p1U niRef100_UPI0019023DEA	Protein disulfide isomerase-like 1-4	3	19192	18008	17488	18180	17125	19007	18229	18104	0,87421	-0,01	UNCHANGED
TRINITY_DN5439_c1_g1_i3_p1sp Q9XF61PDI_DATGL	Protein disulfide-isomerase	14	91932	97034	71945	75615	80353	72258	86970	76075	0,24528	-0,19	UNCHANGED
TRINITY_DN8303_c0_g2_i1_p1sp Q94F20DGR2_ARATH	Protein DUF642 L-GALACTONO-1,4-LACTONE -RESPONSIVE GENE 2	12	173848	179484	195516	130338	129371	128426	182949	129378	0,00119	-0,50	UNCHANGED
TRINITY_DN8231_c0_g1_i1_p1sp Q9FE06EXOL2_ARATH	Protein EXORDIUM-like 2	4	27766	31361	30537	20804	20124	16782	29888	19237	0,00297	-0,64	DOWN
TRINITY_DN4074_c0_g1_i11_p1U niRef100_UPI001902B19B	Protein MET1, chloroplastic	3	15050	20365	18833	15150	22814	19296	18083	19087	0,73081	0,08	UNCHANGED
TRINITY_DN9987_c0_g1_i10_p1U niRef100_UPI001C352259	Protein plastid transcriptionally active 16, chloroplastic	15	58449	90811	84954	110561	100977	116073	78071	109204	0,04597	0,48	UNCHANGED
TRINITY_DN165_c0_g1_i3_p1Uni Ref100_A0A6J1EX23	Protein SIEVE ELEMENT OCCLUSION B-like	3	31245	31043	28455	23892	23102	28567	30248	25187	0,05845	-0,26	UNCHANGED
TRINITY_DN558_c0_g1_i11_p1Un iRef100_A0A6J1CAR6	protein SIEVE ELEMENT OCCLUSION B-like	5	16570	21293	20281	5234	16594	17253	19381	13027	0,20111	-0,57	UNCHANGED
TRINITY_DN558_c0_g1_i12_p1Un iRef100_A0A6J1CAR6	protein SIEVE ELEMENT OCCLUSION B-like	5	11410	15944	5397	5183	8794	7005	10917	6994	0,29100	-0,64	UNCHANGED
TRINITY_DN558_c0_g1_i25_p1Un iRef100_A0A6J1CAR6	protein SIEVE ELEMENT OCCLUSION B-like	6	9008	12109	6877	3746	6253	7069	9332	5690	0,11578	-0,71	UNCHANGED
TRINITY_DN4309_c0_g1_i2_p1sp Q8LPR9TI110_ARATH	Protein TIC110, chloroplastic	7	12908	12812	12652	12998	13414	17140	12791	14517	0,26056	0,18	UNCHANGED
TRINITY_DN8976_c0_g1_i2_p1Un iRef100_UPI001900B876	Protein transport protein SEC23	4	19984	20723	16880	12486	11430	12444	19196	12120	0,00449	-0,66	DOWN
TRINITY_DN4110_c0_g1_i3_p1sp Q8L611SC31B_ARATH	Protein transport protein SEC31 homolog B	6	28039	26908	26321	12148	13596	13518	27089	13087	0,00003	-1,05	DOWN
TRINITY_DN9647_c0_g1_i4_p1sp Q41249PORA_CUCSA	Protochlorophyllide reductase, chloroplastic	18	99987	107386	89628	114762	99846	129391	99000	114666	0,19096	0,21	UNCHANGED

TRINITY_DN4012_c0_g1_i4_p1sp Q41249PORA_CUCSA	Protochlorophyllide reductase, chloroplastic	5	24200	31713	19014	34056	39844	46317	24976	40072	0,04183	0,68	UP
TRINITY_DN7688_c0_g1_i7_p1sp P55826PPOC_ARATH	Protoporphyrinogen oxidase 1, chloroplastic	3	5143	6267	4844	4509	5296	7389	5418	5731	0,76108	0,08	UNCHANGED
TRINITY_DN2123_c1_g1_i1_p187 347at33090 Prp19	Prp19/Pso4-like	2	13352	12354	11967	8459	8817	10190	12558	9155	0,00708	-0,46	UNCHANGED
TRINITY_DN8646_c1_g1_i2_p114 0876at33090 PsbP	PsbP	8	188372	178790	234841	276252	247537	225190	200668	249660	0,09770	0,32	UNCHANGED
TRINITY_DN65_c0_g1_i16_p1spP 82715PPD5_ARATH	PsbP domain-containing protein 5, chloroplastic	2	10794	11650	11097	11509	15209	12713	11180	13144	0,15387	0,23	UNCHANGED
TRINITY_DN4365_c1_g2_i3_p1Un iRef100_A0A6J1DG13	psbP domain-containing protein 6, chloroplastic	5	21794	19313	30700	29357	34596	28938	23936	30963	0,14647	0,37	UNCHANGED
TRINITY_DN10580_c1_g1_i12_p1 spQ9C9W3CAMT1_ARATH	Putative caffeoyl-CoA O-methyltransferase At1g67980	6	14991	14772	20687	13056	11008	15023	16817	13029	0,16853	-0,37	UNCHANGED
TRINITY_DN2898_c0_g1_i1_p1sp Q40784AAPC_CENCI	Putative glucose-6-phosphate 1-epimerase	4	20214	19375	19879	16142	14077	17253	19823	15824	0,01419	-0,33	UNCHANGED
TRINITY_DN1705_c0_g1_i8_p1Un iRef100_UPI001C36D0F4	Putative nucleoredoxin 1	4	4700	7100	4991	4615	4426	6634	5597	5225	0,73756	-0,10	UNCHANGED
TRINITY_DN2507_c0_g1_i10_p2P ALP	Pyridoxal-phosphate	3	7524	8654	7960	6532	7995	9338	8046	7955	0,92221	-0,02	UNCHANGED
TRINITY_DN9648_c1_g1_i3_p1sp Q41140PFPA_RICCO	Pyrophosphate--fructose 6-phosphate 1-phosphotransferase subunit alpha	1 2	30331	29275	28712	21109	19094	21509	29439	20571	0,00056	-0,52	UNCHANGED
TRINITY_DN1815_c0_g1_i3_p1sp Q41141PFPB_RICCO	Pyrophosphate--fructose 6-phosphate 1-phosphotransferase subunit beta	1 2	44087	47365	43649	31997	33653	36092	45033	33914	0,00264	-0,41	UNCHANGED
TRINITY_DN2365_c3_g1_i6_p1sp P21616AVP_VIGRR	Pyrophosphate-energized vacuolar membrane proton pump	7	40750	36355	32262	27143	31065	39539	36456	32582	0,42870	-0,16	UNCHANGED
TRINITY_DN11425_c0_g1_i4_p1s pP51850PDC1_PEA	Pyruvate decarboxylase 1	2	7135	10583	10254	4213	2057	3082	9324	3117	0,00796	-1,58	DOWN

TRINITY_DN14344_c0_g1_i1_p1sp|Q1XDM0|ODPA_NEOYE	Pyruvate dehydrogenase E1 component subunit alpha	4	104825	56714	80842	88275	51414	63135	80794	67608	0,49628	-0,26	UNCHANGED
TRINITY_DN2488_c0_g1_i1_p1sp|P52902|ODPA_PEA	Pyruvate dehydrogenase E1component subunit alpha, mitochondrial	7	20237	30559	30908	18460	26438	26762	27235	23887	0,49185	-0,19	UNCHANGED
TRINITY_DN13007_c0_g3_i1_p1sp|Q6Z1G7|ODPB1_ORYSJ	Pyruvate dehydrogenase E1component subunit beta-1, mitochondrial	6	31037	30238	31789	23502	22077	25054	31021	23544	0,00152	-0,40	UNCHANGED
TRINITY_DN1568_c2_g1_i1_p1sp|O64688|ODPB3_ARATH	Pyruvate dehydrogenase E1component subunit beta-3, chloroplastic	2	10038	11529	11926	10129	10631	13406	11164	11389	0,85707	0,03	UNCHANGED
TRINITY_DN42806_c0_g1_i3_p1sp|B8BJ39|KPYC1_ORYSI	Pyruvate kinase 1, cytosolic	10	26517	28353	29951	16312	17179	22893	28274	18795	0,01439	-0,59	UNCHANGED
TRINITY_DN42806_c0_g1_i11_p1sp|B8BM17|KPYC2_ORYSI	Pyruvate kinase 2, cytosolic	4	2592	3821	3762	1493	2017	2602	3392	2037	0,05741	-0,74	UNCHANGED
TRINITY_DN19910_c0_g1_i18_p1sp|Q42806|KPYC_SOYBN	Pyruvate kinase, cytosolic isozyme	4	11168	14274	11012	5798	7148	8769	12151	7238	0,02283	-0,75	DOWN
TRINITY_DN7272_c0_g1_i6_p1sp|Q42954|KPYC_TOBAC	Pyruvate kinase, cytosolic isozyme	7	26793	25619	24183	17460	19230	22292	25532	19661	0,02142	-0,38	UNCHANGED
TRINITY_DN17773_c0_g1_i1_p1Raffinose_syn	Raffinose	2	5222	7594	9155	8863	11886	11716	7323	10822	0,08093	0,56	UNCHANGED
TRINITY_DN1855_c3_g1_i2_p1sp|P31022|RAB7_PEA	Ras-related protein Rab7	5	13783	13722	15269	12232	9550	12921	14258	11568	0,07872	-0,30	UNCHANGED
TRINITY_DN4544_c3_g1_i1_p1sp|O04486|RAA2A_ARATH	Ras-related protein RABA2a	4	29120	25658	26658	18017	15163	17752	27145	16977	0,00178	-0,68	DOWN
TRINITY_DN4361_c0_g1_i2_p1sp|P92963|RAB1C_ARATH	Ras-related protein RABB1c	2	10321	10175	13405	10692	10354	10981	11300	10676	0,59039	-0,08	UNCHANGED
TRINITY_DN1136_c1_g2_i12_p1sp|O24466|RAE1A_ARATH	Ras-related protein RABE1a	5	29327	26169	33520	20915	19396	22410	29672	20907	0,01893	-0,51	UNCHANGED
TRINITY_DN20632_c0_g1_i5_p1sp|O24456|GBLPA_ARATH	Receptor for activated C kinase 1A	6	3261	4809	3910	2469	3597	4360	3994	3475	0,50563	-0,20	UNCHANGED

TRINITY_DN4877_c0_g1_i2_p1UniRef100_A0A6J1G868	Red chlorophyll catabolite reductase	3	8630	8884	16098	10978	10177	13000	11204	11385	0,94752	0,02	UNCHANGED
TRINITY_DN209005_c0_g1_i1_p1 Redoxin	Redoxin	8	53529	51994	61534	69677	72297	80876	55686	74284	0,01438	0,42	UNCHANGED
TRINITY_DN374_c1_g4_i1_p1RGP	Reversibly	3	7177	8479	8302	9421	10384	11354	7986	10386	0,02553	0,38	UNCHANGED
TRINITY_DN2883_c0_g1_i6_p1UniRef100_A0A0A0LC69	Rhodanese domain-containing protein	4	7116	7348	14615	15285	9828	19121	9693	14745	0,23871	0,61	UNCHANGED
TRINITY_DN6214_c0_g1_i6_p1UniRef100_UPI0019004507	Rhodanese-like domain-containing protein 4, chloroplastic	13	51229	51778	60964	63227	64872	74408	54657	67502	0,05237	0,30	UNCHANGED
TRINITY_DN24690_c0_g1_i7_p1UniRef100_UPI0019014EC5	Rhodanese-like domain-containing protein 9, chloroplastic	5	22341	24637	32074	37370	39214	35770	26351	37451	0,02318	0,51	UNCHANGED
TRINITY_DN6771_c0_g1_i38_p1Ribonuclease_T2	Ribonuclease	8	17901	15733	26985	99300	87884	96202	20206	94462	0,00011	2,22	UP
TRINITY_DN6771_c0_g1_i55_p1UniRef100_UPI0019001883	Ribonuclease MC-like	2	148055	179104	264865	259123	312810	321679	197341	297870	0,06595	0,59	UNCHANGED
TRINITY_DN6771_c0_g1_i35_p1UniRef100_UPI0019001883	Ribonuclease MC-like	6	12523	12149	18339	35236	34734	26967	14337	32312	0,00579	1,17	UP
TRINITY_DN6771_c0_g1_i31_p1UniRef100_UPI0019001883	Ribonuclease MC-like	10	31180	30719	54402	166998	165013	137836	38767	156616	0,00065	2,01	UP
TRINITY_DN233_c0_g1_i27_p1spQ8VZG7TSN1_ARATH	Ribonuclease TUDOR 1	10	19115	22446	20011	12420	13486	15745	20524	13884	0,00895	-0,56	UNCHANGED
TRINITY_DN34967_c0_g1_i5_p1Ribosomal_S24e	Ribosomal	2	48374	42801	80641	98117	62256	53437	57272	71270	0,48133	0,32	UNCHANGED
TRINITY_DN46555_c0_g1_i1_p2Ribosomal_L1	Ribosomal	2	14543	12397	17633	14284	15997	16522	14858	15601	0,67803	0,07	UNCHANGED
TRINITY_DN9602_c0_g1_i1_p1Ribosomal_L15e	Ribosomal	3	26509	33171	33325	17013	27553	28836	31002	24467	0,20900	-0,34	UNCHANGED
TRINITY_DN2248_c0_g1_i2_p1Ribosomal_L1	Ribosomal	3	19919	28263	17439	8715	17192	13315	21874	13074	0,09778	-0,74	UNCHANGED

TRINITY_DN10243_c1_g1_i8_p1Ribosomal_L7Ae	Ribosomal	4	39363	45321	26980	27964	45980	35077	37221	36340	0,91241	-0,03	UNCHANGED
TRINITY_DN3065_c0_g1_i1_p1Ribosomal_S13	Ribosomal	4	23680	30409	14089	5964	16749	17666	22726	13460	0,20007	-0,76	UNCHANGED
TRINITY_DN87351_c0_g1_i5_p1Ribosomal_S7	Ribosomal	6	38921	40860	35053	38625	36876	47887	38278	41129	0,49682	0,10	UNCHANGED
TRINITY_DN1958_c0_g1_i29_p1Ribosomal_S2	Ribosomal	10	101395	157528	153761	103167	123602	123083	137561	116617	0,33942	-0,24	UNCHANGED
TRINITY_DN3383_c0_g1_i17_p1spP98184RIP2_BRYDI	Ribosome-inactivating protein bryodin II	8	50580	55716	85034	38565	46575	44512	63777	43217	0,13490	-0,56	UNCHANGED
TRINITY_DN3383_c0_g1_i20_p1spP98184RIP2_BRYDI	Ribosome-inactivating protein bryodin II	9	6811	7563	15280	72683	88597	71418	9885	77566	0,00039	2,97	UP
TRINITY_DN28850_c0_g1_i3_p1RuBisCO_large	Ribulose	13	286181	291873	255709	309258	343732	345265	277921	332752	0,02796	0,26	UNCHANGED
TRINITY_DN12244_c0_g1_i2_p2spP27064RBL_CUCSA	Ribulose bisphosphate carboxylase large chain	43	995687	864158	903985	1092841	879018	968477	921277	980112	0,46666	0,09	UNCHANGED
TRINITY_DN14071_c0_g1_i5_p1spP08474RBS_CUCSA	Ribulose bisphosphate carboxylase small subunit, chloroplastic	12	10766	11885	7481	9682	10201	9494	10044	9792	0,85995	-0,04	UNCHANGED
TRINITY_DN149515_c12_g1_i1_p1spP08474RBS_CUCSA	Ribulose bisphosphate carboxylase small subunit, chloroplastic	16	585764	678234	491402	541486	551303	564408	585134	552399	0,57941	-0,08	UNCHANGED
TRINITY_DN14071_c0_g1_i2_p1spP08474RBS_CUCSA	Ribulose bisphosphate carboxylase small subunit, chloroplastic	11	10106	10361	8450	16896	19722	17652	9639	18090	0,00123	0,91	UP
TRINITY_DN4542_c1_g1_i3_p1spQ7X9A0RCA1_LARTR	Ribulose bisphosphate carboxylase/oxygenase activase 1, chloroplastic	27	79802	75087	86154	68044	75737	77393	80348	73725	0,19919	-0,12	UNCHANGED
TRINITY_DN443_c2_g2_i1_p1spQ7X999RCA2_LARTR	Ribulose bisphosphate carboxylase/oxygenase activase 2, chloroplastic	33	384473	508717	623126	409053	476097	541789	505439	475646	0,72475	-0,09	UNCHANGED

TRINITY_DN2072_c0_g1_i1_p1sp Q01587RCA_CUCSA	Ribulose bisphosphate carboxylase/oxygenase activase, chloroplastic	18	28156	36233	38311	25172	28605	35457	34233	29745	0,35824	-0,20	UNCHANGED
TRINITY_DN6620_c0_g1_i3_p1sp Q9ZTP5RPE_ORYSJ	Ribulose-phosphate 3-epimerase, chloroplastic	6	26377	36841	50033	56446	83726	91806	37750	77326	0,03565	1,03	UP
TRINITY_DN6688_c0_g1_i4_p1sp P08926RUBA_PEA	RuBisCO large subunit-bindingprotein subunit alpha, chloroplastic	22	91024	101261	93661	74233	79985	93626	95315	82615	0,12317	-0,21	UNCHANGED
TRINITY_DN3433_c0_g1_i6_p1sp Q9AT56METK1_ELAUM	S-adenosylmethionine synthase 1	14	54981	75530	53946	43480	42604	49793	61486	45292	0,09338	-0,44	UNCHANGED
TRINITY_DN13660_c0_g1_i1_p1s pQ9AT56METK1_ELAUM	S-adenosylmethionine synthase 1	15	111741	145374	119526	89612	91768	109393	125547	96924	0,07459	-0,37	UNCHANGED
TRINITY_DN3433_c0_g1_i13_p1s pQ9AT56METK1_ELAUM	S-adenosylmethionine synthase 1	15	31755	42570	29404	26651	30234	30917	34576	29267	0,28114	-0,24	UNCHANGED
TRINITY_DN5924_c2_g1_i4_p1sp Q8LAS8SFGH_ARATH	S-formylglutathione hydrolase	7	27310	38348	45341	28752	28968	36184	37000	31301	0,38068	-0,24	UNCHANGED
TRINITY_DN175_c0_g2_i1_p1Uni Ref100_UPI001900DB8D	Salicylic acid-binding protein 2-like isoform X1	2	8309	16114	15100	8451	10608	12104	13174	10388	0,35556	-0,34	UNCHANGED
TRINITY_DN7585_c0_g1_i19_p1s pO20252S17P_SPIOL	Sedoheptulose-1,7-bisphosphatase , chloroplastic	10	82791	75389	95928	113210	115634	113805	84703	114216	0,00817	0,43	UNCHANGED
TRINITY_DN2134_c0_g1_i10_p1s pQ93WN0SEBP2_ARATH	Selenium-binding protein 2	13	31195	35947	37277	28275	21777	24312	34806	24788	0,01925	-0,49	UNCHANGED
TRINITY_DN5362_c0_g1_i10_p1S HMT	Serine	3	10872	10640	11633	14935	11422	9995	11048	12117	0,51494	0,13	UNCHANGED
TRINITY_DN884_c0_g2_i2_p1spQ 94C74GLYM2_ARATH	Serine hydroxymethyltransferase2, mitochondrial	15	22530	21572	26097	16667	13521	14146	23400	14778	0,00682	-0,66	DOWN
TRINITY_DN12155_c0_g1_i2_p1s pO23254GLYC4_ARATH	Serine hydroxymethyltransferase 4	19	256673	252938	285324	268503	203927	270954	264978	247795	0,51707	-0,10	UNCHANGED
TRINITY_DN884_c0_g1_i4_p1spP 50433GLYM_SOLTU	Serine hydroxymethyltransferase, mitochondrial	22	76824	72165	79401	101073	92555	85937	76130	93188	0,02477	0,29	UNCHANGED

TRINITY_DN170_c0_g2_i3_p1spQ56YA5SGAT_ARATH	Serine--glyoxylate aminotransferase	10	46391	46896	79395	83256	77289	93727	57561	84757	0,08479	0,56	UNCHANGED
TRINITY_DN3087_c0_g1_i4_p1spP48578PP2A4_ARATH	Serine/threonine-protein phosphatase PP2A-4 catalytic subunit	4	21778	22546	16728	16674	16595	14938	20351	16069	0,08852	-0,34	UNCHANGED
TRINITY_DN7_c1_g1_i2_p1UniRef100_UPI000C9D5CCF	Serpin-ZX-like	14	70079	100061	75407	53609	65906	67468	81849	62327	0,12878	-0,39	UNCHANGED
TRINITY_DN7_c1_g1_i4_p1UniRef100_UPI0019020B3B	Serpin-ZX-like	16	63594	78156	58368	52443	60345	72230	66706	61673	0,57489	-0,11	UNCHANGED
TRINITY_DN16895_c0_g1_i5_p1UniRef100_UPI0019005A86	Single-stranded DNA-binding protein WHY2, mitochondrial	2	5540	6433	6825	5820	4872	7056	6266	5916	0,66005	-0,08	UNCHANGED
TRINITY_DN3289_c0_g1_i19_p1spQ9FJ95DHSO_ARATH	Sorbitol dehydrogenase	15	25816	29987	45482	29546	31703	31751	33762	31000	0,67054	-0,12	UNCHANGED
TRINITY_DN14550_c0_g1_i6_p1spO82147SPDE_COFAR	Spermidine synthase	4	26966	27023	12747	13937	21657	23693	22245	19762	0,68052	-0,17	UNCHANGED
TRINITY_DN14550_c0_g2_i12_p1UniRef100_UPI001C355CFF	Spermidine synthase 1	3	6837	7168	4442	3788	7172	6951	6149	5970	0,90378	-0,04	UNCHANGED
TRINITY_DN3261_c0_g1_i14_p1spQ93XK2STSYN_PEA	Stachyose synthase	9	12936	14365	15118	34051	30912	22686	14140	29216	0,01195	1,05	UP
TRINITY_DN7183_c1_g2_i1_p1UniRef100_A0A6J1IG81	Stem-specific protein TSJT1-like n=3 Tax=Cucurbita TaxID=3660 RepID=A0A6J1IG81_CUCMA	3	27172	24690	25737	19489	17850	19942	25866	19094	0,00213	-0,44	UNCHANGED
TRINITY_DN7077_c0_g1_i3_p1UniRef100_UPI00190128C2	Stromal 70 kDa heat shock-related protein, chloroplastic	28	94210	99965	105149	134461	147607	132431	99775	138166	0,00255	0,47	UNCHANGED
TRINITY_DN188734_c0_g1_i1_p1spQ9LVJ1SBT14_ARATH	Subtilisin-like protease SBT1_4	13	31518	35375	36201	28130	28068	29852	34365	28683	0,02180	-0,26	UNCHANGED
TRINITY_DN8802_c0_g2_i1_p1spO65351SBT17_ARATH	Subtilisin-like protease SBT1_7	4	14051	15963	12401	7046	8259	10418	14139	8574	0,01749	-0,72	DOWN
TRINITY_DN7039_c0_g1_i1_p1spO65351SBT17_ARATH	Subtilisin-like protease SBT1_7	7	18376	20722	20082	10713	11375	14924	19726	12338	0,00759	-0,68	DOWN

TRINITY_DN11379_c0_g1_i2_p1sp|O82663|SDHA1_ARATH	Succinate dehydrogenase [ubiquinone] flavoprotein subunit 1, mitochondrial	6	86678	92084	92172	117994	128515	120523	90311	122344	0,00093	0,44	UNCHANGED
TRINITY_DN12178_c0_g2_i2_p1sp|Q941A6|SDH6_ARATH	Succinate dehydrogenase subunit 6, mitochondrial	2	9532	16246	4781	9624	13302	9912	10186	10946	0,84010	0,10	UNCHANGED
TRINITY_DN11661_c0_g1_i1_p1UniRef100_A0A6J1E7W1	Succinate--CoA ligase [ADP-forming] subunit alpha, mitochondrial	4	41998	38614	39559	31637	26823	32557	40057	30339	0,00894	-0,40	UNCHANGED
TRINITY_DN10927_c0_g1_i7_p1sp|O82662|SUCB_ARATH	Succinate--CoA ligase [ADP-forming] subunit beta, mitochondrial	7	25517	29488	23263	13055	18687	22207	26090	17983	0,06592	-0,54	UNCHANGED
TRINITY_DN9606_c0_g1_i12_p1sp|Q9SAK4|SSDH_ARATH	Succinate-semialdehyde dehydrogenase, mitochondrial	3	36069	41298	60693	31741	35466	49193	46020	38800	0,47555	-0,25	UNCHANGED
TRINITY_DN7055_c0_g1_i39_p1sp|O82802|SIR1_TOBAC	Sulfite reductase 1 [ferredoxin], chloroplastic	7	22847	27751	26165	18632	23095	26917	25588	22881	0,38786	-0,16	UNCHANGED
TRINITY_DN2061_c0_g1_i1_p1sp|P28769|TCPA_ARATH	T-complex protein 1 subunit alpha	6	13627	13085	14614	11314	10082	12066	13775	11154	0,02308	-0,30	UNCHANGED
TRINITY_DN3380_c0_g1_i10_p1sp|Q940P8|TCPB_ARATH	T-complex protein 1 subunit beta	2	16612	18497	15850	11976	11835	14359	16986	12723	0,01987	-0,42	UNCHANGED
TRINITY_DN21064_c0_g1_i1_p1sp|Q9LV21|TCPD_ARATH	T-complex protein 1 subunit delta	4	14489	15720	15691	9888	11431	13095	15300	11471	0,01931	-0,42	UNCHANGED
TRINITY_DN169636_c0_g1_i1_p1sp|O04450|TCPE_ARATH	T-complex protein 1 subunit epsilon	6	14345	20250	21121	9803	9619	16554	18572	11992	0,10262	-0,63	UNCHANGED
TRINITY_DN7681_c0_g1_i1_p1sp|Q9SF16|TCPH_ARATH	T-complex protein 1 subunit eta	4	15619	25836	16744	13536	15579	14091	19399	14402	0,20359	-0,43	UNCHANGED
TRINITY_DN12250_c0_g1_i2_p1sp|Q84WV1|TCPG_ARATH	T-complex protein 1 subunit gamma	3	21149	19008	18308	15078	12861	16980	19488	14973	0,03687	-0,38	UNCHANGED
TRINITY_DN189535_c0_g1_i1_p1sp|Q94K05|TCPQ_ARATH	T-complex protein 1 subunit theta	4	13515	16968	14168	8879	10099	11092	14883	10023	0,01713	-0,57	UNCHANGED
TRINITY_DN10411_c0_g1_i1_p1sp|Q9M888|TCPZA_ARATH	T-complex protein 1 subunit zeta 1	2	13233	15340	14726	12461	11209	13789	14433	12486	0,11595	-0,21	UNCHANGED

TRINITY_DN8222_c1_g1_i2_p1sp Q8S8Q6TET8_ARATH	Tetraspanin-8	2	53601	45237	49016	54236	47133	47096	49284	49488	0,95499	0,01	UNCHANGED
TRINITY_DN10214_c0_g1_i8_p1s pO23787THI4_CITSI	Thiamine thiazole synthase, chloroplastic	11	46264	49367	53732	16946	16617	17818	49788	17127	0,00012	-1,54	DOWN
TRINITY_DN9882_c4_g1_i1_p1Un iRef100_UPI000C9D9B55	Thioredoxin H5-like	2	49101	56255	15004	43897	44280	31665	40120	39947	0,99034	-0,01	UNCHANGED
TRINITY_DN18290_c0_g1_i2_p1s pQ39243TRXB1_ARATH	Thioredoxin reductase 1, mitochondrial	6	28051	28284	24332	25097	23096	25082	26889	24425	0,16278	-0,14	UNCHANGED
TRINITY_DN8421_c1_g2_i2_p1Un iRef100_A0A6J1KLC1	Thioredoxin-like protein CDSP32, chloroplastic	5	16681	14111	17414	8402	17897	35153	16069	20484	0,60574	0,35	UNCHANGED
TRINITY_DN1705_c0_g1_i4_p1Th ioredoxin_8	Thioredoxin-like_Thioredoxin_8 Thioredoxin-like	4	18712	22974	13032	7797	13015	12743	18239	11185	0,10241	-0,71	UNCHANGED
TRINITY_DN12296_c0_g1_i3_p1s pO64530STR1_ARATH	Thiosulfate/3-mercaptopyruvate sulfurtransferase 1, mitochondrial	3	15020	12539	17977	13250	13450	11298	15179	12666	0,21679	-0,26	UNCHANGED
TRINITY_DN6528_c1_g1_i16_p1U niRef100_A0A0A0KHC3	Threonine dehydratase	36	173393	171282	190381	65612	72492	96481	178352	78195	0,00085	-1,19	DOWN
TRINITY_DN20207_c0_g1_i3_p1U niRef100_A0A6J1ILR7	Threonine dehydratase	23	97768	101905	145176	101092	109830	143749	114950	118224	0,87776	0,04	UNCHANGED
TRINITY_DN20207_c0_g1_i11_p1 UniRef100_UPI000C9D4603	Threonine dehydratase biosynthetic, chloroplastic-like	31	272972	270335	230945	252638	318508	278151	258084	283099	0,34717	0,13	UNCHANGED
TRINITY_DN5024_c0_g2_i1_p1sp Q9MT28THRC_SOLTU	Threonine synthase, chloroplastic	2	12663	13496	10096	11503	12789	14710	12085	13000	0,54436	0,11	UNCHANGED
TRINITY_DN13142_c0_g1_i3_p1U niRef100_A0A5A7TMS5	Transaldolase	17	75060	95382	100994	45913	50594	62758	90479	53088	0,01609	-0,77	DOWN
TRINITY_DN487_c0_g1_i11_p1sp F4IW47TKTC2_ARATH	Transketolase-2, chloroplastic	22	27170	31025	27427	24782	24238	26510	28541	25177	0,07697	-0,18	UNCHANGED
TRINITY_DN487_c0_g1_i13_p1sp F4IW47TKTC2_ARATH	Transketolase-2, chloroplastic	31	199822	219965	224720	198305	205402	223225	214835	208977	0,61119	-0,04	UNCHANGED
TRINITY_DN149637_c12_g1_i1_p 1spQ2PS27TCTP_CUCMA	Translationally-controlled tumor protein homolog	3	71186	87427	75350	60886	65428	79166	77988	68493	0,26562	-0,19	UNCHANGED

TRINITY_DN6557_c0_g1_i2_p1TRAP_beta	Translocon-associated	2	10327	15279	10293	8894	8502	11484	11966	9626	0,28605	-0,31	UNCHANGED
TRINITY_DN16655_c0_g1_i5_p1UniRef100_A0A0A0LGG6	TRASH domain-containing protein	3	17393	17171	17428	19752	16458	17678	17331	17963	0,54827	0,05	UNCHANGED
TRINITY_DN4477_c1_g1_i4_p1spQ9SYM5RHM1_ARATH	Trifunctional UDP-glucose 4,6-dehydratase/UDP-4-keto-6-deoxy-D-glucose3,5-epimerase/UDP-4-keto-L-rhamnose-reductase RHM1	2	10310	12764	8836	8281	9093	9199	10636	8858	0,20675	-0,26	UNCHANGED
TRINITY_DN131713_c0_g1_i1_p1spP60174TPIS_HUMAN	Triosephosphate isomerase	2	133414	140698	172732	138475	147311	177562	148948	154449	0,76122	0,05	UNCHANGED
TRINITY_DN1803_c0_g1_i4_p1spP48496TPIC_SPIOL	Triosephosphate isomerase, chloroplastic	12	40596	43465	34076	42206	49064	43385	39379	44885	0,19003	0,19	UNCHANGED
TRINITY_DN5269_c0_g1_i2_p1spP21820TPIS_COPJA	Triosephosphate isomerase, cytosolic	13	112697	142581	117451	84789	100201	107911	124243	97634	0,08161	-0,35	UNCHANGED
TRINITY_DN8574_c0_g2_i3_p1Tubulin_C	Tubulin	8	22446	25636	21542	18071	18872	21792	23208	19578	0,09672	-0,25	UNCHANGED
TRINITY_DN8574_c0_g1_i1_p1spP33629TBA_PRUDU	Tubulin alpha chain	17	151619	154551	154370	123455	123461	137846	153514	128254	0,00667	-0,26	UNCHANGED
TRINITY_DN2726_c0_g1_i1_p1spP81947TBA1B_BOVIN	Tubulin alpha-1B chain	7	11701	12612	14061	8438	9341	10411	12791	9397	0,01909	-0,44	UNCHANGED
TRINITY_DN17269_c0_g2_i2_p1spO22349TBA3_ELEIN	Tubulin alpha-3 chain	16	67527	65963	77492	51152	53848	56511	70327	53837	0,01372	-0,39	UNCHANGED
TRINITY_DN17269_c0_g1_i2_p1spQ56WH1TBA3_ARATH	Tubulin alpha-3 chain	16	69165	71020	77760	59406	62015	67215	72648	62879	0,04831	-0,21	UNCHANGED
TRINITY_DN101846_c0_g1_i1_p1spP38669TBA2_NEUCR	Tubulin alpha-B chain	6	38424	19979	20073	11151	6768	8508	26158	8809	0,05034	-1,57	UNCHANGED
TRINITY_DN1397_c0_g2_i1_p1spP93176TBB_HORVU	Tubulin beta chain	18	46511	55155	69868	42400	45996	47829	57178	45408	0,16809	-0,33	UNCHANGED
TRINITY_DN6623_c2_g1_i1_p1spQ43594TBB1_ORYSJ	Tubulin beta-1 chain	21	47721	46154	48046	33904	31583	38250	47307	34579	0,00336	-0,45	UNCHANGED

TRINITY_DN367_c0_g1_i5_p1spP37392TBB1_LUPAL	Tubulin beta-1 chain	24	30028	33320	31143	24232	26884	28462	31497	26526	0,03382	-0,25	UNCHANGED
TRINITY_DN75372_c0_g2_i3_p1spQ3MHM5TBB4B_BOVIN	Tubulin beta-4B chain	12	183399	231477	269131	204283	255854	288381	228002	249506	0,57067	0,13	UNCHANGED
TRINITY_DN367_c0_g1_i2_p1spP29516TBB8_ARATH	Tubulin beta-8 chain	20	110504	117607	114596	90727	98176	97357	114236	95420	0,00386	-0,26	UNCHANGED
TRINITY_DN367_c0_g3_i2_p1Tubulin	Tubulin/FtsZ	13	117628	121442	125706	95166	97375	99051	121592	97197	0,00071	-0,32	UNCHANGED
TRINITY_DN5244_c0_g1_i6_p1spQ84L31RD23C_ARATH	Ubiquitin receptor RAD23c	4	15524	15880	15060	15659	16097	14548	15488	15435	0,92290	0,00	UNCHANGED
TRINITY_DN16002_c2_g2_i1_p1ubiquitin	Ubiquitin_ubiquitin Ubiquitin	3	44477	43922	33139	45317	48338	40911	40513	44855	0,36711	0,15	UNCHANGED
TRINITY_DN5627_c0_g1_i1_p1spP93028UBE11_ARATH	Ubiquitin-activating enzyme E1 1	8	25982	36596	25339	17764	22813	21087	29306	20555	0,09047	-0,51	UNCHANGED
TRINITY_DN9334_c1_g1_i1_p2UQ_con	Ubiquitin-conjugating	2	9421	11488	3577	6358	7374	7598	8162	7110	0,68361	-0,20	UNCHANGED
TRINITY_DN73417_c0_g1_i11_p1spQ94A97UBC35_ARATH	Ubiquitin-conjugating enzyme E2 35	2	31658	37211	23227	13134	19765	16651	30699	16516	0,03432	-0,89	DOWN
TRINITY_DN19739_c0_g1_i1_p1spQ9SHE7RUB1_ARATH	Ubiquitin-NEDD8-like protein RUB1	6	117482	112647	104074	71375	86680	81154	111401	79736	0,00599	-0,48	UNCHANGED
TRINITY_DN7471_c0_g1_i2_p1UniRef100_A0A6J1G623	UBP1-associated protein 2A-like	3	16636	18958	19639	15541	19312	23784	18411	19546	0,67928	0,09	UNCHANGED
TRINITY_DN2523_c1_g1_i3_p1spQ9SGE0AXS2_ARATH	UDP-D-apiose/UDP-D-xylose synthase 2	6	29339	25993	22258	24073	20760	21866	25863	22233	0,18427	-0,22	UNCHANGED
TRINITY_DN5131_c0_g1_i2_p1spO65781GALE2_CYATE	UDP-glucose 4-epimerase GEPI48	12	98792	128301	114885	68027	82245	75998	113993	75424	0,01519	-0,60	UNCHANGED
TRINITY_DN12841_c0_g1_i2_p1spO65781GALE2_CYATE	UDP-glucose 4-epimerase GEPI48	12	30607	34940	34150	19040	20714	31101	33232	23618	0,07411	-0,49	UNCHANGED
TRINITY_DN15029_c0_g1_i1_p1spQ96558UGDH1_SOYBN	UDP-glucose 6-dehydrogenase 1	14	60338	68426	49462	38784	39514	43348	59409	40548	0,02926	-0,55	UNCHANGED
TRINITY_DN15090_c0_g1_i1_p1spQ96558UGDH1_SOYBN	UDP-glucose 6-dehydrogenase 1	7	13504	14283	8759	21800	22238	22020	12182	22019	0,00473	0,85	UP

TRINITY_DN5693_c0_g1_i11_p1spQ9SN95UXS5_ARATH	UDP-glucuronic acid decarboxylase 5	9	29983	37120	29404	21864	18118	22479	32169	20820	0,01601	-0,63	DOWN
TRINITY_DN14690_c0_g1_i1_p1spQ9FN03UVR8_ARATH	Ultraviolet-B receptor UVR8	4	9437	10403	11474	7911	8506	7809	10438	8075	0,01965	-0,37	UNCHANGED
TRINITY_DN6327_c0_g1_i1_p1spQ9SZ83Y4967_ARATH	Uncharacterized oxidoreductase At4g09670	13	38703	44603	37983	32823	38321	42589	40430	37911	0,51383	-0,09	UNCHANGED
TRINITY_DN7291_c0_g1_i1_p187347at33090 Coatomer_WDAD	Uncharacterized protein	4	20285	21104	23324	12185	14599	15585	21571	14123	0,00538	-0,61	DOWN
TRINITY_DN2484_c0_g1_i20_p1UniRef100_A0A6J1DTU1	Uncharacterized protein	8	41208	37700	36833	13175	12118	15588	38580	13627	0,00012	-1,50	DOWN
TRINITY_DN9067_c0_g1_i1_p143683at33090 PK_Tyr_Ser-Thr	Uncharacterized protein	2	5627	7697	9153	3909	4681	6727	7492	5105	0,14584	-0,55	UNCHANGED
TRINITY_DN2138_c0_g1_i31_p1Ras	— Uncharacterized protein	2	7309	8121	6321	7901	6197	7228	7250	7109	0,85376	-0,03	UNCHANGED
TRINITY_DN10380_c0_g1_i2_p1213827at33090	Uncharacterized protein	2	25483	23902	19018	24076	29983	27921	22801	27326	0,15726	0,26	UNCHANGED
TRINITY_DN5830_c0_g1_i2_p1203023at33090	— Uncharacterized protein	2	19343	17009	23205	23270	22565	23145	19852	22993	0,15942	0,21	UNCHANGED
TRINITY_DN9448_c0_g1_i5_p1117191at33090	Uncharacterized protein	2	10950	11739	13571	15075	15432	16578	12087	15695	0,01596	0,38	UNCHANGED
TRINITY_DN7439_c2_g1_i2_p1UniRef100_UPI001C34C71E	Uncharacterized protein	2	9229	9644	13367	15814	16202	13253	10746	15089	0,05406	0,49	UNCHANGED
TRINITY_DN21074_c0_g1_i1_p1UniRef100_A0A6J1JSE0	Uncharacterized protein	2	16081	16540	18092	12121	10826	12035	16904	11661	0,00208	-0,54	UNCHANGED
TRINITY_DN10961_c0_g1_i1_p1MA3	Uncharacterized protein	3	10211	12525	13386	8315	9773	10343	12041	9477	0,08472	-0,35	UNCHANGED
TRINITY_DN72045_c2_g1_i1_p1142077at33090	Uncharacterized protein	3	982	1130	1827	262	432	918	1313	537	0,07636	-1,29	UNCHANGED
TRINITY_DN900_c0_g1_i12_p1101701at33090	Uncharacterized protein	3	9243	8275	9476	8930	7146	8597	8998	8224	0,30589	-0,13	UNCHANGED

TRINITY_DN7898_c0_g1_i6_p187 347at33090	Uncharacterized protein	3	11918	11804	12357	10658	10906	12191	12026	11252	0,19905	-0,10	UNCHANGED
TRINITY_DN7224_c1_g2_i2_p1Un iRef100_A0A6J1J3Y5	Uncharacterized protein	3	11044	11814	18249	14566	15378	16832	13702	15592	0,47134	0,19	UNCHANGED
TRINITY_DN9847_c0_g1_i2_p1Un iRef100_UPI0018FF4180	Uncharacterized protein	3	35523	31618	47748	60884	47049	41045	38296	49659	0,21031	0,37	UNCHANGED
TRINITY_DN4210_c0_g1_i11_p1D AHP_synth_1	Uncharacterized protein	4	7114	6992	8615	6912	5613	11522	7574	8016	0,82453	0,08	UNCHANGED
TRINITY_DN4210_c0_g1_i10_p1D AHP_synth_1	Uncharacterized protein	4	5293	5650	10177	5154	4612	10140	7040	6635	0,87218	-0,09	UNCHANGED
TRINITY_DN5713_c0_g2_i7_p1Pi wi	Uncharacterized protein	4	9353	11950	12508	8238	8341	12200	11270	9593	0,36059	-0,23	UNCHANGED
TRINITY_DN797_c0_g1_i5_p1RCC_reductase	Uncharacterized protein	4	12768	17236	18981	17095	17033	20257	16328	18128	0,44659	0,15	UNCHANGED
TRINITY_DN9923_c0_g1_i5_p120 9015at33090 RRM_1	Uncharacterized protein	4	20672	22072	20006	15409	16734	20086	20917	17410	0,08217	-0,26	UNCHANGED
TRINITY_DN6514_c0_g1_i2_p114 4680at33090	Uncharacterized protein	4	9026	10973	6385	5279	8501	7846	8795	7209	0,39191	-0,29	UNCHANGED
TRINITY_DN10893_c0_g1_i2_p1U niRef100_UPI001C36CB79	Uncharacterized protein	4	12059	14406	11677	15959	18106	19909	12714	17992	0,02078	0,50	UNCHANGED
TRINITY_DN21201_c0_g1_i2_p12 09015at33090 RRM_1	Uncharacterized protein	5	131985	151163	108713	125061	133963	124078	130620	127701	0,82904	-0,03	UNCHANGED
TRINITY_DN3320_c0_g1_i13_p11 90390at33090	Uncharacterized protein	5	13118	26472	26754	16145	15135	34248	22114	21843	0,97345	-0,02	UNCHANGED
TRINITY_DN15363_c0_g1_i2_p15 2795at33090	Uncharacterized protein	5	16815	20831	20796	13210	9592	17836	19481	13546	0,09562	-0,52	UNCHANGED
TRINITY_DN5756_c0_g2_i1_p1Un iRef100_A0A6J1GLI6	Uncharacterized protein	5	16555	16462	26895	13197	14888	21278	19971	16454	0,45428	-0,28	UNCHANGED
TRINITY_DN5128_c2_g1_i2_p1Un iRef100_A0A5E4G6D8	Uncharacterized protein	6	27317	29385	36284	18325	23071	25297	30996	22231	0,06158	-0,48	UNCHANGED
TRINITY_DN41049_c0_g1_i1_p11 82493at33090	Uncharacterized protein	6	168514	140068	142553	144546	127401	122962	150378	131637	0,17037	-0,19	UNCHANGED

TRINITY_DN5819_c0_g1_i2_p1DUF642	Uncharacterized protein	7	48117	56545	76326	34751	37714	51073	60329	41179	0,12102	-0,55	UNCHANGED
TRINITY_DN11549_c0_g1_i10_p1142077at33090	Uncharacterized protein	7	133397	174175	206092	195537	220050	254399	171221	223329	0,12678	0,38	UNCHANGED
TRINITY_DN3437_c0_g1_i3_p1209015at33090 RRM_1	Uncharacterized protein	8	39977	40031	46626	31040	30604	40617	42211	34087	0,10841	-0,31	UNCHANGED
TRINITY_DN2053_c1_g2_i1_p1UniRef100_UPI000C9D818F	Uncharacterized protein	8	27444	34349	23903	40905	40142	19192	28565	33413	0,56541	0,23	UNCHANGED
TRINITY_DN2534_c0_g2_i8_p1UniRef100_UPI0019011D71	Uncharacterized protein	10	143406	197878	124131	143335	179234	158564	155139	160378	0,84056	0,05	UNCHANGED
TRINITY_DN178_c0_g3_i1_p1UniRef100_A0A6J1GPH4	Uncharacterized proteiN—	11	125199	143536	123580	76491	103016	106586	130772	95364	0,03647	-0,46	UNCHANGED
TRINITY_DN1753_c0_g1_i18_p1ATP-synt_ab	Uncharacterized protein	14	71951	90831	68116	59692	69406	69878	76966	66325	0,24247	-0,21	UNCHANGED
TRINITY_DN16637_c0_g1_i1_p1139450at33090	Uncharacterized protein	14	77486	99298	105061	73407	73648	83383	93948	76813	0,13021	-0,29	UNCHANGED
TRINITY_DN18271_c0_g1_i2_p1HEAT	Uncharacterized protein	16	31105	39794	34148	22201	28685	31081	35016	27322	0,10451	-0,36	UNCHANGED
TRINITY_DN3747_c1_g1_i7_p1UniRef100_A0A6J1DMV7	Uncharacterized protein	25	184071	178458	196358	109661	113242	164829	186295	129244	0,03733	-0,53	UNCHANGED
TRINITY_DN5377_c1_g1_i15_p1UniRef100_UPI001900D031	Uncharacterized protein	3	6291	6740	9102	12849	15154	16770	7377	14924	0,00623	1,02	UP
TRINITY_DN171307_c0_g1_i1_p1UniRef100_A0A6J1JQQ4	Uncharacterized protein	4	6023	6362	6982	8812	10410	10686	6456	9969	0,00561	0,63	UP
TRINITY_DN5248_c0_g3_i1_p1UniRef100_UPI0018FFAD65	Uncharacterized protein	4	5961	7073	10603	11477	11678	12892	7879	12016	0,04789	0,61	UP
TRINITY_DN18647_c0_g1_i2_p1UniRef100_A0A6J1J2W9	Uncharacterized protein	5	11063	12603	12485	20565	28083	18784	12050	22477	0,02265	0,90	UP
TRINITY_DN3165_c0_g2_i27_p1190390at33090	Uncharacterized protein	9	15934	22130	25447	42741	41102	29486	21170	37776	0,02967	0,84	UP
TRINITY_DN3542_c0_g1_i1_p1UniRef100_A0A1S3C097	uncharacterized protein	3	15870	21777	13230	10804	15333	12824	16959	12987	0,23534	-0,38	UNCHANGED

TRINITY_DN5553_c0_g1_i1_p1UniRef100_A0A6J1CM96	Uncharacterized protein LOC111012758 isoform X2	5	12576	15165	11221	6739	8335	8051	12987	7708	0,01370	-0,75	DOWN
TRINITY_DN61783_c1_g1_i1_p1UniRef100_A0A6J1FCW5	Universal stress protein PHOS32-like isoform X2	4	32438	39120	16105	24286	28705	23169	29221	25387	0,61505	-0,20	UNCHANGED
TRINITY_DN1684_c0_g2_i10_p1spQ8VXY9UAH_ARATH	Ureidoglycolate hydrolase	2	11418	12209	12328	9585	9520	10735	11985	9947	0,01386	-0,27	UNCHANGED
TRINITY_DN2764_c0_g3_i1_p1spQ42967DCUP_TOBAC	Uroporphyrinogen decarboxylase, chloroplastic	13	56226	52154	63770	63614	57199	80681	57383	67165	0,27758	0,23	UNCHANGED
TRINITY_DN18646_c0_g1_i1_p1UDPGP	UTP--glucose-1-phosphate	6	29002	36488	30165	24919	33233	30078	31885	29410	0,50209	-0,12	UNCHANGED
TRINITY_DN12685_c0_g1_i1_p1spQ9SM09VATA_CITUN	V-type proton ATPase catalytic subunit A	19	55926	69775	75313	45955	56940	56519	67005	53138	0,11080	-0,33	UNCHANGED
TRINITY_DN188835_c0_g1_i1_p1spQ8W4S4VHAA3_ARATH	V-type proton ATPase subunit a3	4	20042	22071	25049	15800	17422	18357	22387	17193	0,03360	-0,38	UNCHANGED
TRINITY_DN5867_c0_g1_i12_p1spQ43432VATB1_GOSHI	V-type proton ATPase subunit B 1	13	55724	56069	66950	41747	43829	50888	59581	45488	0,03772	-0,39	UNCHANGED
TRINITY_DN742_c3_g1_i1_p1spQ9SDS7VATC_ARATH	V-type proton ATPase subunit C	6	10686	12968	11605	11078	12759	11722	11753	11853	0,90905	0,01	UNCHANGED
TRINITY_DN150614_c0_g1_i1_p1spQ9LHA4VA0D2_ARATH	V-type proton ATPase subunit d2	2	38938	22419	28942	12342	10439	11766	30100	11516	0,01842	-1,39	DOWN
TRINITY_DN6677_c0_g1_i1_p1spQ9LX65VATH_ARATH	V-type proton ATPase subunit H	4	17974	16125	17738	19177	16004	15128	17279	16770	0,72721	-0,04	UNCHANGED
TRINITY_DN1529_c1_g1_i6_p1spA2SY66VICHY_VICSN	Vicianin hydrolase (Fragment)	12	80519	92835	102788	99150	103128	113527	92048	105268	0,16265	0,19	UNCHANGED
TRINITY_DN4843_c2_g1_i12_p1UniRef100_A0A6J1EZY2	Xaa-Pro dipeptidase	3	8528	10732	7897	19409	24744	11874	9052	18676	0,06591	1,04	UNCHANGED
TRINITY_DN9145_c0_g1_i1_p1spG5DAC7XTH2_DIOKA	Xyloglucan endotransglucosylase protein 2	9	103580	85607	98825	40785	33498	46341	96004	40208	0,00103	-1,26	DOWN
TRINITY_DN7784_c0_g1_i2_p1spQ38857XTH22_ARATH	Xyloglucan endotransglucosylase/hydrolase protein 22	6	17374	14366	32767	24911	21944	20968	21502	22608	0,85866	0,07	UNCHANGED

TRINITY_DN2495_c0_g1_i4_p1sp Q9FKK7XYLA_ARATH	Xylose isomerase	3	20153	22486	23758	22080	20144	22486	22132	21570	0,68291	-0,04	UNCHANGED